University of Alberta

Clarifying the molecular events of early myofibrillogenesis in zebrafish

by

Layne Myhre

A thesis submitted to the Faculty of Graduate Studies and Research
in partial fulfillment of the requirements for the degree of

Doctor of Philosophy

in

Molecular Biology and Genetics

Biological Sciences

Fall 2013

Edmonton, Alberta

ABSTRACT:

Sarcomeres are highly-structured protein arrays, consisting of precisely-aligned thick and thin filaments. The contractile mechanisms of sarcomeres are generally well understood, but how their patterning is initiated during early striated muscle development remains uncertain. Two of the most widely-accepted hypotheses for this process include the "molecular ruler" model, in which the massive protein titin provides a scaffold along which the myosin thick filament is assembled, and the "pre-myofibril" model, which proposes that thick filament formation rather involves "pre-myofibril" templates, modified stress fibers consisting of non-muscle myosin (NMM) and cytoskeletal actin. These models have proven difficult to test *in vivo*, but zebrafish motility mutants with developmental defects in sarcomere patterning are useful for the elucidation of such mechanisms. One such mutant, *steif*, lacks Unc45b, a molecular chaperone that mediates the folding of thick-filament myosin during sarcomere formation. However, Unc45b may also mediate specific functions of NMMs, and *unc45b* mutants display myocyte detachment, indicative of dysfunctional adhesion complex formation. Given the necessity for non-muscle myosin function in the formation of adhesion complexes and pre-myofibril templates, we tested the hypothesis that the *unc45b* mutant phenotype is not mediated solely by interaction with muscle myosin. Our results demonstrate co-expression and co-localization of Unc45b and NMM in myogenic tissue several hours before any muscle myosin is expressed. We also noted deficiencies in the localization of adhesion complex components and NMM in *unc45b* mutants, that are consistent with a NMM-mediated role for Unc45b during early myogenesis. Further, we report the analysis of the previously uncharacterized *herzschlag* mutant, which has similar striated muscle deficits. The *herzschlag* mutant produces a truncated titin protein, lacking the C-terminal rod domain that is proposed to act as a thick filament scaffold, yet muscle patterning was still initiated, with grossly normal thick and thin filament assembly. Only after embryonic muscle contraction begins is breakdown of sarcomeric myosin patterning observed, consistent with a role for titin in maintaining the contractile integrity of mature sarcomeres. These results support the pre-myofibril model, and conflict with the molecular ruler model of early sarcomere patterning, while demonstrating a novel role for Unc45b in early myogenesis.

ACKNOWLEDGEMENTS

This Ph.D. thesis could not have been completed without the aid, support and guidance of a large number of people, and I would like to take this opportunity to thank them all for their encouragement, expertise and assistance along the way.

First, I would like to express my profound gratitude to my supervisor, Dr. Dave Pilgrim, for taking a chance on an unproven stranger with questionable qualifications, to grant me a space in his lab. Without the opportunity he provided, I would not currently be embarked on an academic career. I'd also like to thank all members of the Pilgrim Lab, both old and new, for providing a warm and stimulating research environment, and for their technical assistance over the years. I would also like to thank the members of my committee for their advice and constructive feedback throughout my Ph.D. program.

Many people contributed to this work, and I would like to make acknowledgement of those contributions. I want to thank Serene Wohlgemuth, who paved the way for my project with her *unc45b* timecourses, and Sophie Comyn, for assistance with zebrafish alcian blue staining. I also thank the various undergraduate students whose research projects formed a significant part of my experiments; Eva Gusnowski, who produced the first transient transgenic *unc45b::GFP* zebrafish; Kendal Prill, who did the high-resolution mapping of the *herzschlag* mutation; and Jordan Hills, who did most of the complementation trials and the myosin antibody staining of *herzschlag* embryos. I must also thank our collaborators on the role of UNC45b in eye development, Dr.s Lars Hansen, Niels Tommerup and Hans Eiberg of the University of Copenhagen. I also want to thank Dr. Heather McDermid for the use of her cell culture facilities; Dr. Mike Belosevic for fish cell culture media and reagents; and Aleah McCorry for all her hard work maintaining our zebrafish stocks over the years. This thesis would also not have been possible without the support of a Discovery Grant from the National Science and Engineering Research Council of Canada.

Finally, I want to thank my parents, Ray and Charlene, without whose unending love and support I would never have embarked on an academic career in the first place; and my better half, Alina Pete, for standing by me through both the hard times and the good, and whose amazing artwork was donated for many of the figures in this thesis.

TABLE OF CONTENTS:

List of Tables and Figures:

List of Abbreviations

This thesis follows the proper gene/protein nomenclature for each species discussed; gene names are italicized, and protein names are capitalized but not italicized. Abbreviated gene names and standard chemical abbreviations are not listed.

Acronym	Definition	Acronym	Definition
ATP	adenosine triphosphate	**NMM**	non-muscle myosin
bHLH	basic helix-loop-helix	**NMR**	nuclear magnetic resonance
bp	base pairs (also kbp, Mbp)	**PBS**	phosphate-buffered saline
dCAPS	derived, cleaved, amplified polymorphic sequence	**PCR**	polymerase chain reaction
DIC	differential interference contrast	**PFA**	paraformaldehyde
DIG	digoxigenin	**rpm**	revolutions per minute
dpf	days post fertilization	**RT**	reverse transcriptase
ECM	extracellular matrix	**se**	single-embryo (as in seZEB)
FBS	fetal bovine serum	**sec**	second
FRAP	fluorescence recovery after photobleaching	**SNP**	single nucleotide polymorphism
GFP	green fluorescent protein (also EGFP, enhanced GFP)	**SSLP**	simple sequence length polymorphism
GST	glutathione S-transferase	**TEM**	transmission electron microscopy
hpf	hours post fertilization	**TPR**	tetratricopeptide repeat
kDa	kilo-Daltons	**UCS**	UNC-45/CRO1/She4p domain
MHC	myosin heavy chain	**UTR**	untranslated region
min	minute	**WT**	wild-type
mMHC	muscle-specific myosin heavy chain	**ZEB**	zebrafish embryonic blastomeres
MO	morpholino	**ZEM**	zebrafish embryo medium

1. INTRODUCTION:

The development of striated muscle tissues, comprising both skeletal and cardiac muscle, involves the assembly of some of the most elaborate protein structures known to molecular biology. This process is exceedingly complex, involving the folding and incorporation of dozens of distinct proteins into a highly-ordered, insoluble, contractile molecular apparatus. The growing recognition of the role of molecular chaperones in the assembly and maintenance of large protein complexes has thus led to a change in our understanding of myogenesis; it has become clear that the development of striated muscle tissue requires more than merely the sequential expression of muscle-specific genes. Rather, myofibrillogenesis must involve highly specific and regulated steps of protein folding and assembly, involving both general and myocyte-specific molecular chaperones, co-chaperones, scaffolding proteins and intermediate structures. The final product of this process are myofibrils; the long, cable-like protein structures that transfer contractile force along the length of a muscle cell, consisting of linear arrays of overlapping protein filaments that function in individual contractile units known as sarcomeres. The structural components of the sarcomere and the mechanisms of sarcomere function have been well-studied, but the initiation of myofibril patterning and assembly, and the specific requirements for scaffolding factors and molecular chaperones during this process, remain poorly understood.

In this thesis, I will explore the two competing models of early myofibrillogenesis. The classic hypothesis is the molecular ruler model, in which the giant protein titin provides a semi-rigid molecular scaffold upon which the myosin thick filament is assembled; the competing hypothesis is the pre-myofibril model, in which myoblast stress fibers, containing non-muscle myosin and actin, act as templates to form the first myofibrils. I will also address the role of a specific molecular chaperone, Unc45b, in this process. Unc45b is known to interact with Hsp90a to mediate folding of muscle myosin during the assembly of the sarcomere thick filament, but recent studies suggest an earlier role for Unc45b in myogenesis, as well as involvement with non-muscle myosin activities in early embryos. My results show that Unc45b is required for early myofibril actin dynamics in cultured myoblasts, and that Unc45b is co-expressed, co-regulated and co-localized with non-muscle myosin in developing myogenic tissues, well before any muscle myosin is present. I also show that the loss of Unc45b results in myofibril attachment deficiencies at the costamere,

which is consistent with the requirement for non-muscle myosin activity in the stabilization of focal adhesions. Further, I show that the loss of the titin rod domain, proposed to act as a myosin scaffold, does not inhibit the formation of regular thick filament striations. These results strongly favour the pre-myofibril hypothesis over the molecular ruler hypothesis. With this thesis, I therefore hope to address the controversy that has prevented the acceptance of a unified model of myofibrillogenesis, and demonstrate the involvement of Unc45b with the earliest events of myofibril patterning and assembly.

1.1 Clinical Significance:

Every tissue in which large quantities of structural proteins are expressed during development is subject to protein aggregation and cellular stress, which may be prevented by the co-expression of developmental molecular chaperones [reviewed by (Akerfelt et al., 2007; Ni and Lee, 2007; Walsh et al., 1999)]. Such developmental events include skeletal matrix deposition, neural axon outgrowth, and muscle differentiation. Protein aggregation in these tissues can lead to developmental defects, including congenital myopathies (detailed in the next section). The necessity for specific molecular chaperones and scaffolding proteins during myofibrillogenesis has thus attracted a great deal of clinical interest, and a number of proteins with important muscle-specific chaperone functions have since been identified [reviewed by (Crawford and Horowits, 2011; Sanger et al., 2010; Willis et al., 2009)]. However, the role of molecular chaperones in early myofibril patterning and assembly is not yet fully known, and additional contributing factors remain to be identified.

1.1.1 Myofibrillar Myopathies:

The mechanics of sarcomere function are now well understood, and many of the genes involved have well-characterized as detailed in the sections below. Many of the genes known to play a role in sarcomere function have also been implicated in congenital skeletal and cardiac myopathies [reviewed by (Bonnemann and Laing, 2004; Laing and Nowak, 2005; Morita et al., 2005)], and it is generally recognized that many of these myopathies represent assembly defects during myofibrillogenesis, rather than merely the loss of sarcomere function. Congenital muscular dystrophy is frequently characterized by severe protein aggregation in striated muscle cells (Garrido et al., 2012; Goebel and Blaschek,

2011), implicating molecular chaperones and other assembly factors. Recently, specific factors involved in the assembly of sarcomeres have become targets for research into congenital myopathy, resulting in the identification of striated muscle myopathies that result from mutations in specific molecular chaperones (Garrido et al., 2012; Selcen and Engel, 2011). Furthermore, muscle is a dynamic tissue that constantly undergoes regeneration and repair, due to the damage of mechanical stress on the cells and connective tissues of working muscular organs. The contractile machinery of sarcomeres must therefore be continuously rebuilt. Because of this constant state of repair, mutations of genes involved in coordinating the assembly and regeneration of muscle often have increasingly deleterious effects later in life, resulting in adult-onset myopathies [reviewed by (Laing and Nowak, 2005; Udd, 2012)]. This is unsurprising, given the established role of chaperones in maintaining protein quality control, coupled with dynamic turnover of proteins through proteasome-mediated degradation [reviewed by (Kim et al., 2008; Willis et al., 2009)]. This results in a constant, dynamic system of development and repair that allows continuous sarcomere assembly while mitigating the risk of protein aggregation.

1.1.2 Myogenesis and Regenerative Medicine:

Recent advances in the field of regenerative medicine have made it more important than ever to elucidate the molecular events surrounding myofibrillogenesis. This field has arisen from the convergence of biomedical tissue engineering and developmental molecular biology (Badylak and Nerem, 2010; Badylak et al., 2010; Badylak et al., 2012; Ingber and Levin, 2007). As new medical treatments begin to achieve the development of whole tissues in adult bodies, rather than the healing of damage to pre-existing tissues, developmental biology is providing the insight to guide our understanding of the molecular events involved in the differentiation of stem cells into functional tissues and organs. The first successful surgeries involving complex, stem-cell-derived muscular organs have been reported (Jungebluth and Macchiarini, 2011; Mase et al., 2010), and these treatments are particularly promising for the regeneration of muscle and connective tissue (Turner and Badylak, 2011; Valentin et al., 2010). Indeed, the use of regenerative medicine for the treatment of striated muscle diseases such as cardiomyopathy has recently made significant progress (Badylak et al., 2010; Turner et al., 2012; Wainwright et al., 2010). While previous research has focused

primarily on the genetic regulation of myogenesis, and on the protein structure of mature sarcomeres, the implications for regenerative medicine have created renewed interest in the early molecular events guiding myofibril assembly during the development and maintenance of striated muscle tissue, involving chaperones, scaffolding proteins and intermediate structures that give rise to functional myofibrils.

1.2 Overview of Myogenesis:

1.2.1 The Early Cellular Events of Skeletal Myogenesis:

Determined myoblast progenitor cells derive from paraxial myotome and dermomyotome, and can first be detected in the vertebrate embryo by the expression of pax3, and by the subsequent expression of myogenesis-regulating basic helix-loop-helix (bHLH) transcription factors of the MyoD family [reviewed by (Brand-Saberi, 2005)]. Activation of downstream myogenic gene programs by these factors results in aggregation of the proliferating myoblasts, followed by the alignment of myotube precursor cells and attachment to the substrate through the formation of focal adhesion complexes. Aligned myoblasts subsequently fuse into linear syncytial myotubes (Figure 1A). Attachment and fusion both require the activity of non-muscle myosins and the presence of a cortical actin wall in proliferating myoblasts (Duan and Gallagher, 2009) (Figure 1B, C). Immediately following fusion, focal adhesion points are modified into integrin attachment complexes called costameres (Figure 1D, E) (Pardo et al., 1983; Sparrow and Schock, 2009), which serve as sites of nucleation for the Z-disk protein, α-actinin (Figure 1E). The proto-costamere sites are visible within the cortical actin, and are sometimes known as I-Z-I brushes (actin-[α-actinin]-actin, described below), appearing under electron microscopy as dense α-actinin clusters with radiating F-actin branches (Holtzer et al., 1997). These intermediate structures associate with the amino-terminus of the giant immunoglobulin-domain protein, titin, and the carboxy-terminus associates with myosin motor proteins, which are then incorporated to form the first cortical myofibrils. Additional myofibrils gradually fill the interior of the cell, anchored to one another and to myocyte organelles by desmin-rich intermediate filaments, until all available space is used, leaving narrow gaps for sarcoplasmic reticulum, proteasomes, and mitochondria, while nuclei are displaced to the cell periphery (Figure 1F). Myofibrils remain anchored at the cell cortex to costameres,

Figure 1: Summary of steps involved in myocyte differentiation and myofibrillogenesis, with regards to actin dynamics. A) The stages of myogenic differentiation, from undifferentiated myotome (left) through proliferation, alignment, fusion and maturation (right) [modified from (Gilbert, 2000)]. B) Proliferating myoblasts are derived from determined myotome cells, and possess an unspecialized actin cytoskeleton (grey lines). C) As differentiation begins, these cells aggregate, characterized by the formation of localized stress fibers in a cortical actin wall (insert). Contractile function of these fibers is provided by non-muscle myosin (NMM, arrow). D) Myoblasts align themselves concurrent to substrate attachment and the elaboration of focal adhesions (arrow). The stress-fiber-like cortical actin and NMM will form the pre-myofibril templates for subsequent myofibril assembly. E) Fusion occurs, resulting in the formation of multinucleated myotubes. Myofibrils begin to form at the cell periphery, centered on costamere attachment points (arrow), constructed from pre-myofibril templates (insert). Pre-myofibrils consist of alternating bands of membrane-associated α-actinin (circles) and NMM (arrow). F) As the myocyte matures, additional myofibrils will fill all available space, interconnected with one another and with organelles by desmin-rich intermediate filaments. New myoblasts will continue to fuse to the terminal ends of the myotube to create a growing myofiber. Artwork in (B-F) generously provided by Alina Pete.

Figure 1:

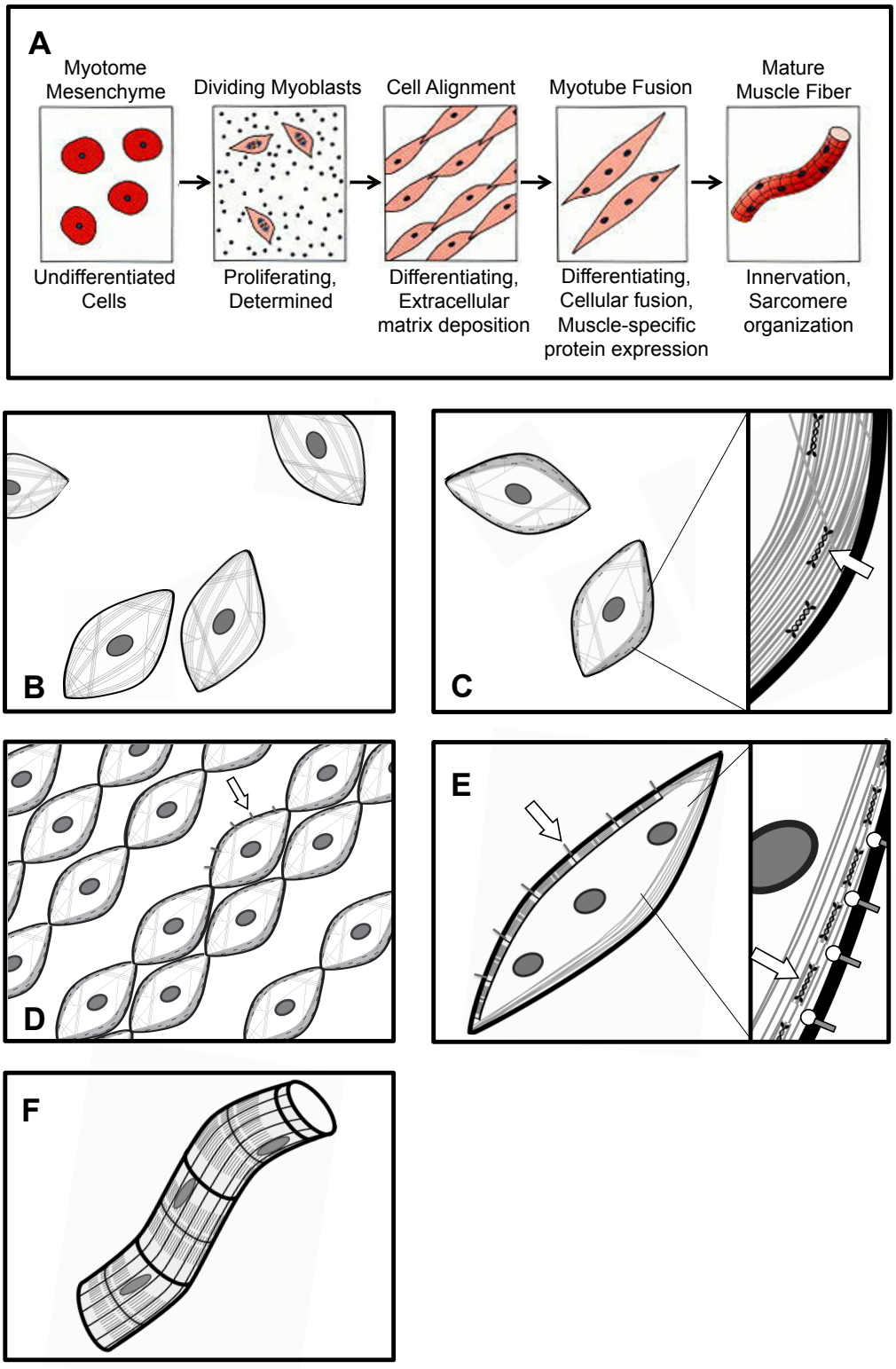
A
Myotome Mesenchyme
Dividing Myoblasts
Cell Alignment
Myotube Fusion
Mature Muscle Fiber
Undifferentiated Cells
Proliferating, Determined
Differentiating, Extracellular matrix deposition
Differentiating, Cellular fusion, Muscle-specific protein expression
Innervation, Sarcomere organization
B
C
D
E
F

which are in turn attached to the extracellular matrix, permitting the transfer of contractile force through the tissue. Additional myoblasts fuse to the growing ends of the myotube until the multinucleated cell becomes a mature, fully-differentiated myofiber (Sanger et al., 2005; Sanger et al., 2010), in which mature isoforms of myosin replace the embryonic and neonatal isoforms as post-natal development continues (Agbulut et al., 2003; Rosser et al., 1998).

1.2.2 Components of the Sarcomere:

The sarcomeres of myofibrils are repeating linear complexes made up of overlapping protein filaments, consisting primarily of myosin, actin, titin, nebulin, and other associated proteins (Figure 2). The overlapping contractile filaments create a recognizable periodic banding pattern, consisting of regularly spaced A-bands and I-bands, which contain the myosin thick filaments and actin thin filaments, respectively, giving striated muscle tissue its characteristic appearance [reviewed by (Ehler and Gautel, 2008; Sanger et al., 2005; Sanger et al., 2010)]. The thick filaments are made up of polymeric muscle myosin II, organized into hexamers consisting of 2 heavy-chain motor subunits and 4 light-chain regulatory subunits (Figure 3A). These individual hexamers organize into higher-order bundles, with globular head domains of heavy-chain subunits jutting outwards from a central filament core, and these bundles associate tail-to-tail with the aid of myomesin, creating a bi-directional thick filament with motor heads extending in both directions. The head domains interact with the overlapping actin-rich thin filaments and perform ATP-dependent motor activity, which is controlled by calcium-mediated association of nebulin/tropomyosin with the actin thin filament [reviewed by (Gordon et al., 2000)]. Actin filaments interact with the Z-disk by cross-linking with α-actinin antiparallel homodimers, and this interaction is stabilized by the PDZ-LIM domain proteins, including ALP, ZASP and CLP36 (Klaavuniemi et al., 2004; Selcen and Engel, 2011; te Velthuis and Bagowski, 2007). At the cell periphery, the Z-disk interacts with costamere attachment sites through two distinct protein binding complexes; the membrane-associated dystrophin/glycoprotein complex, and the vinculin/talin/integrin signaling complex (Figure 4), both of which interact with extracellular laminin and perlecan to anchor the cell and transmit force from the Z-disk to the extracellular environment (Anastasi et al., 2009; Anastasi et al., 2004; Liew and Dzau, 2004). Finally, titin fibril formation occurs in a step-wise fashion as the N-terminal peptide

Figure 2: Schematic diagram of the sarcomere and costamere protein complexes of striated muscle cells. Major components of the mature sarcomere and costamere are shown, along with the cytoskeletal and motor filament systems, in context with the sarcolemma and organelles of syncytial myocytes. Known chaperone or co-chaperone molecules are shown in bold, along with their substrates. Thick arrows indicate regions where chaperone-mediated protein folding is essential to incorporate polymeric filament proteins. Additional artwork generously provided by Alina Pete.

Figure 2:

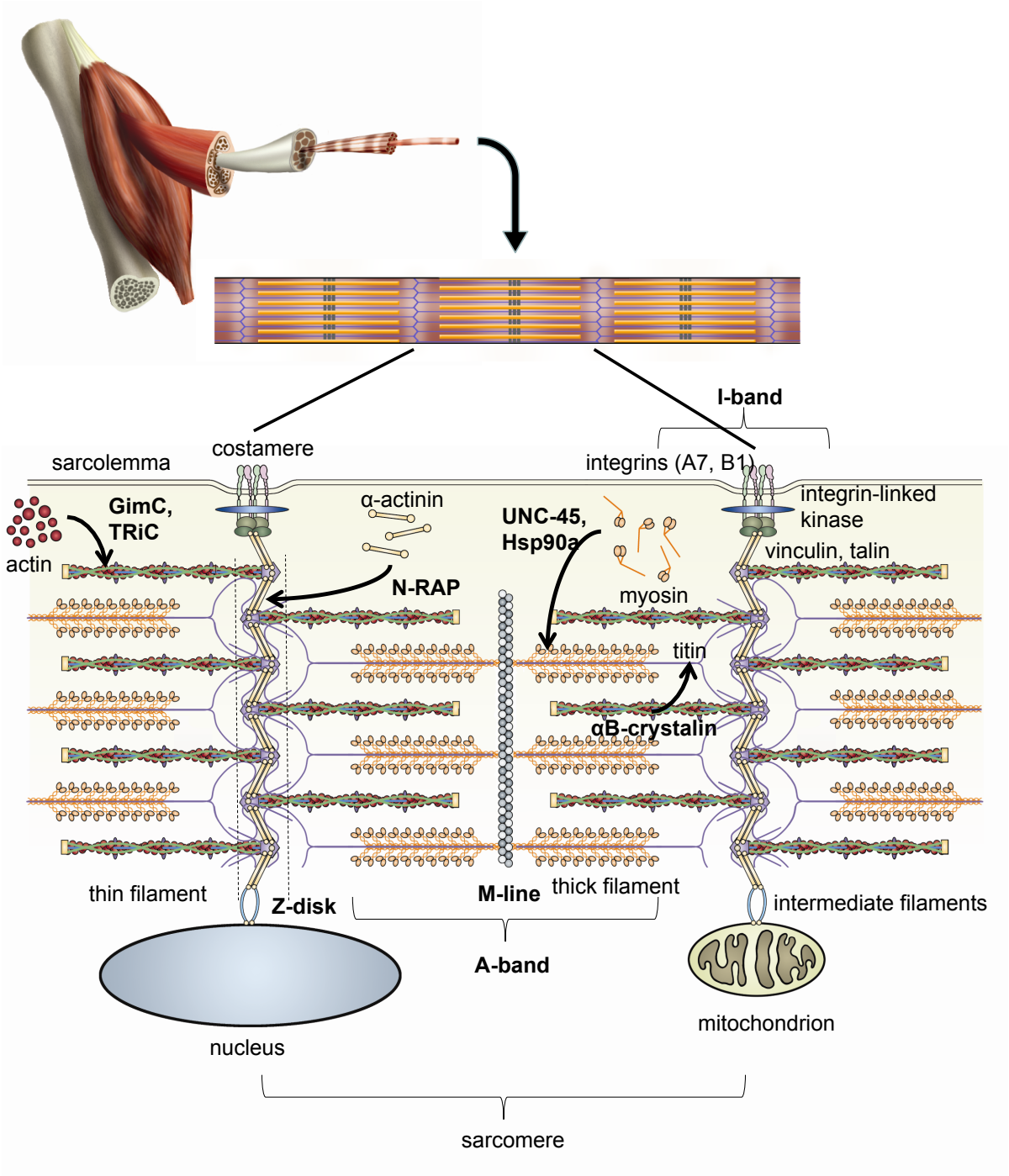
I-band
sarcolemma
costamere
integrins (A7, B1)
integrin-linked kinase
GimC, TRiC
actin
α-actinin
UNC-45, Hsp90a
vinculin, talin
N-RAP
myosin
titin
αB-crystalin
thin filament
Z-disk
M-line
thick filament
intermediate filaments
A-band
mitochondrion
nucleus
sarcomere

Figure 3: Schematic diagram of muscle myosin and titin structures. The protein structures of muscle myosin and titin are shown. A) The myosin hexamer, consisting of two myosin heavy-chains (MHC) and four myosin light chains. All major protein domains (motor head, neck, coiled-coil tail) are shown. Localization of the myosin hexamer within the thick filament is also demonstrated. Modified from (Wohlgemuth, 2007). B) Domain map of titin and context within the sarcomere, showing both the flexible I-band region and the A-band rod domain. Splice variations occur within the indicated I-band section, including the N2A and N2B variants. Domain types are color-coded, including immunoglobulin-rich domains (red), fibronectin-III-like domains (white), the kinase domain (yellow), unique sequences (blue), the flexible PEVK domain (green), and the Z-disk-binding Z-repeat domains (orange). The diagram of titin protein domains is not to scale. Artwork generously provided by Alina Pete.

Figure 3:

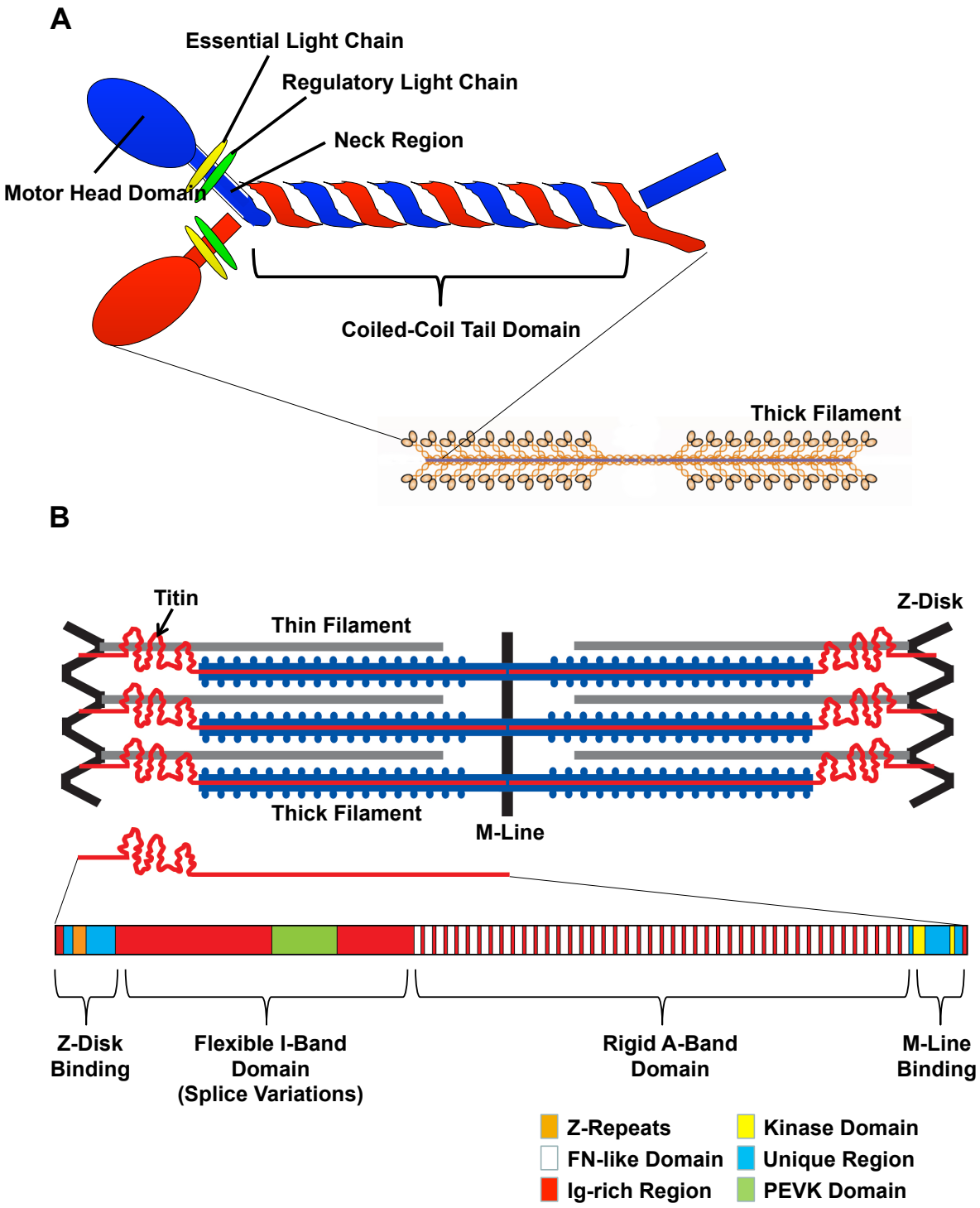
A
Essential Light Chain
Regulatory Light Chain
Neck Region
Motor Head Domain
Coiled-Coil Tail Domain
Thick Filament
B
Titin
Thin Filament
Z-Disk
Thick Filament
M-Line
Z-Disk Binding
Flexible I-Band Domain (Splice Variations)
Rigid A-Band Domain
M-Line Binding
Z-Repeats
FN-like Domain
Ig-rich Region
Kinase Domain
Unique Region
PEVK Domain

first associates with Z-disk proteins, followed by folding and extension of the fibril, and finally association of the C-terminal peptide with proteins of the M-line, concurrently with thick filament assembly (van der Loop et al., 1996; van der Ven and Furst, 1997). The length of the fully-assembled titin protein spans one half-sarcomere, from the Z-disk to the M-line, and is thought to define the final spacing of the sarcomere when at rest, approximately 2.5 microns in mammalian cells (Huxley, 1963; Page and Huxley, 1963). Titin, also known as connectin (Maruyama, 1976), has several important functions in the sarcomere. It acts to stabilize the Z-disk (Gregorio et al., 1998; Peckham et al., 1997), physically limits the maximum extent of sarcomere stretch, and acts as an elastic molecular spring, flexing during muscle contraction and returning the sarcomere to its resting length after the contractile signal is removed (Horowits et al., 1989; Trinick, 1996; Wang et al., 1993).

1.2.3 The Role of Chaperones in Myofibrillogenesis:

Folding of the myosin globular head domain and higher-order assembly of sarcomere thick filaments both require the activity of muscle-specific molecular chaperones (Chow et al., 2002; Liu et al., 1997; Srikakulam and Winkelmann, 1999). Type II myosins fail to maintain motor function when expressed *in vitro* or in bacterial systems, or are subjected to denaturation (Chow et al., 2002; Levitsky et al., 1990), demonstrating the necessity for chaperone-mediated protein folding. "Chaperone" in this context refers to any factor responsible for the prevention of protein aggregation, regardless of a demonstrated ability to facilitate protein folding *in vitro*. For example, some molecular chaperones act by shielding hydrophobic peptides from interacting with one another, while others target mis-folded proteins for rapid proteosome-mediated degradation (Mathew and Morimoto, 1998; Morimoto et al., 1994). Molecules that have been implicated in assisting the proper folding of myosin II include heat-shock family proteins such as Hsp90 and Hsp70, and UNC-45 (Barral et al., 2002; Chow et al., 2002; Liu et al., 2008; Srikakulam and Winkelmann, 1999; Srikakulam and Winkelmann, 2004; Willis et al., 2009). Two α-isoforms of the Hsp90 family (Hsp90a1 and Hsp90a2) are required for proper folding and assembly of the myosin thick filament in vertebrates, and these chaperones are specifically expressed in developing heart and skeletal muscle (Etard et al., 2007; Krone et al., 2003), while other isoforms are more ubiquitously expressed (Etard et al., 2007; Thisse et al., 2004). Likewise, molecular

Figure 4: Schematic diagram of costamere and myocyte attachment components. The two major sub-compartments of the costamere are shown together. The first complex consists of an integrin dimer, bound to a series of stabilizing adaptor proteins (talin, paxillin) and anchored to vinculin, which associates directly with the Z-disk α-actinin. Integrins are also associated with signalling kinases such as focal adhesion kinase (FAK) and integrin-linked kinase (ILK), which transduce ECM-binding signals into the cell. The second complex consists of a series of membrane-inserted glycoproteins called dystroglycans, anchored to the Z-disk by dystrophin, and are thought to provide additional strength to the costamere. Both integrins and dystroglycans bind directly to laminin and perlecan in the ECM, thus transferring force from the sarcomere directly to the extracellular environment. Artwork generously provided by Alina Pete.

Figure 4:

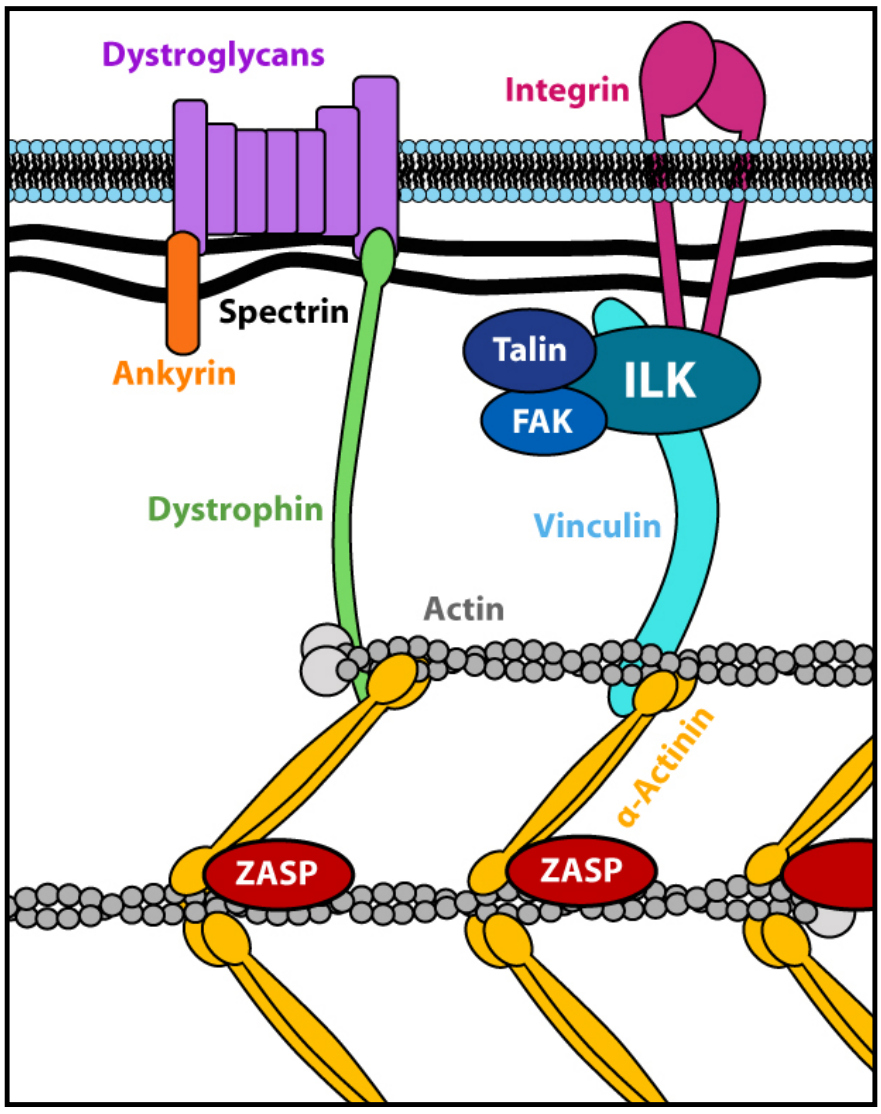
Dystroglycans
Integrin
Spectrin
Ankyrin
Talin
ILK
FAK
Dystrophin
Vinculin
Actin
α-Actinin
ZASP
ZASP

chaperones are involved in the assembly of actin thin filaments, titin filaments, and the desmin-rich intermediate filaments which anchor sarcomeres laterally to each other and to organelles within the myocyte [Figure 2, reviewed by (Crawford and Horowits, 2011; Kim et al., 2008)]. These include N-RAP, which is involved with the organization of α-actinin in the Z-disk (Dhume et al., 2006; Manisastry et al., 2009); GimC and TRiC, which are required for actin thin filament assembly (Grantham et al., 2002; Siegers et al., 1999); and the small heat-shock protein αB-crystallin, which is necessary both for folding of the titin filament (Golenhofen et al., 2002; Inagaki et al., 2006) and for desmin folding in intermediate filaments (Djabali et al., 1997; Wang et al., 2003). Mutations in the genes encoding these molecular chaperones or their substrates are generally associated with disorganized musculature and myopathy in vertebrates (Bonnemann and Laing, 2004; Crawford and Horowits, 2011; Laing and Nowak, 2005; Morita et al., 2005; Vogel et al., 2009), suggesting that the establishment of cytoskeletal scaffolds is essential for subsequent assembly of the functional motor elements of the thick filament. Protein aggregates are often found near Z-disks in myopathies associated with sarcomeric scaffolding proteins, indicating the need for regulation of protein assembly and stability by chaperones in the vicinity of costameres (Kim et al., 2008; Sanger and Sanger, 2008). Furthermore, several sarcomere components and chaperones are known to interact with ubiquitin-recruiting factors (Hoppe et al., 2004; Kim et al., 2008; Landsverk et al., 2007; Lin et al., 2006), and inhibition of proteasome function disrupts fusion and sarcomere formation in cultured myoblasts (Kim et al., 1998; Mugita et al., 1999). This indicates that constant turnover of sarcomere proteins is very likely necessary during myofibrillogenesis, and additional studies have confirmed the rapid turnover of various sarcomere components using FRAP analysis (Ghosh and Hope, 2010; Manisastry et al., 2009). This form of protein quality-control is a common mechanism for molecular chaperones in the prevention of protein aggregation.

1.2.4 Integrins and the Role of Cell-Matrix Interactions in Myofibrillogenesis:

Myofibrillogenesis requires rigid substrate attachment with the extracellular matrix (Discher et al., 2005; Engler et al., 2004; Lin et al., 1989). Not only does the molecular composition (Foster et al., 1987; Funanage et al., 1992; Garcia et al., 1999) and shape (Huang et al., 2006; Lam et al., 2006; Shimizu et al., 2009) of the substrate affect the ability

of myoblasts to differentiate and align themselves prior to fusion, but even mature myocytes cultured in suspension cannot maintain organized myofibrils (Lin et al., 1989; Marino et al., 1987). Mechanical force and tension is important for regulating the formation of complex protein structures in non-muscle cells; the formation of focal adhesion complexes depends on both substrate rigidity (Balaban et al., 2001) and myosin motor function (Helfman et al., 1999); further, the application of external force across non-muscle cells induces focal adhesion growth and elaboration (Riveline et al., 2001). Attachment of myocytes to their surrounding extracellular matrix (ECM) occurs in a similar fashion, via costamere complexes that contain many of the same proteins as focal adhesion structures in non-muscle cells. Indeed, it has been directly demonstrated that force generation between cultured myocytes and their substrates is mediated through costamere junctions (Danowski et al., 1992). Tension across the costamere is essential for the maintenance of sarcomere stability; inhibition of actin/myosin contractility in cultured myocytes causes disassembly of costamere protein complexes concurrent to the disassembly of myofibrils (Sharp et al., 1997), while stimulation of contractility induces or re-establishes costamere organization concurrent to myofibril organization (Fujita et al., 2007), indicating that costamere and myofibril assembly are closely linked. Myofibril formation can be inhibited merely by treating myoblast cultures with an RGD peptide, which antagonizes the matrix-binding region of integrin dimers, even when myosin motor activity is stimulated concurrently (Fujita et al., 2007), demonstrating an essential role for integrin-matrix interaction during myofibrillogenesis.

The first sign of periodic protein alignment similar to that seen in mature sarcomeres occurs at the newly-fused myocyte cortex, where α-actinin co-localizes with integrins, vinculin, and talin during the formation of costameres (Fujita et al., 2007; Tokuyasu, 1989). Accumulated vinculin at integrin-ECM adhesion sites may serve as the initial point of nucleation for α-actinin and the subsequent formation of Z-bodies, indicating that the first step in the higher-order assembly of the sarcomere is cell-substrate attachment [reviewed by (Sparrow and Schock, 2009)]. Integrins and integrin ligands such as perlecan and laminin are indispensable for myofibril and sarcomere formation (Cohn et al., 1999; Rooney et al., 2006; Zoeller et al., 2008), and muscle-specific deficiencies in integrin adhesion result in myopathies characterized by sarcomere disorganization and dissociation of sarcomeres from

the sarcolemma (Hayashi et al., 1998; Rooney et al., 2006). Additionally, work from *C. elegans* and *Drosophila* has shown that integrin requirements are genetically upstream of other essential sarcomeric proteins such as titin (Bloor and Brown, 1998; Hresko et al., 1994; Rui et al., 2010). Muscle cell precursors in the *Drosophila* integrin mutant *mys* differentiate into myoblasts and fuse into multinucleated myotubes, but form no myofibril structures (Volk et al., 1990), further supporting the theory that costamere formation precedes the alignment of Z-bodies along pre-myofibrils to form the Z-disk of mature sarcomeres. Integrin adhesion sites are also thought to be sites of actin nucleation, mediated through Rho-GTPase signaling (DeMali et al., 2002; Dong et al., 2003). Consistent with this, integrin attachment complexes can induce actin nucleation *in vitro*, producing filaments similar to the orientation of actin filaments found in I-Z-I brushes (Butler et al., 2006). Integrins are also proposed to require stabilization by molecular chaperones, and interactions have been demonstrated between β1 integrin, integrin-linked kinase (ILK) and Hsp90 (Aoyagi et al., 2005; Liu and Li, 2008). Stabilization of ILK is required for the assembly of costameres; however, the specific role played by chaperones in this process is not understood, and few of the proteins involved have been characterized (Fujita et al., 2007; Schwander et al., 2003; Sparrow and Schock, 2009).

1.3 Current Models of Myofibrillogenesis:

Although many components of the sarcomere and costamere have been well-characterized, and much is known about the function of the myocyte contractile machinery, the process of myofibril assembly in newly-fused myotubes remains poorly understood, due to the complexity of the system and the number of factors involved. The timing and context of vertebrate muscle development makes it challenging to assay myofibrillogeneis; most studies have been carried out in immortalized cell lines, where contextual cues are lacking. The remaining studies have used mouse embryos, in which only the end result of myogenesis can be readily analyzed, and not the timeline of assembly, making it difficult to assess the order of events. It is thus unclear which components and chaperones are essential for myofibrillogenesis, and which are required only for the maintenance of sarcomeres in mature myocytes, during regeneration and repair. As a result, competing theories exist to

explain the mechanisms of myofibrillogenesis, focused on the step-wise nucleation and incorporation of sarcomere components in differentiating myoblasts.

1.3.1 The Classical Model – Titin as a Molecular Ruler:

A single molecule of the giant muscle protein titin, when folded into its final conformation in mature muscle, spans the distance from one Z-disk to the next M-line, defining a full half-sarcomere (Figure 2). Coupled with the discovery that the actin and titin filaments are both fully formed before myosin thick filament assembly is completed, this led to the "molecular ruler" hypothesis first put forward by Whiting (Whiting et al., 1989). The model proposes that final spacing of the sarcomere depends on the incorporation of titin into the early Z-disk, where it would act as a molecular ruler and scaffold for the assembly of myosin thick filaments (Ehler and Gautel, 2008; Kontrogianni-Konstantopoulos et al., 2009; Tskhovrebova and Trinick, 2003; Whiting et al., 1989). The concept of a protein filament acting as a "molecular ruler", physically limiting the development of a neighbouring structure, is controversial. Similar roles have been proposed for nebulin, which is thought to limit the length of actin thin filaments in the sarcomere (Labeit et al., 1991), and obscurin, which may regulate the lateral alignment of myofibrils (Borisov et al., 2008; Borisov et al., 2006), but evidence for these "ruler" functions is conflicting [reviewed by (Kontrogianni-Konstantopoulos et al., 2009)]. Titin is the largest protein currently known, a highly modular molecule with many splice variants (Guo et al., 2010), consisting mainly of protein-binding immunoglobulin (Ig) and fibronectin-III (fn-III) repeat domains (Figure 3B). In mature muscle, this semi-rigid protein attaches to the Z-disk through a complex with telethonin/T-cap and muscle LIM protein (MLP), which are essential for the Z-disk localization of the titin N-terminus (Knoll et al., 2002; Zou et al., 2003; Zou et al., 2006). The I-band region of titin contains a series of Z-disk-binding Z1-Z2 repeats and a flexible PEVK domain, which is thought to give titin its elasticity during muscle contraction (Linke et al., 1998; Opitz et al., 2003), while the A-band region consists of a rigid rod domain that binds along the length of the thick filament and anchors to the M-line at the C-terminus by direct binding to myomesin (Fig 3B) (Kontrogianni-Konstantopoulos et al., 2009; Muller et al., 2007; Obermann et al., 1997). This rigid rod domain physically limits the maximum extent of contraction, while the flexible I-band region allows sarcomeres to return to their resting state

in the absence of contractile signals [reviewed by (Granzier and Labeit, 2004; Kontrogianni-Konstantopoulos et al., 2009; Tskhovrebova and Trinick, 2003)]. Both regions contain numerous Ig-repeat domains which mediate titin interaction with the thin and thick filaments throughout its length. The A-band rod domain also contains fn-III-repeat domains, and a higher proportion of Ig-repeats, allowing for relatively intimate attachment along the entire length of the thick filament (Figure 3B). Finally, a stretch-sensitive kinase domain lies near the C-terminus, and is thought to activate when titin is stretched, creating a signal cascade that may help to regulate sarcomere protein dynamics and repair (Grater et al., 2005; Kontrogianni-Konstantopoulos et al., 2009; Puchner et al., 2008). N-terminal titin is first detectable by antibody staining concurrent to the nucleation of α-actinin at proto-costamere sites and the formation of I-Z-I brushes (Tokuyasu and Maher, 1987), and this early association provides part of the basis for the molecular ruler model of myofibrillogenesis. Titin association with nucleating α-actinin at developing costameres provides essential stability for the formation of Z-disks (Gregorio et al., 1998; Peckham et al., 1997; Rhee et al., 1994; Turnacioglu et al., 1997), as well as cross-linking the Z-disks to the developing costamere dystrophin complex (Figure 4). The molecular ruler model then predicts that subsequent translation and folding of the remaining titin domains (I-band and A-band) allows titin to act as a scaffold for thick filament incorporation, whereby the newly-folded Ig and fn-III peptides directly recruit individual molecules of muscle myosin as they are released from the hsp90/UNC-45 chaperone complex. This culminates in the formation of the M-line at the titin C-terminus by direct recruitment of myomesin by the C-terminal peptide (Ehler and Gautel, 2008; Kontrogianni-Konstantopoulos et al., 2009; Tskhovrebova and Trinick, 2003). The conformation of titin thus establishes the final periodicity of mature sarcomeres, and holds the sarcomere together through Ig-domain and fn-III domain interactions with the thick and thin filaments throughout its length (Figure 5A).

1.3.2 Evidence For/Against the Molecular Ruler Model:

The length of fully-folded titin, extending from the Z-disk to the M-line, originally led to the hypothesis that titin establishes the periodicity of developing sarcomeres (Ehler and Gautel, 2008; Whiting et al., 1989); it is important to note, however, that the initial pattern formation of α-actinin and vinculin precedes detection of the N-terminal titin peptide

Figure 5: The primary models of myofibrillogenesis. A) the titin "molecular ruler" model of myofibrillogenesis. Following the nucleation of α-actinin at proto-costamere attachment sites, the titin N-terminus is incorporated into the developing Z-disk, helping to stabilize Z-disk polymerization and association with cytoskeletal actin. The subsequent folding of the titin rod domain directly recruits muscle myosin hexamers as they are released from the hsp90 chaperone complex. Theses myosins associate along the titin rod, which thus acts as a scaffold for the thick filaments, and the titin C-terminus recruits myomesin to form the M-line, thus establishing the periodicity of the sarcomere. B) the "pre-myofibril" model of myofibrillogenesis. Stress fibers at the cortex of newly-fused myotubes contain non-muscle myosin (NMM) and α-actinin, which begins to nucleate at focal adhesion sites to form proto-costameres. Tension provided by NMM is essential for this process. The periodicity of costamere attachments creates a pre-myofibril template, characterized by alternating bands of α-actinin and NMM. Muscle myosin then replaces NMM within the sarcomere in a step-wise process that may involve interactions with the hsp90 chaperone complex, resulting in the formation of mature myofibrils.

Figure 5:

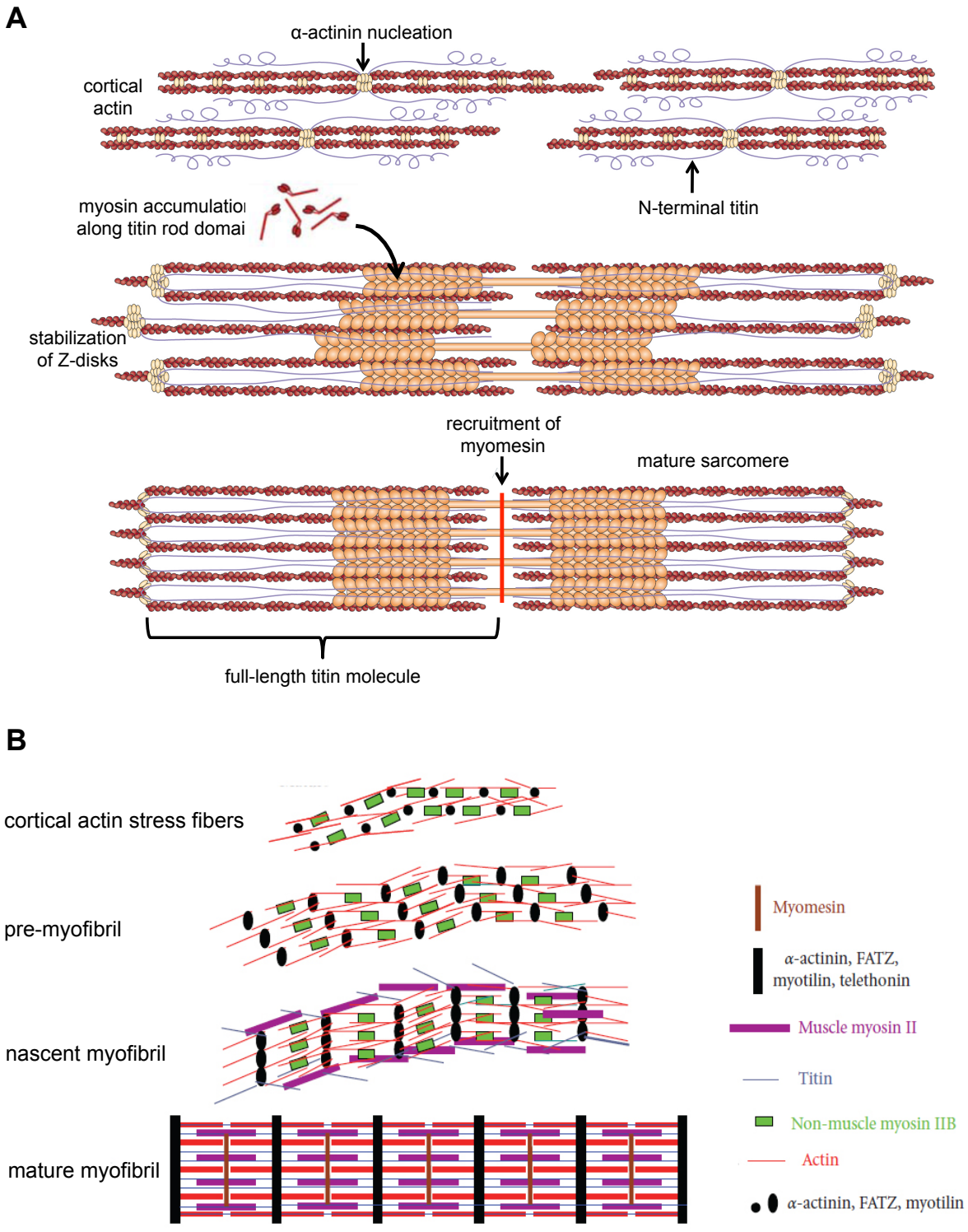
A
α-actinin nucleation
cortical actin
N-terminal titin
myosin accumulatio
along titin rod domai
stabilization of Z-disks
recruitment of myomesin
mature sarcomere
full-length titin molecule
B
cortical actin stress fibers
pre-myofibril
nascent myofibril
mature myofibril
Myomesin
α-actinin, FATZ, myotilin, telethonin
Muscle myosin II
Titin
Non-muscle myosin IIB
Actin
α-actinin, FATZ, myotilin

(Rhee et al., 1994; Sanger et al., 2005; Tokuyasu, 1989), suggesting that only the final positioning of myocyte striations relies on titin. This does not alter the fundamental aspects of the molecular ruler model; that the length of titin establishes the final sarcomere periodicity, and that the rigid rod domain of titin acts as a scaffold for thick filament assembly. A significant amount of correlative data supports these roles for titin, although direct evidence of myosin assembly requiring the titin rod domain is somewhat lacking. Most significantly, antisense oligonucleotide-mediated knockdown of titin disrupts thick filament myosin organization in cultured myoblasts (Person et al., 2000). A loss-of-function mutation of titin has an even more pronounced effect in cell culture (van der Ven et al., 2000), with no visible myosin striations being detected at any time point analysed. Targeted deletion of just the M-line region of titin (the C-terminal peptide) results in the eventual disassembly of myofibrils (Miller et al., 2003; Musa et al., 2006), and several titin mutations have been identified in human myopathies (Hackman et al., 2003; Udd, 2012). However, it is important to note that the M-line C-terminal epitopes of titin are not detectable by immunocytochemistry until well after thick filament assembly has begun (Fulton and Alftine, 1997; Fulton and L'Ecuyer, 1993; Tokuyasu, 1989). Given the established role of N-terminal titin in stabilizing the Z-disk (Gregorio et al., 1998; Peckham et al., 1997; Turnacioglu et al., 1997), it is difficult to directly assess the necessity for the rigid rod domain as a thick filament template; early destabilization of the Z-disk is certain to affect downstream events such as thick filament assembly. Consistent with this, mutant mouse embryos lacking the C-terminus of titin initially develop normal myofibrils with identifiable thick and thin filaments, that are subsequently lost as myofibrils disassemble and muscles atrophy (Peng et al., 2005; Peng et al., 2007; Weinert et al., 2006). This also occurs following targeted ablation of the titin transcript or cardiac-specific knockout of titin in zebrafish (Seeley et al., 2007; Xu et al., 2002). Moreover, despite the high level of conservation of sarcomeric genes between vertebrates and *Drosophila*, the rigid A-band rod domain is not present in *Drosophila* titin (D-titin), although the other functional domains are highly similar to homologous regions of vertebrate titin (Burkart et al., 2007; Machado and Andrew, 2000). Likewise, titin genes in *C. elegans* are structurally different than mammalian titin, and do not span the entire half-sarcomere (Benian et al., 1989; Ferrara et al., 2005), suggesting that the thick-filament-associated functions of mammalian titin in the sarcomere

represent a more recent evolutionary advancement. This is inconsistent with a role for the A-band rod-domain in thick filament assembly in invertebrates.

No study has yet examined the timeline of myofibrillogenesis in cells lacking the titin rod domain, and it is quite possible that myofibril organization occurs normally, with proper thick filament assembly, so long as the Z-disk is stabilized. The lack of full-length titin should impair its function as a molecular spring during sarcomere function, resulting in breakdown of the sarcomere when contractile force is conducted across the myofibril. Embryonic muscle tissue undergoes spontaneous contraction almost immediately after the first myofibrils are formed, which is necessary to promote proper musculoskeletal and neuromuscular development (Kahn et al., 2009; Nowlan et al., 2010; Paulus et al., 2009). This is consistent with the observations that M-line-associated titin appears to act as a signal transducer for sarcomere tension, indicating a possible regulatory role for titin in maintaining sarcomere integrity (Peng et al., 2007; Puchner et al., 2008). In any case, it remains possible that the essential role of A-band titin during myofibrillogenesis occurs later than thick filament assembly, to stabilize the sarcomere rather than to act as a scaffold. To demonstrate otherwise, it would be necessary to examine the timeline of myofibrillogenesis in vertebrate embryos lacking the A-band rod domain of titin (rather than only the C-terminal peptide), showing that the thick filament fails to assemble in the absence of the rod domain. Currently, research has either shown the complete disorganization of sarcomeres in the absence of Z-disk stabilization in cell culture, or the loss of sarcomere organization later in myogenesis, after thick filament assembly and the onset of embryonic muscle contraction.

1.3.3 The Pre-Myofibril Model of Myofibrillogenesis:

A competing model of early myofibrillogenesis is the pre-myofibril model, initially proposed by Rhee (Rhee et al., 1994). This proposes that thick-filament organization is not dependent on the presence of a titin scaffold, although titin is likely still necessary for the stabilization of the Z-disk and maintenance of sarcomere integrity during contraction. Rather, Rhee *et. al*. noted that the I-Z-I brushes at the cortex of newly-fused myocytes are initially associated with non-muscle myosin II, similar to stress fibers of motile cells. They term these structures “pre-myofibrils”, and hypothesize that they act as intermediates in the formation of mature myofibrils, as NMM is replaced by muscle-specific myosin II in a step-

wise fashion (Figure 5B). This allows thick filaments to be incorporated into the expanding actin cytoskeleton concurrent to the incorporation of titin (Sanger et al., 2005; Sanger et al., 2010). Evidence from invertebrates supports this idea; the earliest muscle-specific myosin to be detected in developing *C. elegans* myocytes localizes to nascent bundles of actin that resemble vertebrate stress fibers or I-Z-I brushes (Epstein et al., 1993). Although the titin and pre-myofibril models are not necessarily mutually exclusive, given the apparent role of N-terminal titin in the stabilization of the Z-disk, accumulating evidence favors the pre-myofibril model. The first detectible pattern-forming structures within newly-fused myotubes are the α-actinin nucleation sites, called Z-bodies, which also incorporate cortical cytoskeletal actin to form the stress-fiber-like structures mentioned previously. The titin scaffold model proposes that titin may recruit Z-bodies into I-Z-I brushes, but this would imply that Z-bodies are discrete and randomly distributed, which does not appear to be the case. Rather, as the pre-myofibril model proposes, these membrane-associated clusters of α-actinin form regular periodic patterns, alternating with bands of NMM-II within the actin pre-myofibrils (Du et al., 2008a; Sanger et al., 1986; Sanger et al., 1984). These bands form a mini-sarcomere with a smaller period (0.3-1.5 microns) than the mature sarcomeres of striated muscle, but which appears to act as a fully functional contractile system in early myotubes. The repeat period of mini-sarcomeres was observed to grow over time (Sanger et al., 1986), as thick filament muscle myosin II replaced pre-myofibril NMM-II, concurrent with titin filament elaboration, and titin is likely still responsible for establishing the final distance across the sarcomere.

1.3.4 Evidence For/Against the Pre-Myofibril Model:

The requirement for myosin motor function during myofibrillogenesis has been recognized for some time, since inhibition of myosin heavy chain (MHC) motor activity using pharmacological inhibitors suppresses the formation of organized myofibrils in cultured myoblasts (Kagawa et al., 2006; Soeno et al., 1999). Pharmacological inhibition of contractile signals by calcium channel blockers causes myofibril disassembly and loss of cell-substrate attachment in mature cultured myocytes (De Deyne, 2000; Sharp et al., 1997), indicating a continued need for tension across the cell to maintain sarcomere integrity. Inhibition of myosin contractility also severely reduces sarcomeric actin dynamics in

developing cardiomyocytes (Skwarek-Maruszewska et al., 2009), and even the loss of contractile regulation by a calcium-signal-transducing myosin-light-chain kinase (MLCK) inhibits thick filament assembly during myofibrillogenesis (Du et al., 2003; Ferrari et al., 1998; Ferrari et al., 1996). Moreover, electrical stimulation of contractility can overcome the effects of calcium signal blocking or even accelerate myofibrillogenesis in untreated cells (Fujita et al., 2007). All of these methods of myosin contractile inhibition/excitation affect type II myosins in a non-specific fashion. This means that both muscle-specific and non-muscle myosin activities are likely to be affected by pharmacological motor inhibitors and inhibitors of calcium signalling. Supporting this hypothesis, specific inhibition of a non-muscle myosin light chain kinase results in reversible inhibition of myofibril assembly (Du et al., 2003), and specific depletion of NMM mRNA from undifferentiated myoblasts in culture impairs the polymerization of cortical actin, blocking myoblast fusion and subsequent myofibrillogenesis (Duan and Gallagher, 2009; Swailes et al., 2006). It is now clear that non-muscle myosin II plays an essential role in the formation of pre-myofibrils that precedes the incorporation of muscle-specific myosins into the thick filament, as demonstrated by a number of studies. Most notably, the alignment and fusion of cultured myoblasts requires the presence of an extensive cortical actin network and the activity of non-muscle myosin IIA (Duan and Gallagher, 2009), indicating that the components of stress-fiber-like structures are present at the cortex of newly-formed myotubes from the moment fusion occurs. NMM activity is also necessary for the stabilization of focal adhesion complexes in cultured non-muscle cells (Helfman et al., 1999), suggesting that NMM contractility establishes tension between attachment sites prior to the elaboration of focal adhesions into costameres. Even after the pattern of pre-myofibrils has been fully established, a tension sensor complex including functional NMM and ZASP is necessary for sarcomere integrity in *Drosophila* (Rui et al., 2010). The observed necessity of integrin attachment, substrate rigidity, NMM function and the presence of the cortical actin wall during the earliest stages of myofibrillogenesis all contribute to the pre-myofibril model.

Criticisms of the pre-myofibril model include the observation that the non-muscle myosin isoform generally associated with pre-myofibrils is NMM-IIB, while NMM-IIA is the isoform most often associated with stress fibers in non-muscle cells (Ehler and Gautel, 2008; Sandquist et al., 2006). Since NMM-IIA is specifically necessary for skeletal myoblast

fusion (Swailes et al., 2006), while NMM-IIB appears to be the primary isoform in pre-myofibils of cardiomyocytes, it seems likely that different isoforms possess specialized roles in different processes, and knock-down studies in cultured myoblasts have supported this idea (Swailes et al., 2006). Knockout mice lacking NMM-IIB, which do not survive past birth and have malformed hearts, still contain a significant proportion of normal cardiomyofibrils, indicating that not all myofibril formation depends on NMM-IIB (Bao et al., 2007; Tullio et al., 1997). It is important to note, however, that these embryonic hearts also contain increased levels of the NMM-IIA isoform, which may play a redundant role during myofibrillogenesis; in fact, co-knockdown of NMM-IIA with -IIB demonstrates a more severe phenotype, although overexpression of IIA alone cannot rescue the IIB knockout phenotype (Bao et al., 2007). The newly-discovered and poorly-characterized NMM-IIC may also have redundancy with IIA and IIB (Golomb et al., 2004). All three isoforms of NMM-II are normally detectable in developing myocytes, and both NMM-IIA and -IIB are localized to the cortical actin wall immediately after fusion (Golomb et al., 2004; Wells et al., 1997). Redundancy between myosin isoforms is not unprecedented; in *C. elegans*, one MHC isoform has the ability to fully compensate for the loss of another during thick filament assembly, as we will discuss below (Hoppe and Waterston, 1996; Hoppe and Waterston, 2000; Maruyama et al., 1989), and domain-specific redundancy has been shown between NMM isoforms during cell attachment in mice (Wang et al., 2011). Given that the role of NMM in pre-myofibrils may involve the stabilization of cell attachments, the possibility of redundancy between the NMM isoforms thus remains a strong defence of the pre-myofibril model.

1.3.5 Summary of the Molecular Events of Myofibrillogenesis:

A synthesis of the pre-myofibril model with what is known about titin fibril formation and the role of cell attachment during myocyte differentiation would therefore lead to the following order of events (Figure 6): First, the actin cytoskeleton of proliferating myoblasts is modified to create the cortical actin wall, which associates with NMM in stress-fiber-like conformation, prior to cell aggregation and fusion (Figure 6A-B). Second, formation of integrin-ECM attachments occur, concurrent with myoblast fusion, in a process that requires NMM activity to create tension across the cell. Next, the integrin attachment

Figure 6: Synthesis of the pre-myofibril model with the roles of non-muscle myosin (NMM) in early differentiating myoblasts. Schematic representation of the order of molecular events leading from cytoskeletal actin to mature myofibrils in the pre-myofibril model of myofibrillogenesis. The known roles of NMM during costamere formation are incorporated into this model. A) Elaboration of the actin cytoskeleton in proliferating myoblasts leads to the formation of a cortical actin wall. B) Stress-fiber-like structures in the cortical actin wall contain associated NMM, which allows for alignment and fusion of myoblasts. C) Alignment and fusion are concurrent with proto-costamere formation, resulting in the anchorage of pre-myofibrils to the extracellular matrix. These sites serve as nucleation points for α-actinin, resulting in the formation of mini-sarcomeres with alternating bands of α-actinin and NMM. Incorporation of N-terminal titin occurs at this point as well. D) Folding and lengthening of titin is concurrent with the stabilization of α-actinin in the Z-disk and the incorporation of muscle MHC-II into the thick filament, displacing NMM and widening sarcomeres. E) M-line proteins associate with MHC-II and C-terminal titin, creating the final banding pattern of mature myofibrils.

Figure 6:

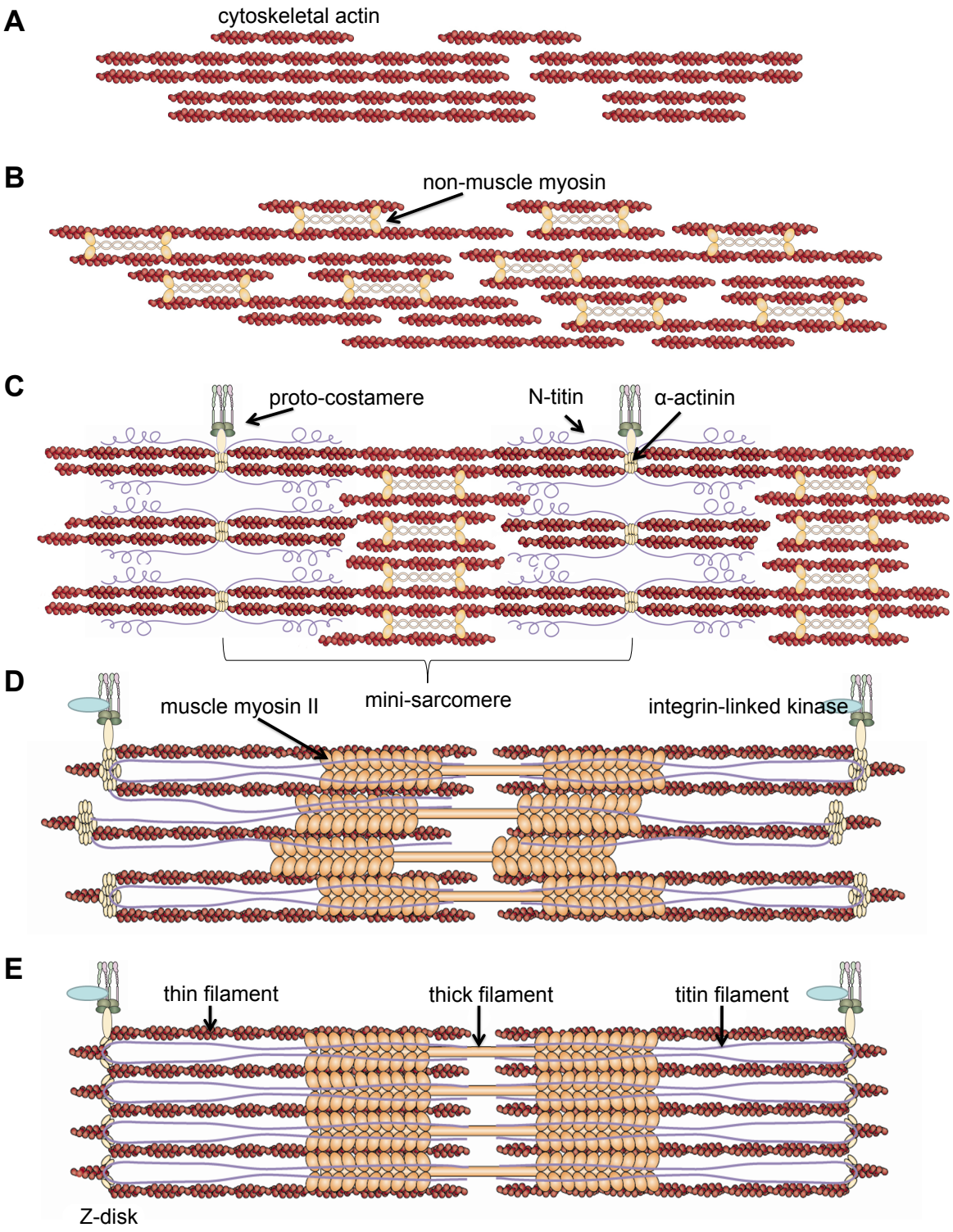
A
cytoskeletal actin
B
non-muscle myosin
C
proto-costamere
N-titin
α-actinin
mini-sarcomere
D
muscle myosin II
integrin-linked kinase
E
thin filament
thick filament
titin filament
Z-disk

complexes serve as nucleation sites for α-actinin, vinculin and talin, creating regularly-spaced, membrane-associated Z-bodies. Further actin polymerization occurs at these sites as well, mediated by formins, resulting in the creation of the mini-sarcomeres that are often called I-Z-I brushes. These are characterized by alternating bands of α-actinin and non-muscle myosin, and are associated with N-terminal epitopes of titin, as well as ZASP and other PDZ-LIM domain proteins, which may help to stabilize the newly-forming Z-disk (Figure 6C). The pre-myofibrils grow, pushing costameres farther apart, as the rod domain of titin is incorporated into the proto-sarcomeres, and desmin-rich intermediate filaments begin to anchor the sarcomeres to one another with the aid of protein folding factors such as αB-crystallin. Incorporation of titin aids the interdigitation of the thick and thin filaments, concurrent with the replacement of NMM with muscle myosin II (Figure 6D). This eventually results in the final spacing of thin and thick filaments with a Z-disk period of 2.5 microns (Figure 6E). Specific chaperone activities are necessary throughout this process, including the stabilization of ILK and integrin attachment complexes by Hsp90 and other chaperones, the nucleation and organization of α-actinin into Z-bodies and mature Z-disks by N-RAP, the polymerization of actin by GimC and TRiC, the folding of titin by αB-crystalin and Hsp70, and folding and assembly of muscle myosin to form the mature thick filaments by Hsp90 and UNC-45 (listed in Figure 2).

1.4 UNC-45 and Myosin Assembly During Myogenesis:

UNC-45 is a myosin-binding protein, initially identified in *C. elegans* through mutations affecting the proper assembly and function of thick filaments in body wall muscle (Ao and Pilgrim, 2000; Venolia et al., 1999). Invertebrates have a single UNC-45 isoform, while two isoforms are found in vertebrates, called Unc45a and Unc45b (Price et al., 2002); Unc45a is expressed ubiquitously, and mutations in zebrafish affect circulation but not striated muscle formation (Anderson et al., 2008). By contrast, Unc45b is expressed specifically in striated muscle, in a pattern virtually indistinguishable from that of Hsp90a (Etard et al., 2007; Thisse et al., 2004; Wohlgemuth et al., 2007). *C. elegans* UNC-45 interacts with Hsp90 family members through an amino-terminal tetratricopeptide repeat (TPR) domain (Barral et al., 2002; Venolia et al., 1999), and with muscle myosin heavy-chain B (MHC-B) through a ~400 residue UNC-45/Cro1/She4p (UCS) domain that is

conserved with fungal homologues (Ao and Pilgrim, 2000; Hutagalung et al., 2002) (Figure 7A). As discussed above, UNC-45/Unc45b is proposed to act as a co-chaperone with Hsp90a, for the folding and assembly of MHC in striated muscle. The specific requirement for Hsp90a chaperone activity in myofibrillogenesis is well-documented (Du et al., 2008b; Hawkins et al., 2008; Krone et al., 2003; Srikakulam et al., 2008), and the mechanisms of Hsp90 ATPase-dependent protein folding are becoming understood [reviewed by (Krukenberg et al., 2011; Mayer, 2010)]. However, less is known about the nature of requirements for tissue-specific co-factors like Unc45b. Reducing or eliminating Unc45b function in zebrafish or *Xenopus* results in loss of thick filament assembly and disorganization of sarcomeres (Etard et al., 2007; Geach and Zimmerman, 2010; Wohlgemuth et al., 2007); indeed, the phenotype of zebrafish *unc45b* mutants (*steif*) (Etard et al., 2007) is very similar to that of *hsp90a1* mutants (*sloth*) (Hawkins et al., 2008), characterized by poorly organized sarcomeres, loss of thick filament assembly, heart dysfunction, pericardial edema and paralysis.

1.4.1 UNC-45 May Exhibit Direct Myosin Chaperone Activity:

UNC-45 has been demonstrated to have chaperone activity *in vitro* (Barral et al., 2002; Melkani et al., 2010), and Unc45b-Hsp90a complexes are necessary for the folding of the MHC motor domain in vertebrates (Liu et al., 2008; Srikakulam et al., 2008). Vertebrate Hsp90a1 and Hsp90a2 are associated only with partially-folded intermediate forms of myosin (Barral et al., 2002), supporting the hypothesis that co-factors such as UNC-45 are necessary for the proper folding and assembly of sarcomeric myosins during myogenesis. *Drosophila* UNC-45 (dUNC-45) is able to reduce heat-induced myosin aggregation *in vitro*, without the addition of any other chaperone or co-factor (Melkani et al., 2010). Hsp90a and Unc45b transcripts are both up-regulated in *unc45b*/*steif* mutant embryos (Etard et al., 2007), and Unc45b expression is increased in response to protein stress in a similar fashion to Hsp90a (Etard et al., 2008). This suggests that Hsp90a and Unc45b may also be co-regulated during zebrafish muscle development or following protein stress. However, vertebrate Unc45b has little effect on MHC folding without the addition of Hsp90a (Liu et al., 2008), and it has not yet been shown that UNC-45 directly mediates protein folding *in vivo*. The primary role of Unc45b in vertebrates may be to act as an adaptor molecule, stabilizing the

Figure 7: Possible roles for Unc45b/non-muscle myosin during early myofibrillogenesis. A) merged protein model of Unc45b, taken from the x-ray crystal structure of *Drosophila* UNC-45 and the solved NMR structure of the human Unc45a TPR domain (protein database ID 2DBA), showing the known active domains of Unc45b. Proposed functions of each section of the protein are indicated. Modified from (Lee et al., 2011a). B) Flowchart of myofibrillogenesis, listing the stages where there is significant evidence to hypothesize the involvement of UNC-45, either because of proposed activities of non-muscle myosin or possible chaperones functions. Specific events that are likely to involve UNC-45 are noted, and probable co-factors for UNC-45 at each stage are indicated.

Figure 7:

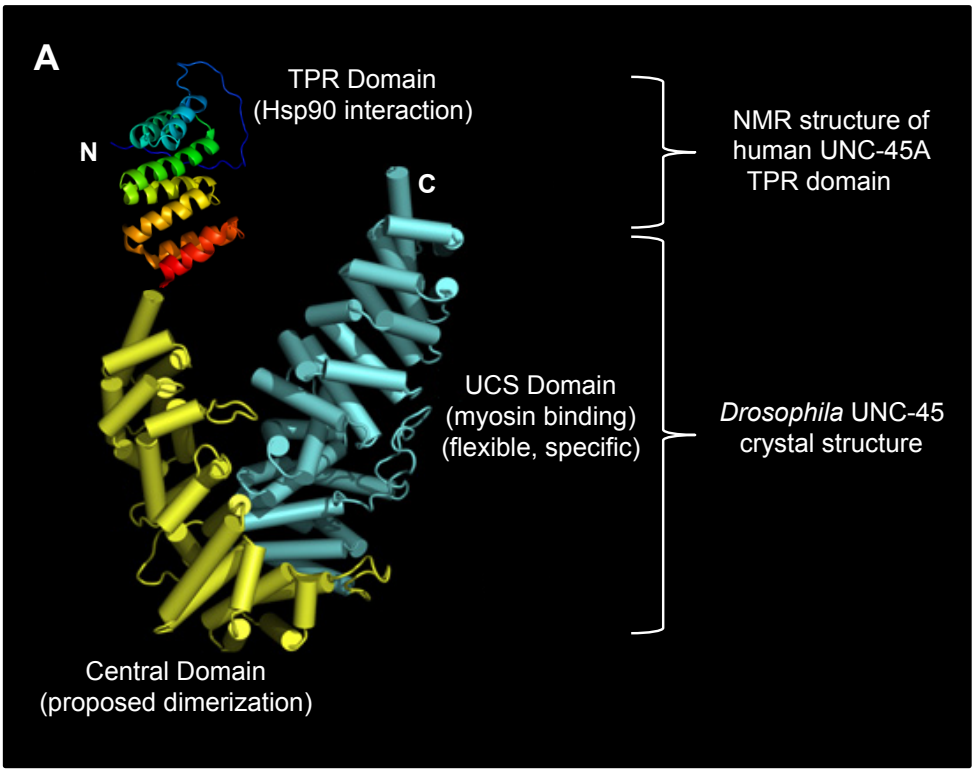

B

Stage of Myogenesis	Events	Steps requiring UNC-45
Myoblast Proliferation		
↓	Growth, Cell Division	No Evidence
Myoblast Aggregation/Alignment		
↓	Stress Fibers/Cortical Actin Wall Forms	**NMM** activity required ← **UNC-45**
Myotube Fusion		
↓	Cell-ECM Attachment, Requires cell tension	**NMM** activity required, Integrin stabilization ← **Hsp90? UNC-45? Apobec2?**
Pre-myofibril Formation		
↓	Costameres Form, Mini-sarcomeres with NMM and α-actinin	**NMM** activity required, ILK folding/stabilization ← **UNC-45**, **Hsp90 UNC-45?**
Thick Filament Assembly		
↓	Muscle MHC replaces NMM	**MHC** folding, Protein quality control ← **Hsp90, UNC-45 UNC-45?**
Mature Myocyte		

interactions between Hsp90a and MHC through the TPR and UCS domains, respectively. However, as noted above, protein aggregation may also be prevented by chaperones that target misfolded proteins for degradation. Such a role has been suggested for UNC-45 in *C. elegans*, studies showing interaction with the CHN-1/UFD-2 ubiquitylation complex (Hoppe et al., 2004). Overexpression of UNC-45 in *C. elegans* results in ubiquitin/proteasome-mediated myosin degradation, indicating that UNC-45 may act to prevent the accumulation of misfolded myosins (Landsverk et al., 2007). In humans, the ubiquitin-selective chaperone p97, known to cause hereditary inclusion-body myopathy in mutants, regulates UNC45B degradation (Janiesch et al., 2007; Kim et al., 2008). *UNC45B* has therefore been proposed as a candidate locus for additional cardiomyopathies (Walker, 2001). This is consistent with the observation that overexpression of vertebrate Unc45b in zebrafish results in a similar phenotype to knockdown embryos, with disorganized sarcomeres and loss of thick filament assembly (Bernick et al., 2010). Despite these reports, however, it remains unclear whether chaperone functions of UNC-45 *in vivo* are directly accomplished in certain situations, or mediated entirely through its association with Hsp90a.

1.4.2 UNC-45 Shows Myosin Isotype Specificity During Development:

Unlike Hsp90 family members, UNC-45 in *C. elegans* is not a general chaperone, but instead shows striking isotype specificity. Thick filaments in *C. elegans* are assembled from two different muscle myosin heavy chains, MHC-A and -B. The minor isoform (MHC-A) is found only in the central 2 μm of the filament, while MHC-B is found along the majority of the lateral arms (Miller et al., 1983). In the region corresponding to the M-line of vertebrate sarcomeres, where only MHC-A is found in *C. elegans*, the myosin molecules adopt an antiparallel alignment. It is possible that the MHC-A tail domain more readily accommodates this alignment than MHC-B, or that it more readily assembles to initiate thick filament organization, perhaps taking a role similar to vertebrate myomesin (Hoppe and Waterston, 1996; Hoppe and Waterston, 2000). This would imply that MHC-B is the more efficient motor protein; however, in mutants lacking MHC-B (*unc-54* null mutants), thick filaments can still be induced to form entirely from MHC-A (Maruyama et al., 1989). In these mutants, UNC-45 no longer localizes to the thick filaments, and additional missense mutations of UNC-45 have no effect on thick filament assembly (Ao and Pilgrim, 2000).

Thus, MHC-A does not seem to require UNC-45 activity despite the fact that the two myosins are 65% identical at the sequence level, and there are no regions of difference in the sequence alignment that would obviously explain this difference in function (Hoppe and Waterston, 1996). There is also no reciprocal rescue; null mutations in MHC-A are embryonic lethal whether or not MHC-B is over-expressed (Fire and Waterston, 1989). In addition to MHC-B, UNC-45 in *C. elegans* interacts with non-muscle myosin NMY-2 (Kachur et al., 2004), but not with the NMY-1 isoform (Kachur and Pilgrim, unpublished data). This isotype specificity is not shared by Hsp90, which associates with a wide variety of target proteins [reviewed by (Jackson, 2013)]. *In vivo*, *C. elegans* UNC-45 co-localizes with NMY-2 during cytokinesis in the early embryo, where it seems to regulate cell contractility (Kachur et al., 2004), and this co-localization has also been shown in the early blastoderm of 2-hour-old *Drosophila* embryos (Lee et al., 2011b). In both species, UNC-45 must be maternally contributed to the oocyte, appearing well before the midblastula transition. The nematode maternal gene product can partially ameliorate the muscle phenotype in UNC-45 mutants, making it unique among muscle genes in *C. elegans* (Venolia et al., 1999). The interaction of UNC-45 with NMY-2 seems to happen at a late stage of myosin assembly, as NMY-2 and actin can fully assemble into identifiable stress fibers, but these structures cannot contract (Kachur et al., 2008), implying that the role of UNC-45 in this context is related to motor function rather than filament assembly. Additionally, crystal analysis of dUNC-45 suggests that its myosin-specific chaperone activity can be attributed to the flexibility of the elastic UCS domain (Lee et al., 2011a). This is in keeping with recent structural studies that suggest a role for the yeast UCS homologue, She4p, in limiting step size during myosin motor action (Shi and Blobel, 2010) (Figure 7A).

1.4.3 UNC-45 Plays an Earlier Role in Myofibrillogenesis – Evidence from Invertebrates:

Although the phenotype of temperature-sensitive *unc-45* mutant alleles is suppressed in *C. elegans* when the thick filaments are assembled from MHC-A as described above, *unc-45* null mutant alleles in this background are still embryonic lethal. One possibility is that small quantities of UNC-45 protein are necessary for reasons unrelated to thick filament assembly. The terminal phenotype of these null alleles, known as Pat (paralyzed and arrested

at two-fold stage) is similar to the Pat phenotype of mutations in genes required for the earliest stages of myoblast differentiation and myofilament assembly (Venolia et al., 1999; Williams and Waterston, 1994), including ECM components and the α and β-subunits of integrin (*pat-2, -3*) (Gettner et al., 1995). Given the myofibrillogenesis models that propose integrin-ECM attachment as the first step in NMM-dependent pre-myofibril assembly [reviewed by (Sanger et al., 2010; Sparrow and Schock, 2009)], and the fact that UNC-45 interacts with NMY-2 (Kachur et al., 2004; Kachur et al., 2008), this phenotype leads to a hypothesis that UNC-45 plays a much earlier role in myofibrillogenesis, independent of muscle myosin, but perhaps requiring other myosins such as NMM. *C. elegans* muscle contains sarcomere-ECM attachment complexes analogous to the Z-disk and costameres of vertebrates (Qadota and Benian, 2010), consistent with a possible role for UNC-45 in stabilizing cell-matrix interactions. Indeed, it has been shown that the *unc-45* mutant phenotype can be partially ameliorated by the expression of truncated UNC-45 lacking the TPR domain (Ni et al., 2011), demonstrating that at least some of UNC-45 function occurs independent of Hsp90. Furthermore, in addition to co-localization with NMM in the early *Drosophila* blastoderm, dUNC-45 protein also co-localizes with both NMM and PS2 integrin at Z-disks during sarcomere formation in third-instar larvae (Bloor and Kiehart, 2001; Lee et al., 2011b). The Z-body nucleation complexes which form downstream of integrin attachment at costameres contain α-actinin, non-muscle myosin, and the PDZ-LIM-domain protein ZASP, all three of which are necessary for subsequent sarcomere formation(Jani and Schock, 2007; Rui et al., 2010). The ZASP-NMM complex is hypothesized to act as a sarcomere-stabilizing tension sensor, and the absence of non-muscle myosin from this complex reduces thick filament organization (Rui et al., 2010). It has thus been suggested that Z-disk non-muscle myosin in *Drosophila* plays a role in cross-linking actin to provide mechanical stability to the sarcomere, and/or stabilizing the formation of cell-matrix attachment complexes, and it is possible that dUNC-45 helps to mediate these functions.

1.4.4 Vertebrate Unc45b is Analogous to Invertebrate UNC-45:

In vertebrates, Unc45b has not been rigorously tested for a role in early embryonic cytokinesis or interactions with non-muscle myosins. Rather, it has been assumed that the

more ubiquitous Unc45a isoform mediates any NMM-related UNC-45 chaperone function during cytokinesis, partly due to the fact that targeted knockdown of Unc45a results in decreased cell proliferation in cell culture (Price et al., 2002). However, little evidence exists to demonstrate interactions between Unc45a and specific NMM proteins, and zebrafish Unc45a null mutants do not display any NMM-related defects (Anderson et al., 2008). Interestingly, a double null mutation of Unc45a and Unc45b has no additive phenotype (Comyn and Pilgrim, 2012), which further supports the notion that Unc45a does not mediate NMM-specific activity during myogenesis, and that compensation does not occur between Unc45a and Unc45b in null mutant embryos. This suggests that the function of Unc45a is divergent from the roles played by UNC-45 in invertebrates, which are likely to be performed entirely by Unc45b in vertebrates. Conservation between vertebrate Unc45b isoforms is greater than between Unc45a isoforms (Figure 8), and Unc45b retains a slightly higher protein identity with invertebrate UNC-45 than does Unc45a. The recent identification of Unc45a as a positive regulator of progesterone receptor activity demonstrates one possible vertebrate-specific function of Unc45a that does not involve myosins (Chadli et al., 2006). It has also often been assumed that the muscle-specific activity of Unc45b is entirely mediated by interactions with Hsp90a and muscle MHC, and yeast two-hybrid screens have not yet indicated NMM as a substrate for Unc45b binding. Given that protein interaction screens with complex-forming chaperone molecules are notoriously difficult to accomplish in yeast, as multiple co-factors are often necessary to stabilize interactions, this hypothesis should not be excluded as a possibility. Multiple lines of evidence now suggest that vertebrate Unc45b may perform a similar muscle-specific function during early myofibrillogenesis as invertebrate UNC-45, prior to thick filament assembly, that may not be mediated by Hsp90a.

1.4.5 UNC-45 Plays an Earlier Role in Myofibrillogenesis – Evidence from Vertebrates:

Zebrafish Unc45b mRNA can be detected in the paraxial mesoderm of developing embryos prior to somite formation or myoblast differentiation (Etheridge et al., 2002; Wohlgemuth et al., 2007), during the earliest stages of myogenesis, as I will show in this thesis. The onset of Unc45b expression in cultured zebrafish blastomeres undergoing

Figure 8: Evolutionary structural conservation between UNC-45 isoforms. Schematic diagram of UNC-45 in various species, showing the major protein domains and their levels of conservation. The amino acid sequence of each domain/region is compared to zebrafish (*Dr*, *Danio rerio*) Unc45a, accession number AAY52462 (upper numbers) or Unc45b, accession number AAL57031 (lower numbers). Comparisons show percentage identity (left) and percentage similarity (right) of each domain. Comparisons were made for *Homo sapiens* UNC45A (accession number AAH37992.1), *Homo sapiens* UNC45B (accession number AAO13384.1), *Caenorhabditis elegans* UNC-45 (accession number AAD01976) and *Saccharomyces cerevisiae* SHE4p (accession number CAA63795.1). Levels of conservation between both zebrafish isoforms and invertebrate UNC-45 were nearly identical, but the percentage of conservation from zebrafish to humans was slightly higher for Unc45b (69/84) than for Unc45a (61/80). Modified from (Wohlgemuth, 2007).

Figure 8:

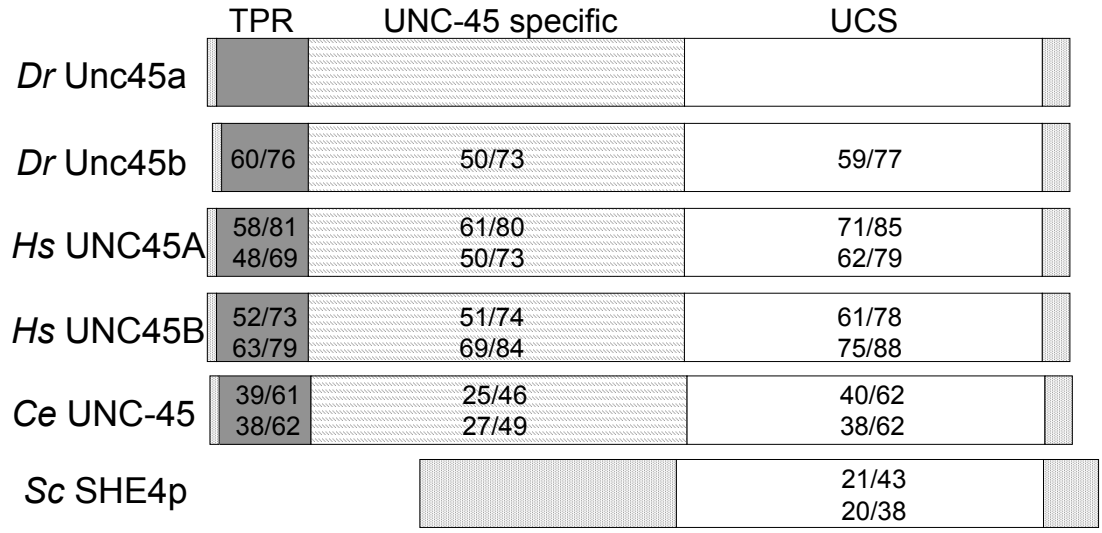
TPR
UNC-45 specific
UCS
Dr Unc45a
Dr Unc45b
60/76
50/73
59/77
Hs UNC45A
58/81
48/69
61/80
50/73
71/85
62/79
Hs UNC45B
52/73
63/79
51/74
69/84
61/78
75/88
Ce UNC-45
39/61
38/62
25/46
27/49
40/62
38/62
Sc SHE4p
21/43
20/38

myogenic differentiation is concurrent with that of the early myoblast marker, MyoD, well before the expression of muscle MHC (Myhre and Pilgrim, 2010). Additionally, the sub-cellular localization and dynamics of Unc45b have been examined in zebrafish embryos expressing fusion proteins (Etard et al., 2008; Etard et al., 2010). Rather than localizing to the myosin thick filament as would be expected for a muscle myosin chaperone, the Unc45b/Hsp90a complex was found to localize to the Z-disks and myosepta (where the myocyte termini of adjacent somites meet) of developing myocytes, which are regions of cell-ECM attachment. It was proposed that the Z-disk may act as a reservoir for stress-response chaperones, as the Unc45b:GFP fusion protein localizes to the A-band following heat-shock; however, this does not explain the localization at the myoseptum, which contains a relatively different protein complement. Alternatively, the Z-disk localization of Unc45b/Hsp90a may represent association with dynamic cell-surface costamere junctions, where they may act to stabilize ILK or other costamere components (Aoyagi et al., 2005). Hsp90 interacts with and stabilizes ILK, a major component of signalling pathways at the costamere (Aoyagi et al., 2005), and Unc45b may also interact with some element of the costamere attachment complex. Supporting this possibility, lateral attachment between myofibers in Unc45b mutants is reduced, with large gaps appearing between mature myocytes in 3 to 5-day-old larvae, although this phenotype has not been reported in Hsp90a mutants (Etard et al., 2007; Etard et al., 2010). This is consistent with a role for Unc45b in the formation or maintenance of costamere anchoring complexes, separate from the role of Hsp90 in stabilizing integrins and ILK.

A recently-identified Unc45b binding partner, Apobec2, appears to co-localize to costamere attachment regions, and interacts with Unc45b but not with Hsp90a in pull-down assays (Etard et al., 2010). Apobec2 is expressed in differentiating myocytes, and knockout mice are characterized by low muscle mass and non-lethal myopathy (Sato et al., 2010), while depletion of Apobec2 in zebrafish results in a dystrophic myopathy with deficiencies in lateral myocyte attachment and disorganization of the myosepta (Etard et al., 2010). These embryos display gaps between myocytes similar to the phenotype observed in Unc45b mutants (Etard et al., 2007; Etard et al., 2010). Mutation of zebrafish *hsp90a1* (*sloth*) disrupts the late stages of thick filament integration, but not pre-myofibril formation or the organization of the Z-disk, while the Z-disk in *unc45b* mutants is highly disorganized,

suggesting that earlier Unc45b activity is required for Z-disk organization in a non-Hsp90-dependant manner (Etard et al., 2007; Hawkins et al., 2008). None of these studies examined Unc45b localization during early myofibrillogenesis, although the initial formation of costameres and the maintenance of the mature attachment complex may both involve similar chaperone activity. Apobec2 is expressed in differentiating myoblasts prior to fusion (Sato et al., 2010), and it is possible that Apobec2 and Unc45b co-localize to developing attachment sites at the Z-disk and myoseptum. Furthermore, mutations in the *Xenopus* Unc45b homologue *dicky ticker* result in delayed formation of Z-bodies and reduced polymerization of α-actinin in developing somites (Geach and Zimmerman, 2010), indicating deficiencies in early cytoskeletal organization at costameres. Given the established theory that α-actinin nucleation occurs at proto-costamere sites where vinculin networks are pre-established [reviewed by (Sparrow and Schock, 2009)], concurrent with pre-myofibril organization from cytoskeletal actin and NMM stress-fibers (Sanger et al., 2010), the *Xenopus* phenotype also supports an early pre-myofibril role for Unc45b.

1.4.6 Possible Roles of Unc45b During Early Myofibrillogenesis:

As UNC-45 plays a role in mediating *C. elegans* non-muscle myosin function during oocyte cytokinesis and later gonad maturation (Kachur et al., 2008), Unc45b may play a similar role in mediating NMM function in vertebrates during the organization of pre-myofibrils and costamere attachment to the ECM [reviewed by (Myhre and Pilgrim, 2012)]. This would explain the deficiencies of myocyte attachment in zebrafish mutants and the early onset of Unc45b expression, and provide a mechanism by which NMM function during myoblast fusion and pre-myofibril organization is coupled to the same chaperone complexes that later mediate the folding and assembly of thick filament myosin. In particular, the lack of contractile function in NMY-2 stress fibers formed in *C. elegans* UNC-45 mutant embryos, which otherwise appear normal (Kachur et al., 2008), indicates that UNC-45 mediates function rather than folding of non-muscle myosins. This is also consistent with the proposed functions of UCS protein homologues in fungal systems (Shi and Blobel, 2010). Given the myofibrillogenesis defects following inhibition or depletion of NMM-IIA and -IIB in cultured myoblasts (Duan and Gallagher, 2009; Swailes et al., 2006) and *Drosophila* larvae (Rui et al., 2010), it is possible that Unc45b may chaperone NMM function during the

pre-myofibrillogenesis of striated muscle, and that only the later stages of MHC thick filament assembly are mediated by Hsp90 family members. It is also possible that Unc45b localization to the Z-disk and myosepta represents a chaperone function completely independent of myosins, either through the stabilization of ILK with Hsp90a or through some other activity mediated by the interaction with Apobec2. The continued localization of Unc45b to these sites in mature muscle cells could also represent the maintenance of costamere tension through NMM chaperoning, as hypothesized in *Drosophila* (Rui et al., 2010).

This is the background to the flowchart shown in Figure 7B, and the hypothesis that UNC-45 may be involved at a number of different points during early myofibrillogenesis, prior to muscle MHC folding and thick filament assembly. These include interactions with NMM-IIA or -IIB to regulate their function during myoblast aggregation, fusion and pre-myofibril formation; the stabilization of integrin attachment points at proto-costameres, possibly in a complex with Apobec2; regulation of signalling at costameres by Hsp90-mediated folding of ILK; or the maintenance of costamere-substrate tension via functional regulation of NMM-IIB. It is unclear whether the mechanisms of Unc45b activity involve direct chaperone folding, stabilization of substrates by targeted degradation of misfolded protein, or regulation of NMM motor function; indeed, all three mechanisms may play a part.

1.5 Identification of Novel Motility Mutants in Zebrafish:

The multitude of possible mechanisms by which Unc45b could act in stabilizing costamere attachments or forming pre-myofibrils suggests that other unknown factors may be involved, particularly in view of how poorly these processes are understood. Since yeast two-hybrid screens have not yet revealed any novel Unc45b binding partners, the identification of additional genes involved with early costamere and pre-myofibril formation might be accomplished by screening for mutants with similar phenotypes to *unc45b/steif*. Genetic analysis of sarcomeric genes has often been carried out in zebrafish, which are quick to develop and highly fecund, allowing for large quantities of embryos to be acquired from each generation. Further, embryos are transparent, allowing for visualization of interior structures when characterizing mutant phenotypes, including birefringence of trunk

musculature and looping of the heart, both of which are indicative of myogenic gene dysfunction. Mutations or targeted knock-downs of known sarcomere assembly genes generally result in embryos with a highly-characteristic phenotype, including reduced motility or paralysis, reduced muscle birefringence and reduced or eliminated heartbeat with pericardial edema, all of which occur in *unc45b/steif* mutants (Etard et al., 2007; Wohlgemuth et al., 2007). These phenotypes are readily identifiable, and can easily be used for phenotypic screening of myofibrillogenesis mutants. Further, loss of genes involved with myofibrillogenesis results in identifiable cellular defects, such as misalignment or complete disruption of Z-disks, shortening of A-bands or I-bands, or lateral separation of myofibers. Examples of sarcomeric mutants with these phenotypes include *titin* (Xu et al., 2002), *desmin*, *vinculin* (Vogel et al., 2009), and of course *hsp90a* and *unc45b*, as mentioned above (Etard et al., 2007).

1.5.1 Selecting Motility Mutants – The Tübingen Genetic Screen:

Forward genetics has been very useful for identifying potential myofibril assembly genes in wide-ranging mutagenesis assays and subsequent phenotypic screens. For example, genetic screens in *C. elegans*, identifying genes falling into the 'Pat' class of embryonic arrest mutants, have provided a wealth of insight into dense body (the *C. elegans* Z-disk) assembly (Moerman and Williams, 2006). A large-scale collaboration between zebrafish laboratories in Tübingen, Germany and Boston, Massachusetts in the early 1990s led to the establishment of methods for a high through-put screen of mutagenized zebrafish lines to identify useful developmental gene loci (Mullins et al., 1994), using *N*-ethyl-*N*-nitrosourea (ENU) to induce point mutations in haploid gametes from wild-type (WT) zebrafish. From a population of about 4000 mutagenized genomes, 894 mutants were identified with visually-identifiable phenotypes and confirmed by complementation crosses (Haffter et al., 1996). The mutants were sorted into a number of phenotypic groups (early embryo defects, axis, mesodermal, CNS, organogenesis, pigment cells, jaws and gills, motility, adult defects, and retinotectal), from which specific phenotypes were screened further. Screens included assessments of cardiac defects (Chen et al., 1996), locomotion and muscle development (Granato et al., 1996; van Eeden et al., 1996), any of which could represent mutations relevant to striated muscle development. A total of ~136 unique mutants were identified,

comprising over 68 affected genes, with phenotypes ranging from complete disruption of somite or heart formation to unusual touch response behaviours. Many of the phenotypes examined were characterized by loss or reduction of muscle striation, pericardial edema, reduced or eliminated heartbeat, heart looping defects or immotility; all of which are shared with sarcomere assembly mutants such as *unc45b* and *hsp90a* (Etard et al., 2007). It therefore seemed reasonable that mutants identified in this screen may reveal other uncharacterized myofibril assembly genes. Several mutants from this study have been subsequently identified as such, including the *sloth* mutant, which maps to the *hsp90a1* gene locus (Hawkins et al., 2008), *softy*, which maps to the laminin B2 gene (Jacoby et al., 2009), and *sapje*, which is dystrophin (Bassett et al., 2003).

1.5.2 Selecting Motility Mutants – *still heart* and *herzschlag*:

Most of the mutants identified by this screen had developmental defects that were restricted to either heart or skeletal muscle, rather than general striated muscle defects as would be expected of genes involved in early sarcomere/costamere organization, and many of the original mutant strains from these screens have been lost. However, of those mutant strains still available, we were able to identify two previously unmapped candidate mutants with defects in both heart and skeletal musculature, and which therefore may represent previously uncharacterized genes involved in sarcomere/costamere assembly; *still heart* (*sth*) and *herzschlag* (*hel*) (Granato et al., 1996). Both mutants were reported to display reduced or eliminated heartbeat and loss of motility. Neither mutant was originally reported to show reduced muscle striation or birefringence; however, we have since shown that reduced birefringence occurs in both mutant strains, and that muscle striation defects occur in at least one strain, *hel* (Figure 9). This is likely due to the fact that muscle striation was examined only by light microscopy of muscle sections stained with toluidine blue, and embryos were screened in bulk, making it likely that such details were overlooked. Regardless, both *sth* and *hel* mutants display phenotypes similar to the sarcomere/costamere assembly chaperone *unc45b*, including reduced or eliminated heartbeat, heart looping defects, pericardial edema, small eyes and head, reduced muscle birefringence, disorganized sarcomeres, and reduced motility or complete paralysis (Figure 9). Each mutant also deviates from the *unc45b* phenotype in a complementary fashion; *sth* mutants retain limited motility, while *hel*

Figure 9: Phenotypic comparison of motility mutants *steif*, *herzschlag* and *still heart*. Whole zebrafish embryos are shown at 3 days post-fertilization, oriented with dorsal sides to the top and anterior to the right (left-hand panels). Mutants are identified by phenotype. Wild-type embryos display very clear birefringence of the trunk/tail musculature (bottom), while all three motility mutants display reduced birefringence. Mutants are also characterized by small eyes and heads and edema of the pericardium and yolk sac. Immunocytochemical staining for slow-muscle myosin (right-hand panels) demonstrates the regularly-spaced myofibrils with clear thick filament striations in wild-type embryos (bottom), which is lost in all three motility mutants. The disorganization of myosin in *still heart* embryos is not as severe as in *steif* embryos, and is most severe in *herzschlag* embryos, in which myosin is localized in large clumps.

Figure 9:

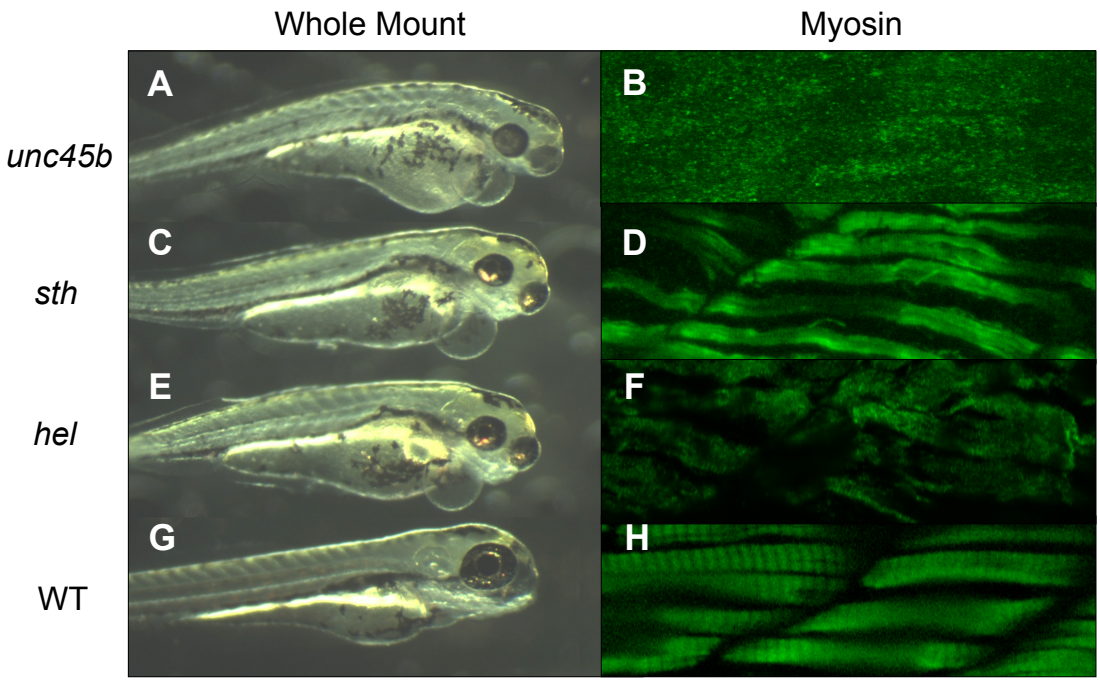

mutants retain a limited heartbeat. This may indicate tissue-specific function during myofibrillogenesis.

1.5.3 Characterization and Mapping of *sth* and *hel*:

Large-scale genetic mapping of mutants from the Tübingen screen was carried on throughout the following decade, and a number of genes have since been identified and cloned, though many remain uncharacterized, including *sth* and *hel*. Low-resolution mapping of these mutant loci has been performed, initially using the bulked-segregant method, followed by recombination analysis of individual embryos (Geisler, 2005). By this method, *sth* has been roughly mapped to a ~500 kbp period on chromosome 8, while *hel* has been roughly mapped to a ~10 Mbp period on chromosome 9 (Geisler et al., 2007). The physical map spanning the *sth* locus on chromosome 8 is highly correlated to genetic maps of SSLP markers from several mapping panels, and previous rough mapping is of sufficiently high resolution for the selection of potential candidate genes (Figure 10A). By contrast, the *hel* locus on chromosome 9 is less well-characterized, although additional bulked-segregant analysis in our laboratory suggests a few possible candidate genes that are associated with myofibrillogenesis (Figure 10B). Very little characterization of the *sth* and *hel* mutant phenotypes was carried out in the original genetic screen, assessing only motility, heartbeat and gross muscle morphology (Chen et al., 1996; Granato et al., 1996); however, previous work in our laboratory with these mutants has also demonstrated heart looping defects, reduced birefringence and disorganization of actinomyosin striations (Wohlgemuth, 2007). Both strains also have defects in lateral and terminal myofiber attachments, resulting in shortened muscle fibers or the formation of lateral gaps between myocytes (Figure 11), suggesting that one or both of these mutations may have an effect on myocyte costamere attachment. Identification of the *sth* and *hel* mutant genes may thus reveal additional players in the initial steps of costamere attachment and myofibrillogenesis.

1.6 Summary and Hypotheses:

In summary, the steps involved in the assembly of myofibrils during early myocyte differentiation remains poorly understood, particularly the specific order of events by which fully-patterned myofibrils initially form at the periphery of differentiated myotubes. The pre-

Figure 10: Physical map of zebrafish genomic DNA spanning the linkage intervals for *sth* and *hel* on chromosomes 8 and 9. A) Physical map of a ~500 kbp region of zebrafish chromosome 8, showing all identified genes in the region in grey. Data collated from the ensembl genome browser (ensembl.org) using the 9th version of the zebrafish genome assembly. The physical locations of reported microsatellite markers with published sequence data are shown above, corresponding to their location in the genomic sequence. The estimated *sth* mutant locus (*tm123a*) is marked in red, based on previously published low-resolution mapping data. B) Physical map of a ~10 Mbp region of zebrafish chromosome 9, showing all identified genes in yellow. The physical locations of reported microsatellite markers with published sequence data are shown above. The estimated *hel* mutant locus (*tg287*) is shown in red, based on low-resolution mapping data.

Figure 10:

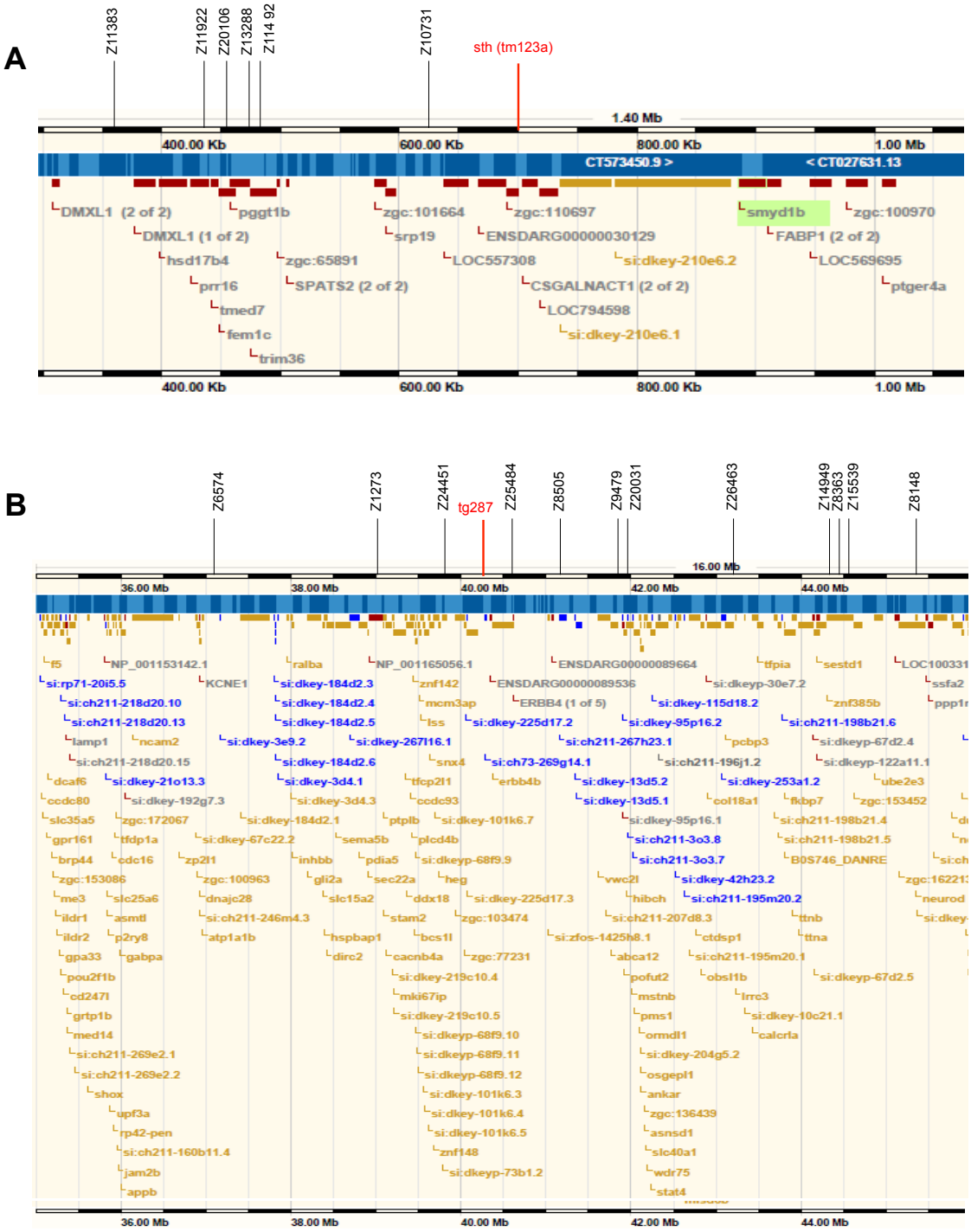
A
Z11383
Z11922
Z20106
Z13288
Z114 92
Z10731
sth (tm123a)
1.40 Mb
400.00 Kb
600.00 Kb
800.00 Kb
1.00 Mb
CT573450.9 >
< CT027631.13
DMXL1 (2 of 2)
pggt1b
zgc:101664
zgc:110697
smyd1b
zgc:100970
DMXL1 (1 of 2)
srp19
ENSDARG00000030129
FABP1 (2 of 2)
hsd17b4
zgc:65891
LOC557308
si:dkey-210e6.2
LOC569695
prr16
SPATS2 (2 of 2)
CSGALNACT1 (2 of 2)
ptger4a
tmed7
LOC794598
fem1c
si:dkey-210e6.1
trim36
400.00 Kb
600.00 Kb
800.00 Kb
1.00 Mb
B
Z6574
Z1273
Z24451
tg287
Z25484
Z8505
Z9479
Z20031
Z26463
Z14949
Z8363
Z15539
Z8148
16.00 Mb
36.00 Mb
38.00 Mb
40.00 Mb
42.00 Mb
44.00 Mb
36.00 Mb
38.00 Mb
40.00 Mb
42.00 Mb
44.00 Mb

Figure 11: Lateral detachment of myofibers in zebrafish motility mutants. A-H) DIC imaging of whole zebrafish embryos at 48 hours post-fertilization (A-D) or 5 days post fertilization (E-H) demonstrates the organization of muscle tissue at the morphological level. Wild-type embryos (A and E) have properly-organized muscle fibers with clearly visible striations at both timepoints. By contrast, all three motility mutants (*herzschlag*, B and F; *still heart*, C and G; and *steif*, D and H) display relatively normal muscle organization at 48 hpf, but without visible striations, and completely disorganized muscle tissue with numerous vacuole-like gaps between fibers by 5 dpf (white arrowheads). At higher magnification (I-K), striations in WT embryos are clearly evident (I); these striations are lost in *hel* and *sth* embryos (J and K, respectively). Modified from (Wohlgemuth, 2007).

Figure 11:

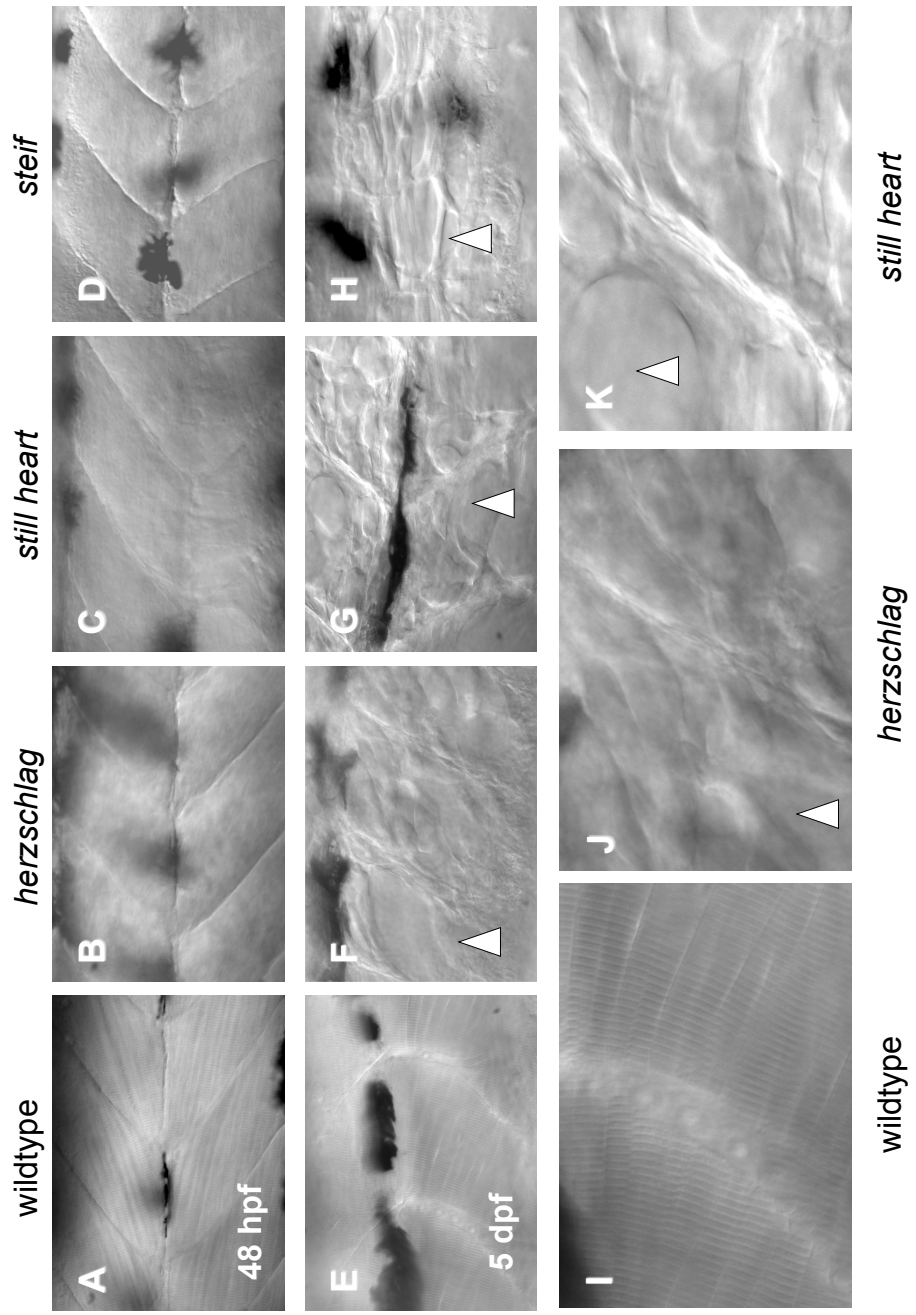
wildtype
herzschlag
still heart
steif
A
B
C
D
48 hpf
E
F
G
H
5 dpf
I
J
K
wildtype
herzschlag
still heart

myofibril model proposes that patterning arises from the arrangement of NMM within the cortical actin cytoskeleton of proliferating myoblasts. Integrin-ECM interactions and subsequent costamere formation are thought to comprise the initial steps involved in establishing the periodicity of regularly-spaced sarcomeres, and NMM is involved in stabilizing costamere attachment. By contrast, the titin molecular ruler model proposes that titin incorporation into the developing Z-disk and subsequent folding of the titin rod domain establishes the periodicity of sarcomeres, while the rod domain acts as a physical scaffold for myosin thick filament assembly. The necessity of NMM in the cortical actin wall and recent evidence supporting a role for Unc45b in mediating NMM function during myogenesis are more consistent with the pre-myofibril hypothesis than the molecular ruler hypothesis, and therefore bear further investigation. Finally, the identification and characterization of novel genes involved with costamere/sarcomere organization will be essential for further elucidation of the early events of myofibrillogenesis, and the characterization of motility mutants such as *sth* and *hel* may prove useful in this endeavour.

1.6.1 First Hypothesis – *Unc45b plays a much earlier role in myofibrillogenesis, concurrent with pre-myofibril formation*:

Due to the pre-somitigenesis expression of Unc45b in zebrafish, which I will establish further in this thesis, there may be a functional role for this protein that is separate from its direct involvement with thick filament assembly. In particular, the reduction of α-actinin nucleation in *Xenopus unc45b* mutants (Geach and Zimmerman, 2010) would seem to indicate a role in early organization of pre-myofibrils. Non-muscle myosin plays a key role in early vertebrate myoblast fusion and patterning of the pre-myofibrils, and the functional dependence of NMY-2 upon UNC-45 chaperone activity in *C. elegans* has been clearly established. This leads to a model whereby UNC-45 has an essential role in the earliest stages of myocyte patterning and myofibrillogenesis separate from its role in thick filament assembly, likely mediated by interaction with NMM. Such a model predicts an interaction between NMM and Unc45b in vertebrates; thus co-localization of NMM and Unc45b would be expected. I therefore predict that NMM and Unc45b expression will be detected in patterns that correlate both spatially and temporally with NMM expression in vertebrate embryos, at both the mRNA and protein level, and precede expression of muscle-

specific myosins during myofibrillogenesis. Also, protein-stress-responsive chaperones such as hsp90 are known to be up-regulated in dystrophic muscle, as mis-assembled sarcomeric proteins begin to aggregate and trigger protein stress pathways (De Paepe et al., 2009; Etard et al., 2007; Sela et al., 2011). This up-regulation has been shown to occur during sarcomere assembly in *unc45b* and *hsp90a* mutants (Comyn and Pilgrim, 2012; Etard et al., 2007), but early stages of myofibril initiation were not examined. I predict that the notable up-regulation of Unc45b expression seen in zebrafish mutants lacking the Unc45b/Hsp90a chaperone complex will be detectable earlier than previously documented, well before the onset of muscle myosin expression. Finally, we predict that the differentiation of single cells (embryonic blastomeres) into myocytes will be impaired specifically at the level of pre-myofibril formation, immediately after fusion/elongation of myotubes. This can be tested in cell culture, while the other predictions can be easily tested in whole zebrafish embryos, using methods that are well-established in our laboratory (*in situ* hybridization and immunocytochemistry). If these predictions can be validated, this would represent further support for the pre-myofibril model and the role of NMMs in myofibrillogenesis, as well as for the involvement of Unc45b with NMM function in vertebrates.

1.6.2 Second Hypothesis – *Unc45b and NMM pre-myofibrils are necessary for costamere assembly*:

The known role of NMM in stabilizing focal adhesions, and the necessity of NMM in the fusion of myotubes, suggests that early expression of Unc45b may relate to the formation of costamere attachment sites during myogenesis. The phenotype of *unc45b*/*steif* mutants, especially the loss of lateral attachment between myofibers in embryos and the co-localization of Unc45b and Apobec-2 to myosepta and the Z-disk of developing myocytes, would seem to support this hypothesis. Unc45b may mediate NMM folding or activity in pre-myofibrils, and/or directly stabilize costameres via some sort of chaperone complex (possibly with Apobec2). It may also mediate the folding of ILK via the Unc45b/Hsp90a chaperone complex, although not all of the molecules involved in ILK stabilization have been characterized to date. These possibilities are not mutually exclusive, as costamere assembly and stabilization has been shown to depend on myosin motor function and the maintenance of tension across the cell, and Unc45b may be involved in stabilizing both non-

muscle myosins as well as specific costamere components. I therefore predict the localization of both Unc45b and NMM to costamere structures during early pre-myofibrillogenesis, which can be tested using immunocytochemistry for costamere markers such as ILK. The zebrafish is a perfect model organism for this analysis, due to the large number of costamere complexes that form at the myosepta, where myocytes are joined end-to-end to transmit force along the entire length of the trunk musculature (Charvet et al., 2011), and which can be visualized easily by immunocytochemistry. Furthermore, our hypothesis predicts that specific defects in costamere formation will occur in *unc45b* mutant embryos, which can be assessed both at the morphological and molecular levels in zebrafish using antibodies or tissue staining.

1.6.3 Third Hypothesis – *Motility mutants still heart and herzschlag may represent novel sarcomeric gene mutations*:

The similarity of the zebrafish *hel* and *sth* mutant phenotypes to those of other sarcomere assembly mutants such as *unc45b/steif* and *hsp90a/sloth* makes it seem likely that these mutations also represent the loss of function of sarcomeric genes. Specifically, the fact that these mutations seem to affect myogenesis in both heart and skeletal muscle, with a phenotype that involves the loss of lateral myofiber attachments, makes *sth* and *hel* good candidates for novel mutations involved in early myofibrillogenesis. Additional high-resolution mapping of the *sth* and *hel* mutant loci can be accomplished using standard microsatellite mapping methods to narrow down the location of mutant loci. This will allow for the selection of likely candidate genes falling within the linkage intervals of *sth* on chromosome 8 and *hel* on chromosome 9. If mutant strains exist for these candidate genes, they can be obtained and used for complementation crosses with *sth* and *hel* to confirm the gene identity. If no mutant strain exists or if mutants cannot be obtained, the candidate genes can be knocked down by antisense oligonucleotide injection to see if the knockdown can phenocopy the *sth* or *hel* mutations. Should these methods fail to reveal the identity of *sth* and *hel*, high-resolution mapping should identify a small enough linkage area to enable DNA sequencing of the mutants and identification of single nucleotide polymorphisms. Microinjection of mRNA can subsequently be used to confirm the identity of the causative lesion.

Even before the *sth* and *hel* genes have been mapped and identified, it would be useful to characterize the myogenesis phenotypes of these mutants. The full details of the specific movement phenotypes of *sth* and *hel* have not been reported, nor has any assessment been made of the morphology of the small-head/small-eye phenotypes, although this has been done for *unc45b* and *hsp90a* mutants, using alcian blue tissue staining and immunocytochemistry to examine cranial skeleton and musculature, respectively. The effects of these mutations on myofibrillogenesis can also be assessed by immunocytochemical staining of specific markers for the Z-disk (α-actinin), M-line (myomesin), costamere (ILK) and ECM components (laminin).

1.6.4 Summary of Experimental Approach:

The above hypotheses will be tested in cell culture and in whole zebrafish embryos using methods outlined in section 2. This will first require the establishment of several technologies, including methods for zebrafish single-embryo cell culture, the generation of an *unc45b::GFP* transgenic zebrafish strain, and the creation of an Unc45b antibody for immunocytochemistry. Thus, to summarize the goals of this thesis: I will show that Unc45b plays a role in early myofibrillogenesis that is independent of its activity as a thick filament myosin chaperone, and is consistent with the pre-myofibril model, by detection of spatial and temporal patterns of Unc45b, NMM and muscle myosin expression in early embryos, and in differentiating myoblasts in culture. No study to date has examined the full timelines of expression of these genes during myogenesis. I will also show that stress-mediated up-regulation of Unc45b precedes the onset of muscle myosin expression. At the same time, I will analyze costamere formation at the myoseptum in both WT and *unc45b* mutant zebrafish embryos, to determine the localization of costamere markers in the absence of Unc45b. I will also complete the mapping and identification of the *sth* and *hel* mutations, and subsequently examine the expression of sarcomere components in these mutants, both in whole embryos and in culture.

The identification of a new role for Unc45b during myogenesis, related to a chaperone function involved in pre-myofibril assembly and/or the stabilization of costamere attachment sites, represents a novel finding that has significant implications for the study of early myofibrillogenesis. Demonstrating the involvement of Unc45b with NMM during this

process will help to elucidate the details of myofibril formation and to resolve the competing models of myofibrillogenesis. This work will also further demonstrate the importance of molecular chaperones during the earliest stages of myocyte differentiation, suggesting a synthesis of the NMM pre-myofibril model with hypotheses about early costamere assembly and the roles of tension and cell attachment during myogenesis. A more comprehensive model of the molecular events of myofibrillogenesis may result, which would be useful in the future for researchers interested in the causes of congenital muscular dystrophies, or in regenerative medicine and the re-growth of muscle tissues.

2. MATERIALS AND METHODS:

2.1 Zebrafish Strains and Husbandry:

2.1.1 Zebrafish Maintenance:

All zebrafish strains were housed at the Biological Sciences aquatic facility in a closed cycled-water system. Adult fish were maintained at 28.5°C with a controlled light cycle of 14 hours light/10 hours dark, and fed twice daily with hatched brine shrimp. Sexually mature adults were naturally mated in pairs using plastic breeding tanks, according to standard procedures (Westerfield, 2000). Offspring were raised in zebrafish embryo medium (ZEM; 15mM NaCl, 50µM KCl, 1.3mM CaCl2, 150µM KH2PO4, 50µM Na2HPO4, 1mM MgSO4 and 0.71mM NaHCO3, modified from (Westerfield, 2000)) for up to 6 days at 28.5°C prior to fixation. Embryos for *in situ* hybridization were raised in embryo medium supplemented with 0.003% phenylthiourea (Sigma) to prevent development of pigmentation from 24 hpf onwards. Embryos were staged by well-established developmental milestones (Kimmel et al., 1995). All procedures were carried out in compliance with the guidelines stipulated by the Canadian Council for Animal Care and the University of Alberta.

2.1.2 Zebrafish Mutant and Wild-Type Strains:

The *unc45b* mutant strain *steif* (*unc45b*^{sb60}) was the generous gift of Dr. Uwe Strähle (Karlsruhe, Germany). This strain possesses a single C-A transversion mutation that creates a premature stop codon at amino acid 788, and was derived from an ethylnitrosourea (ENU) chemical mutagenesis screen for motility mutants in the inbred Tübingen (TB) wild-type genetic background (Behra et al., 2002; Etard et al., 2007). The *herzschlag* (*hel*^{tg287}) and *stillheart* (*sth*^{tm123a}) mutant strains of zebrafish were developed in the TB background by the Nüsslein-Volhard lab in a large-scale ENU chemical mutagenesis screen (Chen et al., 1996; Granato et al., 1996). These strains were obtained from the Max-Planck-Institut für Entwicklungsbiologie (Tübingen, Germany). *Steif, hel,* and *sth* strains were crossed previously in our lab with the inbred wild-type strain AB, developed by George Streisinger (Streisinger et al., 1981). The wild-type strain WIK (Wild Indian Karyotype), developed by Pascal Haffter (Rauch et al., 1997), is highly polymorphic to AB and TB strains, and is thus

useful for microsatellite mapping. AB and WIK fish were both obtained from the Zebrafish International Resource Center (Eugene, OR). WIK fish were crossed with *hel* and *sth* heterozygous fish to generate heterozygous mutant $hel^{+/-}$ and $sth^{+/-}$ strains in an ABTB/WIK background for genetic mapping (Johnson and Zon, 1999). The pickwick mutant strain (pik^{m171}), possessing a single T-G transversion in the cardiac-specific N2B exon (zebrafish e45), was developed in the AB background by ENU mutagenesis in the Fishman lab at the Massachusetts General Hospital (Xu et al., 2002). This strain was a generous gift of Dr. Xiaolei Xu (Rochester, MN). Mutant offspring from heterozygous incrosses were identified phenotypically from 28 hours post-fertilization (hpf) or later by heart deficiencies and/or paralysis. All mutant phenotypes appeared in 1/4 of offspring from crosses of heterozygote parents, consistent with complete penetrance of a single recessive locus. Younger embryos were staged by touch-response, no earlier than the 20-somite stage, or identified by PCR genotyping as described below.

2.1.3 Zebrafish Transgenics:

Stable transgenic *fli1a*:GFP (full name *Tg(fli1a:EGFP)y1,* zfin ID = ZDB-GENO-011017-4) fish were obtained from the Zebrafish Stock Center (Eugene, OR). A stable transgenic *unc45b*:EGFP strain (full name *Tg(unc45b:EGFP)ua1,* zfin ID = ZDB-GENO-110314-2) was generated in our lab by Eva Gusnowski by microinjection of a Tol2-GW-EGFP vector containing the *unc45b* promoter, into wild-type AB embryos. This promoter insert consisted of the region spanning -14 to -1142 (1128bp) upstream of the *unc45b* start site. The fragment was generated from whole zebrafish genomic DNA with the primers Unc45b UTR FOR and REV (Table 1), and purified PCR product was ligated into Tol2-GW-EFGP vectors (lacking the Cfos promoter). Insertion of the fragment was confirmed by PCR sequencing. Purified plasmid DNA was then diluted to 25 ng/µl in 10 µl total volume of sterile water, along with 25 ng/µl of transposase mRNA, and 1 nl of this solution was injected into the cytoplasm of one-cell-stage zebrafish embryos. Embryos were then incubated at 28.5°C in ZEM and fluorescence was monitored to confirm the tissue-specificity of the transgene. Plasmids containing no insert were used for control injections. Surviving injected embryos were grown to adulthood and screened for germ-line insertion. Screened founders were then inbred for two generations to produce a stable transgenic strain.

Table 1: Table of PCR Primers Used

Target	Forward Primer	Reverse Primer
Unc45b UTR FOR	CGCGGATCCGCGGCTTCGTCGTAAGAGAAAATCTGTT	CCGCTCGAGCGGACCCAAAACTGAAAATTACTTGATT
unc45b geno (with SNP)	GTTCATACCTCCTTGCAGCAAACTAGA**A**T[1]	GCTTACCCCAAAATCTTTAAACAAATA
RT unc45b	TGACGATGGGAGAAATTGG	TCTCGGGTTTTCCAGTGTC
RT fli-1	GGGCACAAACGATCAGTAAGAAT	GGCCCAGGATCTGATACGG
RT gapdh	GTGTAGGCGTGGACTGTGGT	TGGGAGTCAACCAGGACAAATA
RT myoD	TGCTTCAACACCAACGAC	CTTATGGCTTAGCGACATCAC
RT HUC	GAAACTCAGGTGTCCAATGGTC	GCGTCCAAATATAGTACCAGG
hsp90a.1 in situ probe	TCTTTTGCGCTACTACACTTCAGCTTC	TAATACGACTCACTATAGG[2]GATAAAATGCAAGAGCAGACACACAAGG
myh9 in situ probe	ACGAGTGGAAGAGGGAGGG	TAATACGACTCACTATAGG[2]GGCCCGCCTCGAACCCCAGAC

1 Mis-matched nucleotide creating the EcoR1 restriction site is underlined

2 The T7 RNA polymerase promoter sequence is highlighted

2.2 Zebrafish Embryonic Blastomere (ZEB) Cell Culture:

Zebrafish embryos at ~3 hpf were washed twice in sterile Hank's saline (Sigma) and sterilized in 0.1% bleach solution for 2 minutes, followed by two more washes in sterile Hank's saline. Embryos were subsequently dechorionated enzymatically in 1 mg/ml pronase and dispensed individually into microfuge tubes before being dissociated in 25% trypsin/EDTA (Sigma) with triturgation, or physically by crushing gently with a plastic tissue homogenizer in Ca_2/Mg_2-free Ringer's saline (8 mg/ml NaCl, 300 µg/ml KCl, 93 µg/ml NaH_2PO_4-$5H_2O$, 25 µg/ml KH_2PO_4, 1 mg/ml $NaHCO_3$). The cells were then pelleted by centrifugation at 2500 rpm and resuspended in 20µl of minimal culture medium (50% Debulcco's modified Eagle's medium (DMEM) and 50% Leibowitz's L-15 medium, with 2 mM L-glutamine, 0.8 mM CaCl, and antibiotics as described below) containing 10% fetal bovine serum (FBS, Sigma) to halt trypsin digestion. Each single-embryo suspension was then seeded as a 20 µl spot onto laminin-coated 8-well glass chamber slides (NUNC). Cells were permitted to attach for 2 hours at 28.5°C in a 5% CO_2 incubator, then fed with 200 µl of the appropriate culture medium (Table 2). Attachment proceeded for 24 hours, after which the media was changed to remove floating unattached/dead cells for genotyping. Removed cells were pelleted by centrifugation at maximum speed in a desk-top centrifuge and set aside for PCR genotyping as described below. For larger-scale RNA collection from wild-type cells, 10-20 embryos per well were dissociated simultaneously and plated in 50 µl aliquots.

2.2.1 Cell Culture Additives:

Several different media were used in order to establish optimal culture conditions (Table 2). Basal culture medium was made up of 25/25/50% DMEM/L-15/Hank's saline, with 10% final volume FBS, 2 mM L-glutamine, and 0.8 mM CaCl. All culture media were supplemented with antibiotics (100 U/ml penicillin, 100 µg/ml streptomycin, 100 µg/ml kanamycin, 50 µg/ml gentamycin and 25 µg/ml amphotericin B). Enriched medium contained 10% whole embryo extract by volume. Embryo extract was made from ~200 zebrafish embryos at 3 dpf per 1 ml of extract solution in basal medium. Embryos for extract were rinsed in sterile Hank's saline and sterilized in 0.5% bleach for 2 minutes, then washed twice again in sterile Hank's saline. The embryos were subsequently dissociated in a

Table 2: Cell Culture Media Tested

Culture Media:	**Ingredients/Additives:**				
A) Basal Medium	25% DMEM, 25% L-15, 50% Hank's	Serum (10% FBS), $CaCl_2$, L-Glutamine	--	--	--
B) Enriched Medium	25% DMEM, 25% L-15, 50% Hank's	Serum (10% FBS), $CaCl_2$, L-Glutamine	10% zebrafish embryo extract	--	--
C) Highly Enriched Medium	25% DMEM, 25% L-15, 50% Hank's	Serum (10% FBS), $CaCl_2$, L-Glutamine	10% zebrafish embryo extract	Hepes / saline buffer (pH 7.4)	Insulin
D) Fish-Specific Enriched Medium	25% DMEM, 25% L-15, 50% Hank's	Serum (10% FBS, 5% Carp Serum), $CaCl_2$, L-Glutamine	10% zebrafish embryo extract	Hepes / saline buffer (pH 7.4)	Insulin

minimal amount of liquid using a dounce tissue homogenizer, then centrifuged to remove tissue debris and sterile-filtered. Other supplements included 5% carp serum (GenWay), HEPES/saline buffer (3.5 mg/ml HEPES, 344 µg/ml KH_2PO_4, 285 µg/ml K_2HPO_4, 375 µg/ml NaOH, 170 µg/ml $NaHCO_3$, and 12.5 mM sodium pyruvate, final medium pH of 7.4), and purified human or bovine insulin (Akron), to a final concentration of 5 µg/ml.

2.2.2 Primary Culture of Zebrafish Embryonic Tail Muscle:

Three-day-old zebrafish embryos were washed twice in sterile Hank's saline and sterilized by incubation for 2 minutes in 0.5% bleach, followed by two more washes in sterile Hank's saline. The embryos were dechorionated manually in sterile embryo medium containing 0.1 mg/ml tricaine, and pinned down with ultra-fine needles for dissection under a stereomicroscope. The ectoderm/skin was removed using fine forceps and the developing striated tail muscle was removed in short strips. Aggregated muscle tissue from 20 embryos was dissociated in 25% Trypsin/EDTA (Sigma) with triturgation, and plated on laminin-coated 8-well glass chamber slides (NUNC). Cultures were fed with Fish-Specific Enriched Medium (Table 2) and cultured for 2-3 days at 28°C in a 5% CO_2 incubator, prior to fixation, antibody staining and imaging.

2.2.3 Cell Culture RT-PCR:

RNA samples were collected in 100 µl of Trizol reagent (Invitrogen) at timed intervals from the point of re-feeding (after 24 hours of cell attachment), which was designated time = 0. Cells were lysed by triturgation and stored in Trizol at -20°C. RNA was extracted in 2/5ths volume of chloroform and precipitated by the addition of 1/2 volume of isopropanol. The RNA was centrifuged for 10 min at 12000 x g at 4°C, washed in 70% ethanol, and air dried before resuspension in nuclease-free DEPC water. One-step RT-PCR was then performed, using a Superscript III RT-PCR kit (Invitrogen) according to the manufacturer's directions, using primers for various developmental markers (Table 1), and the following PCR conditions: cDNA synthesis at 50°C for 30 min; amplification at 94°C, 2 min; (94°C, 15 sec; 55°C, 30 sec; 68°C, 1 min) for 40 cycles; final extension of 68°C for 5 min. Negative controls used non-RT-mix lacking reverse transcriptase, while positive

controls used whole-embryo cDNA from multiple stages between 12 hours and 4 dpf as PCR template.

2.3 Zebrafish Genetics:

2.3.1 Complementation Crossing:

Heterozygous *pickwick* +/- and *herzschlag* +/- adult zebrafish were mated in four separate crosses, two with *pik* +/- males and *hel* +/- females and two with *hel* +/- males and *pik* +/- females. All offspring were collected and unfertilized eggs were removed; surviving offspring were assessed over 3 days for phenotypic variation. Embryos were divided into apparent WT or mutant offspring displaying a *pik* phenotype. Both pools of offspring were counted and expressed as a percentage of total fertilized embryos from all four crosses. These numbers were then compared with predicted Mendelian ratios.

2.3.2 Derived Cleaved Amplified Polymorphic Sequence (dCAPS) Genotyping:

For cell culture genotyping, cell pellets from removed culture medium were dissolved in 20 µl of DNA lysis buffer (50 mM KCl, 10 mM Tris, 5 mM EDTA, 0.01% gelatin, 0.5% IGEPAL, 0.1% Tween) at room temperature. For whole zebrafish embryos, individual embryos were dissociated in 50 µl of DNA lysis buffer plus 1 mg/ml proteinase K and incubated for 3 hours at 65°C, followed by enzyme inactivation at 85°C for 10 minutes. Genotyping primers were designed using dCAPS Finder 2.0 software (Neff et al., 2002), incorporating a single nucleotide mismatch to create an EcoR1 restriction site at the *unc45b* mutant locus (Table 1). PCR was performed using the following conditions: 94°C, 3 min (94°C, 30 sec; 51.5°C, 40 sec; 72°C, 1 min) for 40 cycles, with final extension at 72°C for 5 min. SNP identification of mutant PCR products was achieved by restriction digestion at 37°C with EcoRI and subsequent resolution by 2% agarose gel electrophoresis, revealing homozygous mutants, WT, or heterozygous embryos by differential band migration. Amplification and digestion of DNA from phenotypically-identified 3-day-old mutant and wild-type embryos were used as controls.

2.3.3 Zebrafish Microinjection:

Antisense, morpholino-modified oligonucleotides (morpholinos, MO) or DNA expression constructs were injected into the yolk of 2-cell to 8-cell stage embryos. Each embryo was injected with 5-10 ng of DNA of MO dissolved in Danieau buffer (58 mM NaCl, 0.7 mM KCl, 0.4 mM $MgSO_4$, 0.6 mM $Ca(NO_3)_2$, 5 mM HEPES, pH 7.6) in a total injected volume of ~5-10 nl. Embryos were subsequently raised at 28.5°C in standard embryo medium as above, with 2 changes of fresh medium per day, for up to a maximum of 3 days post-fertilization (dpf). For cell culture, embryos were only raised until the ~1000 cell (high) stage and then bleached and dissociated for culture by the seZEB method as described above. Morpholinos were directed against the translation start site of *p53*, sequence GCG CCA TTG CTT TGC AAG AAT TG (Robu et al., 2007); the translation start site of *unc45b*, sequence ATC TCC AAT TCT CCC ATC GTC ATT (Wohlgemuth et al., 2007); or the exon e47 splice site of *ttnb*, sequence ACC AAA GTC ACA ATC AAA GGT AAT T (Seeley et al., 2007). A GFP expression construct consisted of the Tol2-GW-EGFP plasmid vector containing the *unc45b* promoter, spanning -14 to -1142 (1128bp) upstream of the *unc45b* start site, as described above. Empty Tol2 vector alone was used for control injections.

2.4 *In Situ* Hybridization:

2.4.1 Ribo-probe Generation:

DNA pGEX plasmid vectors containing the entire open reading frame of *unc45b* downstream of a T7 RNA polymerase promoter sequence were generated previously in our lab by Serene Wohlgemuth (Wohlgemuth, 2007). Additional plasmid vectors for probe generation were the generous gifts of Dr. Sarah Childs (*NMM2B*, University of Calgary), Dr. Lisa Maves (*Smyhc1* and *Myhc4*, University of Washington), Dr. Simon Hughs (*Myf5*, Kings College London), and Dr. Eric Weinberg (*MyoD*, University of Pennsylvania). Digoxigenin (DIG)-labeled antisense RNA probes were made from linearized plasmid DNA templates (Table 3), or from PCR amplification of cDNA generating a 956 bp fragment in the case of *hsp90a.1*, or a 319 bp fragment in the case of *myh9* (Table 1). Probes were generated by *in vitro* transcription using ~2 µg of template DNA, a DIG RNA labelling mix (Roche), 1 µl of T3, T7 or SP6 RNA polymerase and the appropriate buffer solutions (Ambion) and 1 µl of

RNase inhibitor in RNase-free water. The transcription reactions were incubated for 2 hours at 37^{o}C, with another 1 μl of RNA polymerase added at the 1 hour point. Template DNA was subsequently removed by digestion with 1 μl of RNase-free DNase for 5 minutes at 37^{o}C, and all reactions were stopped by the addition of 2 μl 0.25 M EDTA (pH 8). Probes were purified either by collection in a quick spin column (Sigma) or by precipitation in 70% ethanol with 0.4 M LiCl overnight at -20^{o}C, followed by centrifugation at 13,000 rpm for 30 minutes at 4^{o}C. Centrifuged pellets were subsequently washed in 70% ethanol and centrifuged again for 15 minutes at 4^{o}C, then resuspended in 50 μl of RNase-free water. All probes were stored at -80^{o}C.

2.4.2 Hybridization Protocol:

Embryos were staged morphologically, dechorionated enzymatically and fixed in 4% paraformaldehyde (PFA) for 1 hour at room temperature or overnight at 4°C. Embryos were subsequently stored at 4°C in PFA (short term) or at -20°C in 100% MeOH (long term). MeOH-stored embryos were rehydrated in a graded methanol series (75%, 50% and 25% MeOH in PBST), and all embryos were washed several times (5 minutes each) in PBST prior to hybridization. Embryos were then permeablized in 10 μg/ml proteinase K for 30 seconds (tailbud to 2-somite stage), 1 minute (5-10 somites), 2 minutes (15-20 somites), 2.5 minutes (24 hpf) or 3 minutes (36 hpf), post-fixed in 4% PFA for 20 minutes at room temperature, and washed another 3x in PBST. *In situ* hybridization was then performed as previously described (Gongal and Waskiewicz, 2008); pre-hybridization was performed by incubation for 2-4 hours at 65°C in hyb buffer (50% formamide, 50 μg/ml heparin, 92mM citric acid, 5X SSC, 0.1% Tween20 and 500 μg/ml tRNA in DEPC water, pH 6.0), and hybridization was performed by overnight incubation at 65°C with the appropriate riboprobe in fresh hyb buffer (probe concentration of between 1:200 and 1:500). Embryos were subsequently washed for 5 minutes at 65°C in each of the following solutions: 66% hyb buffer/33% 2X SSC, 33% hyb buffer/66% 2X SSC, and 2X SSC. Stringency washes were then performed for precisely 20 minutes at 65°C, once in 0.2X SSC + 0.1% Tween20, then twice more in 0.1X SSC + 0.1% Tween20. The embryos were then washed for 5 minutes at room temperature in each of the following solutions: 66% 0.2X SSC/33% PBST, 33% 0.2X

SSC/66% PBST, and PBST. This was followed by incubation for 1 hour at room temperature in blocking solution (2% sheep serum and 2mg/ml bovine serum albumin (BSA) in PBST), and overnight incubation at 4°C in blocking solution containing 1:5000 alkaline-phosphatase (AP)-conjugated anti-DIG FAB fragments (Roche). Antibody washes were performed the next day 4x 10 minutes at room temperature in PBST, followed by four 5-minute washes in coloration buffer (100 mM Tris-HCl, pH9.5, 50mM $MgCl_2$, 100mM NaCl and 0.1% Tween20). Riboprobe localization was then visualized using 0.45% nitro-blue tetrazolium (NBT) and 0.35% 5-bromo-4-chloro-3-indolyl phosphate (BCIP) in fresh coloration buffer. Color development took between 0.5 and 4 hours at room temperature before the reaction was stopped by 4x washes in stop buffer (PBST, pH 5.5). The embryos were imaged immediately or stored in the dark to prevent further color development, up to 5 days. Whole-mount embryos were imaged in 3% methylcellulose, while slide-mounted embryos were de-yolked in PBST using insect pins before being transferred to microscope slides and mounted in 100% glycerol. Whole-mount embryos were imaged using a high-powered Olympus stereomicroscope and photographed with a Q-imaging Micropublisher camera.

2.5 Zebrafish Antibody Staining:

2.5.1 Antibody Generation:

Polyclonal antibodies against unc45b were created using full-length recombinant protein as an antigen. An *E. coli* strain containing the full-length unc45b coding sequence plus a GST tag in the pGEX expression vector was previously generated in our lab (Wohlgemuth, 2007). GST-tagged unc45b recombinant protein was generated by adding a 10ml overnight bacterial culture (in LB broth with ampicillin) to 1 litre of 2x YT medium plus ampicillin and incubating for 3 hours in a 37°C shaking incubator. Protein expression was induced by the addition of 1mM isopropylthio-β-galactoside (IPTG) and the culture was allowed to incubate for another 4 hours at 37°C. The culture was subsequently spun down at 6000g in a 4°C ultracentrifuge, in 250 ml spin bottles. Each pellet was resuspended in 10 ml of ice-cold sonication buffer (50mM Tris - pH 7.5, 100M NaCl, 1mM EDTA, 1% NP-40, 2mM DTT) + protease inhibitors (Roche) and sonicated 3x for 60 seconds. Cellular debris was removed by centrifugation at 16,000g for 30 minutes in a 4°C ultracentrifuge. The

supernatant was then incubated overnight at 4°C with Glutathione Sepharose resin beads (Fisher) that were washed with cold sonication buffer prior to incubation. Beads were then pelleted by centrifugation at 300g for 5 minutes at 4°C, then washed as per manufacturer's instructions in buffers A and B, but not elution buffer. GST-bound beads were separated from recombinant unc45b by digestion with 50U thrombin protease in PBS per 1 ml of saturated resin, overnight at room temperature. Beads with GST tags were then pelleted by centrifugation at 300g for 5 minutes at 4°C and the supernatant removed. The supernatant was centrifuged again at 1300g for 5 minutes at 4°C to remove any remaining beads, then filter-sterilized and supplemented with protease inhibitors. The resulting solution was mixed 1:1 with Freund's complete adjuvant and injected subcutaneously into guinea pigs. Booster injections with additional protein solution mixed 1:1 with Freund's incomplete adjuvant were performed at two-week intervals for a total of 8 weeks prior to sacrifice. Collected blood was heat-inactivated at 37°C for 30 minutes, and clotted overnight at 4°C. Clots were removed and the serum was centrifuged at 10,000g for 10 minutes at 4°C to remove any remaining debris.

2.5.2 Antibody Purification:

Serum was subjected to antibody strip purification and pre-absorption. Full-length unc45b protein was separated from bacteria by SDS-PAGE on 10% polyacrylamide gels and blotted to nitrocellulose. Band detection was accomplished by incubation for 5 minutes in Ponceau stain (0.1% Ponceau-S and 1% acetic acid), followed by destaining in distilled water. The identified bands were marked and the blots were fully destained in distilled water. Blots were then cut into strips to remove all protein other than the identified unc45b band. Serum samples were then incubated overnight at 4°C with the nitrocellulose strips. The strips were then washed twice with PBS and bound antibodies were eluted with 0.1M glycine (pH 2.5). The eluate was subsequently neutralized in 1M Tris-Hcl (pH 8.5) and the resulting antibody solution was tested by western blot for detection of the unc45b band. The antibody solution was then pre-absorbed to increase specificity. Pre-absorption was performed overnight at 4°C by the addition of sonicated debris from *E. coli* containing an empty vector. Pre-absorption debris was then removed by centrifugation at 16,000g for 30

minutes at 4°C, and the final antibody solution was sterile-filtered, supplemented with protease inhibitors, tested by western blot and stored at -80°C.

2.5.3 Western Blot Analysis:

Embryos for Western blot analysis were dissociated mechanically with a plastic tissue homogenizer in protein lysis buffer (50mM Tris - pH 7.4, 150mM NaCl, 1% NP-40, 0.1% SDS), supplemented with protease inhibitors (Roche). Bacterial samples for Western blot were dissociated by triturgation in lysis buffer. All samples were mixed with equal volumes of 2x protein loading buffer (0.12M Tris-HCl - pH 6.8, 4% SDS, 20% glycerol, 0.2% bromophenol blue and 0.2M DTT or β-mercaptoethanol), and subjected to SDS-polyacrylamide gel electrophoresis as follows. Proteins were resolved on 10% polyacrylamide separation gels (10% polyacrylamide/Bis, 0.375M Tris - pH 8.8, 0.1% SDS, 0.05% ammonium persulfate, and 2µl/ml TEMED) with 4% stacking gels (4% polyacrylamide/Bis, 0.125M Tris - pH 6.8, 0.1% SDS, 0.05% ammonium persulfate, and 3µl/ml TEMED), alongside a Precision Plus protein standard ladder (Bio-Rad). SDS-PAGE was performed in running buffer (0.025M Tris, 0.2M glycine, 0.1% SDS), after which gels were placed in ice-cold transfer buffer (0.025M Tris, 0.15M glycine, 20% methanol) to equilibrate for 15 minutes at 4°C. Proteins were then blotted onto pre-soaked nitrocellulose membranes (Bio-Rad) by wet transfer for 1 hour at 100 volts. The blots were subsequently blocked overnight at 4°C with 10% skim milk powder in PBST. Protein detection was accomplished by incubation for 1-3 hours at room temperature with 1:1000 unc45b primary antibody in 1% milk/PBST. Membranes were washed 3x for 5 minutes with PBST, then incubated for 1 hour at room temperature with 1:2500 HRP-conjugated anti-guinea pig secondary antibody in 1% milk/PBST, and washed again 4x 5 minutes with PBST. Bands were visualized by chemiluminescence using Western Blot Chemiluminescence Substrate (Thermo Fisher) as per manufacturer's instructions, followed by exposure to X-ray film.

2.5.4 Whole Embryo Cryosectioning:

Embryos for cryosectioning were fixed at 20-somite, 24 hpf or 48 hpf stages overnight in 4% PFA at 4°C. The embryos were then washed 3x in PBS and incubated in 25% sucrose in PBS for 2 hours at room temperature, then in 35% sucrose in PBS for

another 2 hours or until the embryos had sunk to the bottom of the solution. The embryos were then aligned in plastic cryomolds in tissue freezing medium (Triangle Biomedical Sciences) and frozen in dry ice. Frozen tissue was sectioned to 10 µm thickness onto glass microscope slides as previously described (Barthel and Raymond, 1990), and thawed sections were allowed to adhere to the slides for 2 hours prior to rehydration for 5 minutes in PBST containing 1% DMSO (PBTD). The sections were then placed in a humid box and blocked with 2% BSA in PBST for 30 minutes prior to antibody staining as detailed below, with all washes in PBTD. For staining sections, a minimal volume of antibody solutions or wash buffer was used at each step. Co-staining with Unc45b and NMM antibodies was detected using a mixture of 1:1000 Alexa488 anti-guinea pig and 1:1000 Alexa568 anti-rabbit secondary antibodies. Stained sections were mounted in 100% glycerol prior to confocal imaging.

2.5.5 Immunocytochemistry:

Embryos for whole-mount antibody staining were fixed for 1 hour at room temperature in 4% PFA, washed 3x in PBST, and stored at at 4°C in PBST for a minimum of 3 days to allow embryos to permeabilize, and a maximum of 2 weeks. Embryos were not blocked prior to antibody staining. Cell cultures on glass chamber slides were fixed at 4°C in 1:1 methanol:acetone for 10 minutes, allowed to air-dry, and stored at -20°C. Dehydrated cultures were then rehydrated in PBS blocking solution with 5% bovine serum albumin (BSA) for a minimum of 2 hours prior to staining. For GFP transgenic embryo cultures, cultures were fixed at room temperature in 2% PFA for 15 minutes to prevent loss of GFP signal, washed twice in PBST, and stored at 4°C prior to blocking and staining. Whole embryos, cryosections or cell cultures were then incubated with primary antibody solutions for 1 hour at room temperature or overnight at 4°C. Antibody solutions consisted of 2% BSA in PBST plus primary antibodies against unc45b (as described above), NMMIIA (M8064, Sigma), α-actinin (A7811, Sigma), laminin (L9393, Sigma), titin T11 peptide (T9030, Sigma), titin T12 peptide (generated by Elizabeth Ehler, London, UK), talin (Tln1, GeneTex), integrin linked kinase (ILK, GeneTex), smyhc1 (F59, DSHB), myhc4 (F310, DSHB), myomesin (mMac, DSHB), dystrophin (MANDRA1/7A10, DSHB), dystroglycan (MANDAG2/7D11, DSHB) or mature muscle fibers (MF-20, DSHB). Hybridoma

supernatants (titin T12 and all DSHB antibodies) were used at concentrations of 1:5 to 1:10, while all other (concentrated) antibodies were used at concentrations of 1:50 to 1:100. After staining, primary antibody solutions were removed and the samples were washed 3-4 times in PBST. Secondary antibody solutions consisted of 1:1000 Alexa 488 (green) or 568 (red) fluorescent anti-mouse, anti-rabbit or anti-guinea pig (Invitrogen) in 2% BSA, with or without a counter-stain of 1:50 Alexa 546 or 568 phalloidin (Invitrogen). Incubation in secondary antibody solution was performed for 1 hour at room temperature, after which samples were incubated for 10 minutes with 1 µg/ml DAPI (Sigma) in PBS, then washed 2-3x for 5 minutes in PBST. Whole embryos were mounted under raised coverslips in PBS or 3% methylcellulose prior to imaging. Confocal and fluorescence images were photographed using a Nikon Eclipse 80i confocal microscope, and images were subsequently processed using NIS Elements version C4 software.

2.6 Zebrafish Morphological Analysis and Histology:

2.6.1 Alcian Blue Histochemical Staining:

Dechorionated embryos were fixed at 5 dpf in 4% PFA for 2 hours and then dehydrated in 50% ethanol in PBS for 10 minutes. Dehydrated embryos were then stained overnight in 0.02% Alcian Blue dye in a solution of 70% ethanol, containing 60 mM $MgCl_2$. Excess dye was washed out rinsing 2x in distilled water, and the embryos were bleached for 20 minutes in a solution of 3% H_2O_2 and 2% KOH. The tissue was then permeabilized for 20 minutes in 1 mg/ml trypsin in saturated sodium tetraborate. Embryos were subsequently cleared in a solution of 0.25% KOH and 20% glycerol for 1 hour, followed by 2 hours in 0.25% KOH and 50% glycerol solution, and finally stored in 100% glycerol. Whole-mount embryos were viewed using an Olympus stereomicroscope and photographed with a Q-imaging Micropublisher camera.

2.6.2 Movement and Morphological Analysis:

Live embryo imaging was performed following anaesthetization of hatched embryos in 0.016% tricaine in ZEM. Whole-mount mutant and WT embryos for morphological analysis were mounted and oriented in 3% methylcellulose, viewed under an Olympus stereomicroscope, and photographed or videoed with a Q-imaging Micropublisher digital

camera. Movies of movement phenotypes were prepared using Q-Capture Plus imaging software and edited using Adobe AfterEffects version CS3. Embryos for touch-response analysis were dechorionated in 1 mg/ml pronase and washed 2x in ZEM prior to imaging.

3. RESULTS:

3.1 The Early Role of Unc45b During Myogenic Differentiation in Cell Culture:

(A version of this section has been published as Myhre and Pilgrim, 2010. *Cellular differentiation in primary cell cultures from single zebrafish embryos as a model for the study of myogenesis*. Zebrafish 7(3): 255-266.)

Our hypothesis regarding an early role for Unc45b during myofibrillogenesis suggests that Unc45b is necessary for the earliest stages of myogenic differentiation, possibly involving myoblast alignment, attachment, and fusion, and subsequent formation of pre-myofibrils from actin stress-fibers. In the zebrafish embryo, several of these processes take place almost simultaneously, as segmental plate mesoderm responds to rapidly-changing developmental signals directing migration, elongation, attachment, and myogenic gene expression. Myogenic differentiation also continues to occur throughout embryogenesis, as new somites are added to the elongating tail and differentiate to form striated muscle. To examine some of the early events of myofibrillogenesis independently, we determined that it would be useful to focus on individual differentiating cells in culture, outside the context of somitic mesoderm.

3.1.1 Development of Methods for Single-Embryo Zebrafish Blastomere Cultures:

Cell culture techniques have been previously described in zebrafish, but often rely on the use of immortalized cell lines, including Z4F, PAC2 and SJD cells, which are robust and can be passaged multiple times to increase uniformity and to amplify cell numbers (Chen et al., 2002; Driever and Rangini, 1993; He et al., 2006). However, these advantages must be weighed against the drawback that immortalized cell lines are heavily selected and likely altered from their native form and function, and are therefore of limited use in studying the progression of gene expression during normal *in vivo* development (Obinata, 1997; Pan et al., 2009). Furthermore, frequently-passaged cell lines are often misidentified, aneuploid or contaminated by mycoplasma (Capes-Davis et al., 2010), and confirmation of cell identity is generally difficult and time-consuming. In contrast, primary culture techniques use cells or tissues taken directly from explants or whole embryos, without the immortalization that occurs after multiple passages. Primary cell cultures from embryonic blastomeres have been

used to examine mechanisms of embryonic differentiation in species as diverse as sea urchins (Khaner and Wilt, 1990) and humans (Klimanskaya et al., 2006). In zebrafish, primary cell culture methods using blastula-stage embryos have been previously described (Collodi et al., 1992; Fan and Collodi, 2006; Ghosh and Collodi, 1994; Helmrich and Barnes, 1999), but rely on the dissociation of large numbers of embryos to generate monolayer cultures. One of the advantages of zebrafish as a developmental model is the wide availability of heterozygous mutant strains carrying embryonic-lethal mutations affecting developmental processes, and the ease of genetic manipulation whereby these processes may be studied (Pichler et al., 2003). At the blastula stage, it is impossible to screen offspring of a heterozygous cross in order to derive cultures of a specific genotype, and thus this advantage of zebrafish is lost when using current primary culture techniques.

We therefore set about the optimization of methods to generate primary cultures of zebrafish embryonic blastomeres (ZEB) from single embryos (seZEB), which could then be genotyped after the culture period, allowing the use of genetic and cell culture techniques together in zebrafish for the analysis of differentiation in specific mutant or transgenic cells. We then applied these methods to examine the early stages of cellular differentiation during myogenesis, and the effects of *unc45b* mutation on myofibrillogenesis in individual differentiating cells.

3.1.1.1 Optimization of Cell Culture Conditions for seZEB Cultures:

ZEB cultures have previously been used for the study of myogenesis (Norris et al., 2000; Wang et al., 2005), but it is unknown whether the culture conditions used in those experiments were optimal for myogenic differentiation, nor whether these conditions would be suitable for differentiation of cultures derived from single embryos. Factors which commonly influence myogenesis in cell culture include the attachment substrate (Darmon, 1982; Foster et al., 1987), and media additives such as trophic (growth) factors and nutritional supplements (Dayton and Hathaway, 1991; Pirskanen et al., 2000). We adapted the protocols of Collodi *et al*. (Collodi et al., 1992) and Norris *et al*. (Norris et al., 2000) for the culturing of single zebrafish embryos on 8-well glass chamber slides (Figure 12A). Initial experiments focused on the optimization of culture media and cell substrates to ensure myogenic differentiation in seZEB cultures. We noted three criteria required for optimal

Figure 12: Optimal substrates and media for seZEB cell culture. A) Schematic depiction of the single-embryo ZEB culture method, from embryo collection to seeding of culture slides. B) Substrates were tested for optimal cell attachment and subsequent differentiation of ZEB cultures, including 25 µg/ml laminin, bulk rat-tail collagen, and 0.1 mg/ml poly-L-lysine, as assessed by total cell count after 24 hours of culture (error bars indicate standard deviation, n = 24 single-embryo cultures per treatment). C) Cell culture media were tested to determine qualitative effects on proliferation and cellular differentiation. Cell proliferation was assessed by total cell count after 4 days of culture, and differentiation was assessed by the presence or absence of morphologically distinguishable myocytes. Relative density of myocytes indicated low, medium or high rate of differentiation (n = 40-64 cultures examined per treatment). D) Cell proliferation in highly-enriched media was sufficient to overcome initial cell death following bleaching of embryos, as determined by counts of adherent cells following DAPI staining (black circles). The percentage of differentiated cells was determined by actin co-staining (open circles). Error bars represent standard deviation, n = 24 cultures. E) A representative spot culture stained with DAPI to show the distribution of cell nuclei following differentiation. Arrows indicate clusters of differentiated myocytes. Scale bar = 1 mm.

Figure 12:

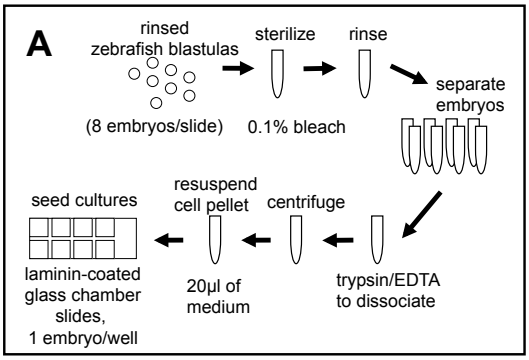

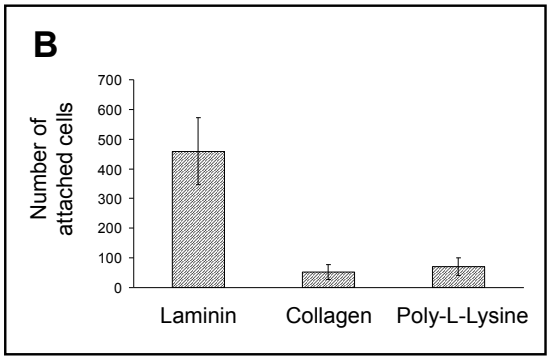

C **Cell Culture Conditions**

	Basal Medium	Enriched Medium (includes whole zebrafish extract)	Highly Enriched Medium (includes pH buffers and insulin)	Fish-Specific Enriched Medium (includes carp serum)	Fish-Specific Enriched Medium (includes carp serum) + morpholino injection
Proliferation	None	low	low	moderate	moderate
Differentiation	none	low	moderate	high	moderate

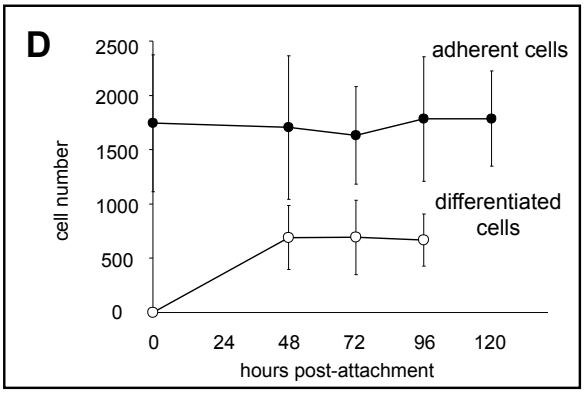

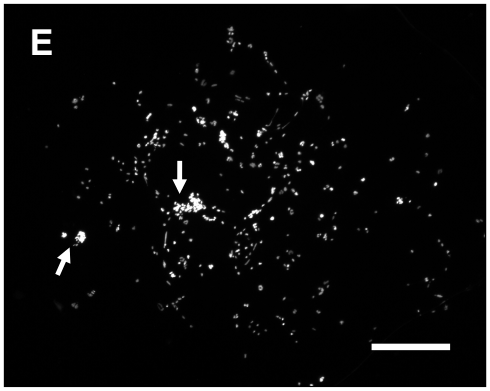

myogenic cell differentiation: Firstly, strong cell-substrate attachment is required to promote a flattened, elongated cell morphology. Mesenchymal cells that are normally capable of undergoing myogenic differentiation when cultured on a laminin substrate often fail to do so when attached to fibronectin/poly-lysine substrates (Foster et al., 1987; von der Mark and Ocalan, 1989). We therefore attempted to establish single-embryo cultures on various common cell culture substrates, including bulk rat-tail collagen, poly-L-lysine, and laminin (Fig 12B). Of these, laminin substrates were most efficient for cell attachment of early blastomeres, as measured by counting total attached cells following 4 days of culture.

Secondly, nutritional and trophic factors in mesenchymal cell cultures must favor sufficient proliferation to ensure cell-cell communication between attached cells, and finally, growth factors that favor myogenic differentiation must be present in the culture medium. In basal medium (Table 2), cells failed to proliferate and phenotypic differentiation was not observed (Fig 12C). Some proliferation was seen under nutritionally-enriched conditions (Enriched Medium and Highly Enriched Medium, Table 2 and Fig 12C), attended by an increased rate of differentiation where cell density was highest. The addition of supplemental insulin gave slightly better results (Fig 12C). Insulin-like growth factors are trophic factors known to increase both cell proliferation and differentiation in cultured myoblasts (Pirskanen et al., 2000). The further addition of carp serum gave the best results of all media tested (Fig 12C), presumably because it contains numerous fish-specific trophic factors. The rate of differentiation in cultures containing both carp serum and insulin was very high, with morphologically distinct myocytes detectable in almost every culture. Cell proliferation in highly-enriched media was sufficient to overcome initial cell death following bleaching of embryos (Fig 12D), as determined by counts of adherent cells in each culture following DAPI staining (Fig 12E). Relatively constant cell numbers were maintained up to the point of cellular differentiation, which took place in our cultures between 2 and 4 days following attachment. Differentiated cells in highly-enriched media constituted between 20-50% of the total cell count (Fig 12D), lower than but comparable to the rates of differentiation reported in mammalian C2C12 cell cultures (50-90+%) (Silberstein et al., 1986; Yaffe and Saxel, 1977).

3.1.1.2 Characterization of Myogenesis in seZEB Cell Cultures:

Initial cell attachment in single-embryo cultures resulted in the formation of isolated clusters of blastomeres of varying sizes (Fig 13A), which remained rounded and poorly-attached for several hours thereafter. Cell death was observed during the sterilization and dissociation process, but proliferation was sufficient to keep cell numbers relatively constant (Fig 13B), and floating or dead cells were removed. Surviving cells proliferated slowly under these conditions, even in the most enriched media (Fig 13C). Proliferation was restricted to regions of higher cell density, resulting in piled-up clusters of cells by 2 days of culture (Fig 13E, arrows), which had a flattened, fibroblast-like phenotype. Cells began fusing and elongating over the next 24 hours to form isolated bundles of elongated cells (Fig 13B, arrows), which displayed an apparent myogenic phenotype. Multinucleated cell bundles were similar in appearance to those formed in differentiating mammalian C2C12 cells (Abe et al., 2004; Liu et al., 2010), however fusion of myocytes was often incomplete, resulting in elongated or partially-fused nuclei rather than larger numbers of small, discrete nuclei (Fig 13G). Unlike C2C12 cells, proliferating seZEB cells were not contact-inhibited, and continued to pile up during myoblast fusion and subsequent differentiation. Comparison of the progression of myoblast fusion in seZEB cells to C2C12 cells indicated that proliferation, elongation and fusion in seZEB cultures were likely concurrent, rather than sequential.

The cultures at this point contained two morphologically distinct types of myocyte-like cells (Fig 13D-G). Elongated myotube-like cell bundles were detected towards the periphery of the cultures (Fig 13D) or in cell-dense clusters throughout the culture (Fig 13B), while cells between these bundles remained flattened, often in contact with their neighbors, but with numerous filamentous cell extensions (Fig 13E, arrows). Both the myotubes and the filamentous extensions of flattened cells contained the highly-identifiable banding patterns characteristic of sarcomere arrangement in developing skeletal muscle (arrow in 13C). Elongated cells were determined to be multinucleated (Fig 13D), while flattened myoblast-like cells towards the center of the cultures often remained single-nucleated (Fig 13F, arrowhead), despite the presence of sarcomere bands. The banded cell extensions in both types of myocytes stained positive for muscle markers such as actin (Figure 14A, C, F) and myosin heavy chain (Fig 14E, F). Actin staining in myocyte-like

Figure 13: Phenotypic characterization of seZEB cell cultures. A) Live embryonic blastomeres from a single zebrafish embryo at the time of initial plating, imaged using a stereo dissecting microscope (scale bar = 0.1 mm). B) Differential interference contrast (DIC) microscopy of a single-embryo culture at low magnification (40x). Scale bar = 1 mm. Arrows indicate piled-up regions of differentiating myocytes. C-G) DIC microscopy of differentiated myocytes in single-embryo cultures. Nuclei are indicated by DAPI staining in D and F (scale bars = 0.1 mm). Arrows highlight the periodic banding pattern characteristic to striated muscle cells in panels C and E (scale bars = 0.05 mm). Arrow in F indicates an isolated, single-nucleated myocyte. G) DAPI stained single myocyte, demonstrating multiple and elongated nuclei (scale bar = 0.05 mm).

Figure 13:

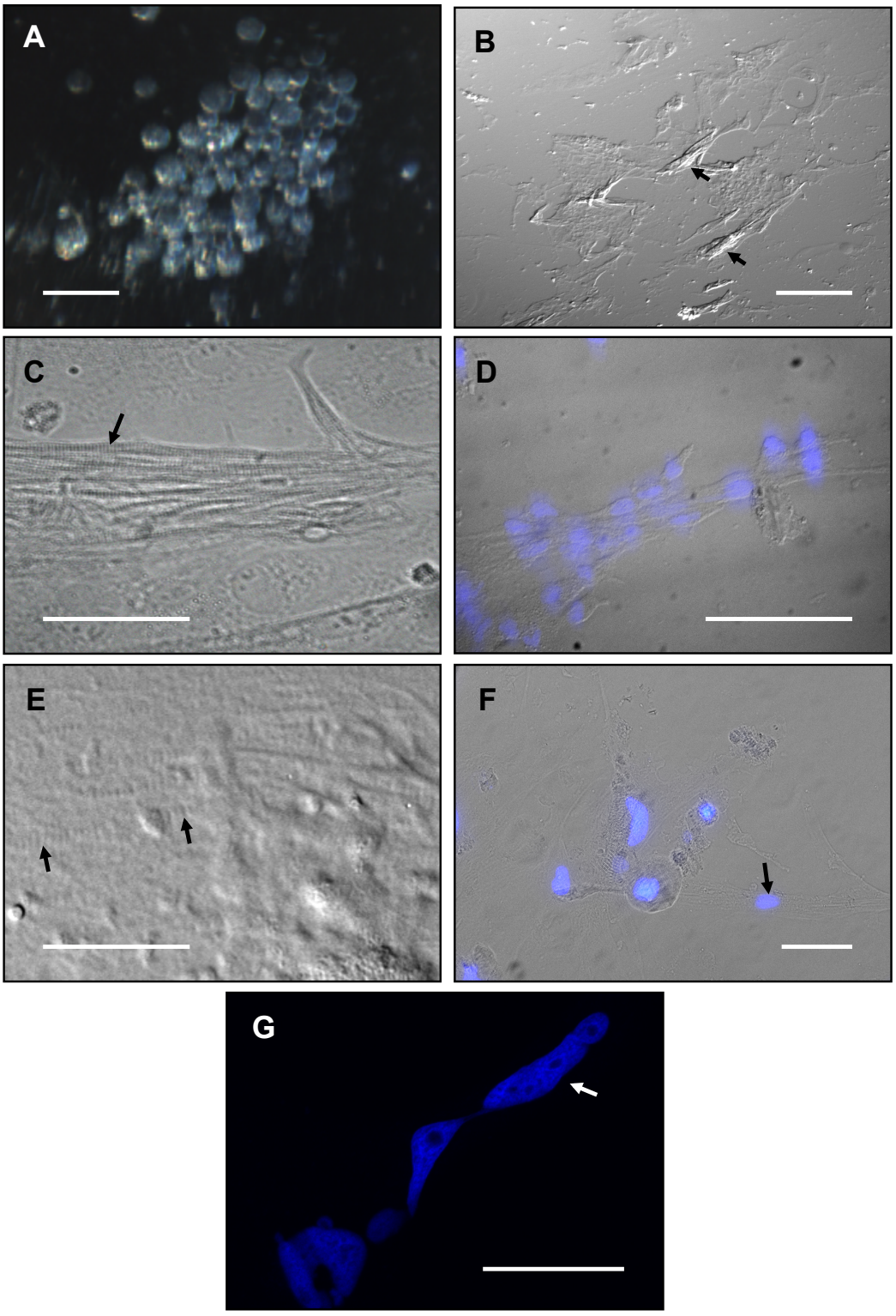

Figure 14: Molecular characterization of myogenesis in seZEB cell cultures. Single-embryo cultures were stained for several markers of myocyte differentiation. Actin expression in seZEB cultures is shown by phalloidin staining (labeled with Alexa 546) in panels A and C (orange), while nuclei are indicated by DAPI staining (blue). Single-nucleated myocytes (A, insert) and multi-nucleated myocyte bundles (C) both demonstrate distinct banded patterns of actin expression. B and D) Phase contrast images of the stained cultures from A and C, demonstrating a single cell body (A) versus a bundle of elongated cells (C). E) Muscle myosin was detected using F-59 anti-myosin heavy chain antibody (green), with DAPI counter-stain (blue). Myosin-negative cells are indicated with arrows. F) Myosin and actin co-stained cultures, showing alternating patterns of myosin and actin sarcomere bands characteristic of differentiating muscle. Higher magnification is shown in the insert. Comparison with cultures of differentiated tail myocytes from 3-day-old zebrafish embryos demonstrated a similar phenotype (G) and pattern of muscle myosin expression (H). Scale bars = 0.05 mm (A-H), 0.1 mm (G).

Figure 14:

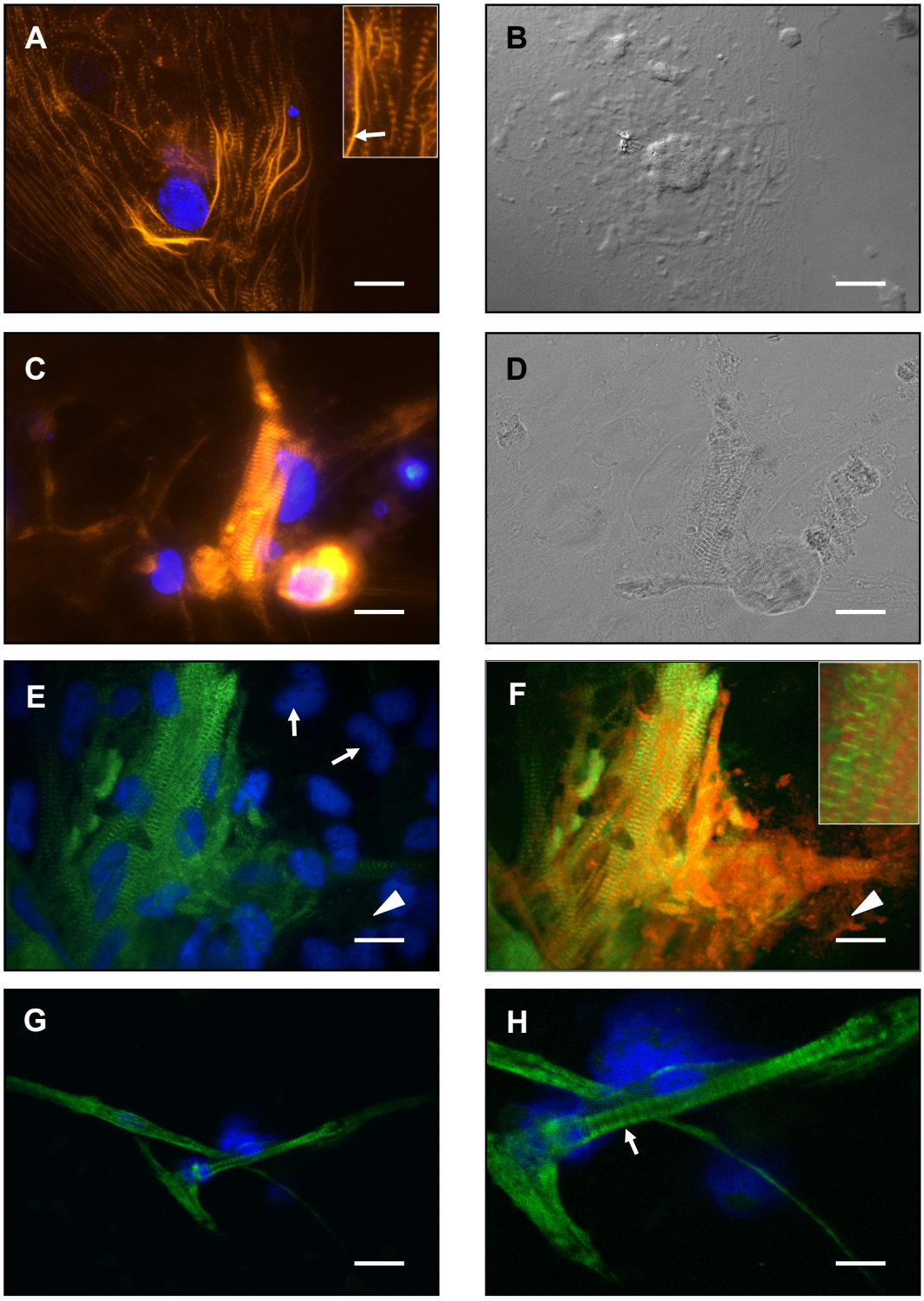

cells was present in a distinctive banded pattern that is characteristic of developing sarcomeres. This pattern was detected in both the single-nucleated, flattened myocytes (Fig 14A) and the elongated, multinucleated myocyte bundles (Fig 14C, D). Interestingly, myofibril-like organization of actin was preceded by unbroken, elongated strands of cytoskeletal actin (Fig 14A, arrow). Further, staining for muscle-specific myosin heavy chain (mMHC) revealed that expression was limited to cells with myocyte-like banding patterns (Fig 14E), while the undifferentiated cells in between did not express detectable myosin (arrows), myosin did not co-localize with elongated cytoskeletal actin filaments (arrowheads). Most importantly, co-staining for myosin and actin together (Fig 14F) revealed clearly separate, alternating red and green bands which correspond to the A band and I band respectively of functional sarcomeres (14F insert). To compare these seZEB cells morphologically with fully differentiated myocytes, we cultured developing tail muscle tissue from 3-day-old zebrafish embryos in our fish-specific enriched medium. The phenotypes of these cells (Fig 14G) appeared very similar to those of our seZEB cultures, with elongated cells containing multiple nuclei, and the banding patterns following myosin antibody staining (Fig 14H) were identical (arrow).

3.1.1.3 Expression of Sarcomere Components in seZEB Cell Cultures:

It is noteworthy that fast muscle fibers in zebrafish are multinucleated, while slow muscle fibers are single-nucleated (Devoto et al., 1996). It is therefore possible that flattened, single-nucleated cells in culture represent slow-muscle fiber differentiation, while elongated, multi-nucleated cells represent differentiating fast-muscle fibers. This does not seem to be the case, however, as immunofluorescent staining with an antibody specific to the slow-muscle MHC isoform was frequently detected in multi-nucleated cell bundles (Fig 14E), and staining with an antibody specific to fast-muscle MHC was detected in flattened cells (Fig 15A). This is not unexpected, since early embryonic muscle in zebrafish has been shown to co-express both isoforms (Bryson-Richardson et al., 2005). Although the patterns of myosin and actin expression in single-embryo cultures were characteristic of myocyte differentiation, we also examined the expression of other muscle cell markers in differentiating cell clusters, in order to provide further evidence that the seZEB culture system is optimized for myogenic differentiation (Figure 15). These included α-actinin to

Figure 15: Expression of sarcomere markers demonstrates myofibrillogenesis in early seZEB cultures. Single-embryo ZEB cultures were stained with antibodies against additional markers of myocyte differentiation (green), including fast-muscle myosin isoform (A), α-actinin (C), myomesin (E) and dystroglycan (G). Expression and localization was assessed after 2 days of culture, and DAPI nuclear counter-staining was used to demonstration the scale of differentiating cell clusters (B, D, F, H). Fast muscle myosin was expressed throughout differentiating cells, and also localized to A-bands of nascent myofibrils (arrow in A). Expression of α-actinin was also rapid, but restricted to myofibrils (C). Fully-formed Z-disks were visible at this stage (arrowhead), but newly-differentiating cells also contained small rows of punctae that indicate pre-myofibril formation (arrow). Myomesin expression was minimal in early cultures, localized to the oldest fibrils (arrow in E), while dystroglycan expression was broadly distributed throughout the differentiating cells (G). Scale bars = 0.05 mm.

Figure 15:

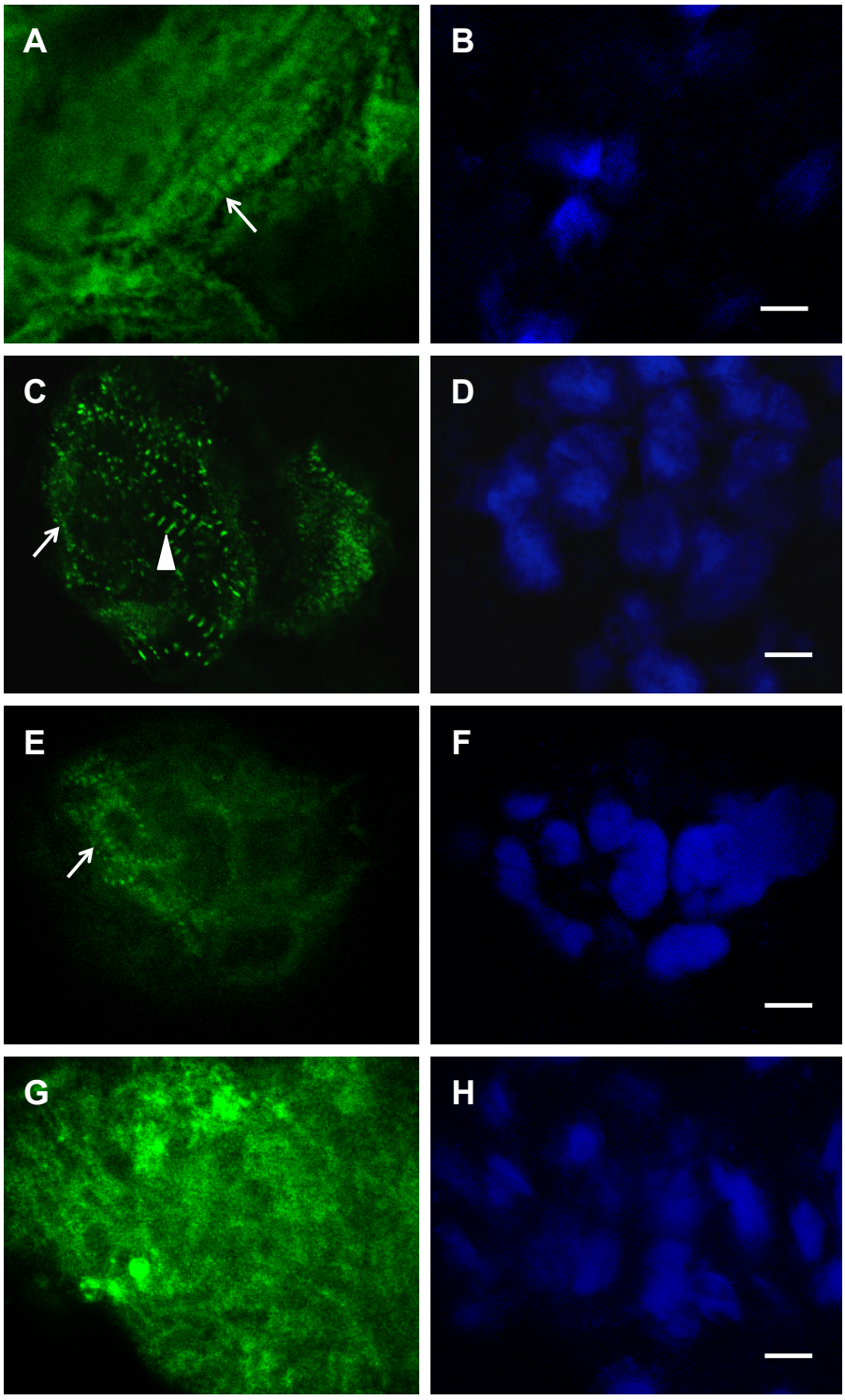

mark the developing Z-disk (Fig 15C), myomesin to mark the developing M-line (Fig 15E), and dystroglycan to mark sites of cell attachment (Fig 15G). Immunostaining of early cultures (48 hours of culture) revealed extensive networks of α-actinin expression in nascent myofibrils (Fig 15C), including both full-formed Z-disk bands (arrowhead) and punctate nucleation sites (arrow). In contrast, early cultures expressed myomesin in relatively few clusters (Fig 15E), and localization was restricted to the oldest myofibrils (arrow). This is in keeping with previous research showing that α-actinin expression far precedes that of A-band and M-line components (Sanger et al., 2005; Sparrow and Schock, 2009; Tokuyasu and Maher, 1987). Interestingly, expression of dystroglycan, a major component of the sarcoglycan complex that helps maintain contact between the sarcolemma and the extracellular matrix (Figure 4), was broadly distributed throughout cell clusters in seZEB cultures, rather than localizing to nascent costameres at the Z-disk periphery (Fig 15G). This may be due to the lack of ECM patterning on the laminin-coated glass substrate, or represent a general difference between *in vivo* and *in vitro* myogenic differentiation.

As an independent assay to confirm that ZEB cultures grown under our optimized culture conditions specifically favored myogenic differentiation, we performed RT-PCR analysis using primers for a set of developmental marker genes (Table 1) over a 48-hour time-course of cell culture. Since other cell types may differentiate in zebrafish cell cultures, especially endothelial cells, which are also known to form from cells of fibroblastic lineage (Tamaki et al., 2007), we first examined the expression of the transcription factor *fli1*. *fli1* is a marker of early differentiating endothelial cells (Brown et al., 2000), which are also known to develop from squamous fibroblast-like mesenchymal cells in culture (Wang et al., 2006). The absence of PCR product generated from these primers (Figure 16A, top row) supports the conclusion that these culture conditions were optimized for non-endothelial differentiation. By contrast, expression of the muscle-specific transcription factor *myoD* and the myosin chaperone *unc45b* were both detected at early time-points (Fig 16A, second and third rows). The neural-specific transcription factor *HUC* and the housekeeping gene *gapdh* were used as negative and positive controls respectively (Fig 16A, fourth and fifth rows). The *HUC* neuronal marker was not detected, indicating that the cells in ZEB cultures were exclusively of mesenchymal fate, since spontaneous neuronal differentiation occurs only in

Figure 16: RT-PCR shows that ZEB culture conditions favor myogenic over endothelial or neuronal differentiation. ZEB cultures derived from multiple WT embryos were established and collected at 24-hour intervals to obtain RNA for analysis by RT-PCR. A) Detection by RT-PCR of endothelial (top row), myogenic (second and third row), and neuronal (fourth row) marker transcript expression. No *fli1* (endothelial) or *HUC* (neuronal) marker transcription was detected in optimized ZEB cultures, while *myoD* and *unc45b* (muscle) transcripts were detected throughout the two days of culture, commencing as early as 24 hours after cell attachment. *gapdh* (fifth row) served as a positive control. B) Control RT-PCR used bulk RNA prepared from combined embryos ranging from 4 hours to 3 days post-fertilization.

Figure 16:

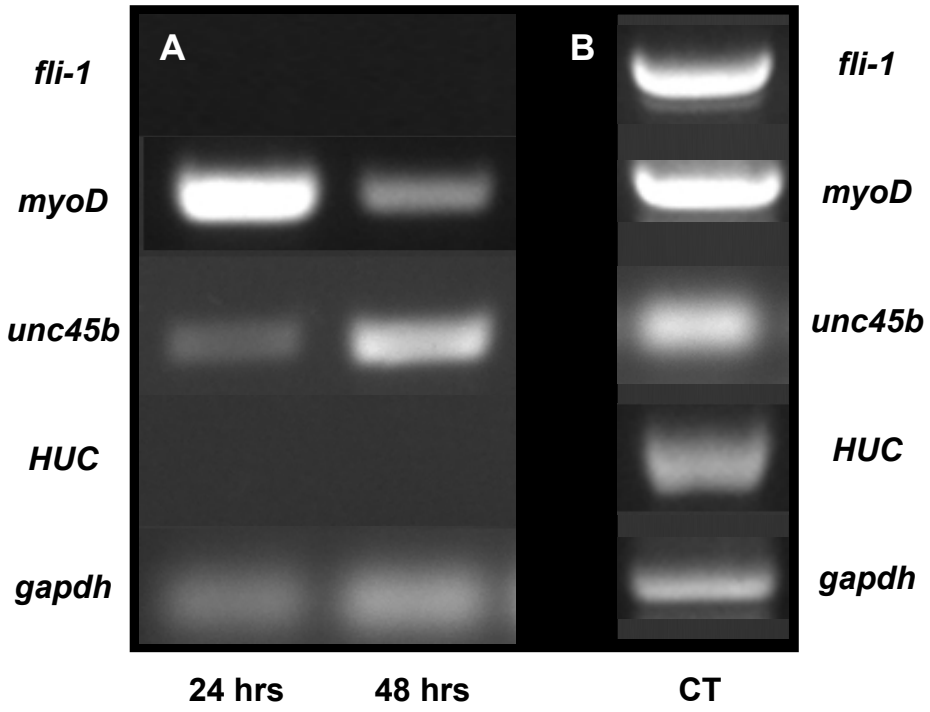
A
B
fli-1
myoD
unc45b
HUC
gapdh
fli-1
myoD
unc45b
HUC
gapdh
24 hrs
48 hrs
CT

ectodermal cells. Positive control RT-PCR using whole-embryo extract from combined embryonic stages (4 hpf to 3 days) demonstrated the expression of all markers (Fig 16B).

3.1.2 Expression of Unc45b in Early seZEB Cultures is Robust but Restricted to Myogenic Cells:

The expression of *unc45b* detected by RT-PCR in 24-hour ZEB cultures, concurrent with *myoD* expression, was somewhat surprising. MyoD is an early marker of myoblast differentiation, whose expression far precedes myofibrillogenesis (Brand-Saberi, 2005), and the formation of identifiable myofibrils with organized muscle myosins was not detected by immunostaining until around 48 hours of culture. It is possible that this general expression, which was found even at the earliest time-points, merely reflects a stress response in newly-dissociated blastomeres, since Unc45b is known to be stress-responsive (Etard et al., 2008) However, this result is consistent with the rapid detection of early pre-myofibrils showing punctate α-actinin localization in Figure 15. To further test our hypotheses, we generated seZEB cultures from transgenic zebrafish strains, including the *fli1::GFP* transgenic line *Tg(fli1a:EGFP)y1*, and the *unc45b::GFP* transgenic line *Tg(unc45b:EGFP)ua1*, the latter of which was created previously in our laboratory (Myhre and Pilgrim, 2010), and is described in more detail below (see Fig 27). The purpose of this experiment was threefold: first, to determine if transgene expression could be readily detected in seZEB cultures from transgenic embryos; second, as a further assay for any endothelial differentiation in the seZEB culture model; and finally to more closely examine *unc45b* expression in cell culture in order to determine if the early expression detected in Figure 16 was specific to myogenic cells. At 36 hours, cultures from zebrafish embryos containing the *unc45b::GFP* transgene displayed GFP expression only in phenotypically-differentiating myocyte bundles (Figures 17A and B). DAPI nuclear staining revealed numerous isolated fibroblast-like cells (arrows) that did not express GFP, both at the periphery of cultures (Fig 17A) and between the myoblast bundles towards the center of cultures (Fig 17B), demonstrating that *unc45b* promoter activity was specific to myogenic differentiation, rather than stress response, in seZEB cultures. Cells that were positive for GFP expression were also shown to display characteristic actin staining patterns (Fig 17C) typical of differentiating myocytes. To test for endothelial cell differentiation, we also examined GFP expression in cultures from

Figure 17: seZEB cultures from transgenic or injected embryos allow uncomplicated manipulation of gene expression. Single-embryo cell cultures were derived from *unc45b::GFP* or *fli1::GFP* transgenic zebrafish embryos, or WT embryos that had been microinjected with DNA expression constructs or morpholino oligonucleotides. A, B) Expression of *unc45b::GFP* (green) was limited to bundles of differentiating myocytes, while isolated cells (indicated by DAPI staining in blue) at the edges of the culture (A) or between the myocyte bundles (B) displayed no detectable GFP (arrows). C) Actin staining (red) revealed that GFP-positive cells also displayed actin banding patterns characteristic of myocytes (insert). All cultures examined in A-C contained visibly-differentiating myocytes which were positive for *unc45b::GFP* expression (n = 40 single-embryo cultures). D) Expression of *fli1::GFP* was not detected in any culture, although differentiating cells still appeared normal under phase contrast microscopy (E). Scale bars = 0.1 mm. F) WT zebrafish embryos were injected at the 2- to 4-cell stage with *unc45b::GFP* expression constructs. GFP expression was detectable in bundles of differentiating cells as early as 2 days of culture (scale bar = 0.5 mm). G) Blastomeres from embryos injected with *p53* control morpholinos were able to undergo attachment and differentiation in culture, forming visible striations (arrowhead, scale bar = 0.05 mm). H, I) Embryos injected with a morpholino against *unc45b* were co-stained with phalloidin (H, red) and F59 anti-myosin antibody (I, green). Actin and myosin expression were disorganized in nearly all cultures from *unc45b* MO-injected embryos (arrows). Scale bars in H and I = 0.1 mm.

Figure 17:

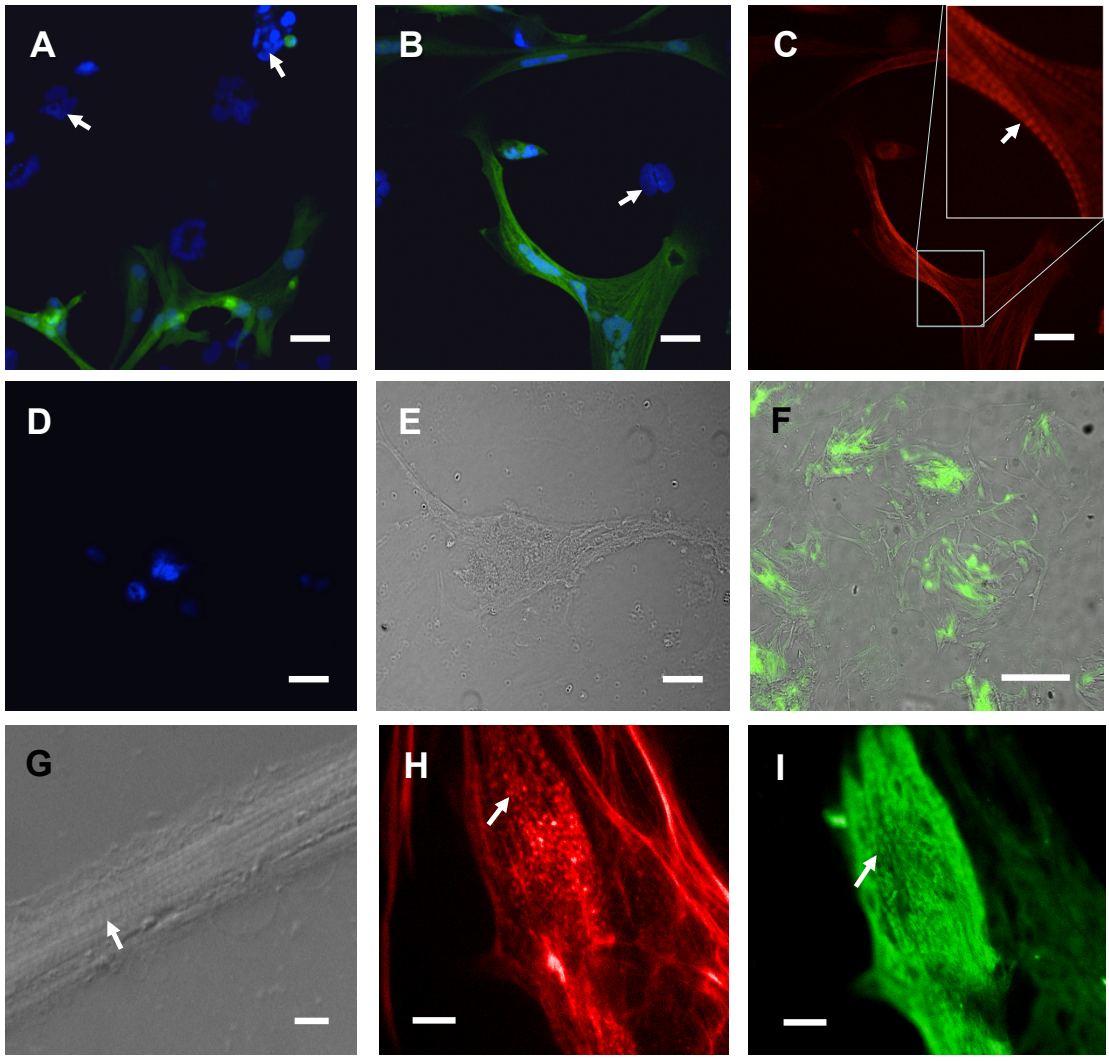

Tg(fli1a:EGFP)y1 zebrafish. In the *fli1::GFP* transgenic cultures, no GFP signal was detected in any cell (Fig 17D). This is consistent with the hypothesis that our cell culture method specifically favors myogenic differentiation over other pluripotent fibroblast fates.

3.1.3 seZEB Cultures are Useful for Studying Myogenesis Following Manipulations of Gene Expression:

The detection of transgene expression in seZEB cultures indicates the usefulness of our single-embryo culture system as a model for genetic studies in zebrafish. In addition to the wealth of transgenic zebrafish lines, another of the useful aspects of zebrafish as a developmental model is the ease with which gene expression can be manipulated in embryos by microinjection of antisense oligonucleotides (to down-regulate gene expression) or *in vitro* synthesized mRNA or DNA expression constructs (to up-regulate gene expression). If seZEB cultures could be created from microinjected embryos, it would be possible to examine the effects of changes to specific gene expression on subsequent myogenesis, including Unc45b. Therefore, we injected individual embryos at the two- to four-cell stage with antisense morpholino-modified oligonucleotides (MOs) or DNA expression constructs prior to dissociation for seZEB cell culture. Injection with a plasmid DNA containing GFP under the control of the *unc45b* upstream promoter region was used to determine whether gene expression can be up-regulated in the seZEB culture system (Fig 17F). After two days of culture, GFP expression was readily detectable in differentiating myocytes. Additionally, injection with MOs was used to determine whether gene expression can be effectively down-regulated in this culture system. Injection with a *p53* MO (routinely co-injected in zebrafish gene-knockdown experiments to reduce apoptosis) did not prevent the differentiation of myocytes (Fig 17G) identifiable by the formation of elongated cell bundles with visible striations (arrow). Furthermore, injection of single embryos with an *unc45b* MO (Fig 17H, I) resulted in a similar phenotype to developing myocytes in whole *unc45b/steif* mutant embryos, displaying disorganized localization of actin (Fig 17H) and myosin (Fig 17I), with scattered punctae (arrows) rather than the organized bands normally seen in myofibrils. Nearly all viable cultures derived from *unc45b* MO-injected embryos displayed this phenotype (n = 56). Microinjection of embryos resulted in only a slight reduction in proliferation and differentiation compared to WT embryos, and viability of cultures from

injected embryos was lower than uninjected WT embryos by only ~15% (Fig 18A, third column, n = 144).

3.1.4 Unc45b Mutation Results in Failed Myofibril Organization but Not Morphological Differentiation in seZEB Cultures:

To further demonstrate the usefulness of seZEB cultures for zebrafish developmental genetics, and to address our hypothesis regarding the early role of Unc45b in myofibrillogenesis, we assayed the progress of myogenic differentiation in cultures derived from *unc45b/steif* mutant embryos (Fig 18B). Specifically, we in-crossed heterozygous mutant *unc45b*$^{+/-}$ zebrafish and dissociated individual progeny at the blastula stage for ZEB culture. We were unable to phenotypically distinguish between WT and mutant embryos at the blastula stage; therefore, cell culture supernatant from *steif* in-crossed seZEB cultures was drawn off and replaced following 24 hours of cell attachment. Dead or unattached cells in the media supernatant were collected by centrifugation for DNA extraction and PCR amplification using dCAPS primers (Table 1). This allowed us to identify the genotypes (mutant, WT or heterozygous) of the cells in the cultures prior to examination of cellular morphology and marker expression (Fig 18C). Genotyping revealed that the expected 1:2:1 ratio of WT, heterozygous, and homozygous mutant embryos was obtained from heterozygote crosses. After 4 days of culture, the percentage of genotyped WT cultures in all experiments that were viable and contained phenotypically-identifiable myocytes with characteristic banding patterns was over 66% (Fig 18A, first column, n = 256). Of genotyped *steif* cultures, however, somewhat fewer were viable (Fig 18A, second column, n = 64) and almost none contained fully differentiated myocytes with identifiable striations. Furthermore, after blind-scoring a number of apparently-homozygous *steif* cultures (determined by lack of visible striations and punctate patterns of actin staining), identification was confirmed by dCAPS-genotyping at over 90% accuracy (Fig 18D).

Given the muscle-specific defects of *steif* mutant embryos, it was unsurprising that myofibrillogenesis was severely reduced in cells derived from cultured *steif* embryonic blastomeres (Fig 18E). Mutant cells underwent morphologically-identifiable myogenic differentiation in these cultures, with peripheral cells forming long fibril-like bundles (Fig 18E) that were often multi-nucleated and morphologically similar to myocytes. However,

Figure 18: Myocyte marker expression and genotyping of seZEB cultures from *unc45b* mutant embryos. Single-embryo cultures of ZEB cells were established from embryos obtained by crossing *steif* mutant heterozygote parents. A) The percentage of cultures with viable, differentiating cells was measured for genotyped WT, *steif* and injected embryos. B) Phenotype of 3-day-old *steif* mutant embryo as compared to wild-type (bottom), demonstrating heart edema and reduced birefringence of tail muscle. Cell cultures from mutant embryos were identified by dCAPS genotyping of culture media (C), compared to control DNA amplified from phenotypically-identified mutant embryos or wild-type adults. *steif* alleles detected in cultured embryos gave the expected 1:2:1 ratio of homozygous WT, heterozygous, and homozygous mutants (n = 88). D) In the reverse experiment, phenotypic identification of *steif* mutants and WT embryos was confirmed by dCAPS genotyping, demonstrating nearly 100% accuracy. Only a few cultures identified phenotypically as derived from WT/heterozygous or mutant embryos were found to be otherwise. D) Genotype-confirmed mutant seZEB cultures were stained for actin with phalloidin to visualize sarcomere banding patterns (red), with DAPI as a nuclear counter-stain (blue). Mutant cultures demonstrated deficiencies in sarcomere organization, and punctate expression of actin (arrows in D). E, F) Co-staining of actin (red) with the F59 anti-myosin antibody (green) demonstrated co-localization of disorganized, punctate actin and myosin expression (arrows). Scale bars in all panels = 0.1 mm.

Figure 18:

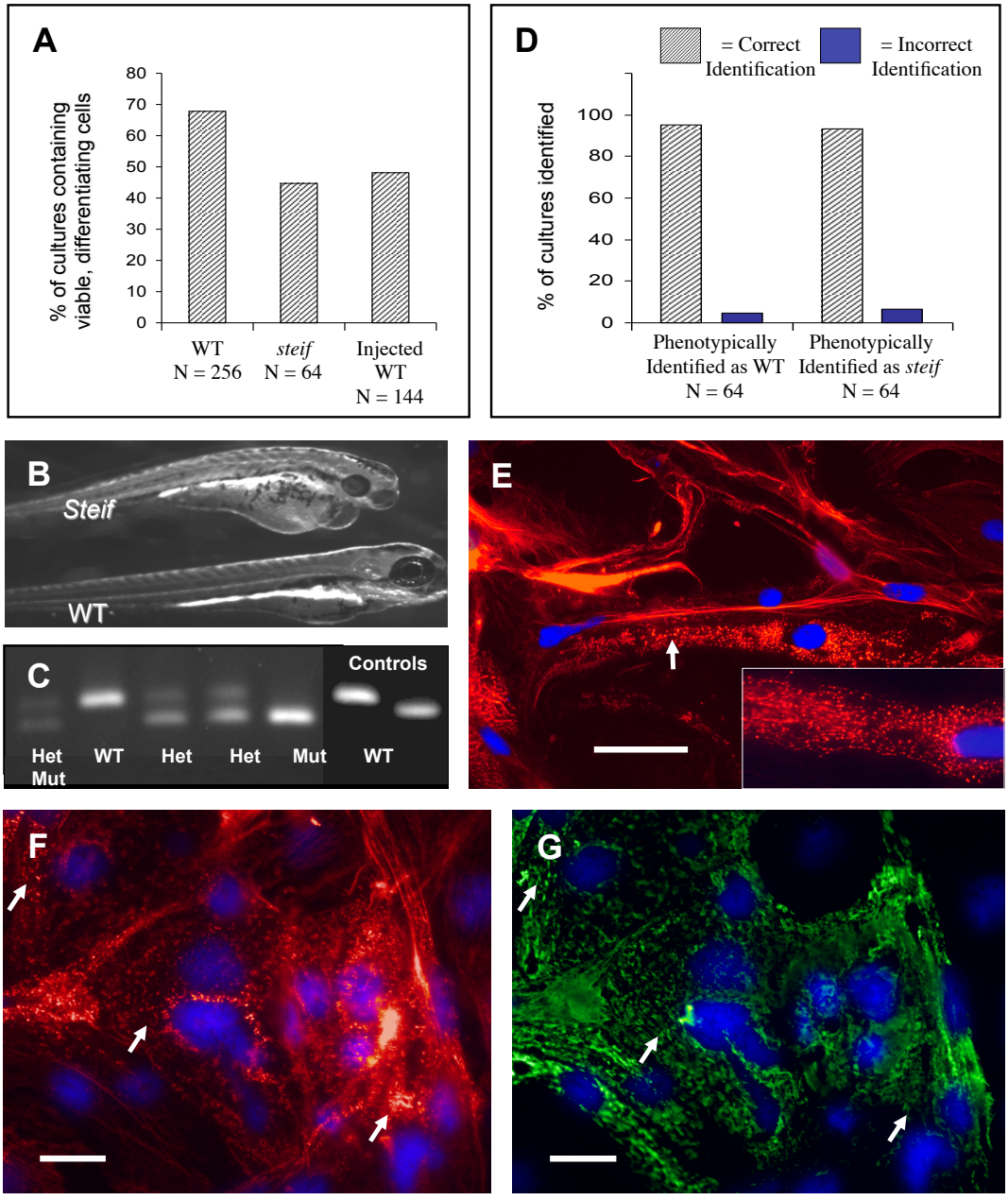
A
% of cultures containing viable, differentiating cells
80
70
60
50
40
30
20
10
0
WT N = 256
steif N = 64
Injected WT N = 144
D
= Correct Identification
= Incorrect Identification
% of cultures identified
100
80
60
40
20
0
Phenotypically Identified as WT N = 64
Phenotypically Identified as steif N = 64
B
Steif
WT
C
Controls
Het Mut
WT
Het
Het
Mut
WT
E
F
G

actin dynamics in these cells were very different, with fewer elongated actin filaments and no regular banding patterns forming; rather, actin in elongated myocytes was punctate and poorly-organized, without regularity (arrow and insert in Fig 18E, arrow in Fig 18F). This scattered punctate actin possibly corresponds to regions of failed sarcomere assembly. Further, when cells were co-stained with antibodies against mMHC, a similar punctate pattern of expression was detected (Fig 18G). The disorganized patterns of actin and myosin expression co-localized in these cultures throughout the cell body (compare arrows in 18F and G). Interestingly, the quantity of elongated actin fibrils, which are common in cultured fibroblasts (Kharitonova and Vasiliev, 2004; Toh et al., 1979), was much increased in mutant cultures (Fig 18E). In the context of the pre-myofibril model of myofibrillogenesis, these structures are pre-myofibril precursors; this suggests the possibility that the loss of Unc45b impedes the progress of actin fibril elaboration to form the pre-myofibril templates. However, given that there was little or no reduction in cell attachment in *unc45b* mutant cultures (Fig 18A), and that the cell morphology of differentiating myocytes in cultures did not seem to be affected by the mutation (Fig 18E-G), it is not possible to draw any firm conclusions from these *in vitro* experiments regarding any role of Unc45b prior to myosin deposition. For this elucidation, we turn to *in vivo* experiments.

3.2 The Early Role of Unc45b in Zebrafish Myofibrillogenesis:

The expression of Unc45b at early stages of myogenesis and the loss of all myofibril assembly in *unc45b/steif* mutant cells in culture both support an early role for Unc45b that may be consistent with the pre-myofibril model of myofibrillogenesis. However, within the timeline of myogenic differentiation in cell culture, outside the context of normal somite formation, it is difficult to separate the myosin-chaperone role of Unc45b with roles that may precede the formation of the thick filament. The myocyte attachment defects apparent in *unc45b* mutant embryos is also absent in cell culture, likely due to the ubiquity of the laminin substrate. Therefore, in order to further test our hypothesis that Unc45b plays an earlier role in myogenesis than previously thought, we set about establishing the specific timeline and spatial patterning of *unc45b* and myosin gene expression throughout the early stages of zebrafish somite development, at both the mRNA and protein levels. We accomplished this at the mRNA level by *in situ* hybridization, and at the protein level by

generating a polyclonal antibody against zebrafish Unc45b protein that could be used for whole-mount or cryosection immunostaining. Although *in situ* hybridization and protein localization of Unc45b have been previously reported (Etard et al., 2007; Etard et al., 2010; Wohlgemuth et al., 2007), a rigorous timeline of expression at early stages, and comparison to myosin expression, has not yet been described.

3.2.1 The Timeline of Somite Morphogenesis in Zebrafish:

Myofibrillogenesis can be followed via the dynamic changes of actin deposition within the differentiating paraxial mesoderm, depicted for zebrafish schematically in Figure 19. Disorganized segmental plate mesoderm initially flanks a row of cuboidal adaxial cells, immediately adjacent to the developing neural tube (Fig. 19A, E). Organization of the segmental mesoderm causes the alignment of cortical actin, which forms the initial somite boundaries (arrowheads), while adaxial cells begin to undergo apical constriction (Fig. 19B, F) (Daggett et al., 2007). Adaxial cells eventually fuse and form elongated actin structures, which denote the first differentiated myocytes (Fig 19C, G). The elongated adaxial cells then migrate laterally to form the superficial slow-muscle fibers (arrow in Fig. 19H). This begins to occur in the oldest somites between the 15- and 20-somite stages of embryo development (Devoto et al., 1996). Meanwhile the remaining deep cells elongate and fuse (Fig. 19D, H), resulting in the formation of myotubes that stretch completely from one myoseptum to the next, with thick cortical actin walls (Fig. 19I, K). Cortical actin in these cells forms periodic bands that represent early myofibrils (arrows in Fig. 19I, L). Eventually, growing myofibrils fill the entire cell, displacing nuclei and creating mature muscle tissue (Fig. 19J, M). Striations may be noted at higher magnification (Fig. 19L, N). The localization of periodic NMM to the cortical actin in newly-fused myotubes is well-established (Du et al., 2003; Du et al., 2008a; Duan and Gallagher, 2009; Sanger et al., 2005; Sanger et al., 2009), and NMM is required for the organization and fusion of myoblasts in cell culture (Duan and Gallagher, 2009; Swailes et al., 2006). Despite this, the early temporal and spatial patterns of NMM expression prior to myotube fusion have not been reported in zebrafish, nor has any comparison been made with the patterns of Unc45b expression during these early stages of myogenesis.

Figure 19: Diagrammatic representation of zebrafish somite maturation during myogenesis. A representative dorsal view of paraxial mesoderm extending laterally from the edge of the developing neural tube (only the mesoderm is shown). Sample embryos at each stage are stained with phalloidin to show actin dynamics (E-H, K-N). Pre-somitic mesoderm in early embryos is made up of disorganized proliferative cells with thickened cortical actin structures (A, E). A columnar epithelium can be found immediately adjacent to the developing neural tube; these are the early adaxial cells. B) Adaxial cells undergo apical constriction as the cells of the segmental plate align to create continuous actin barriers between the somites (arrowheads in B, F), and somites first become visible within the embryo. Fusion of adaxial cells results in the formation of the first contractile structures (C, G) containing slow-fiber myosin isoforms. Clockwise rotation of the somites beginning around the 15-somite stage creates a curvature of the myosepta (D, H), giving rise to the characteristic chevron shape. Concurrently, adaxial slow muscle fibers migrate laterally towards the somite periphery (arrow in H). At this stage, somite cells of the segmental plate begin to elongate and fuse. Once somite cells are fully fused (I, K), striations appear in the cortical actin as the first myofibrils are constructed (arrows). As myocytes mature, they fill completely with striated myofibrils (J, M). Panels L and N show the formation of striated myofibrils at higher magnification. All artwork generously provided by Alina Pete.

Figure 19:

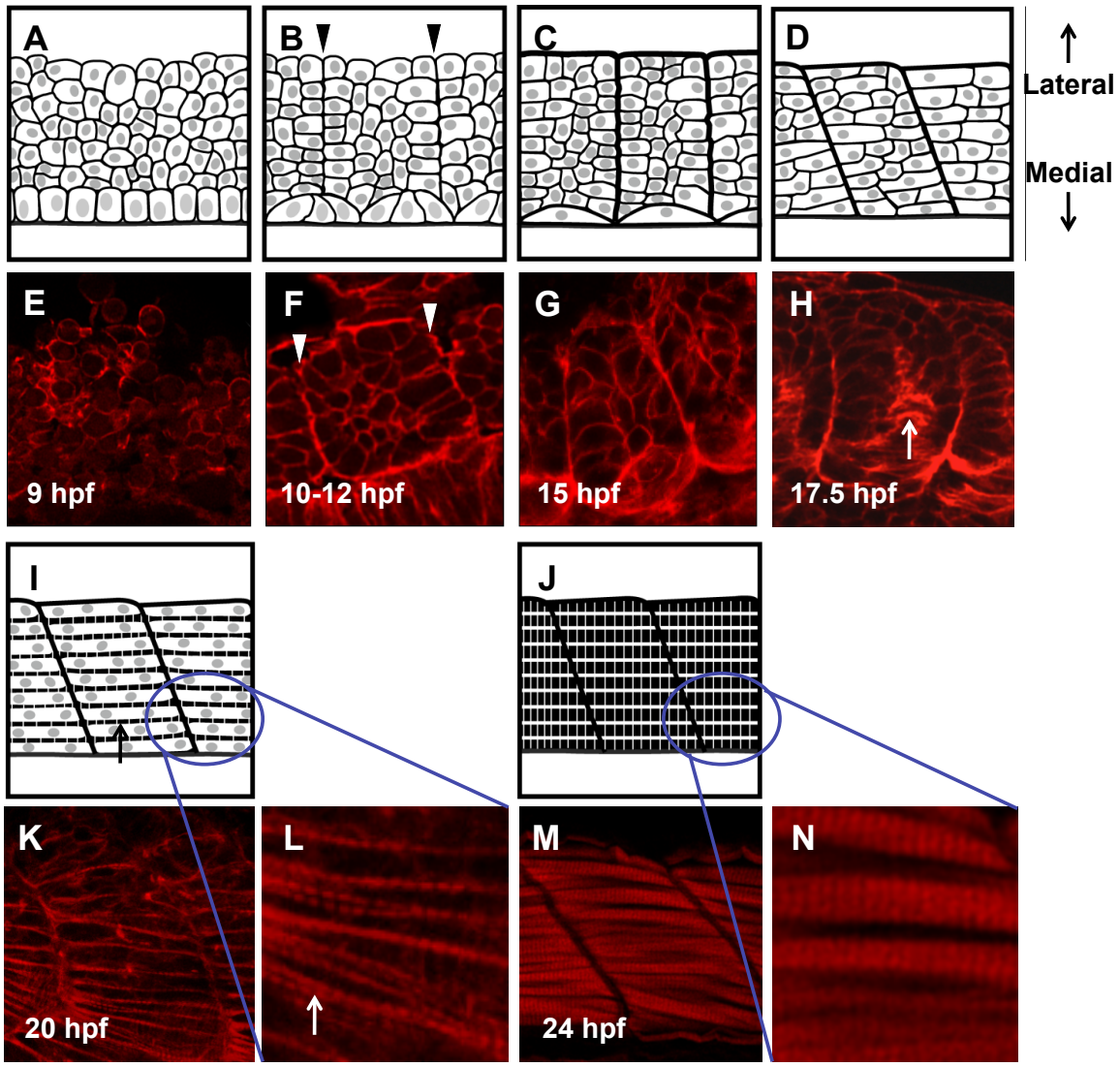
A
B
C
D
Lateral
Medial
E
9 hpf
F
10-12 hpf
G
15 hpf
H
17.5 hpf
I
J
K
20 hpf
L
M
24 hpf
N

3.2.2 Early Expression of *unc45b* Matches Spatially and Temporally with NMMs but not with Muscle Myosins:

3.2.2.1 Expression Timecourse of *unc45b* and Non-Muscle Myosins:

To establish a timeline of gene expression during early myogenesis, we performed side-by-side mRNA *in situ* hybridizations of *unc45b* with non-muscle (Figure 20) and muscle myosin probes (Figure 21), between the tailbud stage at ~10 hours post-fertilization (hpf), and the 10-somite stage at ~15 hpf. *unc45b* mRNA expression was noted in pre-adaxial mesoderm at the tailbud stage (Fig 20A), prior to any detectable myosin expression (compare Fig 20A and E with Fig 20A, E, I and M), subsequently spreading to encompass all pre-somitic adaxial mesoderm by the 2-somite stage (arrow in Fig 20B). Lateral segmental plate expression of *unc45b* mRNA was initially detected only in developing somites and not in pre-somitic mesoderm (arrowhead in Fig 20B), but extended throughout the pre-somitic segmental plate mesoderm by the 5-somite stage (Fig 20C), coincident with NMM up-regulation. Expression of the NMM genes *myh9* (coding for NMMIIA) and *myh10* (coding for NMMIIB) has not previously been described in early zebrafish embryos. Since the isoform detected in pre-myofibrils is NMMIIB (Rhee et al., 1994), we selected the zebrafish NMMIIB gene *myh10* for primary analysis. *myh10* NMM expression at the tailbud stage was restricted to the tailbud itself (white arrow in Fig 20I), and transcripts were detected most strongly in developing neural tissues from the 2-somite stage (~11 hpf) onwards (Fig 20J-L). However, *myh10* mRNA expression was also detectable at significant levels in somitic and presomitic mesoderm, both in adaxial cells (arrows) and segmental plate cells (arrowheads). This expression pattern was consistent from 2 to 10 somites, although a qualitative increase in NMM staining was noted in somites around the 5-somite stage (Fig 20K). By the 10-somite stage, *myh10* and *unc45b* mRNA were co-expressed throughout the developing somites and pre-somitic mesoderm (compare Fig 20D with 20L), with very little difference between patterns of adaxial mRNA expression (arrows) and lateral segmental plate expression (arrowheads) for either gene.

Although NMMIIB is the primary non-muscle myosin isoform of premyofibrils, expression of NMMIIA in embryonic muscle has also been reported (Takeda et al., 2000). To account for a possible role for NMMIIA in myofibrillogenesis, we also determined the timeline of mRNA expression of the zebrafish NMMIIA gene *myh9*. Given the known role

Figure 20: *unc45b* mRNA expression correlates spatially and temporally with NMM. *In situ* hybridization of zebrafish embryos at the tailbud (A, E, I, M), 2 somite (B, F, J, N, Q, T), 5 somite (C, G, K, O, R, U) and 10 somite (D, H, L, P, S, V) stages of development, photographed from dorsal (A-D, I-L, Q-S) and lateral (E-H, M-P, T-V) views. *In situ* probes were generated against *unc45b* (A-H), *myh10* (I-P) and *myh9* (Q-V). *unc45b* expression was detectable in presomitic adaxial mesoderm at the tailbud stage (A), extending to the tail from the 2-somite stage (arrow in B) onwards. Expression of *unc45b* in the segmental plate mesoderm was detected initially in differentiating somite cells only (arrowhead in B). However, from the 5-somite stage onwards (C-E), *unc45b* was detectable throughout the segmental plate mesoderm (arrowheads) in both differentiating somites and caudal pre-somitic mesoderm (G, H, white arrowheads). Non-muscle myosin IIB (*myh10*) expression was detectable at the tailbud stage (I) in the bud itself (arrowhead), spreading throughout the neural tube by the 2-somite stage (J). Expression was also detectable in adaxial cells (arrows) and the segmental plate mesoderm (arrowheads), growing more pronounced from the 5-somite stage onwards (K-L). Expression of *myh10* was not limited to the differentiating somites, extending throughout the pre-somitic mesoderm as well. By contrast, expression of *myh9* was ubiquitous at low levels, but was not significantly detectable in axial or paraxial tissues until the 5-somite stage, at which point enrichment of *myh9* transcript in the neural tube was detected (R). In myogenic tissues, some enrichment of *myh9* was detected in adaxial cells (arrowheads). Arrowhead positions are the same between dorsal and lateral views.

Figure 20:

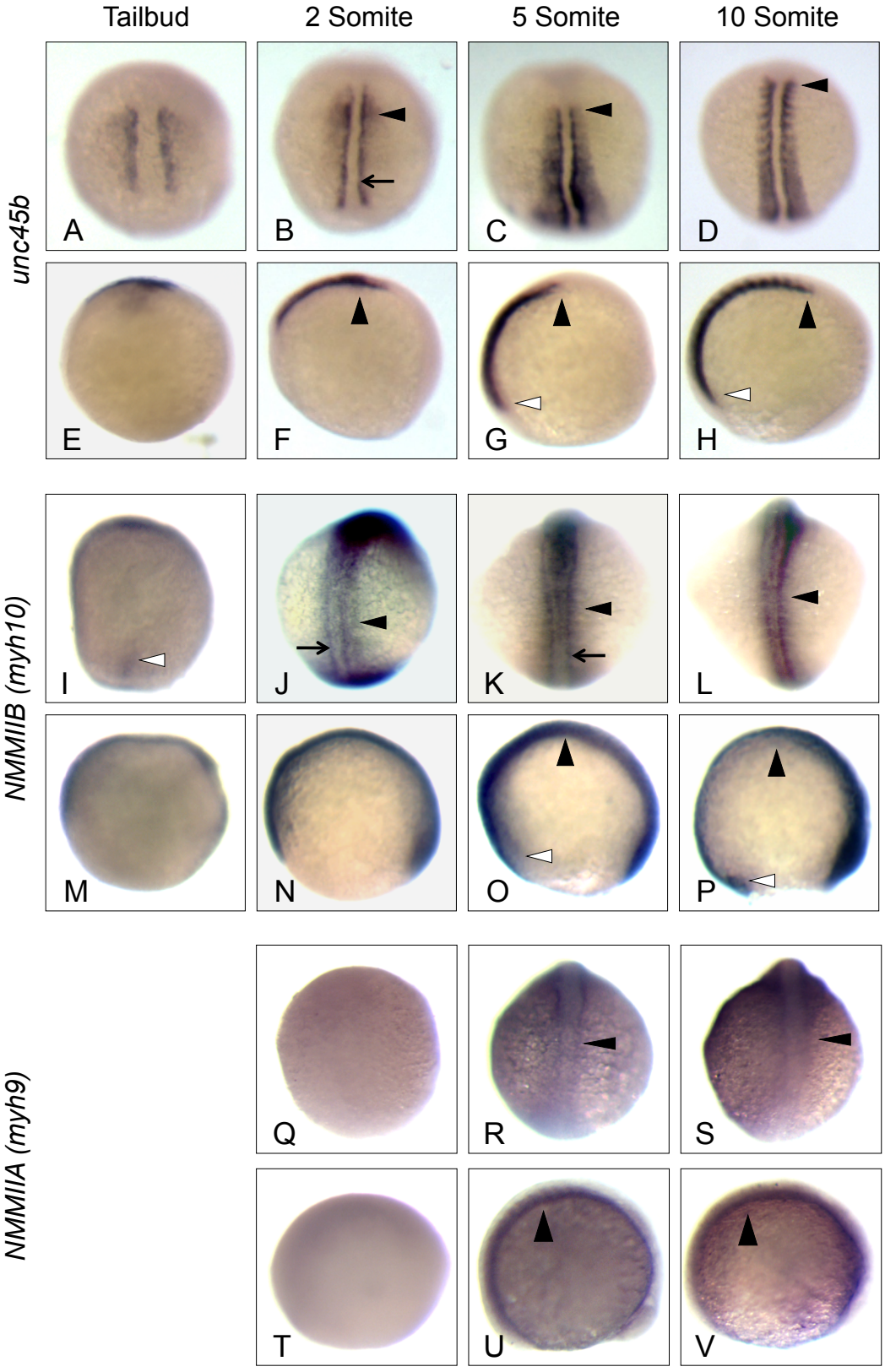
Tailbud
2 Somite
5 Somite
10 Somite
unc45b
NMMIIB (myh10)
NMMIIA (myh9)
A
B
C
D
E
F
G
H
I
J
K
L
M
N
O
P
Q
R
S
T
U
V

Figure 21: *unc45b* mRNA expression occurs long before muscle myosin expression.
In situ hybridization of zebrafish embryos at the tailbud (A, E, I, M), 2 somite (B, F, J, N), 5 somite (C, G, K, O) and 10 somite (D, H, L, P) stages of development, photographed from dorsal (A-D, I-L) and lateral (E-H, M-P) views. *In situ* probes were generated against *smyhc1* (A-H), and *myhc4* (I-P). By contrast with *unc45b* and *myh10* in Figure 20, the earliest slow-muscle myosin (*smyhc1*) was expressed at very low levels at the 2-somite stage (B), and not expressed in significant quantities until the 5-somite stage (C). Expression was restricted to adaxial cells as expected (black arrowheads). Expression extended into the first few pre-somites (white arrowhead in C) but not to the caudal-most presomitic tissue (white arrowhead in H). Likewise, fast-muscle myosin (*myhc4*) was not detectable at all before the 5-somite stage (K), and was also restricted initially to adaxial cells (arrowheads in K and P), extending into the first few pre-somites (white arrowhead in K), but not to the caudal-most tissue (white arrowhead in P). No expression was detected in segmental plate mesoderm at any time-point investigated.

Figure 21:

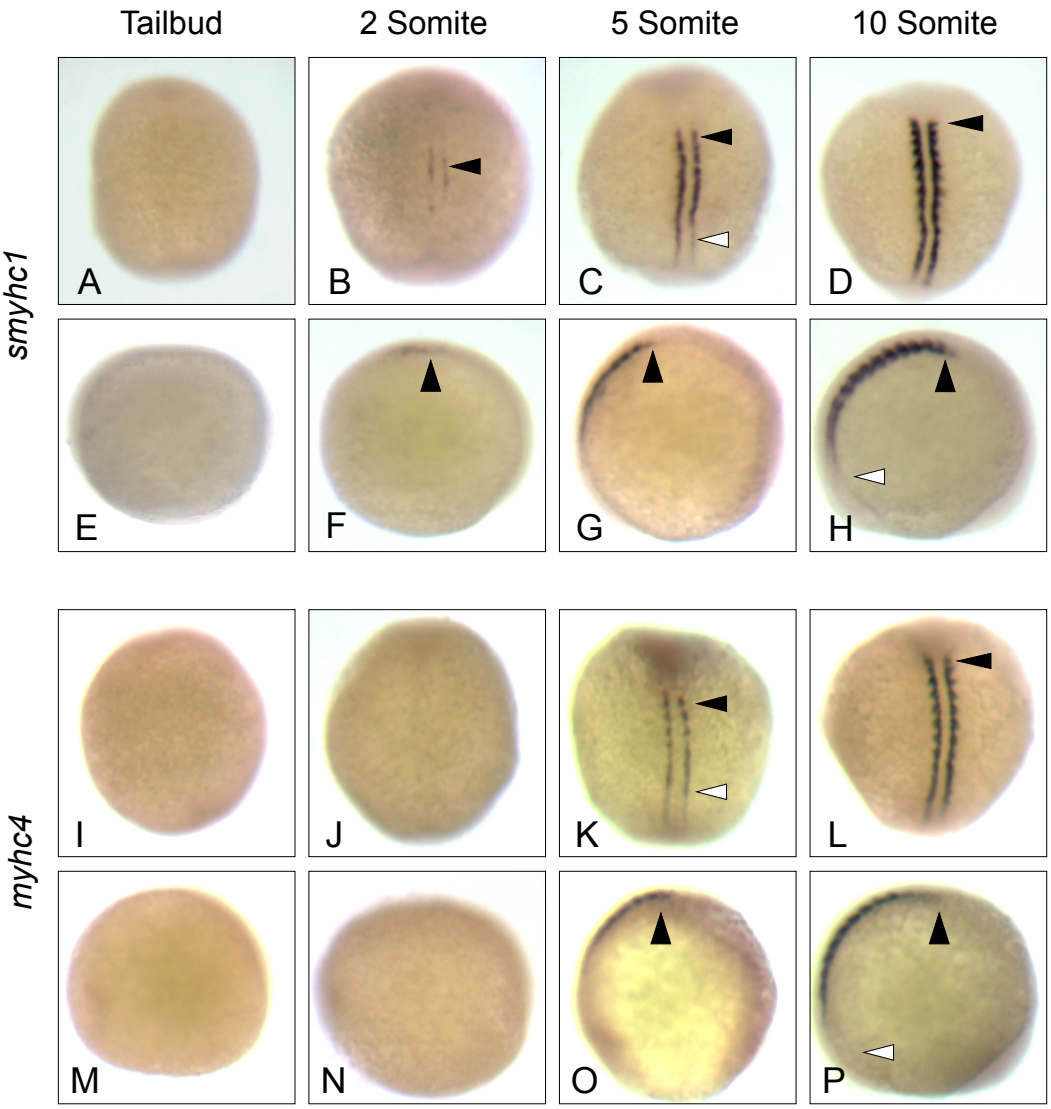
Tailbud
2 Somite
5 Somite
10 Somite
smyhc1
myhc4
A
B
C
D
E
F
G
H
I
J
K
L
M
N
O
P

of NMMIIA in cell division and motility, the seeming ubiquitous low-level expression of *myh9* at all stages examined was unsurprising (Fig 20Q-V); however, transcripts were enriched in adaxial and segmental plate mesoderm (arrowheads) at both the 5-somite (Fig 20R) and 10-somite stages (Fig 20S). The expression of both isoforms of NMM in pre-somitic mesoderm is consistent with previous reports in mice (Takeda et al., 2000), and further supports the probability that both isoforms are involved in myofibrillogenesis to some degree.

3.2.2.2 Expression Timecourse of Muscle Myosins:

By contrast, the first muscle-specific myosin (mMHC) isoform that is expressed during development, *smyhc1* (Devoto et al., 1996; Elworthy et al., 2008; Thisse et al., 2004), was weakly detectable at the mRNA level only in adaxial cells at the 2-somite stage (Fig 21B). As expected, this slow-muscle specific myosin was not detectable outside of adaxial cells at any time-point examined (Fig 21A-H), since lateral migration of slow-muscle fibers does not begin until ~16-17 hpf (Devoto et al., 1996). *smyhc1* expression in pre-somitic mesoderm was limited to the first few segments (white arrowhead in Fig 21C), even at the 10-somite stage when NMM and *unc45b* mRNA expression had extended throughout the pre-somitic mesoderm (compare white arrowheads in Fig 21D with 20G, H, O, and P). mRNA for the fast-muscle specific myosin, *myhc4*, was not detected at all until the 5-somite stage (Fig 21K), and transcripts were likewise limited to the adaxial tissue from the 5-10 somite stages (Fig 21K-L). Since fast-muscle fibers do not differentiate until later in development (Burguiere et al., 2011; Devoto et al., 1996), this adaxial expression of *myhc4* likely denotes early slow-muscle fibers, which have been shown to express both muscle myosin isoforms (Bryson-Richardson et al., 2005).

3.2.2.3 High Magnification of *in situ* Gene Expression:

Spatial patterns of mRNA expression may be clearer in Figure 22, where adaxial tissue (arrows) and lateral segmental plate (arrowheads) expression of *myh10* mRNA can be seen at the 2-somite stage (Fig 22A), while *unc45b* expression is primarily adaxial (Fig 22D). At the 5-somite stage (Fig 22B), *myh10* mRNA expression was increased, particularly in the segmental plate mesoderm, corresponding to up-regulation of *unc45b* expression in

Figure 22: *unc45b* mRNA expression correlates to non-muscle myosin but not muscle myosin in segmental plate mesoderm. *In situ* hybridization, high magnification view of developing somites in de-yolked zebrafish embryos at the 2-somite, (A, D, G, J), 5-somite (B, E, H, K) and 10-somite (C, F, I, L) stages. Non-muscle myosin (*myh10*, A-C) and *unc45b* (D-F) were expressed consistently in both adaxial cells (arrows) and lateral segmental plate mesoderm (arrowheads) at all stages. In contrast, slow-muscle myosin (*smyhc1*, G-I) was expressed only in adaxial cells (arrows) at these stages, beginning lateral migration into the segmental plate only at the latest stages examined (white arrowhead in I). Fast-muscle specific myosin (*myhc4*, J-L) was expressed after the 5-somite stage, and only in adaxial cells (arrows).

Figure 22:

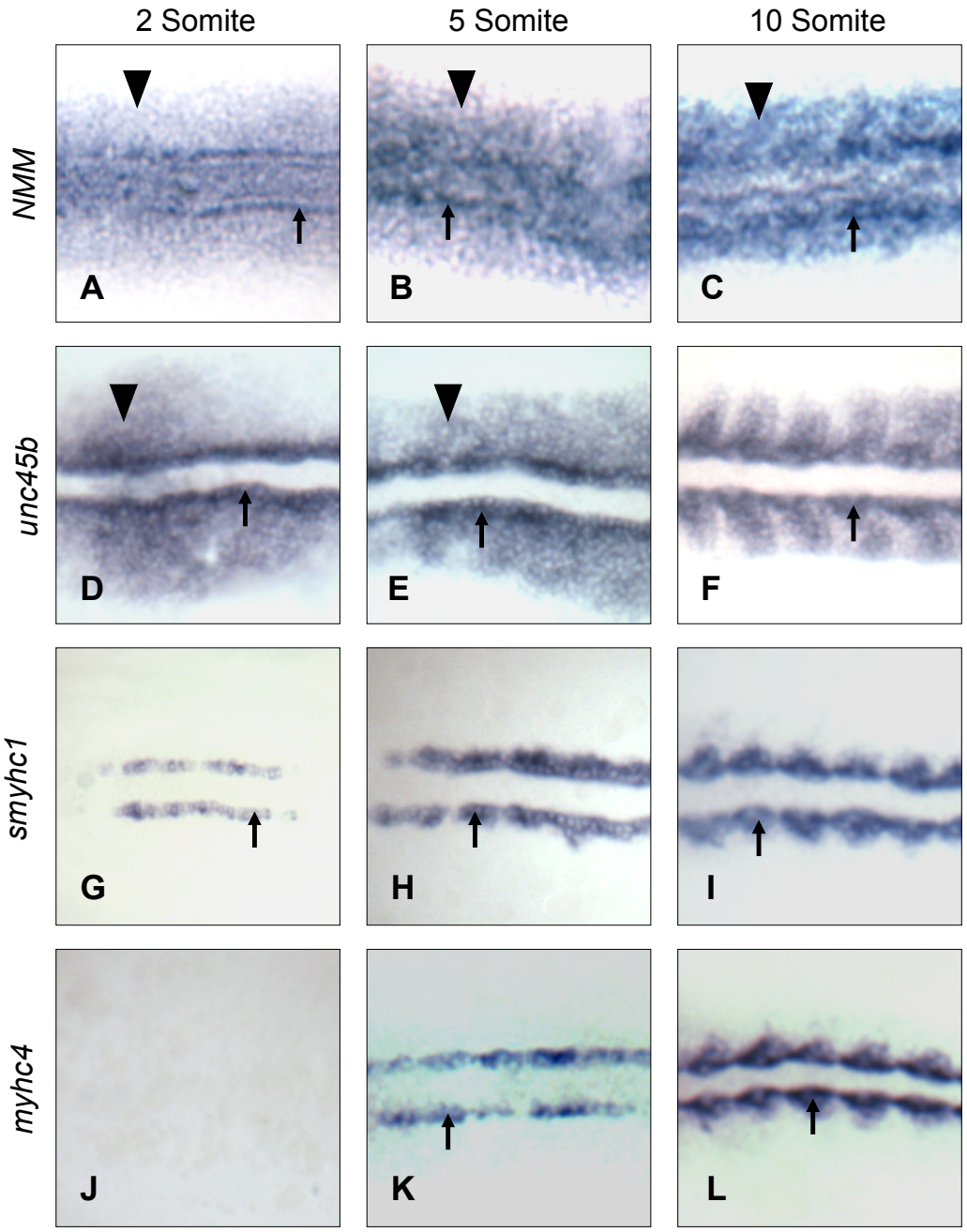
2 Somite
5 Somite
10 Somite
NMM
unc45b
smyhc1
myhc4
A
B
C
D
E
F
G
H
I
J
K
L

the same tissue (Fig 22E). By the 10-somite stage, *myh10* and *unc45b* mRNA were co-expressed throughout the developing somites and pre-somitic mesoderm (compare Fig 20H with 20P, and Fig 22C with 22F), with very little difference between patterns of adaxial mRNA expression (arrows) and lateral segmental plate expression (arrowheads) for either gene (compare Fig 22C and 22F). This co-expression of NMM and *unc45b* mRNA in segmental plate mesoderm was concurrent with myoblast alignment and elongation (Figure 19B-C and 19E-F).

The limits of muscle myosin mRNA expression can also be seen more clearly in Figure 22, where *smyhc1* mRNA detection was limited exclusively to adaxial cells (Fig 22G-I). Only a handful of somites weakly expressed *smyhc1* mRNA at the 2-somite stage (Fig 22G), and considerable expression was only seen at the 5-somite stage (Fig 22H). Fast-muscle-specific MHC isoform (*myhc4*) was not detected prior to the 5-somite stage (Fig 22J, K), and was also confined to adaxial tissue at all time-points examined (Fig 22L). While gene expression does not automatically denote necessity, the expression of *unc45b* mRNA at early time-points, in the absence of either slow or fast mMHC, supports our first hypothesis, that Unc45b plays an earlier role in myofibrillogenesis. These results strongly suggest that the previous view of Unc45b exclusively as a muscle myosin co-chaperone is incomplete, and is at least consistent with the pre-myofibril model and a role for NMM in myofibril formation.

3.2.3 Protein Expression of Unc45b Matches Spatially and Temporally with NMM but not with Muscle Myosin:

Since *unc45b* mRNA was detectable much earlier than mRNA for the primary contractile components of the sarcomere, it was important to determine whether this gene expression profile reflected Unc45b protein production. We therefore examined the localization of Unc45b, NMM and mMHC proteins by whole-mount or cryosection immunostaining. It has been suggested that NMMIIA and IIB isoforms may compensate for one another during myogenesis, and both isoforms are found in developing skeletal muscle (Takeda et al., 2000). Antibodies against mammalian NMMIIB localize to pre-myofibrils in mouse cells (Du et al., 2003; Du et al., 2008a; Sanger et al., 2005; Sanger et al., 2009). No antibodies specific to zebrafish NMM peptides are currently available, although some

mammalian NMM antibodies show cross-reactivity to zebrafish (Gutzman and Sive, 2010; Sanger et al., 2009). Mammalian NMMIIB antibodies fail to detect NMMIIB isoform in zebrafish myoblasts, while NMMIIA isoform is detected instead (Sanger et al., 2009). The specificity of these antibodies in zebrafish is not established, and it is possible that the NMMIIA antibody, which is derived from a partially-conserved (<50% similar) mammalian peptide, recognizes both zebrafish isoforms (which are ~80% similar). This hypothesis is supported by the fact that the NMMIIA antibody reacts with developing retinal cells in zebrafish, which express NMMIIB but not the IIA isoform (Lin-Jones et al., 2009). For our purposes, it is less relevant which isoform of zebrafish NMM is detected by these antibodies. Based on the above data (Figures 20-22), and the well-established use of NMM antibodies in zebrafish (Gutzman and Sive, 2010; Sanger et al., 2009), we have therefore used the NMMIIA antibody as a general marker of NMM localization in all subsequent experiments.

Antibodies against zebrafish Unc45b are not commercially available, and our trials using commercial antibodies raised against mammalian Unc45b peptides were unsuccessful. We therefore generated a polyclonal antibody in guinea pigs using full-length recombinant Unc45b as an antigen. The specificity of this antibody was confirmed by Western blotting against purified recombinant Unc45b protein and tissue extracts (Fig 23A); the protein detected by the antibody migrated faster than its predicted molecular weight (over 100 kDa), resolving to ~85 kDa; however, this is very similar to reports for mammalian Unc45b, which also resolves below its predicted molecular weight, at ~90 kDa (Srikakulam et al., 2008). The antibody failed to recognize the truncated *steif* mutant protein in Western blots (Fig 23A, lane 7). We also tested the antibody by whole-mount immunostaining of whole 3-day embryos (Fig23B). We then used this antibody to confirm the expression of Unc45b protein at all stages where mRNA was detected (Fig 24A-D); as expected, Unc45b protein was seen in adaxial tissue and segmental plate as early as the 2-somite stage (Fig 24A), extending throughout the pre-somitic mesoderm from the 5-somite stage onwards (Fig 24B-D). By the 5-10 somite stage, expression in developing somites (Fig 24E) was detected both in adaxial cells (arrowheads) and the lateral segmental plate mesoderm, particularly at the cortices of differentiating myoblasts and the myosepta, where cytoskeletal actin was also enriched (Fig 24F). NMM expression was also detected at the 5-10 somite stage in both adaxial and lateral mesoderm (Fig 24G), in a similar pattern to Unc45b, while mMHC was only detected in

Figure 23: The zebrafish Unc45b antibody is specific to WT Unc45b protein. Western blot analysis (A) and whole-mount immunostaining (B) confirm the specificity of the Unc45b polyclonal antibody. Proteins were resolved by 10% SDS-PAGE and blotted to nitrocellulose using the standard Laemmli protocol, then blocked in 5% skim milk solution prior to antibody staining. Lane 1, protein extract from 72-hpf WT embryos detected with pre-bleed serum shows only a little background at lower molecular weights. Lanes 2 and 3, two different protein extracts from 72-hpf WT embryos (ZF1 and ZF2) stained with final bleed serum containing the Unc45b antibody detects multiple bands. Lanes 3-5 were stained with purified Unc45b antibody. Lane 3, staining of blotted bacterial extract containing full-length recombinant zebrafish Unc45b reveals a primary band of ~85 kDa. Lanes 4 and 5, staining of blotted ZF1 and ZF2 extract reveals a single specific band. Lane 6, staining of ZF extract from *unc45b* mutant embryos reveals a loss of antigenicity in the truncated protein. ZF extract was generated from 20 embryos per 50µl of protein lysis buffer. B) whole-mount immunostaining of 72-hpf embryos reveals Unc45b antibody reactivity throughout all striated muscle tissue with very little background signal.

Figure 23:

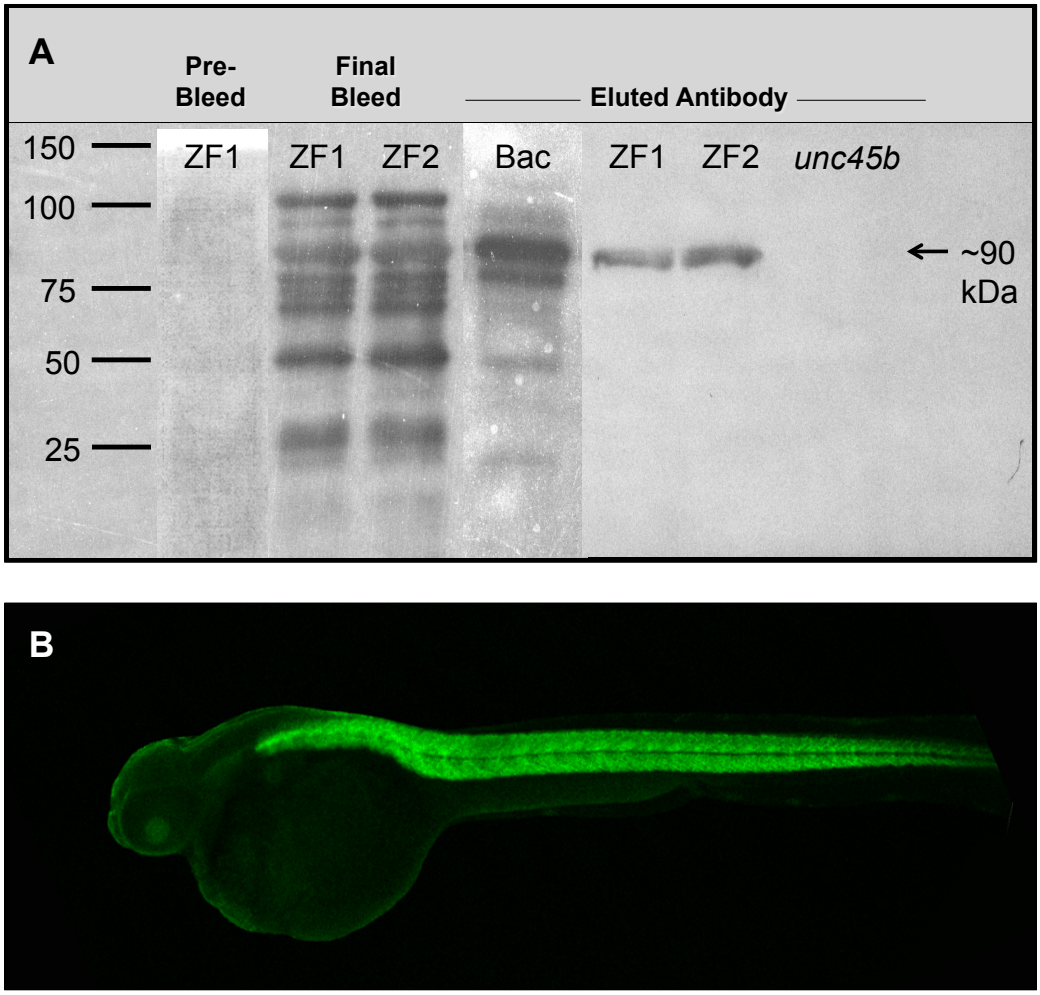
A
Pre-Bleed
Final Bleed
Eluted Antibody
150
100
75
50
25
ZF1
ZF1
ZF2
Bac
ZF1
ZF2
unc45b
~90 kDa
B

Figure 24: Unc45b protein is co-localized with non-muscle myosin protein in early segmental plate mesoderm. Immunofluorescent staining of Unc45b at the 2-somite (A), 5-somite (B), 10-somite (C) and 15-somite (D) stages of development demonstrates the same pattern of protein expression as was seen for mRNA expression at similar stages; enriched expression in adaxial cells, spreading throughout the segmental plate laterally and extending caudally throughout the pre-somitic mesoderm. Higher magnification of 5-somite (E-H) zebrafish embryos demonstrates protein accumulation of Unc45b (E) and non-muscle myosin (G) in both adaxial cells (arrowheads) and lateral segmental plate mesoderm, demonstrating enrichment at the myoblast cortex (arrows) and somite boundaries, where cytoskeletal actin is also enriched (F). By contrast, muscle myosin protein accumulation (H) was limited to adaxial cells that form the superficial layer of slow muscle fibers. In cryosections of developing zebrafish muscle tissue (I-N), co-localization of Unc45b (green, I, L) and NMM (red, J, M) protein can be seen as yellow fluorescence. At the 20-somite stage (I-K), localization to myoblast cortices (arrows) and nascent myofibrils (arrowheads) are both evident. This co-localization persists at 28 hpf (L-N). Merged NMM and Unc45b staining is shown in panels K and N.

Figure 24:

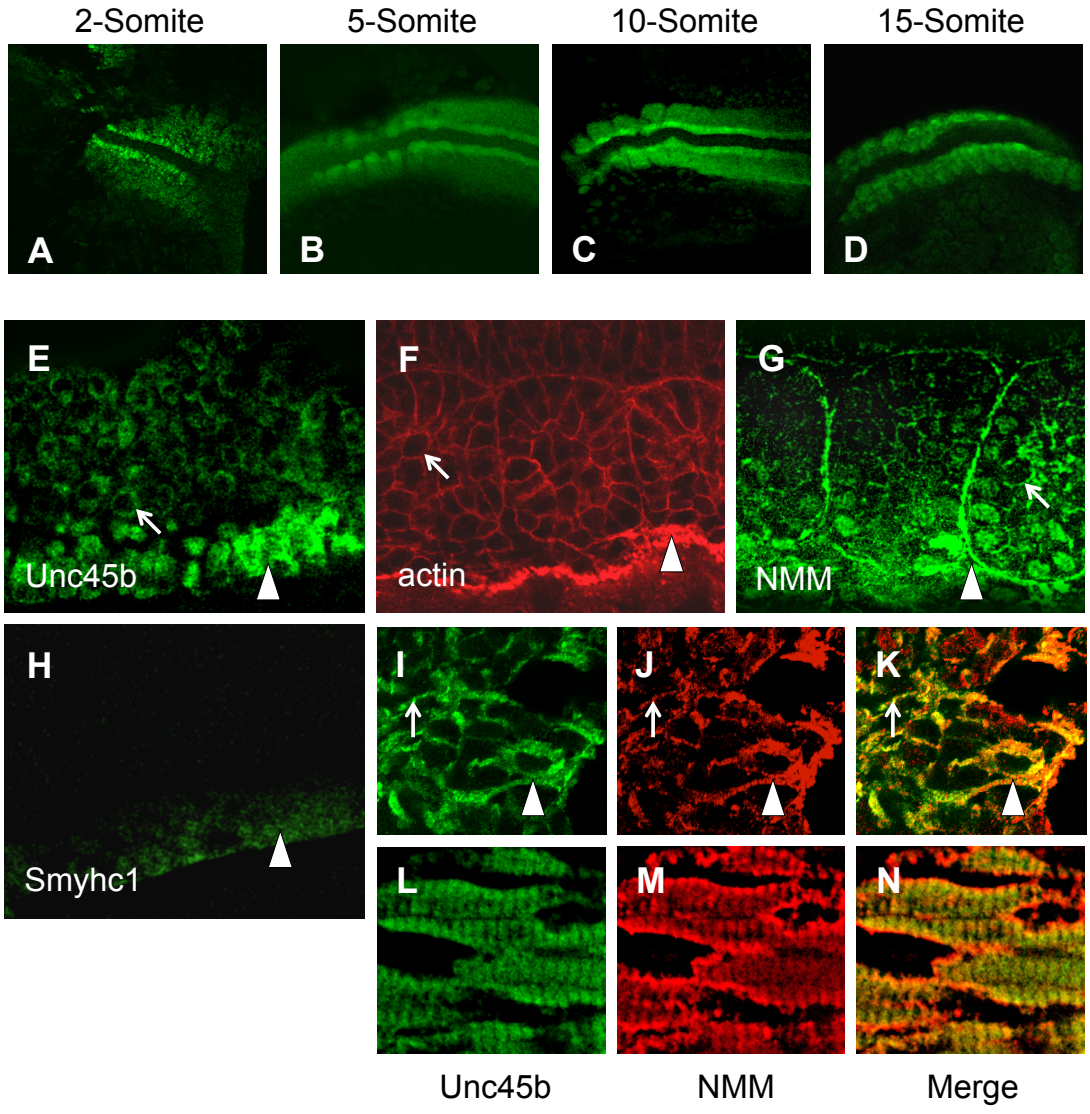
2-Somite
5-Somite
10-Somite
15-Somite
A
B
C
D
E
Unc45b
F
actin
G
NMM
H
Smyhc1
I
J
K
L
M
N
Unc45b
NMM
Merge

adaxial cells (Fig 24H). To determine the localization of these proteins during myofibrillogenesis, we used thin cryosections to better expose the relevant peptides for antibody staining (Fig 24I-N). At the 15-20 somite stage (Fig 24I-K), partial co-localization of Unc45b (green) and NMM (red) was readily apparent as yellow fluorescence, both at the cortices of elongating myoblasts (arrows) and along nascent myofibrils (arrowheads). This co-localization persisted even after myofibrillogenesis was complete, as shown in 28-hpf embryos (Fig 24L-N), where both proteins localize to myocyte cortices and I-bands. This sub-cellular localization of Unc45b and NMM protein is consistent with an attachment-related role during myogenesis, consistent with *unc45b* mutant myocyte detachment phenotypes. Co-localization was not complete, however; red fluorescence in the merged panels K and N indicate NMM staining in the absence of Unc45b, and green staining indicates Unc45b staining in the absence of NMM.

3.2.4 NMM and Unc45b Localize with Components of the Costamere in Developing Myocytes

As noted above, the partial co-localization of NMM with cortical actin during pre-myofibril formation in newly-fused myotubes has been well-established. However, NMM and cortical actin show similar expression patterns between 12 and 16 hpf, prior to the formation of pre-myofibrils (Figure 24, panels F and G). The known requirement for NMM activity during myoblast alignment and fusion in cell culture, and the early pre-somitic expression of NMM detected in our experiments, both suggest an early role for NMM during zebrafish myogenesis. As discussed above, NMM activity also stabilizes the formation of focal adhesion complexes in differentiating myoblasts in culture (Sharp et al., 1997; Simpson et al., 1993). In addition, components of costameres, which form as modifications of focal adhesion complexes, are among the earliest identifiable structural elements expressed in differentiating myocytes (Sparrow and Schock, 2009). In addressing our second hypothesis, that Unc45b is necessary for the formation and/or stability of costameres, we therefore investigated the localization of NMM and Unc45b protein as well as several components of costameres in early zebrafish embryos (Figure 25). In younger embryos (tailbud to 2-somite stage), we noted expression of α-actinin (Fig 25B), integrin-linked kinase (Fig 25C), NMM (Fig 25D), Unc45b (Fig 25E) and cortical actin (Fig 25F) at the

Figure 25: Non-muscle myosin and Unc45b localize with costamere components at myoblast cell peripheries and at myosepta. Immunofluorescent staining of early zebrafish embryos (10-12 hpf) demonstrates the localization of early sarcomere components (including non-muscle myosin) to the cortices of myoblasts during somite organization (depicted in panel A). Myocyte costamere components such as α-actinin (B) and integrin-linked kinase (ILK, C) localize to the myoblast cell cortex prior to costamere formation (arrowheads). Punctae in these panels indicate nucleation of costamere components at cell attachment sites (arrows). NMM and Unc45b are similarly localized to myoblast cortices (D and E, respectively). Phalloidin staining against actin marks the myoblast cortex (F). Subsequently, at 12-15 hpf, costamere components organize at the myosepta (arrowheads) as depicted in G, including α-actinin (H) and ILK (I). Non-muscle myosin and Unc45b were also localized to the developing myosepta at these stages of development (J and K, respectively).

Figure 25:

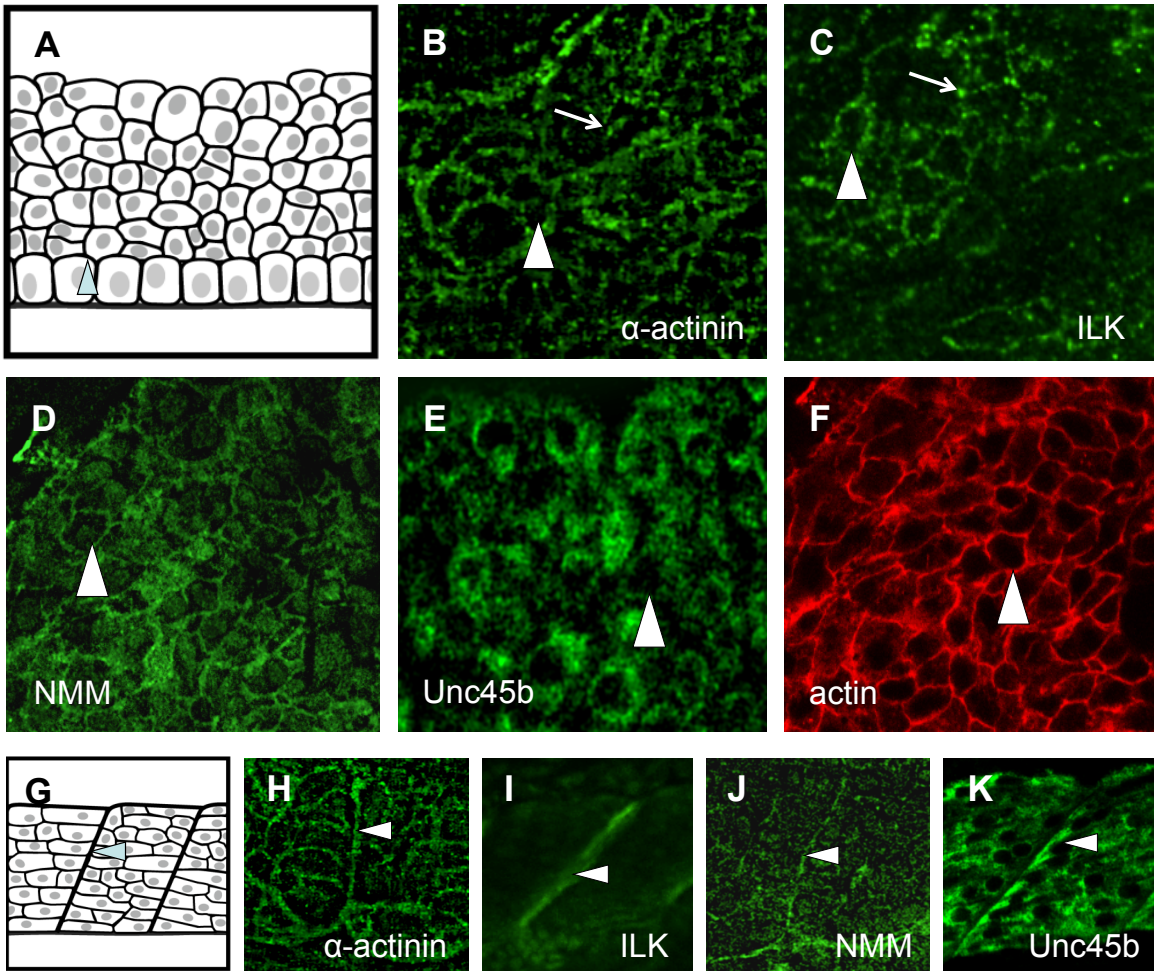
A
B
α-actinin
C
ILK
D
NMM
E
Unc45b
F
actin
G
H
α-actinin
I
ILK
J
NMM
K
Unc45b

periphery of proliferating myoblasts (arrowheads in all panels, compare with diagram in 25A). The periphery of these cells corresponds to sites of cell attachment, and the individual punctae of localized α-actinin and ILK in panels 25B and 25C likely correspond to individual focal adhesions (arrows). At later stages of development (> 10-somite) there was also a significant enrichment of NMM, Unc45b and costamere components at the myosepta (see diagram in Fig 25G), where strong attachment of costameres to extracellular matrix components is required in differentiated myofibers (arrowheads in Fig 25H-K). This supports a cell-attachment role for NMM and Unc45b during the early stages of myogenesis, as previously implied by the myocyte attachment defects that have been reported in *unc45b* mutant embryos (Etard et al., 2008; Etard et al., 2010).

3.2.5 Unc45b Localizes with NMM in Developing Lens of WT Embryos but not *steif*:

Unc45b antibody staining also revealed protein localization in the developing lenses of 2- and 3-dpf embryos (Figure 23B). We therefore examined the expression patterns of the *unc45b::GFP* transgene in our *Tg(unc45b:EGFP)ua1* transgenic line, described above. We found that Unc45b promoter activity was reported by GFP expression throughout the skeletal (Fig 26A) and cardiac muscle (Fig 26B), recapitulating the pattern of endogenous Unc45b protein expression. Expression was also detected in the developing lens, starting in the lens vesicle at ~30 hpf (arrow in Fig 26B), and persisting in elongating cortical lens fibers between 2 and 4 dpf (Fig 26C). Antibody staining of acetone-washed, dissected eyes from 2 dpf embryos revealed a consistent Unc45b signal. These discoveries are consistent with the recent identification of a mutation in human UNC45B causing congenital cataracts (Hansen et al., 2013). Since NMMIIB is expressed in developing retinal cells in zebrafish (Lin-Jones et al., 2009), we examined the localization of NMM and Unc45b in cryosections of retinal tissue from 48 hpf zebrafish embryos (Figure 27). Both proteins were expressed throughout the developing retina (Fig 27A, B), localized to cell cortices of elongating laminar cells (Fig 27G, H) and exhibiting strong co-localization (Fig 27I). Co-localization was also detected in lens fiber cells (arrows). Interestingly, in *unc45b* mutant fish, which express a truncated and non-functional protein (Etard et al. 2007) that still partially cross-reacts with our polyclonal antibody (Fig 27D, J), the pattern of NMM expression was not

Figure 26: GFP reporter expression in *unc45b::GFP* transgenic embryos. A transcriptional GFP reporter under the control of the *unc45b* promoter is expressed in all striated muscle tissues. A) GFP reporter expression in developing somites of a 25-somite-stage embryo. B) GFP reporter expression in the developing heart tube of a 30-hpf embryo. Reporter expression also occurs in the developing lens vesicle (arrow). C) Close-up view of a 48-hpf zebrafish eye shows GFP expression in cortical lens fibers (arrows). Lens-specific activity of the *unc45b* promoter was confirmed in WT animals by whole-mount immunostaining of dissected zebrafish eyes at 48 hpf, using a polyclonal antibody against full-length Unc45b (E). Staining was detected throughout the developing lens. D) Nuclear DAPI staining shows the locations of lens and retinal tissue for comparison.

Figure 26:

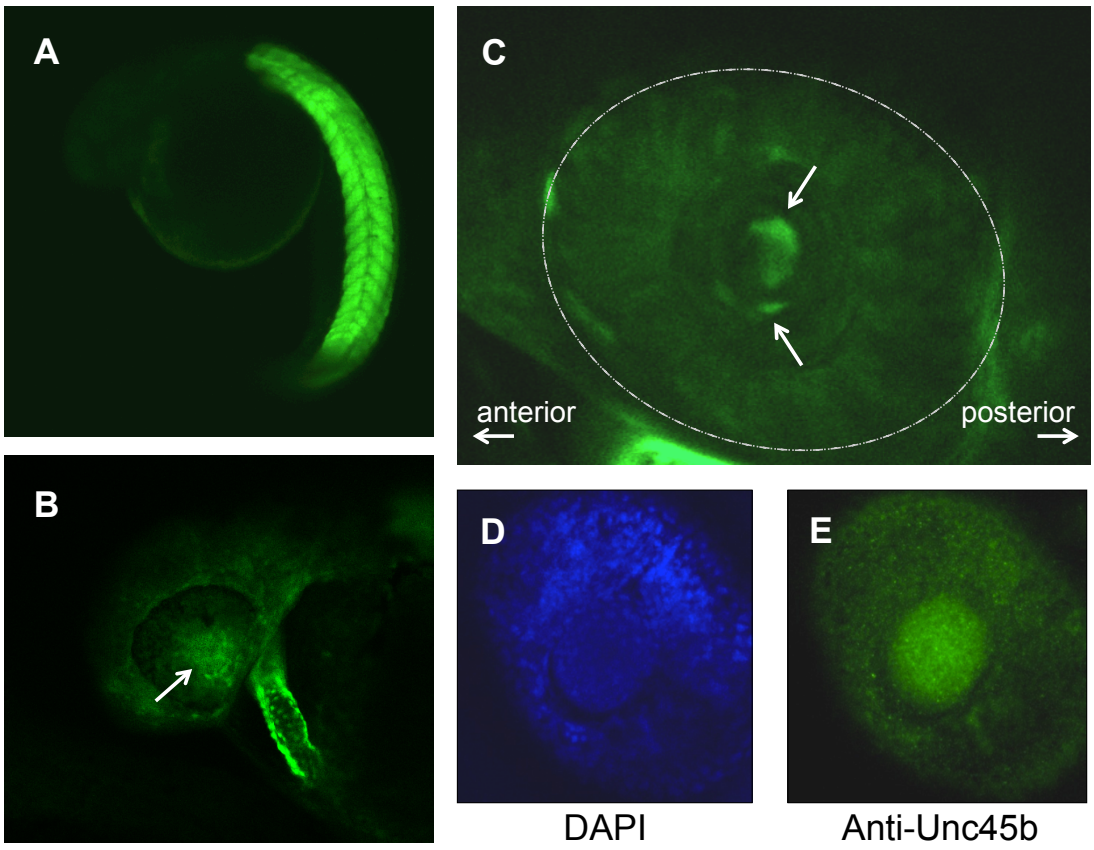

Figure 27: Unc45b and NMM co-localization in the developing eye is lost in *unc45b* mutant embryos. Antibody staining of cryosections of zebrafish eyes from 2 dpf embryos. Wild-type (A-C, G-I), and homozygous *steif unc45b* mutant embryos (D-F, J-L) were immunostained with polyclonal antibodies against zebrafish Unc45b (A, D, G, J), or NMM (B, E, H, K), or DAPI nuclear stain (C, F). Co-localization of Unc45b and NMM is visible in retinal tissues as well as the developing lens (arrows). At higher magnification (G-L), localization of Unc45b and NMM expression to the cell cortex can be seen, and co-localization becomes much more apparent (I). In *unc45b* mutant embryos (J, K), the pattern of NMM expression remains the same (K), but Unc45b no longer localizes to the cell cortex (J) and co-localization is lost (L).

Figure 27:

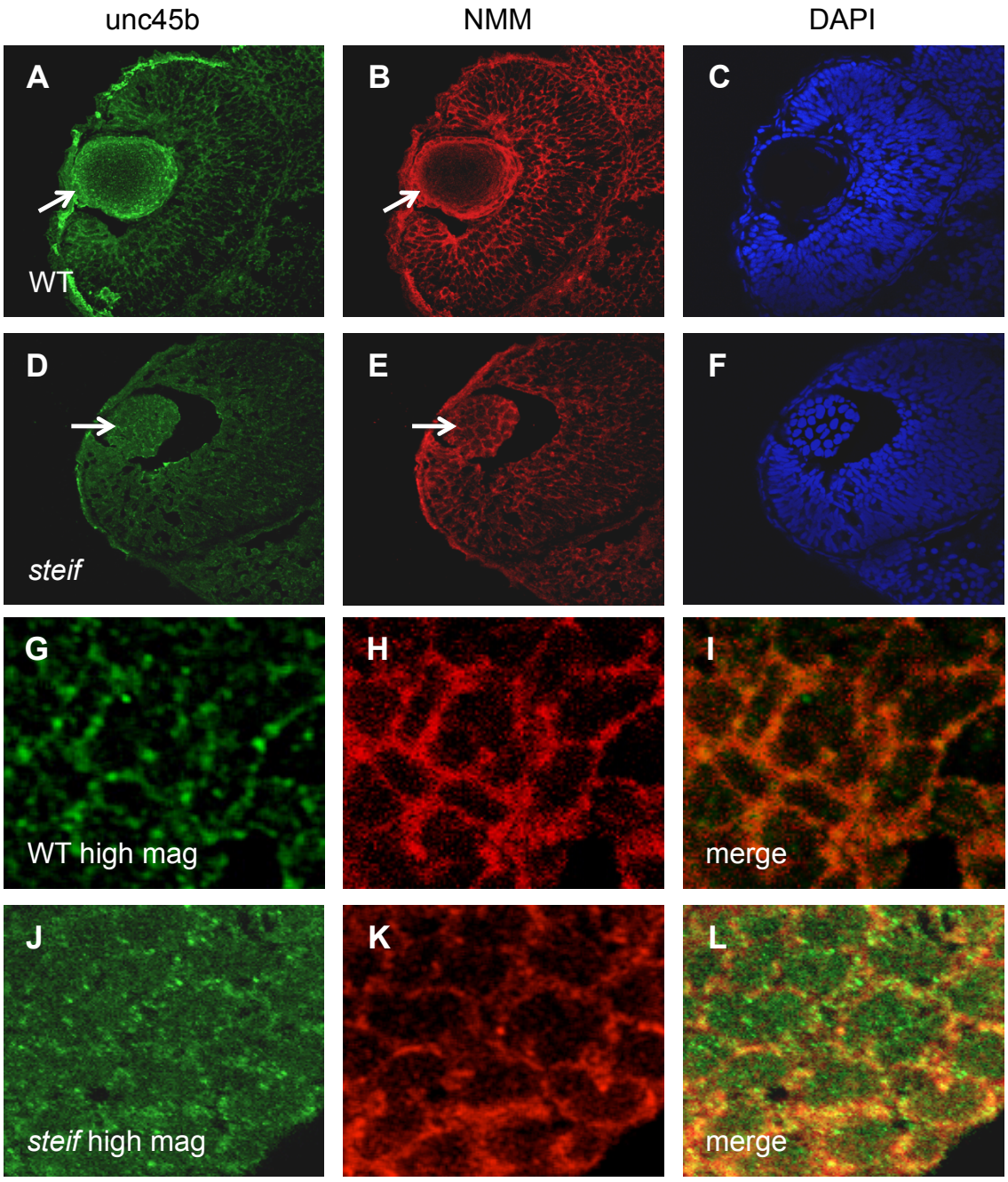
unc45b
NMM
DAPI
A
B
C
WT
D
E
F
steif
G
H
I
WT high mag
merge
J
K
L
steif high mag
merge

notably altered, even though the clearing of the lens was much delayed (Fig 27E, K), but the co-localization of truncated Unc45b with NMM was lost (Fig 27L). The loss of NMM and Unc45b co-localization in the developing retina and lens may contribute somewhat to the small-eye and lens phenotypes seen in *steif* mutants. Indeed, injection of the human mutant *UNC45B* mRNA into wild-type zebrafish embryos causes similar lens defects (Hansen et al., 2013).

3.2.6 *unc45b* Mutant Zebrafish Display Costamere Deficiencies, Including Delayed Nucleation of α-Actinin and Loss of NMM and ILK Localization to the Myoseptum:

The nucleation of α-actinin at the developing Z-lines of early somites is one of the initial stages of myofibrillogenesis, representing the formation of costamere attachments that are vital to sarcomere integrity. *Xenopus unc45b* mutants have been reported to show delayed α-actinin nucleation in the caudal-most developing somites, characterized by elongated myofibers that lack the periodic banding pattern of α-actinin localization (Geach and Zimmerman, 2010). We examined α-actinin localization in 20 hpf WT and mutant zebrafish embryos (identified phenotypically) by immunostaining (Figure 28). As expected, caudal somitic mesoderm in WT embryos (Fig 28A-C) was characterized by elongated myofibers with limited actin organization (Fig 28B) that did not yet span the entire somite. Localization of α-actinin in these cells already resembles fully-assembled Z-lines in older somites (to the left in each panel) and the initial organization of periodic rows of punctae may be seen (arrowheads) in the youngest somites (right). This is in contrast to the non-periodic punctate staining of α-actinin in early, un-elongated myoblasts shown previously in Figure 5 (Fig 25B and 25H). The striated pattern of staining in the 20th somite can be seen more clearly at higher magnification (inserts). In *unc45b* mutant embryos (Fig 28D-F), this pattern of localization was lost, and resembled the disorganized punctae of younger somites, although the pattern was retained in older somites (compare panels 28G and F), indicating a delay in α-actinin nucleation similar to that seen in *Xenopus*.

Unc45b localizes to the Z-line and myofibril termini in WT embryos, and *unc45b* mutants are characterized by lateral separation of myofibrils in mature muscle tissue (Etard et al., 2010; Wohlgemuth et al., 2007). A loss of tension between myocyte cell/matrix

Figure 28: Nucleation of α-actinin is delayed in zebrafish *unc45b* mutants.
Immunofluorescent staining of WT (A-C) and *unc45b* mutant embryos (D-F) at 20 hours post-fertilization, displaying the 19th to 22nd somites. The caudal-most somites of these embryos were still undergoing myogenesis, as shown by the incomplete elongation of myofibers and localization of α-actinin and actin staining in WT embryos (A and B, inserts). Nucleation of α-actinin is the first indication of periodic myofibril patterning (arrowhead). In mutant embryos, organization of α-actinin at costamere attachment sites was not yet complete, and nucleation has just begun (D, insert). Actin counter-staining with phalloidin (B, E) demonstrates the ongoing organization of actin in early myofibers, which can be compared with the pattern of α-actinin localization in merged images (C, F). Blue fluorescence indicates DAPI nuclear stain. The cranial-most somites at 24 hpf display relatively normal patterns of α-actinin staining in mutants (H) compared to WT embryos (G).

Figure 28:

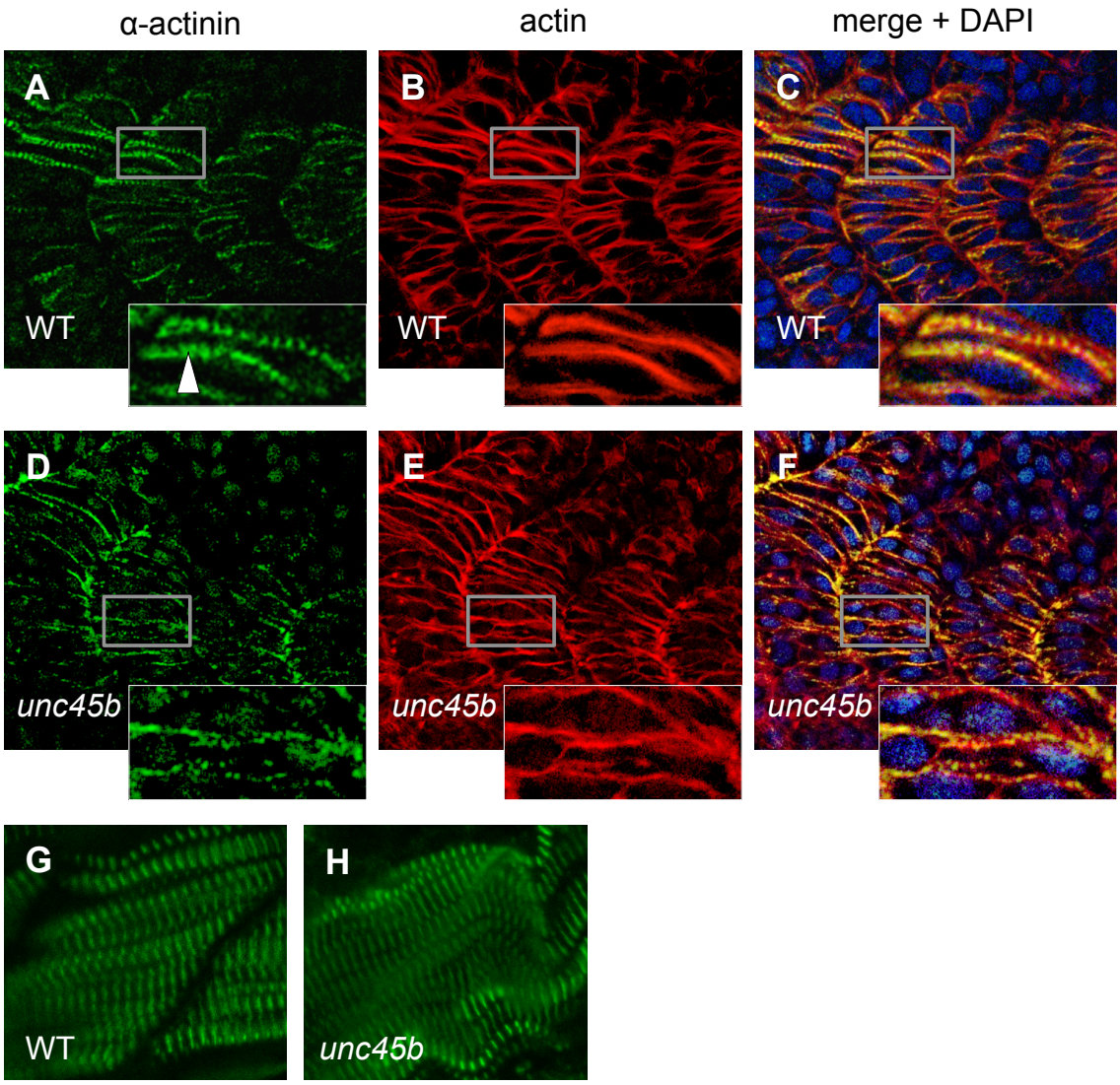
α-actinin
actin
merge + DAPI
A
B
C
WT
WT
WT
D
E
F
unc45b
unc45b
unc45b
G
H
WT
unc45b

attachment points, either through inhibition of general myosin activity or blocking of integrin binding, results in sarcomere disorganization (De Deyne, 2000; Sharp et al., 1997). Given the reported defects in myocyte attachment and the delay of α-actinin nucleation we have showed in caudal somites of *unc45b* mutants, it is possible that the *unc45b* mutant phenotype is at least partially due to deficiencies in myocyte attachment, particularly at the costameres of the myosepta (Figure 29). Myofibrils in *unc45b* mutants frequently do not fully extend from myoseptum to myoseptum (compare Fig 29A with 29D), with large lateral gaps between the fibrils (arrowhead in Fig 29D). Localization of NMM to the myosepta was disrupted in *unc45b* mutants (compare Fig 29B with 29E), which corresponds with the loss of localization of costamere components to the myosepta such as ILK (compare Fig 29C with 29F). At higher magnification, it is also possible to note the punctate Z-line localization of ILK (arrow in Fig 29G), which was lost in *unc45b* mutants (Fig 29J). Further, this loss of localization does not represent a secondary effect of gross tissue defects, as the organization of myofibrils along the myoseptum was not changed in mutants (arrowhead in Fig 29J). Likewise, there was no change in laminin organization at the myosepta (compare panels 29H with 29K), indicating no change in extracellular matrix deposition; nor was there a change in dystrophin organization (compare panels 29I with 29L), indicating no change in dystroglycan complex formation at the sarcolemma. Furthermore, higher magnification (Figure 30) shows that both Unc45b and NMM protein (Fig 30A and B, respectively) are enriched at the myosepta (arrowheads) with significant co-localization (Fig 30C), as seen in Figures 24 and 25. In *unc45b* mutants, enrichment of Unc45b and NMM at the myosepta is lost (Fig 30D and E, respectively), and co-localization of these proteins is greatly reduced (Fig 30F). Taken together, these data support our second hypothesis, showing that the loss of Unc45b function has a direct impact on the organization of costameres, both laterally and at myosepta, which may be mediated by the folding or stabilization of NMM.

3.2.7 Unc45b is Co-Regulated with NMMIIB During Protein Stress:

Unc45b and Hsp90 transcripts are significantly up-regulated in response to protein-denaturing stresses such as heat-shock (Etard et al., 2008; Krone et al., 1997). A similar up-regulation occurs in *unc45b* mutant embryos (Etard et al., 2007), suggesting that the accumulation of mis-folded mMHC in the absence of myosin chaperones may also trigger

Figure 29: Localization of NMM and costamere components to the myoseptum is lost in *unc45b* mutant embryos. Immunofluorescent staining of WT (A-C, G-I) and *unc45b* mutant embryos (D-F, J-L) at 24+ hours post-fertilization. The positions of myofiber attachment points at the myosepta were made visible by actin staining (A, E). Like earlier embryos, mature muscle tissue was characterized by the localization of non-muscle myosin (B) and integrin-linked kinase (C, G) to the myosepta in WT embryos. This localization was lost in *unc45b* mutants (E, F, J). At higher magnification (G, J), ILK co-localizes with actin striations at lateral costamere attachment points (arrow in G); this pattern of staining was also lost in *unc45b* mutant embryos (J). Green fluorescence to the right of the actin staining represents background staining outside of the muscle tissue, and blue fluorescence indicates DAPI counter-staining. However, the tissue morphology was not changed in mutants, and the disorganized myofibers were still separated by myosepta (arrowhead in J) containing ECM components such laminin (compare panels H and K), and ECM/glycoprotein complex components such as dystrophin (compare panels I and L).

Figure 29:

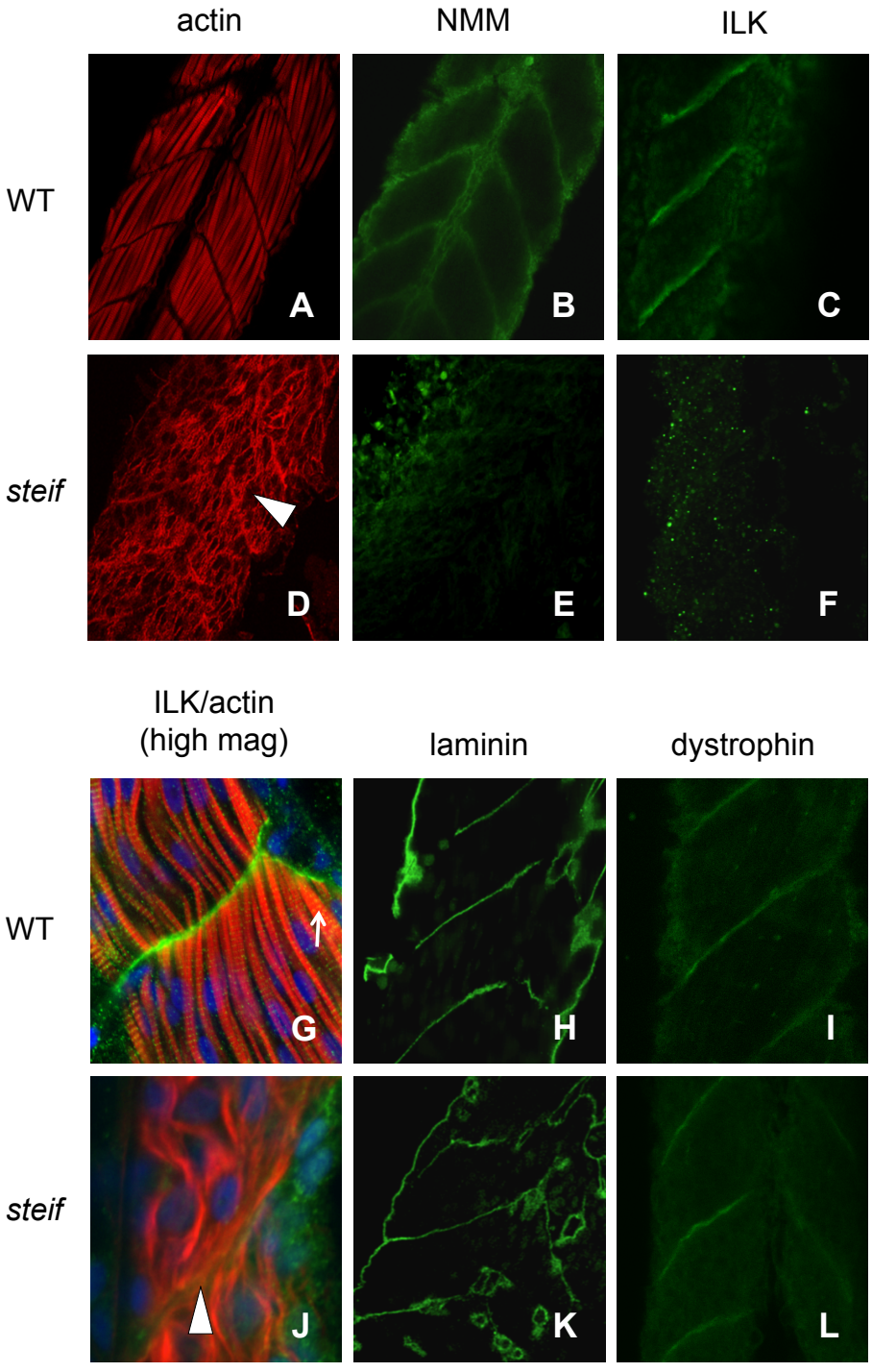
actin
NMM
ILK
WT
A
B
C
steif
D
E
F
ILK/actin
(high mag)
laminin
dystrophin
WT
G
H
I
steif
J
K
L

Figure 30: Co-localization of Unc45b and NMM at the myoseptum is lost in *unc45b* mutant embryos. Immunofluorescent staining of cryosections from 48 hpf zebrafish embryos, using antibodies again Unc45b (A, D) and NMM (B, E). In WT embryos (A-C), immunostaining revealed the enrichment of both proteins at the developing myosepta (arrowheads), with strong co-localization both at myosepta and throughout the I-bands of mature myocytes (C). The enrichment of both proteins at the myosepta was lost in *unc45b* mutants (D, E), although myosepta were still clearly visible (arrowheads). The co-localization of the two proteins at the myosepta was also greatly reduced (compare C and F).

Figure 30:

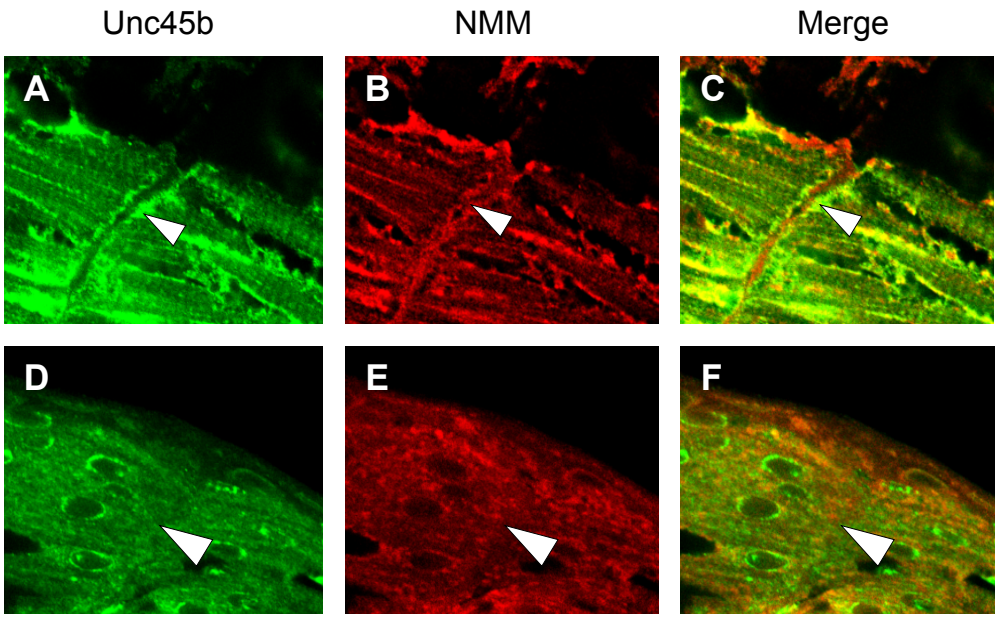

protein stress pathways. For example, overexpression of UNC-45 in *C. elegans* triggers proteosome-mediated protein degradation of muscle myosins (Landsverk et al., 2007). Upstream myogenic transcription factors such as *myf5* and *myoD* are not greatly affected in older *unc45b* mutant embryos (Comyn and Pilgrim, 2012; Wohlgemuth et al., 2007), indicating that the mis-folded protein stress response does not simply induce a general up-regulation of myogenic genes. However, these studies have only examined Unc45b expression in embryos older than 30 hpf, after somitogenesis and the differentiation of myofibers throughout the trunk musculature is complete. It is important to establish whether the increased expression of *unc45b* mRNA in these mutants was triggered exclusively by the accumulation of mis-folded mMHC, or if up-regulation begins before any mMHC is present in the embryo. Embryos were collected in bulk from crosses of heterozygous *unc45b* mutants and *in situ* hybridization was used to examine the qualitative expression of *unc45b*, myosins, or myogenic regulators (Figure 31). PCR genotyping (dCAPS) was used to identify mutants among the stained embryos and for comparison with WT ($n > 10$ for each stage and marker). Even at earlier (11-12 hpf) stages of development, side-by-side imaging of WT and *unc45b* embryos demonstrated significant up-regulation of *myh10* mRNA in mutants (Fig 31A). This up-regulation persisted through the 10-15 somite stage (Fig 31B). The expression of *unc45b* mRNA was affected similarly at both early and later stages (Fig 31C and 31D, respectively), as has been previously reported (Etard et al., 2007). This increase in *unc45b* transcription seen in mutant embryos does not seem to be accompanied by increased protein accumulation, at least as measured by immunostaining (compare Fig 31C and D with Unc45b protein staining in Fig 31). UNC-45 is known to associate with the ubiquitin ligase UFD2a/Ube4B in *C. elegans* (Hoppe et al., 2004; Janiesch et al., 2007), and it is possible that increased expression of the truncated Unc45b protein results in rapid proteosome-mediated degradation of excess Unc45b. Indeed, overexpression of Unc45b in zebrafish results in a reduction of myosin protein expression and organization (Bernick et al., 2010), indicating that Unc45b protein levels are likely to be precisely regulated during development.

As expected, no significant change of mRNA expression was detected for the upstream myogenic transcription factor *myoD* at earlier (11-12 hpf) stages of development (Fig 31E), although staining may have been somewhat increased by the 10-somite stage (~15

Figure 31: Non-muscle myosin and *unc45b* mRNAs are co-up-regulated in early *unc45b* mutant embryos. *In situ* hybridization of embryos at the 5-somite (A, C, E, G, I) and 10-somite (B, D, F, H, J) stages. Approximately 50 embryos were examined for each stage and marker. WT and *unc45b* mutant embryos were identified by dCAPS genotyping. Color development in *unc45b* mutant embryos (right-hand embryo in all panels) was much more rapid than in WT embryos (left-hand embryo in all panels) for non-muscle myosin *myh10* (A, B), indicating up-regulation of mRNA expression. This increase is concurrent with the up-regulation of *unc45b* mRNA expression (C, D). RNA expression of myogenic regulators *myoD* (E, F) and *myf5* (G, H) were not increased detectably in mutants at the 5-somite stage (compare left and right embryos in panels E and G). At the 10-somite stage, *myf5* remained unaffected (H), but *myoD* mRNA expression was somewhat increased in *unc45b* mutants (F), concurrent with the onset of significant muscle myosin expression. *smyhc1* mRNA expression was not affected at either stage (J, I).

Figure 31:

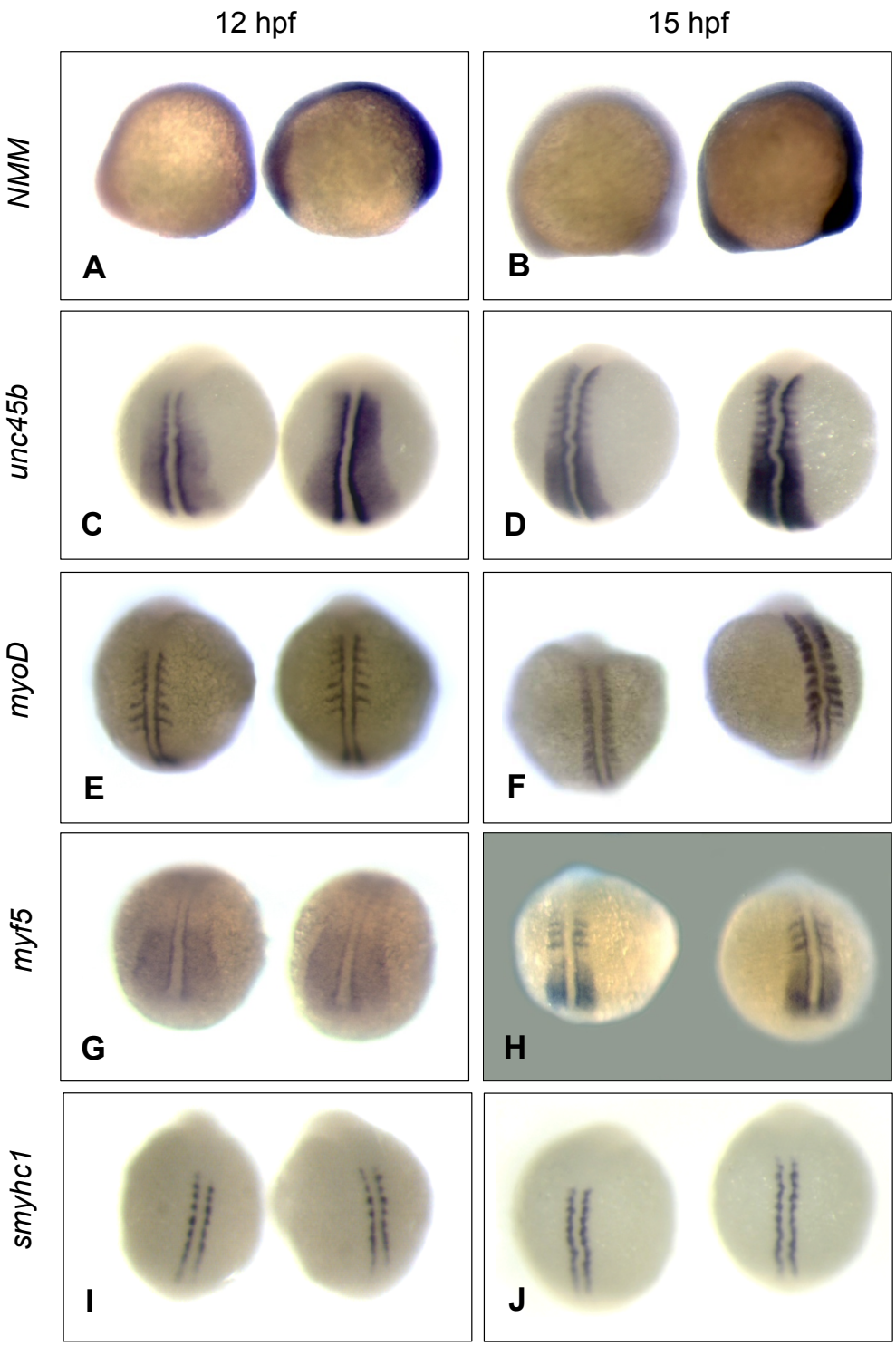

hpf) (Fig 31F). Expression of another upstream myogenic regulator, *myf5*, was not affected at any time point (panels 31G, H), indicating that the up-regulation of *myh10* and *unc45b* mRNA did not merely represent a global increase in myogenesis. The expression of muscle myosins was not affected in mutants at these early stages (Fig 31I, J), and no significant mMHC is detectable at the earliest stages, indicating that the up-regulation of *unc45b* in early mutant embryos cannot be due to the accumulation of mis-folded mMHC, but rather reflects an earlier defect in *unc45b* mutants, possibly relating to the function of NMM.

3.3 Characterization of Novel Motility Mutants in Zebrafish - Implications for the Titin Molecular Ruler Model of Myofibrillogenesis:

It is clear that not all of the factors necessary for early sarcomere patterning have yet been identified, nor what molecular characteristics would allow additional players to be discovered. Genetic screens in animal model systems have served as powerful tools for the identification of new factors involved with developmental patterning pathways; for example, large-scale deletion screens in *C. elegans* (Ahnn and Fire, 1994) have led to the identification of many of the sarcomere components currently known [reviewed by (Moerman and Williams, 2006)]. We can take advantage of similar screens in zebrafish that have previously identified loci involved in muscle development. Of particular interest would be those mutant loci that produce phenotypes similar to known sarcomere components, including defects of motility, muscle organization, heart development and circulation. The most suitable mutant phenotypes should include defects in both heart and skeletal muscle. Mutant lines from past genetic screens that match these criteria include *herzschlag (hel)*, *still heart (sth)*, *slinky (sky)*, and *jam* (Chen et al., 1996; Granato et al., 1996). Of these, only *hel*, *sth* and *jam* were available as stock fish, and preliminary characterization in our laboratory (Wohlgemuth, 2007) suggested that *hel* and *sth* were the most likely to be involved in the early stages of myofibrillogenesis. These previously-uncharacterized motility mutants may represent novel sarcomere/costamere gene mutations, and we thus began to identify the genes containing the relevant causative polymorphisms. As mentioned above (Figure 10), previous low-resolution mapping of these loci has isolated the *sth* mutation to a ~500 kbp region of on chromosome 8, while the *hel* mutation has been isolated to a ~10 Mbp region of chromosome 9 (Geisler et al., 2007). By analyzing published expression data for genes in

these regions [(Thisse et al., 2004); (http:/ZFIN.org)], we were able to limit our initial focus to genes that are specifically expressed in striated muscle. In the case of *sth*, only one such candidate was identified, *smyd1b* (Tan et al., 2006). *smyd1b* is a histone methyltransferase that is expressed specifically in developing heart and skeletal muscle precursors, and targeted knockdown of this gene results in motility defects, eliminated heartbeat and pericardial edema (Du et al., 2006; Just et al., 2011), making this a very likely candidate gene for the *sth* mutation. The broader region containing the *hel* locus contains several candidate genes, including titin, which is already known to play a role in myofibrillogenesis. Zebrafish have two paralogous titin isoforms due to a historical gene duplication event, *ttna* and *ttnb*, which are located in tandem over a ~500 kbp span of chromosome 9, oriented head-to-tail (Seeley et al., 2007). Further microsatellite mapping of the *sth* and *hel* mutant loci at higher resolution (recombination of ~200 individual meioses) has been performed in our laboratory, and confirmed linkage to these two gene candidates; microsatellite SSLP markers that lie very close to *smyd1b* on the zebrafish physical sequence map (Figure 10) segregated with *sth*, while markers lying close to the titin genes segregated with *hel* (Kendal Prill, personal communication).

While these candidates represent known, rather than novel, myofibrillogenesis genes, characterization of these mutations and their phenotypes has the potential to elucidate various outstanding questions regarding the early stages of myofibril formation. Other members of our laboratory are pursuing the *sth* mutation and the role of *smyd1b* in myofibrillogenesis. The *hel* mutation, on the other hand, may present an opportunity to more closely examine the role of titin and the "molecular ruler" model, which is directly relevant to our hypotheses. The *hel* mutant phenotype (Figure 9) includes paralysis of trunk muscle, reduced heartbeat, small head and eyes, and pericardial edema. Since these phenotypic features are all induced by targeted *ttna* knockdown in zebrafish, but not by knockdown of *ttnb* (Seeley et al., 2007), the *ttna* gene was chosen as the best candidate for further analysis and comparison with *hel* mutants.

3.3.1 The *herzschlag* mutation is an allele of the zebrafish *ttna* gene:

The most well-characterized *ttna* mutation in zebrafish is the *pickwick* (*pik*)^{m171} allele, which bears a point mutation within the heart-specific N2B exon of *ttna* (Figure 32),

Figure 32: Schematic diagram of the zebrafish titin gene cassette, showing all exons and introns. A) Diagram of the titin tandem gene cassette on zebrafish chromosome 9. B) Exon diagram of the zebrafish *ttna* and *ttnb* genes. Exons are color-coded to indicate the protein domains they contribute to, including immunoglobulin-like domains (Ig, red), fibronectin-III-like domains (FN-III, white), Z-disk associated repeat domains (Z-repeats, black), the flexible PEKV-rich domain (PEKV, yellow), the C-terminal kinase domain (black), the 3' and 5' UTR regions (grey) and various unique regions (blue). Exons corresponding to the Z-disk, I-band, A-band and M-line segments of titin protein are noted. From (Seeley et al., 2007).

Figure 32:

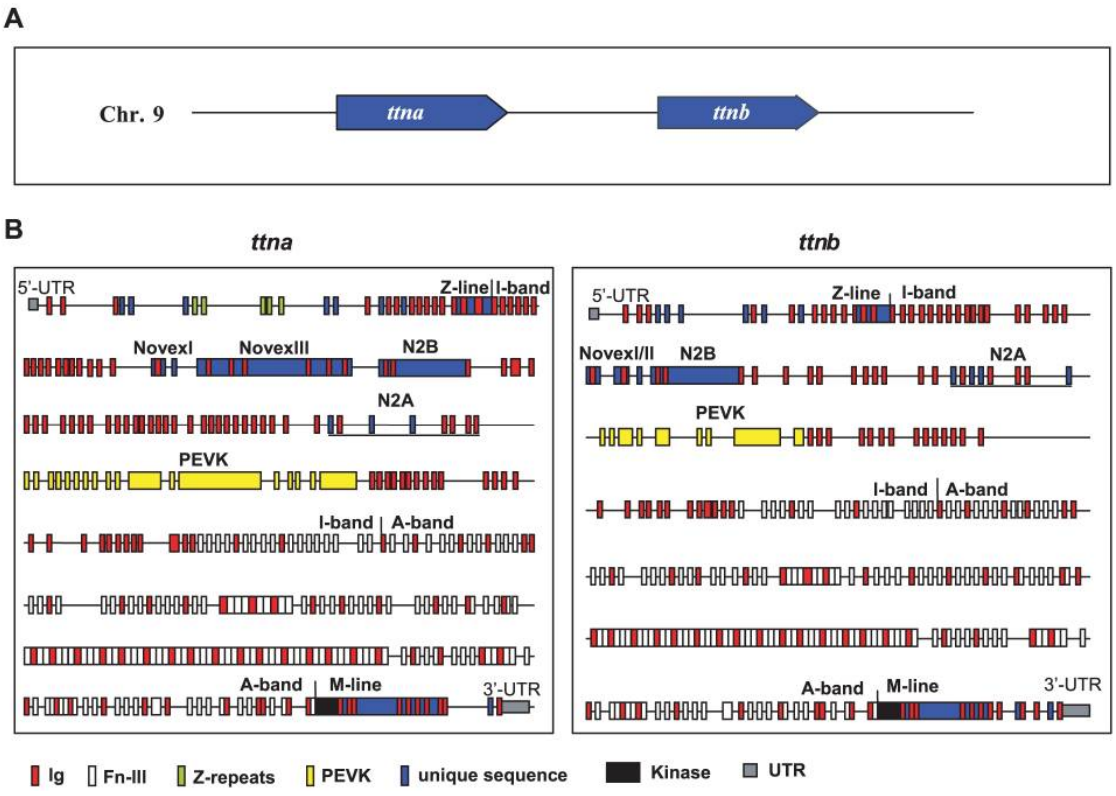
A
Chr. 9
ttna
ttnb
B
ttna
ttnb
5'-UTR
Z-line
I-band
NovexI
NovexIII
N2B
N2A
PEVK
I-band
A-band
A-band
M-line
3'-UTR
5'-UTR
Z-line
I-band
NovexI/II
N2B
N2A
PEVK
I-band
A-band
A-band
M-line
3'-UTR
Ig
Fn-III
Z-repeats
PEVK
unique sequence
Kinase
UTR

creating a premature stop codon in cardiac muscle (Seeley et al., 2007; Xu et al., 2002). This exon is spliced out of *ttna* mRNA in skeletal muscle, and therefore has no effect on skeletal muscle myofibrillogenesis. The specific cardiac phenotype of *hel*, involving a reduction but not complete elimination of heartbeat with severe looping defects, is identical to the cardiac phenotype of *pik*. Since *hel* mutants possess a strong skeletal muscle phenotype in addition to this heart defect, *hel* may represent the first null mutation of *ttna*, affecting titin function in all myogenic tissues. The existence of *pik* as a known *ttna* mutant allowed us to assess the *hel* mutant locus by genetic complementation as mentioned in section 1.6.3, above (depicted diagrammatically in Figure 33A). Heterozygous mutant *hel* +/- and *pik* +/- adult fish were crossed, and the offspring were assessed phenotypically (n = 822 offspring from 4 different individual crosses). As the *pik* mutation creates a premature stop codon in the heart-specific N2B exon of *ttna*, non-complementation would be expected to result in an identical heart phenotype; reduced heartbeat, small head and eyes, and pericardial edema, but no skeletal muscle paralysis (Fig 33B). This was indeed the case; 25% of all larvae from the complementation cross displayed the *pik* mutant phenotype, confirming a failure to complement and Mendelian segregation consistent with full penetrance (Fig 33C). Since neither *pik* nor *hel* alleles display apparent defects as heterozygous larvae or adults, the results of this complementation test demonstrate that the *hel* and *pik* mutations are alleles of the same gene.

Although the *ttnb* gene is neither strongly expressed nor appears to be necessary for normal cardiac function in zebrafish (Seeley et al., 2007; Steffen et al., 2007), it remains possible that the *hel* mutation represents a recessive *ttnb* allele that acts together with the $ttna^{pik}$ allele to produce a heart phenotype. However, co-knockdown of *ttna* and *ttnb* with morpholino-oligonucleotides (MOs) does not create a more severe heart phenotype than the loss of *ttna* alone (Seeley et al., 2007). To directly test this with a *ttna* genetic lesion, we crossed heterozygous mutant *pik* fish together, and injected the resulting embryos with antisense MO against *ttnb*. If the *pik ttna* lesion and the loss of *ttnb* act synergistically to create a phenotype, then we expected greater than 25% of the embryos to display heart defects. This did not occur (Fig 33D); the same percentage of embryos had the heart phenotype as the uninjected controls (n = 84).

Figure 33: The *herzschlag* mutation is an allele of the *ttna* gene. A) Diagram of the complementation cross between the unknown *herzschlag* mutation and the known heart-isoform-specific *ttna* mutant *pickwick*. B) The outcome of the complementation cross demonstrates that the two mutations fail to complement, indicating that the two lesions are allelic. The phenotype of the heteroallelic mutant (top) is indistinguishable from the *pickwick* mutant phenotype (*pik*), displaying pericardial edema, reduced heartbeat, small head and eyes, but with normal locomotion. The complementation cross produced this mutant phenotype with the expected Mendelian ratios (C), whether *hel* males and *pik* females were used, or vice versa (n=822 total offspring from 4 individual, independent crosses). D) the offspring of a cross between *pik* heterozygous parents were injected with a morpholino against the *ttnb* gene. The same percentage of *ttnb*-MO-injected embryos had the *pik* heart defect phenotype as the uninjected controls (n = 84).

Figure 33:

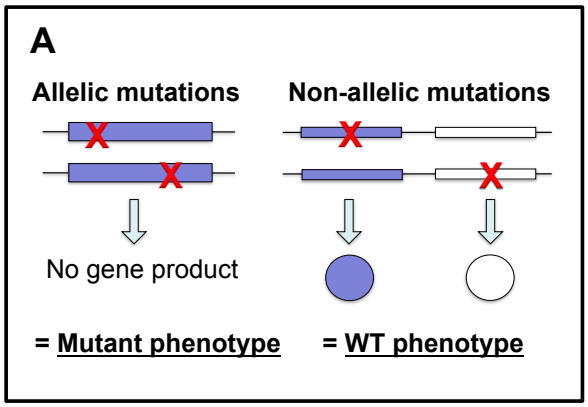

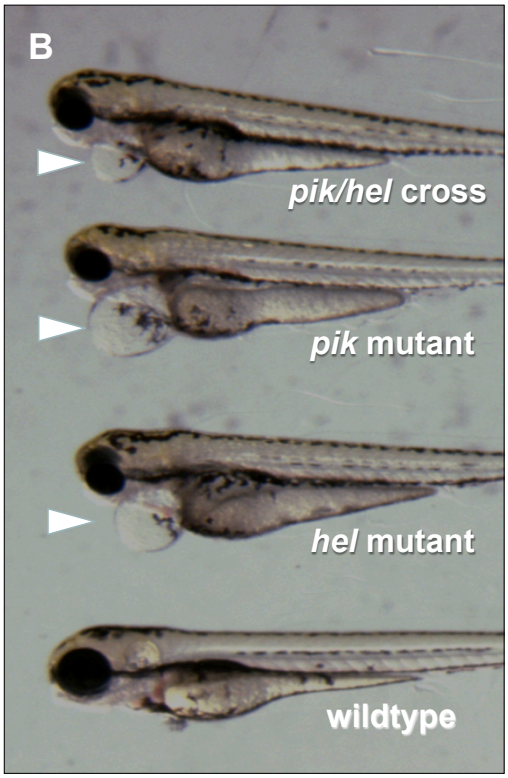

C

pik /hel cross	% wildtype	% mutant
Totals (n=822)	74.9%	25.1%
Expected Ratio (1:2:1)	75%	25%

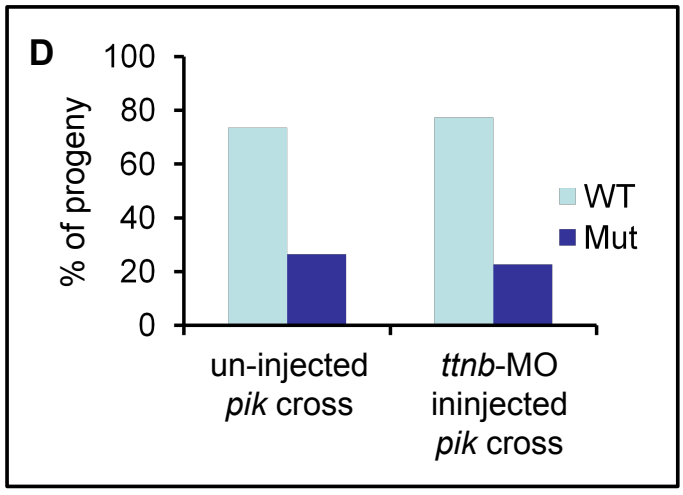

3.3.2 The *herzschlag* phenotype shares features with the mutant phenotypes of other genes involved in myofibrillogenesis:

Several aspects of the *hel* and *sth* mutant phenotypes are reminiscent of other mutants with defects in early myofibrillogenesis, including small eyes and head, heart defects with pericardial edema, reduced muscle birefringence and organization of muscle fibers, and reduced motility (Figure 9). The small head and small eye phenotypes common to several sarcomere mutants in zebrafish may arise from decreased circulation attendant to cardiomuscular defects (Etard et al., 2007; Hawkins et al., 2008; Raeker et al., 2010; Xu et al., 2002). Reduced circulation is also attended by retention of fluid, leading to pericardial edema (Zhu et al., 2013). Consequently, little difference in head and heart defects was noted when comparing *hel* mutants with those showing severe skeletal muscle deficiency due to an independent mutation such as *steif* or *sth* (Fig 9), or those with heart but no skeletal muscle deficiency, such as *pik* (Fig 33B). The small head/small eye phenotype also did not seem to depend upon whether heartbeat was completely absent (*steif, sth*) or merely reduced (*hel, pik*). In embryos older than 4 dpf, pericardial edema in *hel* or *sth* mutants (Figure 34) lead to severe dysplasia of muscular (upper panels) and skeletal (lower panels) elements of the head. Occulomotor muscles were much reduced in size (arrowheads), and the origin of the interhyoideus muscle (arrows) was extremely displaced laterally, with poorly-defined or absent hyoideus muscles posterior to the interhyoideus. Likewise, the ceratohyal cartilage was severely displaced laterally (arrowheads in lower panels), greatly affecting the shape of the jaw. These skeletomuscular phenotypes were not specific to the *hel* and *sth* mutations, and were also seen in other mutants with reduced circulation, such as *steif* (Comyn and Pilgrim, 2012).

In older embryos (>4 dpf) the trunk musculature of *hel* and *sth* embryos was completely disorganized (Figure 11) lacking in muscle fiber striations (Fig 11J, K), indicating a loss of sarcomere organization. Muscle fibers were shortened, universally failing to span the entire somite, with vacuole-like spaces between fibers (arrowheads). Immunofluorescent staining for muscle myosin and sarcomeric actin in *hel* mutants more clearly demonstrates these shortened fibers (Figure 35). As early as 3 dpf, overlapping pattern of myosin and actin striations characteristic of WT muscle tissue (Fig 35A-C) is completely lost in *hel* mutants (compare Fig 35A with 35D, 35B with 35E, and 35C with

Figure 34: The mutant phenotypes of *still heart* and *herzschlag* are characterized by circulation and edema-related defects. Reduced heartbeat in motility mutants results in pericardial edema and dysplasia of muscular (upper panels) and skeletal (lower panels) elements of the head by 5 dpf. Musculature of the head was highlighted by immunofluorescent staining with a general muscle fiber antibody and subsequent 3D reconstruction of optical sections via confocal microscopy (upper panels). Both *sth* (A) and *hel* (B) mutants have smaller eyes and attached occulomotor muscles (arrows) compared with wildtype embryos (C). Additionally, both mutants have laterally displaced interhyoideus muscles with reduced or absent hyoideus muscles, compared with wildtype fish (arrowheads). Alcian blue histochemical staining (lower panels) revealed that ceratohyal cartilages (arrowheads) were also laterally displaced compared to wildtype embryos, with severely truncated lower jaws (arrows).

Figure 34:

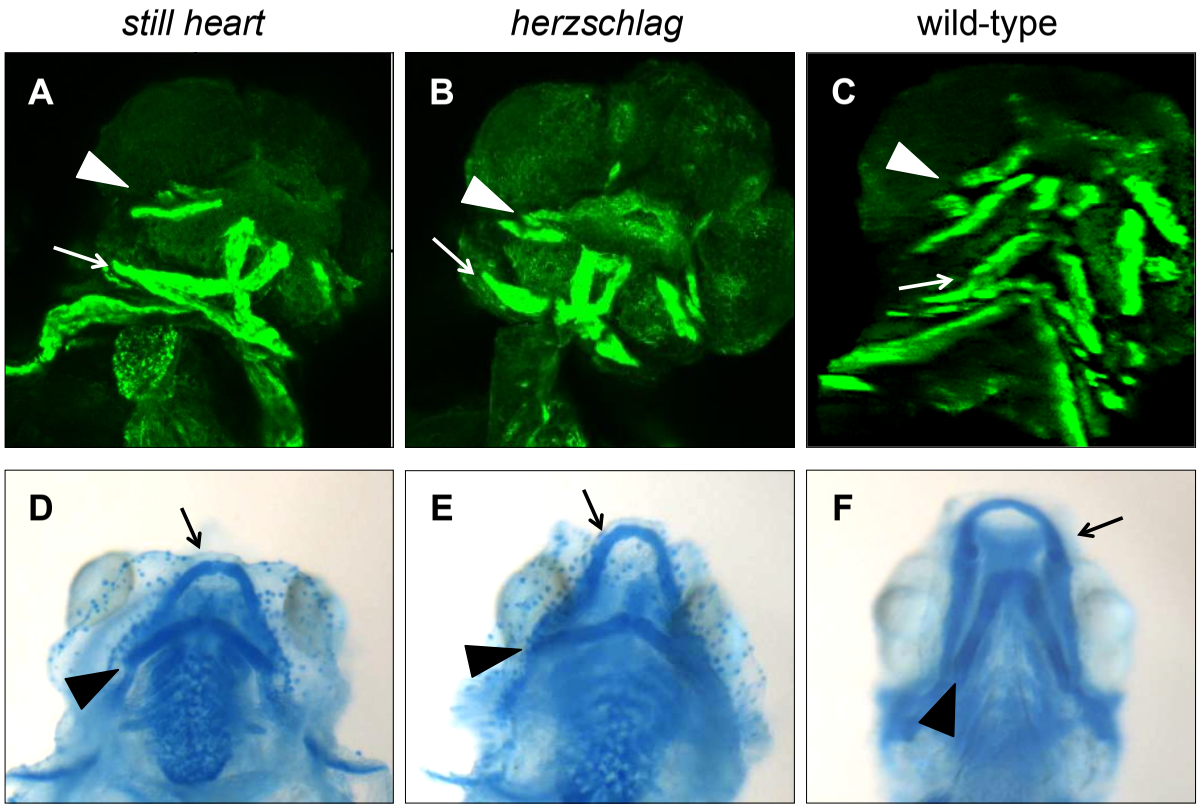

Figure 35: The mutant phenotype of *herzschlaq* is characterized by shortened myofibers and disorganized sarcomeres. Comparison of thick filament myosin and thin filament actin patterning in *hel* mutants with WT embryos at 3 days post-fertilization (dpf). WT muscle myosin (A) and actin (B) create an overlapping pattern of striations that clearly delineates the repeating sarcomeres of myofibrils (C). By contrast staining in *hel* mutants for myosin (D) and actin (E) demonstrates the extreme myofibril disorganization, with greatly shortened myofibers and lateral separations between cells. F) A merged image shows co-localization of myosin and actin in mutant embryos. At higher magnification (G, H), it can be seen that some myosin periodicity (arrow) seems to remain in *hel* mutants (bars in G), but at a much shorter period than in wild-type embryos (bars in H), approximately 0.6 microns compared to ~2 microns in WT zebrafish muscle. The integrity of myosepta was not affected by the *hel* mutation (arrowheads in D, E, and F). This is particularly evident following immunostaining of extracellular laminin in WT (I) and *hel* mutant embryos (J).

Figure 35:

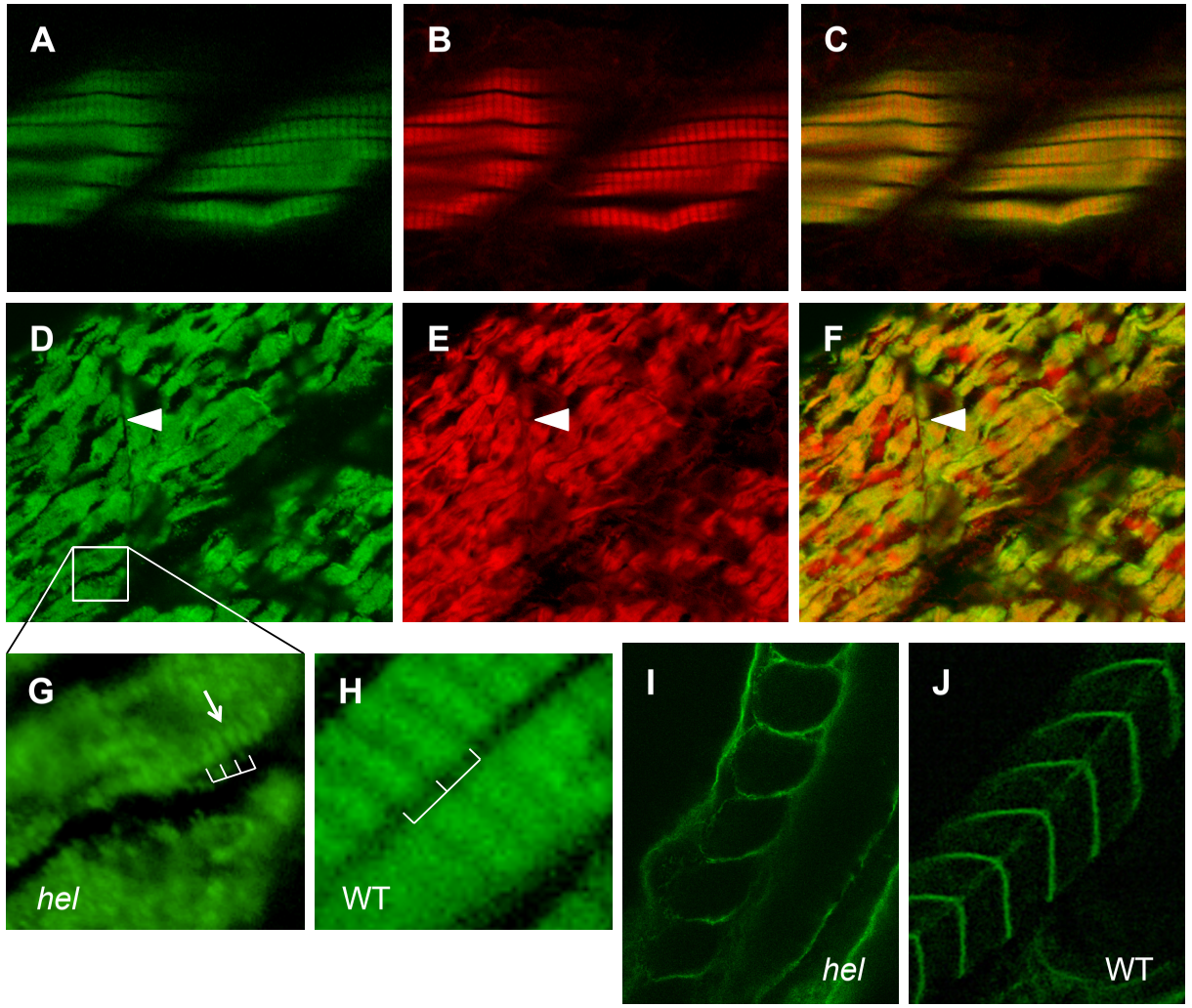

35F). The shortening of muscle fibers is clearly visible in these mutants; however, the integrity of myosepta was maintained in *hel* mutants (arrowheads in Fig 35D, E, F), and immunofluorescent staining of the myoseptum extracellular matrix with an antibody against laminin (Fig 35I, J) showed that the molecular structure of myosepta was unaffected in mutants (Fig 35J), even though myofiber organization was lost. This indicates that the shortened myofibers were physically detached from the myosepta. The loss of myofiber striation and disorganization of fibers within the somite are consistent with the original description of the *hel* phenotype (Granato et al., 1996). However, after digital magnification (Fig 35G, H), immunostaining of thick filament myosin suggested a residual pattern, albeit with a greatly reduced period from normal sarcomere organization (compare bars in 35G with 35H), of ~0.6 microns, compared to the ~2 microns of WT zebrafish sarcomeres. This suggested the possibility that the *ttna* mutation was causing the compression of sarcomeres rather than their destabilization, in view of titin's function as a molecular spring. Indeed, upon closer inspection and despite the original report that *hel* mutants are paralyzed (Granato et al., 1996), early embryos are seen to retain a limited spontaneous twitch response following dechorionation (Figure 36, compare WT movement in videos S1 and S3 with *hel* mutants in videos S2 and S4), rather than displaying total paralysis as in the case of other sarcomere mutants, such as *unc45b/steif* (Etard et al., 2007).

3.3.3 The *hel* mutation lies within the flexible I-band region of ttna; *hel* mutants thus lack the of the titin A-band rod domain:

The *hel* mutation was isolated in a screen using ENU to induce point mutations in zebrafish (Granato et al., 1996). At least 11 missense polymorphisms have been annotated within the coding sequence of *ttna* (ensembl genome database); given the rate of genomic polymorphism in zebrafish, even within inbred strains (~2-5 per 10 kbp (Bradley et al., 2007)), the size of the *ttna* gene (176 kbp and 235 exons in zebrafish (Seeley et al., 2007)) and the difficulty of testing each sequence difference for functional effect, it was important to establish whether *hel* was likely a protein truncation or a missense mutation. Fortunately, peptide-specific antibodies are available to determine whether protein expression of titin still occurs in *hel* mutants. A widely-used polyclonal antibody against the T11 peptide of titin (Barthel and Raymond, 1990), which recognizes the end of the flexible I-band at the I-to-A

Figure 36: *hel* mutant embryos are not totally paralyzed as previously reported when compared to WT control embryos. WT embryos begin twitching from random muscle contractions as soon as the tail becomes free from the yolk, between the 20 and 25 somite stages (video S1). *hel* mutant embryos of the same stage (video S2) retain this random twitch activity, although the movements generated are smaller in magnitude. By 30 hpf, twitching in WT embryos is rapid and involves complete lateral curvature of the body axis (video S3), while curvature in twitching *hel* mutants is severely limited, appearing similar to twitching movements at early stages (video S4). The overall frequency of tail movements is roughly the same in both WT and *hel* mutants of the same stage.

Figure 36:

This figure can be viewed online at the following URLs:

Video S1 - http://youtu.be/Ii7D8rKj6nI

Video S2 - http://youtu.be/D1OX2gf0Kys

Video S3 - http://youtu.be/V6UL9JAC2Z4

Video S4 - http://youtu.be/74yjwQ5n_ao

transition (Fig 37A), failed to produce an immunofluorescent signal in *hel* mutant embryos at 30 hpf, despite strong specific staining in WT embryos of the same stage (compare 37B with 37C and 37F with 37G). However, an antibody against the T12 peptide (Barthel and Raymond, 1990), which is found in the N-terminal region of titin, just parallel to the Z-disk (Fig 37A), consistently showed staining localized to the center of the I-band (arrow in Fig 37H) in both WT and *hel* mutant embryos (compare Fig 37D with 37E and 37H with 37I). Given that single-nucleotide changes are unlikely to affect the folding of large structural peptides to such an extent as to prevent antigenicity, this detection of the T12 peptide in *hel* mutants in the absence of detectable T11 peptide strongly indicates the presence of a truncated protein, likely due to a premature stop codon. The epitope recognized by the T12 antibody has been narrowed to within a 300 kbp region of rabbit *titin* (Tskhovrebova and Trinick, 2002) which corresponds to exons 26-27 in zebrafish (Seeley et al., 2007). This means that the *hel* truncation likely lies somewhere between exons 27 and ~103 (the end of the flexible PEVK domain near the I-A transition) of *ttna*.

3.3.4 New hypothesis: the titin rod domain is not essential for thick filament assembly:

Given the support for the pre-myofibril model of myogenesis from our experiments with Unc45b and NMM, we determined that it would be informative to use the *ttna hel* mutation to examine the role of titin in the initiation of myofibrillogenesis. In the titin molecular ruler model, as discussed in the introduction above, the A-band rod domain of titin is theorized to recruit muscle myosin and act as a scaffold for thick filament assembly. Since titin plays multiple roles in myogenesis, including the stabilization of the Z-disk (Gregorio et al., 1998; Peckham et al., 1997; Turnacioglu et al., 1997), and the maintenance of tension dynamics through the C-terminal kinase domain (Grater et al., 2005; Kontrogianni-Konstantopoulos et al., 2009; Puchner et al., 2008), it is difficult to test this hypothesis. The $(pik)^{m171}$ allele of *ttna*, resulting in heart-specific defects but no skeletal muscle defects, is thus not useful for the analysis of the molecular ruler model. An additional mutant allele of the *ttna* gene, $(pik)^{uw2}$, characterized by Paulus *et al*. (Paulus et al., 2009), has a skeletal muscle phenotype as well as the cardiac phenotype, which suggests a more general truncation of ttna that reduces or eliminates its function in all tissues. The phenotype

Figure 37: The *herzschlag* mutation produces titin protein that fails to cross-react with antibodies specific for the rod domain. Immunofluorescent staining with antibodies directed against specific peptides of the titin protein shows that mutant embryos lack the T11 peptide, found at the I-band to A-band transition, but retain the T12 peptide, which localizes just lateral to the Z-disk. A) schematic diagram of a sarcomere, showing the binding sites of the anti-titin-T11 (blue line) and anti-titin-T12 (purple line) antibodies, relative to the position of a titin molecule (red). Whole-mount WT *hel* siblings (B, D, F, H) and *hel* mutant embryos (C, E, G, I) were identified phenotypically at 30 hpf and stained with antibodies against these respective peptides (green in B-E). Embryos were also counter-stained with fluorescently-labelled phalloidin to show actin organization (red in F-I). Anti-titin-T11 antibody staining was clearly visible in WT embryos (B, F) but not in *herzschlag* mutants (C, G). By contrast, the anti-titin-T12 staining was clearly visible in both WT (D, H) and *hel* mutant embryos (E, I), localizing to the Z-disk as expected (arrow), despite apparent disorganization of the myofibrils (E, I). Artwork generously provided by Alina Pete.

Figure 37:

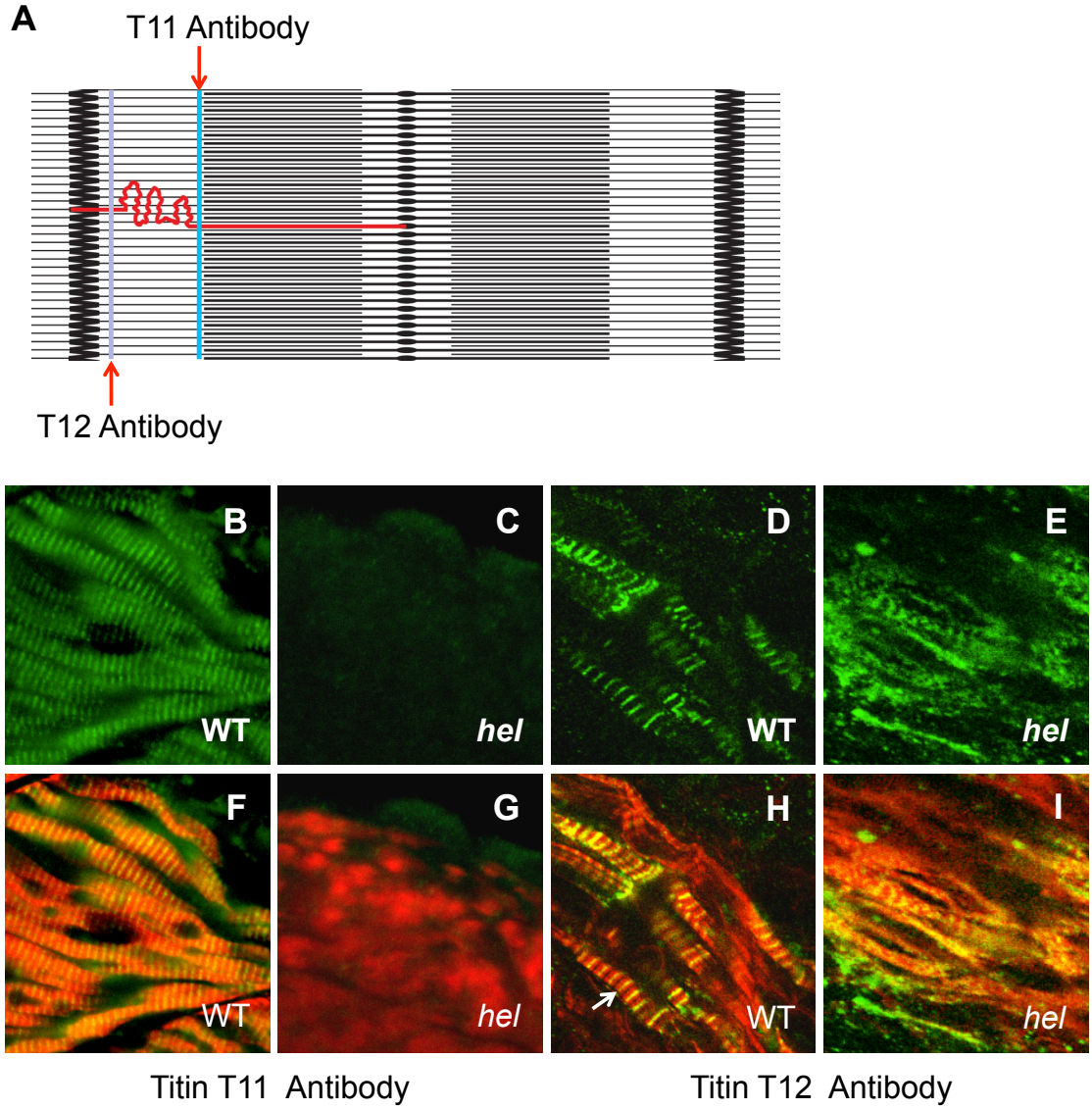
A
T11 Antibody
T12 Antibody
B
WT
C
hel
D
WT
E
hel
F
WT
G
hel
H
WT
I
hel
Titin T11 Antibody
Titin T12 Antibody

of (*pik*)^{uw2} is very similar to the *herzschlag* phenotype, but not as severe in terms of movement or skeletal muscle disorganization. Taken with the broad effects of the *hel* mutation on both cardiac and skeletal muscle, this suggests that the *hel* mutation represents a more extreme truncation of *ttna*. In any case, immunostaining with specific antibodies against different sub-regions of the ttna protein demonstrates that the *hel* mutation represents a truncation of the *ttna* A-band rod domain (Fig 37), making it possible to directly test the titin molecular ruler hypothesis for the first time.

Given the appearance of shortened myofibers with a residual pattern of compressed myosin bands in *hel* mutants (Fig 35G) and the retention of limited muscle function in the heart and trunk (Fig 36), we hypothesize that *ttna* in zebrafish plays a later role in myofibrillogenesis, related to sarcomere stability rather than thick filament formation. This may be further tested in *hel* mutant embryos by examining the progression of myofibrillogenesis in *hel* mutants at early stages of development, particularly during the formation of the thick filament, by myosin antibody staining. If our hypothesis is correct, we expect to see the formation of myosin striations in early *hel* mutant embryos, which will subsequently be lost as contractions in the absence of titin cause sarcomere disassembly.

3.3.4.1 *Herzschlag* mutants display normal myosin thick filament organization during early myofibrillogenesis, despite lacking the A-band rod domain:

Normal myofibrillogenesis in zebrafish is first apparent between the formation of 15-25 somites, beginning in the oldest somites and progressing caudally, as the elaboration of cortical actin at the periphery of elongating myocytes (Figure 38). Once elongation is complete, thick filament myosin immunostaining can be detected in the early myofibrils (Fig 38A). Striations (arrows) are readily apparent in these early fibrils. Within a few hours, myofibrils completely fill the nascent myofibers (Fig 38B and C). The pattern of myosin (Fig 38A-C) and actin (Fig 38D-F) staining corresponds to the thick and thin filaments of individual sarcomeres, respectively. In comparison, myosin deposition at the cortices of elongating myocytes proceeded normally in *hel* mutants (Fig 38G). Surprisingly, these fibers still retained noticeable striations with a normal period for thick filament myosin (arrow), although striations in the actin were not readily apparent (Fig 38J). Myosin accumulation in these cells was somewhat delayed initially, but the pattern of normal A-band striations

Figure 38: Myosin thick filament organization still occurs in *hel* mutants despite the absence of the titin rod domain. *Herzschlag* mutants and wild-type embryos were followed through a time-course of myogenesis, and stained at 24, 30 and 48 hpf with antibodies against slow-muscle myosin (green). In wild-type embryos (A-F), the striations of organized thick filaments can be seen at all time-points throughout myofibrillogenesis (arrows in A-C). Counter-staining with fluorescently-labelled phalloidin to show actin organization (red) reveals a similar pattern of thin filament organization (D-F). In *hel* mutant embryos, the striated pattern of myosin thick filaments was retained at 24 hours (G, arrow). By 30 hpf, myofibers were clearly disorganized (H), but retained a striated pattern of thick filament myosin (arrow). This pattern was only lost completely after 48 hpf (I). Thin filament striations, as show by phalloidin counter-staining, were never visible at any timepoint in *hel* mutant embryos (J-L).

Figure 38:

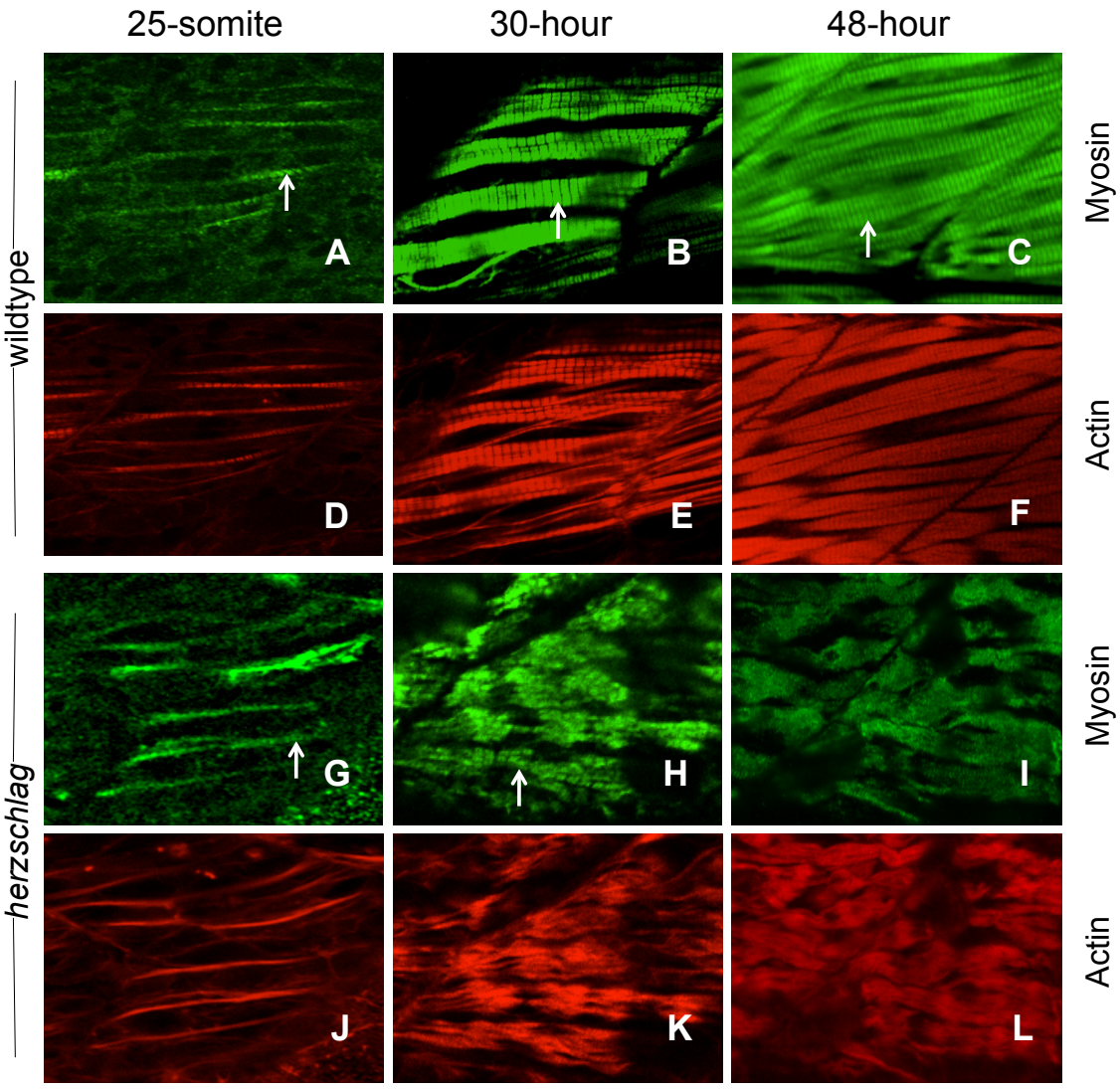
25-somite
30-hour
48-hour
wildtype
herzschlag
Myosin
Actin
Myosin
Actin
A
B
C
D
E
F
G
H
I
J
K
L

persisted at 30 hpf, well after myogenesis was complete (Fig 38H), which may explain the residual movement seen in mutants at 30 hpf mutants (Fig 36). Only after 48 hours did this pattern of myosin striation begin to disappear, as the sarcomeres collapsed (Fig 38I), resulting in the shortened myofibers seen at later stages (compare Fig 38I and 38L to Fig 38F-H). The formation of recognizable thick filament striations in early myocytes shows that normal organization of muscle myosin is initiated during myofibrillogenesis in *hel* mutants, even though they lack the A-band rod domain of titin. Taken together, these results strongly indicate that initial thick filament patterning and assembly does not require the presence of a titin A-band-domain scaffold.

3.3.4.2 The titin paralog *ttnb* does not compensate for loss of *ttna* in zebrafish *hel* mutants:

Due to the presence in zebrafish of a titin paralog, *ttnb*, it was necessary to test whether compensation occurs in *hel ttna* mutants. The *ttnb* gene is predicted to encode a protein which is truncated relative to *ttna*, lacking most of the NOVEX III domain from the flexible I-band region, but containing almost the entire A-band rod domain, which suggests that *ttnb* may have some redundancy with *ttna*. *In situ* hybridization using probes directed against the N2A and N2B exons detects *ttnb* expression in developing striated muscle tissue (Seeley et al., 2007), but this gives no indication whether the A-band rod domain is expressed in these tissues, nor whether protein translation occurs. Furthermore, MO-mediated knockdown of *ttnb* produces only a mild phenotype in skeletal muscle tissue even at very high MO concentrations (Seeley et al., 2007; Steffen et al., 2007), suggesting that *ttnb* may not function directly in myofibrillogenesis. It was therefore important to establish whether expression of *ttnb* could partially compensate for the loss of *ttna* in *hel* mutants, thus accounting for the initial formation of organized myosin thick filaments. We injected *ttnb* MO into the offspring of heterozygous in-crossed $hel^{+/-}$ adults at a variety of concentrations, and assayed myosin thick filament assembly by immunostaining with antibodies for muscle myosin (Figure 39). Even at the highest levels of *ttnb* MO concentration, which had only mild effects on *hel* non-mutant siblings (Fig 39A), thick filament myosin striations were detected in MO-injected *hel* mutants (Fig 39B, arrow). Actin striations as detected by phalloidin counter-staining were also normal in MO-injected

Figure 39: Myosin organization is not disrupted following knockdown of ttnb in hel mutant embryos. *Herzschlag* mutants and WT siblings were injected at the 1-4 cell stage with splice-blocking morpholinos directed against *ttnb* at high concentration, and raised until 30 hpf before fixation and immunofluorescent staining with antibodies against slow-muscle myosin (green, A, C). WT embryos were afflicted with mild defects in motility and some myofiber disorganization, as previously reported. A) myosin striations were mostly normal in injected WT embryos, as were actin striations following phalloidin staining (red, C). In injected *hel* mutant embryos, patterns of myosin striation (B, arrow) appeared identical to uninjected *hel* mutants in all embryos examined (n = 30 mutants). As in uninjected *hel* embryos, actin striations were not visible, though myofibers were still brightly stained with phalloidin (D).

Figure 39:

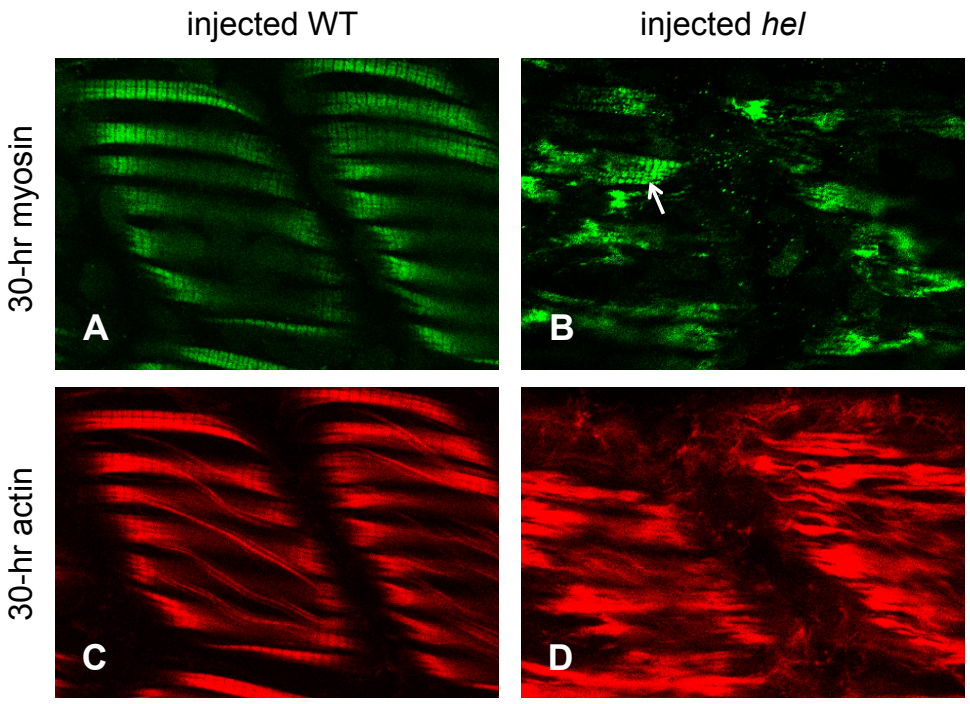

siblings (Fig 39C). These striations were absent in injected *hel* mutants (Fig 39D), exactly as seen in uninjected mutants (Fig 38). These results were the same in all mutant embryos examined by immunostaining (n = 30).

3.3.5 *hel* mutant embryos show M-line deficiencies but retain organization of Z-disks:

The titin C-terminus interacts directly with the M-line protein, myomesin (Obermann et al., 1997), and is thought to be responsible for the recruitment of myomesin to the sarcomere, since mice lacking the C-terminus of titin show defects in M-line assembly (Peng et al., 2005). Titin also plays a role in stabilizing the Z-disk via interactions of the N-terminal domains with Z-disk components, including α-actinin, telethonin and LIM-domain proteins (Gregorio et al., 1998; Zou et al., 2003). The truncated *hel* titin protein is most useful for the study of myofibrillogenesis if it retains N-terminal functions related to the Z-disk while losing the C-terminal A-band domains. To test whether the *hel* mutation results in the loss of C-terminal functions of titin while retaining N-terminal functions, we examined the integrity of different regions of the sarcomere at 30 hpf, using immunofluorescent staining of α-actinin as a marker for the Z-disk and of myomesin as a marker for the M-line (Figure 40). In WT embryos, α-actinin localizes to the Z-disk (Fig 40A), demonstrated by counter-staining for actin, which labels the entire I-band (Fig 40C). Staining of α-actinin was localized to the center of the I-band (insert), with non-staining gaps between I-bands marking the M-line (arrow). In *hel* mutant embryos, myofibrils were disorganized as shown in Figure 38; however, a regular striated pattern of α-actinin remained detectable (Fig 40B, 40D). Myomesin staining localized to the M-line in wild-type embryos (Fig 40E), corresponding to the gaps between actin I-bands (Fig 40G, arrow). In *hel* mutants, the immunofluorescent staining of myomesin was completely lost (Fig 40F, 40H), indicating that myomesin was either not expressed or scattered throughout the cells in *hel* mutant muscle. This result is in keeping with the hypotheses that C-terminal titin peptides are required for recruiting myomesin to the M-line, and strongly supports our conclusion that *hel* mutants lack the C-terminal region of *ttna* due to the truncation mutation.

Figure 40: Localization of myomesin but not α-actinin is lost in the titin truncation mutant. Wild-type (left) and *herzschlag* mutant embryos (right) were examined at 30 hpf to determine the effects of titin truncation on the organization of specific regions of the sarcomere. Integrity of the Z-disk was assessed by immunofluorescent labelling of α-actinin (A-B), while integrity of the M-line was assessed by labelling of myomesin (E-F). All markers can be seen in their normal arrangement in WT embryos when merged with a phalloidin counter-staining to show actin (red), which leaves a narrow gap at the M-line (arrows). Narrow bands of green fluorescence correspond to the Z-disk for α-actinin (C, insert) and the M-line for myomesin (G, insert). In *hel* embryos (right), expression of α-actinin was detected (B), and sarcomere organization was reduced as in Figure 38, with α-actinin striations detectable in some myofibers (D, insert). By contrast, myomesin localization was not detectable in *hel* mutant embryos at all (F, H).

Figure 40:

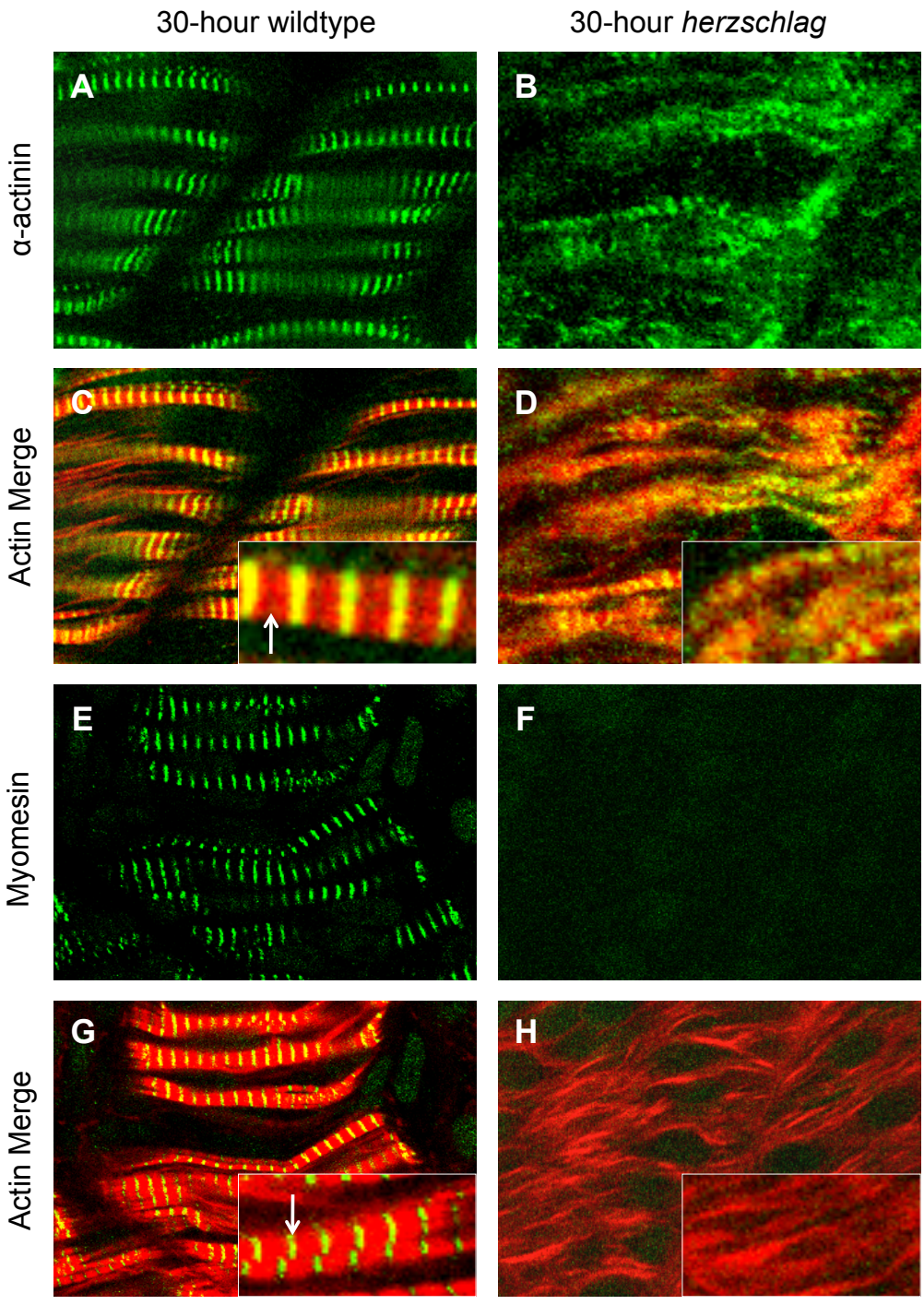
30-hour wildtype
30-hour *herzschlag*
α-actinin
Actin Merge
Myomesin
Actin Merge
A
B
C
D
E
F
G
H

3.3.6 Expression of stress responsive chaperones that are up-regulated in response to myosin misfolding is not affected in *hel* mutants:

The myosin chaperones Hsp90a1 and Unc45b, which are both up-regulated in response to protein-denaturing stresses such as heat-shock, also show up-regulation of transcripts in zebrafish mutants that have deficiencies in myosin folding and thick filament assembly (Comyn and Pilgrim, 2012; Etard et al., 2007; Peng et al., 2005). This increased expression of myosin-specific chaperones likely occurs in response to the aggregation of misfolded or disorganized myosin during myofibrillogenesis in thick filament assembly mutants, as is known to occur for other substrate-specific chaperones (Lisse et al., 2008; Vleminckx et al., 2002). In order to determine whether the *hel* mutation results in the misfolding or aggregation of disorganized myosin during early myofibrillogenesis due to loss of the proposed myosin scaffold, we performed *in situ* hybridization to qualitatively assess increases in mRNA expression for these myosin-specific chaperones (Figure 41). Expression of *hsp90a1* was detected throughout the trunk muscle of 24 hpf embryos, outlining the somites (Fig 41A). By 36 hpf, expression was mostly restricted to the caudal-most somite tissue (Fig 41B). In *hel* mutants, the pattern of *hsp90a1* mRNA in 24-hpf embryos was not distinguishable from WT embryos (Fig 41C). At 36 hpf, there was still little difference between WT and *hel* mutant embryos (compare Fig 41B with 41D), although the region of caudal expression was somewhat expanded to include more somites (arrow). This expanded expression was localized to a few somites, and did not represent a global increase in mRNA levels; as such, it likely corresponds to a delay in development, rather than an increase in response to protein aggregation. Similar results were obtained for *unc45b* expression. WT embryos expressed *unc45b* mRNA throughout the developing trunk muscle at 24 hpf (Fig 41E), constricting to somite boundaries and caudal somite tissue by 36 hpf (Fig 41F). An identical pattern of expression was seen in *hel* mutants at both 24 hpf (Fig 41G) and 36 hpf (Fig 41H), with a slight expansion of the darker-staining caudal somites at 36 hpf (arrow in Fig 41H). These results demonstrate that no misfolding or aggregation of myosin (which is known to trigger chaperone up-regulation) occurs in *ttna* mutants until 36 hpf or later, further supporting the hypothesis that myosin thick filament assembly occurs independent of the presence of the titin rod domain.

Figure 41: Stress-responsive gene expression is not increased in *hel* mutant embryos during early myofibrillogenesis. Expression of myosin-folding stress-responsive chaperone genes *hsp90a1* (A-D) and *unc45b* (E-H) did not significantly change in *hel* mutant embryos (C-D and G-H) when compared with wild-type controls (A-B and E-F). Increased mRNA expression of stress-responsive genes was assessed by *in situ* hybridization at 24 (left) and 36 hpf (right). At 24 hpf, when increased expression of myosin chaperones is expected in mutants with myosin assembly defects that result in accumulation of misfolded protein, no qualitative change could be detected between WT and *hel* mutant embryos for either chaperone gene (compare A with C and E with G). Even at 36 hpf, expression was not greatly increased (compare B with D and F with H), although the extent of mRNA expression in the tail somites was somewhat greater in mutants (arrows).

Figure 41:

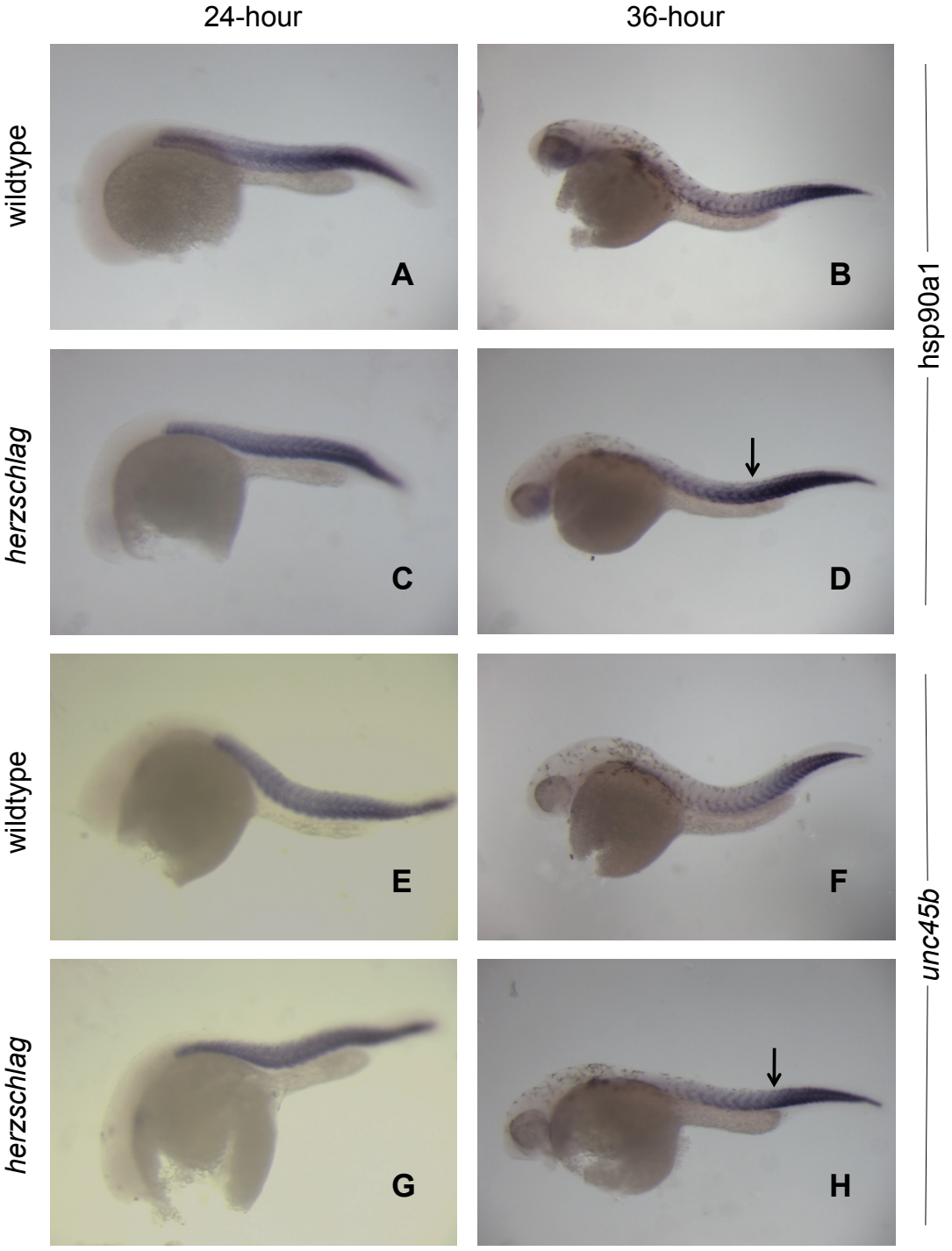
24-hour
36-hour
wildtype
herzschlag
wildtype
herzschlag
A
B
C
D
E
F
G
H
hsp90a1
unc45b

3.3.7 In the absence of contractile signals, myosin and actin filaments in *hel* mutant cells are less disorganized.

I suggest that the lack of a titin A-band rod domain in *hel* mutants does not impede the initial folding and assembly of myosin into organized thick filaments. Instead, given the apparent compression of sarcomeres that are observed in later *hel* mutant embryos (Fig 35G), and the known role of titin in returning the sarcomere to resting length after contraction, the loss of sarcomere integrity and break-down of myofibrils observed in older *hel* mutants (Fig 35D-F) may be due to the loss of titin`s molecular spring function. While the flexible I-band may not be lacking in *hel* mutants, the strong anchoring of titin within the sarcomere through the many Ig- and FN-like domains located within the A-band may be essential for the long-term stability of sarcomeres in response to contraction. To test this, I used our seZEB culture system to examine embyronic myocytes from individual *hel* mutant embryos in standard media, lacking any contractile stimulation (Figure 42). The genotype of individual cultures was assessed by PCR amplification of SSLP markers that were determined to be closely linked to the *hel* locus. Myosin thick filament striations were readily detectable by immunostaining in WT cultures (Fig 42A). Myocytes in *hel* mutant cultures also formed myosin thick filaments with a recognizable banding pattern, and the striations maintained a similar period to WT cultures even after 5 days of culture (Fig 42B). Actin counterstaining also clearly demonstrated the retention of sarcomere spacing in *hel* mutant cultures compared to WT (compare Fig 42C and 42D). This is in stark contrast to the sarcomeres of whole mutant embryos even at 30 hpf (Figure 38). The greater retention of sarcomere organization in the absence of contractile signals, taken with our other findings, suggests that it is the loss of titin`s molecular spring function during muscle contraction that results in the disassembly of sarcomeres in *hel* mutants, rather than any scaffolding function during myofibrillogenesis.

Figure 42: *hel* mutant myocytes that are not subject to contractile signals in culture retain sarcomere organization. Dissociated blastomeres from individual WT (left) and *hel* mutant (right) embryos were cultured on laminin substrate to induce myogenesis for 5 days prior to fixation. Individual cultures were genotyped by PCR to confirm the identity of mutants and siblings. Immunofluorescent staining for myosin (green, A and B) and phalloidin counter-staining for actin (red, C and D) demonstrated relatively normal sarcomere patterning in mutants as compared with WT (compare banding patterns in A with B and in C with D). Overall reduced sarcomere organization was reduced in mutants, but to a much lesser degree than even 30-hpf mutant embryos. Myosin A-band and actin I-band patterning with the standard sarcomere period could be readily discerned in all cultures (B, D).

Figure 42:

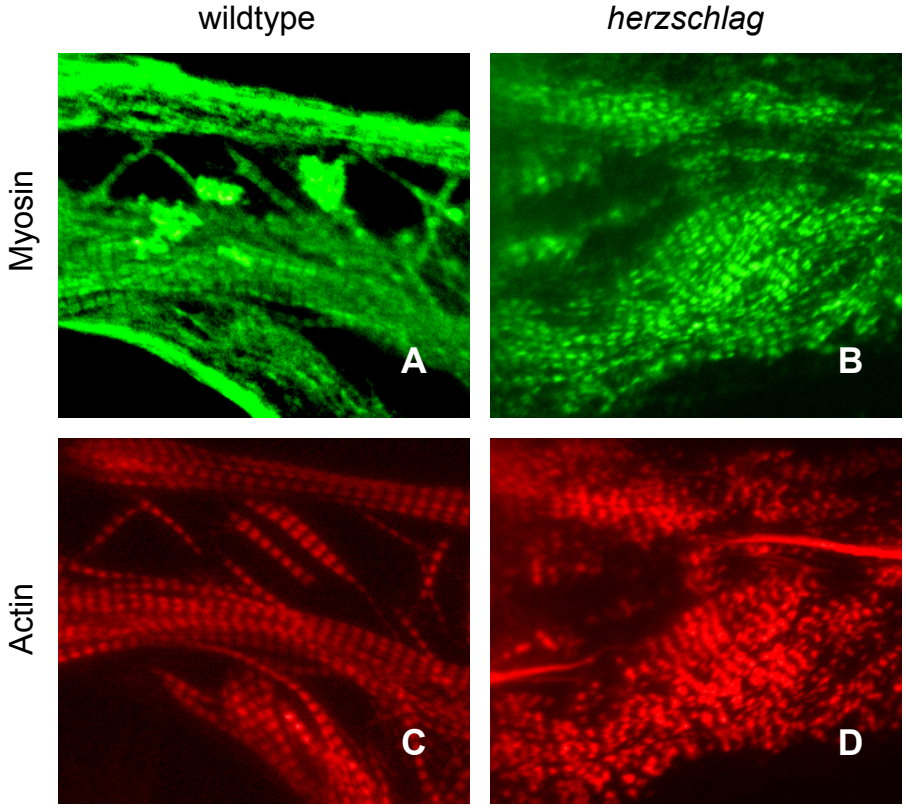

4. DISCUSSION:

4.1 The early role of Unc45b in myofibrillogenesis - *in vitro* evidence:

A number of lines of evidence support an earlier role for Unc45b in myofibrillogenesis, challenging the previous view that Unc45b merely plays the part of a muscle myosin co-chaperone. This evidence includes the NMM-mediated activity of Unc45b in early *C. elegans* embryos (Kachur et al., 2004; Kachur et al., 2008), expression of dUNC-45 in early blastoderm and later Z-disk localization in *Drosophila* (Lee et al., 2011b), Z-disk localization and myofiber attachment defects in *steif* mutant zebrafish (Etard et al., 2007; Etard et al., 2010), and the reports of an earlier expression profile in zebrafish and *Xenopus* (Geach and Zimmerman, 2010; Wohlgemuth et al., 2007). To assess whether early Unc45b activity during myofibrillogenesis is necessary, we began by looking at the myogenic differentiation of zebrafish blastomeres in culture from WT and *unc45b* mutant embryos. This first required the optimization of cell culture methods for deriving ZEB cultures from single embryos, a system which could prove very useful for developmental studies of myogenesis in cell culture.

4.1.1 Development of the seZEB cell culture system for the study of myofibrillogenesis:

Previous studies have made use of the ZEB culture protocols established by Collodi *et al*. (Collodi et al., 1992) for the study of zebrafish muscle cells in culture, although little emphasis has been put on the molecular mechanisms of myogenic differentiation in these cells. In other vertebrate developmental models, cellular differentiation studies have generally focused on easy-to-maintain cell lines such as mouse C2C12 or tumor-derived cells. While fibroblast-like cell lines of this type are highly competent for myogenic differentiation in culture, these cells have the disadvantage of being selected for immortality (or at least continued proliferation after repeated passaging), which likely result in altered genetic programs and/or aneuploidy. The variation from WT gene expression in these lines is generally not examined (Capes-Davis et al., 2010). By contrast, primary cell culture using ZEB protocols seems a preferable method for the study of gene expression in cultures undergoing myogenic differentiation. Primary cell culture methods are well-established for

many vertebrates; however, zebrafish have the advantage of being a relatively inexpensive and therefore widely-used model for genetic manipulation. The use of microinjection to introduce RNA or DNA for overexpression studies, transgene vectors for genomic insertion, or antisense oligonucleotides for knock-down experiments make these organisms one of the most versatile genetic models currently in use (Ackermann and Paw, 2003; Patton and Zon, 2001). Further, the wide availability and wealth of mutant and transgenic zebrafish lines means that a large number of genes thought to be involved in myogenic differentiation could be studied using our single-embryo cell culture system.

4.1.1.1 Optimization and characterization of myogenesis in seZEB cell cultures:

Un-determined mesenchymal cells from vertebrate embryos have been shown to assume a fibroblast-like phenotype in cell culture and undergo spontaneous myogenic differentiation, under a variety of culture conditions (Dayton and Hathaway, 1991; Tamaki et al., 2007). Even mature, differentiated cells of mesenchymal origin can be induced to undergo dedifferentiation and subsequent myogenesis in culture (Geoghegan and Byrnes, 2008). Some culture conditions, however, can minimize or eliminate myogenic differentiation in mesenchymal cell cultures. For example, too high or too low cell density (De Angelis et al., 1998; Lindon et al., 2001), trophic factors such as TGF-ß family members (Filvaroff et al., 1994; Pirskanen et al., 2000), and improper cell culture substrates (von der Mark and Ocalan, 1989) can all affect myogenic differentiation and even prevent myogenesis from occurring in culture. Our results establish a set of favorable conditions for single-embryo cultures to undergo myogenic differentiation in terms of culture method, substrate, and media. Although previous studies have made use of few media supplements for ZEB primary culture, most commonly bovine serum and zebrafish embryo extract alone (Fan and Collodi, 2006; Ghosh and Collodi, 1994; Helmrich and Barnes, 1999), we found that both insulin and carp serum had a profound impact on the proliferation and differentiation of ZEB cultures, to the extent that a single blastula-stage embryo was capable of proliferating and differentiating .

We have also established that seZEB cultures did not express ectodermal markers, consistent with a uniformity of mesenchymal cell-type. Although ectoderm-inducing factors are present in the zebrafish yolk even prior to fertilization (Ober and Schulte-Merker, 1999),

the dilution of these factors during the dissociation of the embryo may prevent ectodermal or chordamesodermal specification. It is also known that embryonic fibroblast cultures of mesenchymal origin can be induced to undergo other types of cellular differentiation, including endothelial (Tamaki et al., 2007; Wang et al., 2006), and hematopoietic differentiation (Keller et al., 1993). Under the conditions and methods outlined here, endothelial markers were not detected, further demonstrating the uniformity of cell type in single-embryo cultures under our specific culture conditions. It is noteworthy that some myogenic cells were flattened and single-nucleated, while others were multinucleated cell bundles. Slow muscle precursors in zebrafish are larger, flattened, and single-nucleated, and found at the periphery of the myotome (Devoto et al., 1996; Roy et al., 2001), and the two myogenic cell populations in our culture system could thus represent regionalized slow-muscle and fast-muscle differentiation. However, immunofluorescent staining using fast-muscle- or slow-muscle-specific anti-MHC antibodies resulted in similar staining patterns in both types of myocytes. This may indicate that our ZEB myocytes express both isoforms, as has been previously reported in early embryonic muscle in zebrafish (Bryson-Richardson et al., 2005).

4.1.1.2 Usefulness of the seZEB cell culture system as a model for developmental cell biology:

The microinjection of antisense oligonucleotides for knock-down of genes involved with myogenesis prior to cell culture is a useful tool for developmental genetics, and it is noteworthy that the injection of *unc45b* morpholinos resulted in a phenocopy of the *steif* mutant phenotype in cells derived from nearly 100% of embryos cultured. The fact that any stress from microinjection resulted in only a 15-20% reduction in viability and differentiation indicates the feasibility of routine knock-down experiments in the seZEB culture system. Moreover, microinjection with a GFP reporter construct prior to culture resulted in detectable GFP expression under the control of a myocyte-specific promoter. These experiments show that both up-regulation and down-regulation of gene expression can be achieved in zebrafish embryos prior to cell culture with a high success rate. Further, it is possible to drive ZEB cultures towards alternate cell fates, such as smooth muscle (Norris et al., 2000), by the addition of specific trophic factors to the cell culture media. Sun *et al*. (Sun

et al., 1995) have also observed the differentiation of ZEB cells into morphologically-identifiable neurons and astrocytes following two weeks of culture in the presence of sodium selenite on poly-D-lysine substrates, and Collodi *et al*. (Collodi et al., 1994) have detected hepatocyte P450 in ZEB cultures treated with 10 nM TCDD (2,3,7,8-tetrachlorodibenzo-P-dioxin). Although these methods are not well-characterized outside of mammalian cells, and attachment on non-laminin substrates was limited in our seZEB cultures (Fig 1B), these studies suggest that it may be possible to expand the usefulness of the seZEB culture system for studies of genetic mechanisms of differentiation and development in a wide variety of cell and tissue types. Future studies may therefore focus on the development of zebrafish-specific markers and methods for characterizing the differentiation of seZEB cell cultures into alternate cell fates. In any event, the ability to examine cellular differentiation in isolated, pluripotent cells in monolayer, which can be easily and instantly treated with pharmacological reagents and viewed in real time, without immobilizing live embryos, is of singular value. Moreover, cultures from *unc45b* mutant embryos demonstrated that mutations that are zygotic lethal when homozygous in whole embryos do not necessarily impair the ability of cells in seZEB cultures to undergo myogenic differentiation to the point of phenotypic identification. Therefore, zebrafish strains possessing early embryonic lethal mutations in genes of interest could potentially still be used for the study of cellular differentiation *in vitro* by our methods. This represents a major advantage of the seZEB culture system, which permits the examination of mutant cells in culture that could not be obtained from early embryonic lethal larval fish. However, the limitations of this technology are very clear: cells in culture are by definition removed from their normal embryonic context, are therefore only useful for studying processes which are cell-autonomous and for which culture conditions have been at least partially defined.

4.1.2 Myofibrillogenesis in *unc45b* mutant cultures fails from the outset, though myocyte morphology was not affected:

The expression of Unc45b during myogenesis has been reported to occur quite early in whole zebrafish embryos, beginning at ~9 hpf, prior to any myoblast elongation or fusion, or to the organization of sarcomeres in striated muscle (Etard et al., 2007; Wohlgemuth et al., 2007). This was confirmed in our culture system, as expression of transcripts for *unc45b*

and the early muscle transcription factor MyoD were detectable at high levels within 24 hours of plating, indicating only a short (~12 hour) delay in developmental timing of gene expression due to cell stress and the substrate attachment period. The absence of functional Unc45b is known to lead to decreased myofibrillogenesis and sarcomere organization in *steif* mutant zebrafish (Etard et al., 2007) and *unc45b* morphants (Wohlgemuth et al., 2007), which is consistent with our results showing actin disorganization in cultured mutant cells. Despite the early onset of *unc45b* expression, cells in *unc45b* mutant cultures still became elongated and multi-nucleated, and displayed increased actin expression, suggesting that Unc45b is not required for the early stages of myoblast alignment and fusion. However, the persistence of actin stress fibers in newly-differentiated mutant cells, and the appearance of actin punctae throughout elongated myocytes, suggest that the lack of Unc45b affects actin dynamics during the earliest stages of myofibrillogenesis. The pre-myofibril model is based on the reported growth of actin stress fibers into early myofibrils (Manisastry et al., 2009; Rhee et al., 1994; Sanger et al., 2005), and the persistence of stress fibers in elongated myocytes in *unc45b* mutant cultures is thus consistent with our hypothesis that Unc45b plays a role in these early stages of myofibrillogenesis. Moreover, the lack of organized myosin in any mutant culture examined suggests that the formation of actin punctae is not indicative of the eventual breakdown of organized myofibrils, but rather the failure of myofibrils to form.

Despite the cell detachment phenotype seen in whole *unc45b* mutant embryos, we saw no evidence of substrate attachment deficiencies in mutant cultures. This may simply reflect the differences between native ECM organization and the over-abundance of laminin substrate provided in cell culture, or it could point to an increased necessity for myofiber tension in whole embryos that cannot translate to individual cultured cells. Given the limitations of cell culture models, these experiments were unable to address these questions regarding the effects of *unc45b* mutation on costamere attachment. We were also unable to address the timeline of gene expression as would be seen in specific tissues during development. To elucidate these subjects, we thus also examined the spatial and temporal patterns of *unc45b* and myosin mRNA expression and protein localization in whole zebrafish embryos, and the effects of *unc45b* mutation on NMM protein localization, α-actinin nucleation, and costamere organization in intact muscle tissue.

4.2 The early role of Unc45b in myofibrillogenesis - whole embryo studies:

This is the first study to examine the involvement of vertebrate Unc45b in early sarcomere development, during the initial stages of myofibril formation, rather than focus on its role as a chaperone to mMHC. Through *in situ* mRNA analysis and antibody staining of protein localization in whole embryos, we have demonstrated that Unc45b expression commences long before the onset of mMHC production in both pre-somitic and segmental plate tissues, corresponding to differentiating myoblasts that are undergoing elongation and the establishment of costamere attachments. This supports our first hypothesis, regarding the timeline of Unc45b expression in zebrafish. We have also shown and that significant up-regulation of *unc45b* transcription in mutants also precedes the onset of mMHC expression, ruling out mMHC misfolding as the trigger for the previously noted increased chaperone and co-chaperone expression. Given the involvement of Unc45b homologues with non-muscle myosin function in invertebrates outlined above, our findings propose a mechanism of Unc45b activity during myogenesis that is consistent with the pre-myofibril model of myofibrillogenesis, whereby Unc45b is involved with the assembly of NMM pre-myofibrils. Our results also show that the loss of Unc45b function results in costamere deficiencies in the early embryo, which were concurrent with the loss of NMM localization to the costamere. This is consistent with the necessity for NMM function during substrate attachment and the subsequent stabilization of costameres, further supporting the model above, that the early myogenesis defects in *unc45b* mutant zebrafish involve processes that are mediated by NMM. These data also support our second hypothesis, that loss of *unc45b* should result in costamere defects.

4.2.1 Possible chaperone activities of Unc45b during early myofibrillogenesis:

Vertebrates possess two distinct UNC-45 genes, reported to be a general-cell isoform (Unc45a) and a striated-muscle-specific isoform (Unc45b) (Price et al., 2002). It was assumed that the general-cell isoform mediates any NMM-related UNC-45 chaperone function during cytokinesis, due to the fact that targeted knockdown of Unc45a results in decreased cell proliferation in cell culture (Price et al., 2002). However, little evidence exists to demonstrate interactions between Unc45a and specific NMM proteins, and zebrafish *unc45a* null mutants do not display any NMM-related defects (Anderson et al., 2008). A

double null mutation of *unc45a* and *unc45b* has no additive phenotype (Comyn and Pilgrim, 2012), which further supports the notion that Unc45a does not mediate NMM-specific activity during myogenesis, and that compensation does not occur between Unc45a and Unc45b in null mutant embryos. Unc45b has been shown to act as an Hsp90 co-chaperone, mediating the assembly of thick filament myosin in muscle tissue, and is known to interact with both Hsp90 and MHC *in vivo* and *in vitro* (Ao and Pilgrim, 2000; Barral et al., 2002; Srikakulam et al., 2008). The expression of specific molecular chaperones often briefly precedes the expression of their target substrates during development. For example, Hsp90a1 expression can be detected in zebrafish adaxial cells at the 5-somite stage throughout the pre-somitic mesoderm (Rauch, 2003), even though the expression of mMHC at this stage was limited to the somites and anterior-most presomitic mesoderm. However, given that the expression of Unc45b significantly preceded not only mMHC production, but also the earliest reported Hsp90a1 expression in both adaxial cells and segmental plate mesoderm, the early expression of Unc45b is consistent with a non-mMHC-related role in early myogenesis.

Other Hsp90 genes are expressed somewhat earlier in development, prior to the expression of mMHC. *hsp90a2* expression, for example, commences as early as the 2-somite stage at low levels in adaxial and segmental plate mesoderm, while *hsp90ab1* is expressed ubiquitously as early as the 2-cell stage (Rauch, 2003). Stabilization of costamere components by Hsp90 beta isoforms has previously been shown, specifically ILK and integrins (Aoyagi et al., 2005; Liu and Li, 2008). Mouse cell culture experiments have demonstrated that alpha and beta forms of Hsp90 can both interact with Unc45b (Srikakulam et al., 2008). However, the depletion of the Hsp90a1 isoform has the ability to phenocopy at least the later effects of Unc45b knockdown in zebrafish (Etard et al., 2007), while depletion of Hsp90a2 or Hsp90ab1 do not, suggesting that the Hsp90a2 and Hsp90 beta isoforms do not contribute significantly to the *unc45b* mutant phenotype. Still, we have not ruled out the possibility that the early role of Unc45b at least partly involves a Hsp90a2-mediated interaction with NMM, or an Hsp90ab1-mediated stabilization of ILK and/or integrins at the costamere that may or may not involve interaction with NMM. In addition, Unc45b binds to Apobec2 *in vitro*, which co-localizes with Unc45b at the Z-line in older embryos, but not in *Unc45b* mutants (Etard et al., 2010). Apobec2, a blocker of TGF-β signalling, is expressed

earlier than muscle myosins in developing somites (Thisse et al., 2004), and the loss of costamere organization in *Unc45b* mutants may therefore involve binding with Apobec2 rather than Hsp90, or both, although the potential role of Apobec2 in costamere stabilization is unknown.

4.2.2 Implications of the early role of Unc45b for the pre-myofibril model of myofibrillogenesis:

The precise involvement of non-muscle myosins during early myofibrillogenesis remains somewhat controversial. Periodic banding of cortical actin stress fibers with non-muscle myosin IIB in newly-fused myotubes has been well-documented (Du et al., 2003; Du et al., 2008a; Sanger et al., 2005; Sanger et al., 2009), yet knockout of NMMIIB in mice does not seem to inhibit myofibril formation, although NMMIIA in these embryos is up-regulated (Tullio et al., 1997). Likewise, depletion of NMMIIA or IIB in C2C12 cell cultures inhibits myoblast fusion, but limited myofibril formation still occurs (Swailes et al., 2006). It has been suggested that NMMIIA and NMMIIB play at least partially compensatory roles during myofibrillogenesis (Sanger et al., 2010), although the NMMIIB mutant phenotype in mouse cardiomyocytes is not fully rescued by expression of NMMIIA (Bao et al., 2007), and co-depletion of both isoforms in cell culture seems to have little additive effect (Swailes et al., 2006). To date, no study has examined how the different isoforms of muscle and non-muscle myosin may compensate for one another during development. For example, NMMIIB can compensate for the contractility defects in NMMIIA-depleted fibroblast cells, but not cell motility defects (Even-Ram et al., 2007), and over-expression of invertebrate muscle MHC-A can compensate for the loss of MHC-B during myofibrillogenesis in *C. elegans* mutants (Ao and Pilgrim, 2000; Maruyama et al., 1989). We found that the expression of NMMIIB mRNA was confined to the developing neural tube and somitic tissue, while NMMIIA expression was more ubiquitous, though enriched in somites and neural tissue. This may indicate a co-operative or at least compensatory interaction between NMMIIA and IIB in developing myoblasts in zebrafish.

4.2.2.1 The role of Unc45b in eye development:

Expression of Unc45b in the developing lens and retinal tissue was unexpected, as no previous study has addressed any eye-related role for Unc45b during development. It has been noted, however, that the loss of *unc45b* in zebrafish causes a small-eye, small-head phenotype in addition to striated muscle-specific defects (Etard et al., 2007; Wohlgemuth et al., 2007). Since a number of genes involved with heart muscle function result in small-eye and small head phenotypes when lost (Etard et al., 2007; Granato et al., 1996; Xu et al., 2002), it has generally been assumed that these defects are caused by the reduction in circulation from the yolk, and represent a global developmental delay. Indeed, heart defects in zebrafish are also generally attended by retention of fluid that causes edema of the pericardium and yolk sac (Zhu et al., 2013). However, the specific eye defects of *unc45b/steif* embryos include a small lens with retention of lens fiber nuclei, and disorganization of laminar actin (Comyn, 2011), which persist much longer than other effects of developmental delay in *unc45b* mutants (Etard et al., 2007). Moreover, the persistence of nuclei and actin disorganization are not seen in the small-eye phenotype of other heart muscle mutants, such as *pickwick* (Hansen et al., 2013), suggesting that the loss of Unc45b causes a specific effect on developing lens fibers. Our results show that co-localization of NMM and Unc45b in cell cortices of lens fibers and differentiating retinal epithelium is lost in *unc45b/steif* mutants. Given that studies in rats have suggested that NMM plays an role in the shaping of lens fiber cells (Al-Ghoul et al., 2010; Ledee et al., 2007), this supports our hypothesis that Unc45b mediates NMM activity in specific tissues, which may also include early differentiating myocytes.

4.2.2.2 Loss of costamere stabilization in *unc45b* mutants and implications for the pre-myofibril model:

Myofibril formation can be inhibited completely in C2C12 myotubes by the blocking of integrin binding with competing RGD peptides (Fujita et al., 2007), demonstrating the necessity of substrate attachment for myofibrillogenesis. Furthermore, this loss of myofibrillogenesis was not merely due to the lack of integrin signalling, because C2C12 myocytes cultured on highly-elastic polymer gels undergo alignment and fusion, but also fail to undergo myofibrillogenesis (Engler et al., 2004), indicating that mechanical tension at

costamere attachment sites is essential for myofibril formation. NMM activity is necessary for the maintenance of focal adhesion complexes in cultured fibroblasts (Chrzanowska-Wodnicka and Burridge, 1996), and NMM localizes to costamere sites in differentiating myoblasts (Takeda et al., 2000). Unc45b also co-localizes with NMM at costamere sites in zebrafish, as shown in Figures 25 and 29 above. Since costamere attachment complexes are built upon focal adhesion sites to begin with, it seems likely that the maintenance of focal adhesion stability by NMM activity in early myoblasts would be necessary for costamere tension and subsequent myofibril formation in differentiating myocytes. UNC-45 binds to the non-muscle myosin NMY-2 in *C. elegans,* and is necessary for NMY-2 function, but not for its folding or assembly (Kachur et al., 2008). It has also been theorized that UNC-45 plays a part in mediating the step-size of the myosin head domain during motor function in yeast (Shi and Blobel, 2010), and this could explain the activity of Unc45b at costamere attachments in vertebrates. Although no study has yet shown a direct interaction between the vertebrate Unc45b and NMM *in vivo,* interaction between Unc45b and another costamere-localizing protein, Apobec-like2 (Apo2), has been demonstrated in zebrafish. It is also worth noting that *in vitro* interactions between chaperones and their target proteins are often disrupted in the absence of specific co-factors. More importantly, a targeted knockdown of Apo2 is able to phenocopy the myofiber attachment defects seen in *unc45b* mutants (Etard et al., 2010). It therefore seems likely, given the cell detachment phenotype of *unc45b* mutants, the loss of tension in focal adhesion complexes when NMM is inhibited, and the necessity of substrate rigidity for myofibrillogenesis, that a NMM-mediated role for Unc45b may exist at costameres of the Z-line and myosepta in zebrafish.

4.2.3 The effects of *unc45b* mutation on NMM localization in zebrafish supports the pre-myofibril model:

NMM and UNC-45 co-localization has also been previously shown in *Drosophila* and *C. elegans,* (Kachur et al., 2008; Lee et al., 2011b) and both of these molecules localize to costameres and the myoseptum in zebrafish at late stages of myogenesis (Etard et al., 2008; Sanger et al., 2009), but our data further demonstrate that NMM and Unc45b expression are also correlated spatially and temporally in the early embryo, which occurs before the onset of muscle myosin expression. This strongly supports our first hypothesis,

that Unc45b plays a much earlier role in myofibrillogenesis than previously thought; at the very least, the view of Unc45b as merely an Hsp90 co-chaperone, assisting the folding of mMHC, is incomplete. We also showed that these genes are co-regulated to some degree following the protein stress response in early embryos, and that this up-regulation occurs in the absence of mMHC. Given the myofiber attachment defects and delayed nucleation of α-actinin in *unc45b* mutants, the loss of NMM localization to the myosepta would seem to indicate quite strongly that the stabilization of costamere attachment is dependent on Unc45b expression during myofibrillogenesis, supporting our second hypothesis. Further, the loss of co-localization between Unc45b and NMM in eye tissues and at the myoseptum in *unc45b* mutants suggests a direct role for Unc45b in mediating NMM folding or function. The localization was only partially overlapped, suggesting that Unc45b plays other roles that do not involve NMM, and that NMM activity does not always involve Unc45b. The detection of green fluorescence in merged images, indicating Unc45b with no NMM localization, is unsurprising, as Unc45b has already been implicated in multiple processes during myogenesis, including mMHC folding, interactions with Apobec2, stabilization of ILK, etc. Red fluorescence, on the other hand, is unsurprising because of the promiscuity of the NMM antibody, which likely binds to multiple NMM isoforms, while only NMMIIB has been directly implicated in pre-myofibril formation. Regardless, the high level of co-localization directly adjacent to the myosepta displayed in Figure 30 is very much in keeping with previous reports (Etard et al., 2010; Sanger et al., 2009). Taken together, these findings support the pre-myofibril model of myofibrillogenesis, in which NMM plays a vital part in the initial patterning of myofibrils from actinomyosin stress fibers. This represents a novel role for the Unc45b chaperone during early myocyte differentiation that has not previously been described.

4.3 The characterization of motility mutants - implications for the titin molecular ruler model of myofibrillogenesis:

Analysis of the zebrafish *herzschlag* mutation through genetic mapping, complementation and peptide-specific antibody staining is consistent with *hel* being a nonsense allele of the *ttna* gene, with a mutation lying somewhere between the T12 and T11 antibody binding sites, corresponding to exons 27 and ~103, therefore lacking the A-band

rod domain of titin that has been proposed to act as a myosin thick filament scaffold. Complementation indicates that the *hel* mutation is allelic with *pik*, a known lesion of *ttna*. The *pik* mutant allele of *ttna* produces a heart-specific phenotype, as the *pik* lesion lies within the heart-specific N2B exon, while *hel* embryos display a more severe phenotype, affecting both heart and skeletal muscles. This suggests that the *hel* mutation lies within an exon retained in striated muscle isoforms of titin. As expected, the *pik/hel* complementation cross displayed a heart phenotype but not a skeletal muscle phenotype. This is because the *pik* allele still produces a normal functioning titin protein in skeletal muscles (Xu et al., 2002). The *hel* mutation thus represents a more severe lesion that is not specific to trunk muscle, and peptide-specific antibody staining strongly suggests the loss of the A-band rod domain. Many point mutations have been identified within the coding sequence of *ttna*, and given the structural nature of the titin protein, single-nucleotide changes in Ig-like or FN-III domains seem unlikely to cause significant defects in titin function; it is also unlikely that a single-nucleotide change would affect the antigenicity of the T11 antibody binding site, given that the antibody was generated from a large trypsin-generated peptide (Barthel and Raymond, 1990). Taken together, this evidence suggests that the *hel* mutation is a nonsense allele of *ttna*.

4.3.1 The *hel* mutant offers an opportunity to test the molecular ruler model:

Our phenotypic analysis of the *sth* and *hel* mutants, and the mapping of these mutant loci to specific genes, did not support our third hypothesis; the mutations did not reveal novel components of the sarcomere or costamere. However, since *hel* animals produce a protein lacking the A-band rod domain but retaining the Z-disk-binding N-terminal domains, this mutant presents an opportunity to address models for the function of titin as a myosin thick filament scaffold. Any Z-disk-stabilizing functions of titin are likely to be performed normally by the protein product of *hel*, as demonstrated by α-actinin staining in Figure 40. This is important because the N-terminal splice variants of titin, including the ~700 kDa NOVEX-III isoform, are known to bind to obscurin and α-actinin, helping link the Z-disk to the I-band (Bang et al., 2001). In contrast, any C-terminal rod domain functions, including the recruitment of myomesin, as well as any myosin-specific scaffold functions, will be deficient in these embryos. The *hel* mutant thus represents a domain-specific loss-of-

function mutation, and as such, should prove useful for addressing the role of titin in the patterning of the thick filament.

Evidence for the involvement of "molecular rulers" in sarcomere formation is both contradictory and controversial [reviewed by (Kontrogianni-Konstantopoulos et al., 2009)], although the existence of "ruler" mechanisms has been shown to exist in viral systems, such as the assembly of the bacteriophage λ tail (Katsura, 1987). In view of our evidence in support of the pre-myofibril model, we proposed a final hypothesis, that the initiation of myofibrillogenesis and assembly of the thick filament does not require the titin rod domain scaffold. Pursuant to this hypothesis, we investigated the timeline of myofibrillogenesis in *hel* mutant animals. Our analysis demonstrates that the loss of the titin rod domain does not impede the initial patterning and assembly of the myosin thick filament, as *hel* mutant embryos underwent normal thick filament assembly, producing typically-spaced A-bands. Moreover, these sarcomeres retained limited function up to 48 hours, permitting limited twitch movement of mutant embryos, thus suggesting a longer-term degeneration of sarcomeres in titin mutants rather than deficiencies in initial thick filament assembly. The shortened muscle fibers of older *hel* mutants likely correspond to a collapse of the sarcomere, resulting from impaired molecular spring function of truncated *ttna*.

4.3.2 Sarcomeres degrade over time in the absence of the titin molecular spring:

Our results are consistent with evidence from a number of sources suggesting that titin deficiency results in longer-term degradation of muscle rather than failure of sarcomere assembly during myogenesis. For example, mouse embryos lacking the C-terminus of titin initially form normal myofibrils with identifiable thick and thin filaments that are later lost as sarcomeres begin to disassemble (Peng et al., 2005). This also occurs following MO-mediated knockdown or cardiac-specific knockout of titin in zebrafish (Seeley et al., 2007; Xu et al., 2002). Additionally, human myopathies involving mutations of the titin gene tend to be late-onset and degenerative, rather than affecting perinatal muscle function (Hackman et al., 2003; Udd, 2012), although recent advances in next-generation sequencing have identified several infant-onset titinopathies, resulting in non-lethal centronuclear hypotonia (Ceyhan-Birsoy et al., 2013), or myopathy with early respiratory failure in at least 8 families (Pfeffer et al., 2013). However, given the known role of titin in stabilizing the Z-disk

(Gregorio et al., 1998; Peckham et al., 1997), and the many Ig- and FN-like protein-binding domains located throughout the titin rod domain, it seems likely that interactions between titin and other proteins throughout the sarcomere play a role in stabilizing contracting myofibrils over time. The well-established molecular spring function of the flexible I-band domain of titin has long been hypothesized to be the primary mechanism by which sarcomeres return to their resting length after contraction or stretching (Granzier and Labeit, 2004; Tskhovrebova and Trinick, 2002; Tskhovrebova and Trinick, 2003; Whiting et al., 1989). In the absence of the titin rod domain binding to the A-band, it seems likely that the re-folding of compressed titin would be less efficient in pushing the A-band away from the Z-disk following contraction. This hypothesis is consistent with our observations of compressed A-band-like patterns in the shortened skeletal muscle fibers of older *hel* mutant embryos, and the reduced disorganization of sarcomeres in *hel* mutant seZEB cultures, even after 5 days.

As mentioned above, titin is one of the largest genes known, and other mutations have been linked to *ttna* in zebrafish, possibly representing other useful domain-specific deletions. One such mutation, dubbed *pik*^{uw3}, (Paulus et al., 2009), was theorized to be an early truncation of *ttna*. Myosin staining using the F59 antibody in these embryos showed a different pattern of staining at 24 hpf than in *hel* embryos; myosin staining was present in elongating myocytes, but appeared as scattered punctae similar to background in WT embryos, rather than displaying normal thick filaments as in *hel* embryos. However, we have observed that *hel* mutant embryos experience a global developmental delay, similar to that seen in other circulation mutants such as *unc45b/steif*, and the organization of myosin and actin into cortical myofibrils at ~20-24 hpf is likewise generally delayed in *hel* mutants compared to WT embryos; older somites in mutants are comparable to younger WT ones. Since no actin controls or embryos older than 24 hpf were used in the *pik*^{uw3} experiments, it is impossible to say whether thick filament organization was actually deficient in *pik*^{uw3} mutants, or merely delayed at 24 hours. Unlike in *hel* embryos, the T11 titin epitope was detected in *pik*^{uw3} mutants, although in a disorganized pattern, suggesting that the *pik*^{uw3} mutation is a less severe truncation or even a missense mutation of *ttna*. This is supported by the reported movement phenotype of *pik*^{uw3}, which is also less severe than the phenotype of *hel* mutants prior to 24 hpf. The pattern of α-actinin localization was also disorganized in *pik*^{uw3} embryos, indicating that this mutation may create a

defect in Z-disk binding and stabilization, rather than producing a truncated protein. In any case, given the size and multi-functional nature of titin, the production of truncated *ttna* proteins lacking specific domains by mutations such as *hel* or *pik*^{uw3} (or other mutations currently being identified by genome-wide sequence-based screens in zebrafish (Kettleborough et al., 2013) or *C. elegans* (Thompson et al., 2013)), should prove to be powerful tools for elucidating the many roles of this giant protein.

4.3.3 Loss of the titin C-terminal kinase domain may contribute to eventual sarcomere degradation in *hel* mutants:

The C-terminus of titin contains a unique self-inhibitory kinase domain, which is activated during muscle stretching (Puchner et al., 2008). This domain has been proposed to transduce a stretch-sensing signal through a signalling complex with nbr1 and p62/SQSTM1 (Lange et al., 2005), activating ubiquitin-mediated protein turnover pathways, and may also activate myogenic gene programs for the repair of damaged sarcomeres (Gautel, 2011). It has also been shown to phosphorylate the Z-disk-stabilizing protein T-cap, leading to the hypothesis that it may be required to regulate Z-disk assembly through T-cap activation (Mayans et al., 1998). The selective deletion of the titin kinase domain in mice results in eventual disassociation of sarcomeres (Weinert et al., 2006), well after the assembly of thick filaments, as occurs in the zebrafish *hel* mutant phenotype. It is therefore possible that the *hel* sarcomere degeneration phenotype is caused at least in part by the loss of this domain and its stretch-signalling function, rather than deficiencies of the molecular spring role of titin due to reduced A-band anchoring. This possibility does not alter the fact that thick filament assembly in both mutants appears normal, with the usual striation pattern and sarcomere period. However, sarcomeres in the mouse M-line mutants do not reduce in length, instead failing to mature laterally up to 11 days post-coitus, after which total dissociation of sarcomere components occurs (Weinert et al., 2006). This is in stark contrast to the *hel* mutants, in which sarcomeres and muscle fibers were drastically shortened by 48 hpf, a phenotype not seen at all in the mouse M-line mutants. Moreover, these possibilities are not necessarily mutually exclusive; shortening of sarcomeres due to the loss of the molecular spring function and the loss of stabilizing tension signals from the absent kinase domain may act in concert to cause the eventual complete breakdown of the sarcomeres.

4.3.4 The *ttnb* gene does not compensate for the loss of *ttna* function in *hel* mutants:

Although teleosts possess *ttnb*, a second titin gene whose mRNA is expressed in muscle tissue (Seeley et al., 2007), the specific role, if any, of *ttnb* protein in myogenesis is not clear. Morpholino-mediated knockdown of *ttnb* produces no phenotype in heart muscle, and only produces a mild phenotype in skeletal muscle at very high MO concentrations (~100 ng/embryo, (Seeley et al., 2007)). It is possible that *ttnb* expression is evolutionarily retained only because the presence of additional titin molecules helps to further stabilize the sarcomere through protein interactions with Ig- and FN-like domains. Indeed, the aforementioned mRNA expression studies have only reported the expression of N-terminal I-band domains of *ttnb*. A probable zebrafish *ttnb* mutant, *runzel* (*ruz*) retains normal movement and heartbeat for the first few days of development, and has no sarcomere disorganization up to 3.5 dpf, although myofibrils in these embryos eventually become mis-oriented and sarcomeres collapse after 6-7 days (Steffen et al., 2007), suggesting that some longer-term role is likely being played by *ttnb*, possibly in aiding the stabilization of the Z-disk, similar to the role of the short NOVEX-III titin isoforms (Bang et al., 2001). In any case, co-injection of zebrafish embryos with morpholinos against both titin isoforms has no additive effect beyond injection of *ttna* MO alone (Seeley et al., 2007), and our injections of *ttnb* MO into *hel* or *pik* mutant embryos had no additional effects beyond the expected mutant phenotypes. Most importantly, *hel* embryos injected with the *ttnb* MO still had normal patterning of thick filament myosin at 24 and 30 hpf, even at high MO concentrations, strongly indicating that *ttnb* has no ability to compensate for the loss of the *ttna* rod domain in *hel* mutants.

4.4 Summary and Conclusions:

These results support our final hypothesis, indicating that the titin rod domain, long thought to act as a scaffold for thick filament assembly, is dispensable for the initial patterning of myofibrils. The alternative pre-myofibril model suggests that no thick filament scaffold is necessary, and our findings regarding an early, NMM-mediated role for Unc45b in myogenesis, and the necessity for Unc45b in costamere assembly at the myoseptum, supports this over the older titin molecular ruler model. The necessity of Unc45b for the differentiation of actin stress fibers into pre-myofibrils in seZEB cell culture, the early

expression of *unc45b* mRNA in cultured myoblasts and in somitic and pre-somitic tissue in whole embryos and the up-regulation of *unc45b* and NMM in the absence of mMHC are all consistent with our first hypothesis, that Unc45b plays an earlier role in myogenesis than previously thought. In addition to this, the co-localization of Unc45b protein with NMM and early costamere components, the loss of costamere components at the myoseptum in *unc45b/steif* embryos, and the loss of NMM and Unc45b co-localization in mutant eye and muscle tissue strongly support our second hypothesis, that Unc45b helps to mediate NMM activity in the formation of cell attachments and costameres. It does not seem likely that Unc45b mediates NMM folding in the absence of Hsp90; however, evidence from *C. elegans* suggests that the interaction may be necessary for NMM function (Kachur et al., 2008), possibly by mediating myosin step size (Shi and Blobel, 2010).

Our analysis of the *hel* mutation, which we identify as a nonsense truncation within the flexible I-band of *ttna*, suggests that muscle MHC is able to assemble into thick filaments without the need for a titin scaffold; thick filament organization was seen in embryos as old as 36 hpf, and even longer in cell culture where no contractile signals are encountered. Further, no up-regulation of myosin chaperones was seen in response to the mutation, suggesting that myosin mis-accumulation does not occur. This is in keeping with the pre-myofibril model, which states that NMM in the pre-myofibrils provides scaffolding for thick filament construction, and thus myosin folding should not be impacted by titin deficiencies. Alternatively, the recent discovery that Unc45b is able to form short-chain polymers during myosin folding (Gazda et al., 2013) suggests that myosin may be added to thick filaments in a stepwise fashion by chaperone activity alone. It is very likely that all of these mechanisms come in to play simultaneously; that Unc45b helps to mediate costamere stability during the formation of pre-myofibrils, that the Unc45b/Hsp90 complex mediates a step-wise addition of myosin to replace NMM as myofibrils mature, and that titin helps to stabilize the filaments as they are laid down. Regardless, all of our results taken together strongly support the pre-myofibril model of myofibrillogenesis over the titin molecular ruler model, and should help lay to rest the long-standing controversy between these models of early myofibril patterning and assembly.

5. REFERENCES:

Abe, T., K. Takano, A. Suzuki, Y. Shimada, M. Inagaki, N. Sato, T. Obinata, and T. Endo. 2004. Myocyte differentiation generates nuclear invaginations traversed by myofibrils associating with sarcomeric protein mRNAs. *J Cell Sci*. 117:6523-6534.

Ackermann, G.E., and B.H. Paw. 2003. Zebrafish: a genetic model for vertebrate organogenesis and human disorders. *Front Biosci*. 8:1227-1253.

Agbulut, O., P. Noirez, F. Beaumont, and G. Butler-Browne. 2003. Myosin heavy chain isoforms in postnatal muscle development of mice. *Biol Cell*. 95:399-406.

Ahnn, J., and A. Fire. 1994. A screen for genetic loci required for body-wall muscle development during embryogenesis in Caenorhabditis elegans. *Genetics*. 137:483-498.

Akerfelt, M., D. Trouillet, V. Mezger, and L. Sistonen. 2007. Heat shock factors at a crossroad between stress and development. *Ann N Y Acad Sci*. 1113:15-27.

Al-Ghoul, K.J., T.P. Lindquist, S.S. Kirk, and S.T. Donohue. 2010. A novel terminal web-like structure in cortical lens fibers: architecture and functional assessment. *Anat Rec (Hoboken)*. 293:1805-1815.

Anastasi, G., G. Cutroneo, R. Gaeta, D. Di Mauro, A. Arco, A. Consolo, G. Santoro, F. Trimarchi, and A. Favaloro. 2009. Dystrophin-glycoprotein complex and vinculin-talin-integrin system in human adult cardiac muscle. *Int J Mol Med*. 23:149-159.

Anastasi, G., G. Cutroneo, F. Trimarchi, G. Santoro, D. Bruschetta, P. Bramanti, A. Pisani, and A. Favaloro. 2004. Evaluation of sarcoglycans, vinculin-talin-integrin system and filamin2 in alpha- and gamma-sarcoglycanopathy: an immunohistochemical study. *Int J Mol Med*. 14:989-999.

Anderson, M.J., V.N. Pham, A.M. Vogel, B.M. Weinstein, and B.L. Roman. 2008. Loss of unc45a precipitates arteriovenous shunting in the aortic arches. *Dev Biol*. 318:258-267.

Ao, W., and D. Pilgrim. 2000. Caenorhabditis elegans UNC-45 is a component of muscle thick filaments and colocalizes with myosin heavy chain B, but not myosin heavy chain A. *J Cell Biol*. 148:375-384.

Aoyagi, Y., N. Fujita, and T. Tsuruo. 2005. Stabilization of integrin-linked kinase by binding to Hsp90. *Biochem Biophys Res Commun*. 331:1061-1068.

Badylak, S.F., and R.M. Nerem. 2010. Progress in tissue engineering and regenerative medicine. *Proc Natl Acad Sci U S A*. 107:3285-3286.

Badylak, S.F., D. Taylor, and K. Uygun. 2010. Whole-Organ Tissue Engineering: Decellularization and Recellularization of Three-Dimensional Matrix Scaffolds. *Annu Rev Biomed Eng*.

Badylak, S.F., D.J. Weiss, A. Caplan, and P. Macchiarini. 2012. Engineered whole organs and complex tissues. *Lancet*. 379:943-952.

Balaban, N.Q., U.S. Schwarz, D. Riveline, P. Goichberg, G. Tzur, I. Sabanay, D. Mahalu, S. Safran, A. Bershadsky, L. Addadi, and B. Geiger. 2001. Force and focal adhesion assembly: a close relationship studied using elastic micropatterned substrates. *Nat Cell Biol*. 3:466-472.

Bang, M.L., T. Centner, F. Fornoff, A.J. Geach, M. Gotthardt, M. McNabb, C.C. Witt, D. Labeit, C.C. Gregorio, H. Granzier, and S. Labeit. 2001. The complete gene sequence

of titin, expression of an unusual approximately 700-kDa titin isoform, and its interaction with obscurin identify a novel Z-line to I-band linking system. *Circ Res*. 89:1065-1072.

Bao, J., X. Ma, C. Liu, and R.S. Adelstein. 2007. Replacement of nonmuscle myosin II-B with II-A rescues brain but not cardiac defects in mice. *J Biol Chem*. 282:22102-22111.

Barral, J.M., A.H. Hutagalung, A. Brinker, F.U. Hartl, and H.F. Epstein. 2002. Role of the myosin assembly protein UNC-45 as a molecular chaperone for myosin. *Science*. 295:669-671.

Barthel, L.K., and P.A. Raymond. 1990. Improved method for obtaining 3-microns cryosections for immunocytochemistry. *The journal of histochemistry and cytochemistry : official journal of the Histochemistry Society*. 38:1383-1388.

Bassett, D.I., R.J. Bryson-Richardson, D.F. Daggett, P. Gautier, D.G. Keenan, and P.D. Currie. 2003. Dystrophin is required for the formation of stable muscle attachments in the zebrafish embryo. *Development*. 130:5851-5860.

Behra, M., X. Cousin, C. Bertrand, J.L. Vonesch, D. Biellmann, A. Chatonnet, and U. Strahle. 2002. Acetylcholinesterase is required for neuronal and muscular development in the zebrafish embryo. *Nat Neurosci*. 5:111-118.

Benian, G.M., J.E. Kiff, N. Neckelmann, D.G. Moerman, and R.H. Waterston. 1989. Sequence of an unusually large protein implicated in regulation of myosin activity in C. elegans. *Nature*. 342:45-50.

Bernick, E.P., P.J. Zhang, and S. Du. 2010. Knockdown and overexpression of Unc-45b result in defective myofibril organization in skeletal muscles of zebrafish embryos. *BMC Cell Biol*. 11:70.

Bloor, J.W., and N.H. Brown. 1998. Genetic analysis of the Drosophila alphaPS2 integrin subunit reveals discrete adhesive, morphogenetic and sarcomeric functions. *Genetics*. 148:1127-1142.

Bloor, J.W., and D.P. Kiehart. 2001. zipper Nonmuscle myosin-II functions downstream of PS2 integrin in Drosophila myogenesis and is necessary for myofibril formation. *Dev Biol*. 239:215-228.

Bonnemann, C.G., and N.G. Laing. 2004. Myopathies resulting from mutations in sarcomeric proteins. *Curr Opin Neurol*. 17:529-537.

Borisov, A.B., M.G. Martynova, and M.W. Russell. 2008. Early incorporation of obscurin into nascent sarcomeres: implication for myofibril assembly during cardiac myogenesis. *Histochem Cell Biol*. 129:463-478.

Borisov, A.B., S.B. Sutter, A. Kontrogianni-Konstantopoulos, R.J. Bloch, M.V. Westfall, and M.W. Russell. 2006. Essential role of obscurin in cardiac myofibrillogenesis and hypertrophic response: evidence from small interfering RNA-mediated gene silencing. *Histochem Cell Biol*. 125:227-238.

Bradley, K.M., J.B. Elmore, J.P. Breyer, B.L. Yaspan, J.R. Jessen, E.W. Knapik, and J.R. Smith. 2007. A major zebrafish polymorphism resource for genetic mapping. *Genome Biol*. 8:R55.

Brand-Saberi, B. 2005. Genetic and epigenetic control of skeletal muscle development. *Ann Anat*. 187:199-207.

Brown, L.A., A.R. Rodaway, T.F. Schilling, T. Jowett, P.W. Ingham, R.K. Patient, and A.D. Sharrocks. 2000. Insights into early vasculogenesis revealed by expression of the

ETS-domain transcription factor Fli-1 in wild-type and mutant zebrafish embryos. *Mech Dev*. 90:237-252.

Bryson-Richardson, R.J., D.F. Daggett, F. Cortes, C. Neyt, D.G. Keenan, and P.D. Currie. 2005. Myosin heavy chain expression in zebrafish and slow muscle composition. *Dev Dyn*. 233:1018-1022.

Burguiere, A.C., H. Nord, and J. von Hofsten. 2011. Alkali-like myosin light chain-1 (myl1) is an early marker for differentiating fast muscle cells in zebrafish. *Dev Dyn*. 240:1856-1863.

Burkart, C., F. Qiu, S. Brendel, V. Benes, P. Haag, S. Labeit, K. Leonard, and B. Bullard. 2007. Modular proteins from the Drosophila sallimus (sls) gene and their expression in muscles with different extensibility. *J Mol Biol*. 367:953-969.

Butler, B., C. Gao, A.T. Mersich, and S.D. Blystone. 2006. Purified integrin adhesion complexes exhibit actin-polymerization activity. *Curr Biol*. 16:242-251.

Capes-Davis, A., G. Theodosopoulos, I. Atkin, H.G. Drexler, A. Kohara, R.A.F. MacLeod, J.R. Masters, Y. Nakamura, Y.A. Reid, R.R. Reddel, and R.I. Freshney. 2010. Check your cultures! A list of cross-contaminated or misidentified cell lines. *Int J Cancer*. 127:1-8.

Ceyhan-Birsoy, O., P.B. Agrawal, C. Hidalgo, K. Schmitz-Abe, E.T. Dechene, L.C. Swanson, R. Soemedi, N. Vasli, S.T. Iannaccone, P.B. Shieh, N. Shur, J.M. Dennison, M.W. Lawlor, J. Laporte, K. Markianos, W.G. Fairbrother, H. Granzier, and A.H. Beggs. 2013. Recessive truncating titin gene, TTN, mutations presenting as centronuclear myopathy. *Neurology*.

Chadli, A., J.D. Graham, M.G. Abel, T.A. Jackson, D.F. Gordon, W.M. Wood, S.J. Felts, K.B. Horwitz, and D. Toft. 2006. GCUNC-45 is a novel regulator for the progesterone receptor/hsp90 chaperoning pathway. *Mol Cell Biol*. 26:1722-1730.

Charvet, B., M. Malbouyres, A. Pagnon-Minot, F. Ruggiero, and D. Le Guellec. 2011. Development of the zebrafish myoseptum with emphasis on the myotendinous junction. *Cell and tissue research*. 346:439-449.

Chen, J.N., P. Haffter, J. Odenthal, E. Vogelsang, M. Brand, F.J. van Eeden, M. Furutani-Seiki, M. Granato, M. Hammerschmidt, C.P. Heisenberg, Y.J. Jiang, D.A. Kane, R.N. Kelsh, M.C. Mullins, and C. Nusslein-Volhard. 1996. Mutations affecting the cardiovascular system and other internal organs in zebrafish. *Development*. 123:293-302.

Chen, W., S. Burgess, G. Golling, A. Amsterdam, and N. Hopkins. 2002. High-throughput selection of retrovirus producer cell lines leads to markedly improved efficiency of germ line-transmissible insertions in zebra fish. *J Virol*. 76:2192-2198.

Chow, D., R. Srikakulam, Y. Chen, and D.A. Winkelmann. 2002. Folding of the striated muscle myosin motor domain. *J Biol Chem*. 277:36799-36807.

Chrzanowska-Wodnicka, M., and K. Burridge. 1996. Rho-stimulated contractility drives the formation of stress fibers and focal adhesions. *J Cell Biol*. 133:1403-1415.

Cohn, R.D., U. Mayer, G. Saher, R. Herrmann, A. van der Flier, A. Sonnenberg, L. Sorokin, and T. Voit. 1999. Secondary reduction of alpha7B integrin in laminin alpha2 deficient congenital muscular dystrophy supports an additional transmembrane link in skeletal muscle. *J Neurol Sci*. 163:140-152.

Collodi, P., Y. Kamei, T. Ernst, C. Miranda, D.R. Buhler, and D.W. Barnes. 1992. Culture of cells from zebrafish (Brachydanio rerio) embryo and adult tissues. *Cell Biol Toxicol*. 8:43-61.

Collodi, P., C.L. Miranda, X. Zhao, D.R. Buhler, and D.W. Barnes. 1994. Induction of zebrafish (Brachydanio rerio) P450 in vivo and in cell culture. *Xenobiotica*. 24:487-493.

Comyn, S. 2011. Phenotypic Characterization of a Zygotic-Lethal unc45b-/-; unc45a-/- Mutant in Zebrafish, Danio rerio. *In* Biological Sciences. Vol. Master of Science. University of Alberta, Edmonton.

Comyn, S.A., and D. Pilgrim. 2012. Lack of Developmental Redundancy between Unc45 Proteins in Zebrafish Muscle Development. *PLoS One*. 7:e48861.

Crawford, G.L., and R. Horowits. 2011. Scaffolds and chaperones in myofibril assembly: putting the striations in striated muscle. *Biophys Rev*. 3:25-32.

Daggett, D.F., C.R. Domingo, P.D. Currie, and S.L. Amacher. 2007. Control of morphogenetic cell movements in the early zebrafish myotome. *Dev Biol*. 309:169-179.

Danowski, B.A., K. Imanaka-Yoshida, J.M. Sanger, and J.W. Sanger. 1992. Costameres are sites of force transmission to the substratum in adult rat cardiomyocytes. *J Cell Biol*. 118:1411-1420.

Darmon, M.Y. 1982. Laminin provides a better substrate than fibronectin for attachment, growth, and differentiation of 1003 embryonal carcinoma cells. *In Vitro*. 18:997-1003.

Dayton, W.R., and M.R. Hathaway. 1991. Myogenic cell proliferation and differentiation. *Poult Sci*. 70:1815-1822.

De Angelis, L., S. Borghi, R. Melchionna, L. Berghella, M. Baccarani-Contri, F. Parise, S. Ferrari, and G. Cossu. 1998. Inhibition of myogenesis by transforming growth factor beta is density-dependent and related to the translocation of transcription factor MEF2 to the cytoplasm. *Proc Natl Acad Sci U S A*. 95:12358-12363.

De Deyne, P.G. 2000. Formation of sarcomeres in developing myotubes: role of mechanical stretch and contractile activation. *Am J Physiol Cell Physiol*. 279:C1801-1811.

De Paepe, B., K.K. Creus, J.J. Martin, J. Weis, and J.L. De Bleecker. 2009. A dual role for HSP90 and HSP70 in the inflammatory myopathies: from muscle fiber protection to active invasion by macrophages. *Ann N Y Acad Sci*. 1173:463-469.

DeMali, K.A., C.A. Barlow, and K. Burridge. 2002. Recruitment of the Arp2/3 complex to vinculin: coupling membrane protrusion to matrix adhesion. *J Cell Biol*. 159:881-891.

Devoto, S.H., E. Melancon, J.S. Eisen, and M. Westerfield. 1996. Identification of separate slow and fast muscle precursor cells in vivo, prior to somite formation. *Development*. 122:3371-3380.

Dhume, A., S. Lu, and R. Horowits. 2006. Targeted disruption of N-RAP gene function by RNA interference: a role for N-RAP in myofibril organization. *Cell Motil Cytoskeleton*. 63:493-511.

Discher, D.E., P. Janmey, and Y.L. Wang. 2005. Tissue cells feel and respond to the stiffness of their substrate. *Science*. 310:1139-1143.

Djabali, K., B. de Nechaud, F. Landon, and M.M. Portier. 1997. AlphaB-crystallin interacts with intermediate filaments in response to stress. *J Cell Sci*. 110 (Pt 21):2759-2769.

Dong, Y., D. Pruyne, and A. Bretscher. 2003. Formin-dependent actin assembly is regulated by distinct modes of Rho signaling in yeast. *J Cell Biol*. 161:1081-1092.
Driever, W., and Z. Rangini. 1993. Characterization of a cell line derived from zebrafish (Brachydanio rerio) embryos. *In Vitro Cell Dev Biol Anim*. 29A:749-754.
Du, A., J.M. Sanger, K.K. Linask, and J.W. Sanger. 2003. Myofibrillogenesis in the first cardiomyocytes formed from isolated quail precardiac mesoderm. *Dev Biol*. 257:382-394.
Du, A., J.M. Sanger, and J.W. Sanger. 2008a. Cardiac myofibrillogenesis inside intact embryonic hearts. *Dev Biol*. 318:236-246.
Du, S.J., H. Li, Y. Bian, and Y. Zhong. 2008b. Heat-shock protein 90alpha1 is required for organized myofibril assembly in skeletal muscles of zebrafish embryos. *Proc Natl Acad Sci U S A*. 105:554-559.
Du, S.J., J. Rotllant, and X. Tan. 2006. Muscle-specific expression of the smyd1 gene is controlled by its 5.3-kb promoter and 5'-flanking sequence in zebrafish embryos. *Dev Dyn*. 235:3306-3315.
Duan, R., and P.J. Gallagher. 2009. Dependence of myoblast fusion on a cortical actin wall and nonmuscle myosin IIA. *Dev Biol*. 325:374-385.
Ehler, E., and M. Gautel. 2008. The sarcomere and sarcomerogenesis. *Adv Exp Med Biol*. 642:1-14.
Elworthy, S., M. Hargrave, R. Knight, K. Mebus, and P.W. Ingham. 2008. Expression of multiple slow myosin heavy chain genes reveals a diversity of zebrafish slow twitch muscle fibres with differing requirements for Hedgehog and Prdm1 activity. *Development*. 135:2115-2126.
Engler, A.J., M.A. Griffin, S. Sen, C.G. Bonnemann, H.L. Sweeney, and D.E. Discher. 2004. Myotubes differentiate optimally on substrates with tissue-like stiffness: pathological implications for soft or stiff microenvironments. *J Cell Biol*. 166:877-887.
Epstein, H.F., D.L. Casey, and I. Ortiz. 1993. Myosin and paramyosin of Caenorhabditis elegans embryos assemble into nascent structures distinct from thick filaments and multi-filament assemblages. *J Cell Biol*. 122:845-858.
Etard, C., M. Behra, N. Fischer, D. Hutcheson, R. Geisler, and U. Strahle. 2007. The UCS factor Steif/Unc-45b interacts with the heat shock protein Hsp90a during myofibrillogenesis. *Dev Biol*. 308:133-143.
Etard, C., U. Roostalu, and U. Strahle. 2008. Shuttling of the chaperones Unc45b and Hsp90a between the A band and the Z line of the myofibril. *J Cell Biol*. 180:1163-1175.
Etard, C., U. Roostalu, and U. Strahle. 2010. Lack of Apobec2-related proteins causes a dystrophic muscle phenotype in zebrafish embryos. *J Cell Biol*. 189:527-539.
Etheridge, L., P. Diiorio, and C.G. Sagerstrom. 2002. A zebrafish unc-45-related gene expressed during muscle development. *Dev Dyn*. 224:457-460.
Even-Ram, S., A.D. Doyle, M.A. Conti, K. Matsumoto, R.S. Adelstein, and K.M. Yamada. 2007. Myosin IIA regulates cell motility and actomyosin microtubule crosstalk. *Nat Cell Biol*. 9:299-U104.
Fan, L., and P. Collodi. 2006. Zebrafish embryonic stem cells. *Methods Enzymol*. 418:64-77.
Ferrara, T.M., D.B. Flaherty, and G.M. Benian. 2005. Titin/connectin-related proteins in C. elegans: a review and new findings. *J Muscle Res Cell Motil*. 26:435-447.

Ferrari, M.B., K. Ribbeck, D.J. Hagler, and N.C. Spitzer. 1998. A calcium signaling cascade essential for myosin thick filament assembly in Xenopus myocytes. *J Cell Biol*. 141:1349-1356.

Ferrari, M.B., J. Rohrbough, and N.C. Spitzer. 1996. Spontaneous calcium transients regulate myofibrillogenesis in embryonic Xenopus myocytes. *Dev Biol*. 178:484-497.

Filvaroff, E.H., R. Ebner, and R. Derynck. 1994. Inhibition of myogenic differentiation in myoblasts expressing a truncated type II TGF-beta receptor. *Development*. 120:1085-1095.

Fire, A., and R.H. Waterston. 1989. Proper expression of myosin genes in transgenic nematodes. *Embo J*. 8:3419-3428.

Foster, R.F., J.M. Thompson, and S.J. Kaufman. 1987. A laminin substrate promotes myogenesis in rat skeletal muscle cultures: analysis of replication and development using antidesmin and anti-BrdUrd monoclonal antibodies. *Dev Biol*. 122:11-20.

Fujita, H., T. Nedachi, and M. Kanzaki. 2007. Accelerated de novo sarcomere assembly by electric pulse stimulation in C2C12 myotubes. *Exp Cell Res*. 313:1853-1865.

Fulton, A.B., and C. Alftine. 1997. Organization of protein and mRNA for titin and other myofibril components during myofibrillogenesis in cultured chicken skeletal muscle. *Cell Struct Funct*. 22:51-58.

Fulton, A.B., and T. L'Ecuyer. 1993. Cotranslational assembly of some cytoskeletal proteins: implications and prospects. *J Cell Sci*. 105 (Pt 4):867-871.

Funanage, V.L., S.M. Smith, and M.A. Minnich. 1992. Entactin promotes adhesion and long-term maintenance of cultured regenerated skeletal myotubes. *J Cell Physiol*. 150:251-257.

Garcia, A.J., M.D. Vega, and D. Boettiger. 1999. Modulation of cell proliferation and differentiation through substrate-dependent changes in fibronectin conformation. *Mol Biol Cell*. 10:785-798.

Garrido, C., C. Paul, R. Seigneuric, and H.H. Kampinga. 2012. The small heat shock proteins family: the long forgotten chaperones. *Int J Biochem Cell Biol*. 44:1588-1592.

Gautel, M. 2011. Cytoskeletal protein kinases: titin and its relations in mechanosensing. *Pflugers Archiv : European journal of physiology*. 462:119-134.

Gazda, L., W. Pokrzywa, D. Hellerschmied, T. Lowe, I. Forne, F. Mueller-Planitz, T. Hoppe, and T. Clausen. 2013. The myosin chaperone UNC-45 is organized in tandem modules to support myofilament formation in C. elegans. *Cell*. 152:183-195.

Geach, T.J., and L.B. Zimmerman. 2010. Paralysis and delayed Z-disc formation in the Xenopus tropicalis unc45b mutant dicky ticker. *BMC Dev Biol*. 10:75.

Geisler, R. 2005. Mapping and cloning. *In* Zebrafish: A Practical Approach. C. Nusslein-Volhard, editor. Oxford University Press, Oxford. 175-212.

Geisler, R., G.J. Rauch, S. Geiger-Rudolph, A. Albrecht, F. van Bebber, A. Berger, E. Busch-Nentwich, R. Dahm, M.P. Dekens, C. Dooley, A.F. Elli, I. Gehring, H. Geiger, M. Geisler, S. Glaser, S. Holley, M. Huber, A. Kerr, A. Kirn, M. Knirsch, M. Konantz, A.M. Kuchler, F. Maderspacher, S.C. Neuhauss, T. Nicolson, E.A. Ober, E. Praeg, R. Ray, B. Rentzsch, J.M. Rick, E. Rief, H.E. Schauerte, C.P. Schepp, U. Schonberger, H.B. Schonthaler, C. Seiler, S. Sidi, C. Sollner, A. Wehner, C. Weiler,

and C. Nusslein-Volhard. 2007. Large-scale mapping of mutations affecting zebrafish development. *BMC Genomics*. 8:11.
Geoghegan, E., and L. Byrnes. 2008. Mouse induced pluripotent stem cells. *Int J Dev Biol*. 52:1015-1022.
Gettner, S.N., C. Kenyon, and L.F. Reichardt. 1995. Characterization of beta pat-3 heterodimers, a family of essential integrin receptors in C. elegans. *J Cell Biol*. 129:1127-1141.
Ghosh, C., and P. Collodi. 1994. Culture of cells from zebrafish (Brachydanio rerio) blastula-stage embryos. *Cytotechnology*. 14:21-26.
Ghosh, S.R., and I.A. Hope. 2010. Determination of the mobility of novel and established Caenorhabditis elegans sarcomeric proteins in vivo. *Eur J Cell Biol*. 89:437-448.
Gilbert, S.F. 2000. Developmental Biology. Sinauer Associates, Incorporated.
Goebel, H.H., and A. Blaschek. 2011. Protein aggregation in congenital myopathies. *Semin Pediatr Neurol*. 18:272-276.
Golenhofen, N., A. Arbeiter, R. Koob, and D. Drenckhahn. 2002. Ischemia-induced association of the stress protein alpha B-crystallin with I-band portion of cardiac titin. *J Mol Cell Cardiol*. 34:309-319.
Golomb, E., X. Ma, S.S. Jana, Y.A. Preston, S. Kawamoto, N.G. Shoham, E. Goldin, M.A. Conti, J.R. Sellers, and R.S. Adelstein. 2004. Identification and characterization of nonmuscle myosin II-C, a new member of the myosin II family. *J Biol Chem*. 279:2800-2808.
Gongal, P.A., and A.J. Waskiewicz. 2008. Zebrafish model of holoprosencephaly demonstrates a key role for TGIF in regulating retinoic acid metabolism. *Hum Mol Genet*. 17:525-538.
Gordon, A.M., E. Homsher, and M. Regnier. 2000. Regulation of contraction in striated muscle. *Physiol Rev*. 80:853-924.
Granato, M., F.J. van Eeden, U. Schach, T. Trowe, M. Brand, M. Furutani-Seiki, P. Haffter, M. Hammerschmidt, C.P. Heisenberg, Y.J. Jiang, D.A. Kane, R.N. Kelsh, M.C. Mullins, J. Odenthal, and C. Nusslein-Volhard. 1996. Genes controlling and mediating locomotion behavior of the zebrafish embryo and larva. *Development*. 123:399-413.
Grantham, J., L.W. Ruddock, A. Roobol, and M.J. Carden. 2002. Eukaryotic chaperonin containing T-complex polypeptide 1 interacts with filamentous actin and reduces the initial rate of actin polymerization in vitro. *Cell Stress Chaperones*. 7:235-242.
Granzier, H.L., and S. Labeit. 2004. The giant protein titin: a major player in myocardial mechanics, signaling, and disease. *Circ Res*. 94:284-295.
Grater, F., J. Shen, H. Jiang, M. Gautel, and H. Grubmuller. 2005. Mechanically induced titin kinase activation studied by force-probe molecular dynamics simulations. *Biophys J*. 88:790-804.
Gregorio, C.C., K. Trombitas, T. Centner, B. Kolmerer, G. Stier, K. Kunke, K. Suzuki, F. Obermayr, B. Herrmann, H. Granzier, H. Sorimachi, and S. Labeit. 1998. The NH2 terminus of titin spans the Z-disc: its interaction with a novel 19-kD ligand (T-cap) is required for sarcomeric integrity. *J Cell Biol*. 143:1013-1027.
Guo, W., S.J. Bharmal, K. Esbona, and M.L. Greaser. 2010. Titin diversity--alternative splicing gone wild. *J Biomed Biotechnol*. 2010:753675.

Gutzman, J.H., and H. Sive. 2010. Epithelial relaxation mediated by the myosin phosphatase regulator Mypt1 is required for brain ventricle lumen expansion and hindbrain morphogenesis. *Development*. 137:795-804.

Hackman, J.P., A.K. Vihola, and A.B. Udd. 2003. The role of titin in muscular disorders. *Ann Med*. 35:434-441.

Haffter, P., M. Granato, M. Brand, M.C. Mullins, M. Hammerschmidt, D.A. Kane, J. Odenthal, F.J. van Eeden, Y.J. Jiang, C.P. Heisenberg, R.N. Kelsh, M. Furutani-Seiki, E. Vogelsang, D. Beuchle, U. Schach, C. Fabian, and C. Nusslein-Volhard. 1996. The identification of genes with unique and essential functions in the development of the zebrafish, Danio rerio. *Development*. 123:1-36.

Hansen, L., S. Comyn, H. Eiberg, Y. Mang, N. Tommerup, A. Lind-Thomsen, T. Rosenberg, F. Jean, J.L. Myhre, and D.B. Pilgrim. 2013. The myosin chaperone UNC45B is involved in lens development and autosomal dominant infantile cataract. *Hum Mol Genet*. Submitted.

Hawkins, T.A., A.P. Haramis, C. Etard, C. Prodromou, C.K. Vaughan, R. Ashworth, S. Ray, M. Behra, N. Holder, W.S. Talbot, L.H. Pearl, U. Strahle, and S.W. Wilson. 2008. The ATPase-dependent chaperoning activity of Hsp90a regulates thick filament formation and integration during skeletal muscle myofibrillogenesis. *Development*. 135:1147-1156.

Hayashi, Y.K., F.L. Chou, E. Engvall, M. Ogawa, C. Matsuda, S. Hirabayashi, K. Yokochi, B.L. Ziober, R.H. Kramer, S.J. Kaufman, E. Ozawa, Y. Goto, I. Nonaka, T. Tsukahara, J.Z. Wang, E.P. Hoffman, and K. Arahata. 1998. Mutations in the integrin alpha7 gene cause congenital myopathy. *Nat Genet*. 19:94-97.

He, S., E. Salas-Vidal, S. Rueb, S.F.G. Krens, A.H. Meijer, B.E. Snaar-Jagalska, and H.P. Spaink. 2006. Genetic and transcriptome characterization of model zebrafish cell lines. *Zebrafish*. 3:441-453.

Helfman, D.M., E.T. Levy, C. Berthier, M. Shtutman, D. Riveline, I. Grosheva, A. Lachish-Zalait, M. Elbaum, and A.D. Bershadsky. 1999. Caldesmon inhibits nonmuscle cell contractility and interferes with the formation of focal adhesions. *Mol Biol Cell*. 10:3097-3112.

Helmrich, A., and D. Barnes. 1999. Zebrafish embryonal cell culture. *Methods Cell Biol*. 59:29-37.

Holtzer, H., T. Hijikata, Z.X. Lin, Z.Q. Zhang, S. Holtzer, F. Protasi, C. Franzini-Armstrong, and H.L. Sweeney. 1997. Independent assembly of 1.6 microns long bipolar MHC filaments and I-Z-I bodies. *Cell Struct Funct*. 22:83-93.

Hoppe, P.E., and R.H. Waterston. 1996. Hydrophobicity variations along the surface of the coiled-coil rod may mediate striated muscle myosin assembly in Caenorhabditis elegans. *J Cell Biol*. 135:371-382.

Hoppe, P.E., and R.H. Waterston. 2000. A region of the myosin rod important for interaction with paramyosin in Caenorhabditis elegans striated muscle. *Genetics*. 156:631-643.

Hoppe, T., G. Cassata, J.M. Barral, W. Springer, A.H. Hutagalung, H.F. Epstein, and R. Baumeister. 2004. Regulation of the myosin-directed chaperone UNC-45 by a novel E3/E4-multiubiquitylation complex in C. elegans. *Cell*. 118:337-349.

Horowits, R., K. Maruyama, and R.J. Podolsky. 1989. Elastic behavior of connectin filaments during thick filament movement in activated skeletal muscle. *J Cell Biol*. 109:2169-2176.

Hresko, M.C., B.D. Williams, and R.H. Waterston. 1994. Assembly of body wall muscle and muscle cell attachment structures in Caenorhabditis elegans. *J Cell Biol*. 124:491-506.

Huang, N.F., S. Patel, R.G. Thakar, J. Wu, B.S. Hsiao, B. Chu, R.J. Lee, and S. Li. 2006. Myotube assembly on nanofibrous and micropatterned polymers. *Nano Lett*. 6:537-542.

Hutagalung, A.H., M.L. Landsverk, M.G. Price, and H.F. Epstein. 2002. The UCS family of myosin chaperones. *J Cell Sci*. 115:3983-3990.

Huxley, H.E. 1963. Electron Microscope Studies on the Structure of Natural and Synthetic Protein Filaments from Striated Muscle. *J Mol Biol*. 7:281-308.

Inagaki, N., T. Hayashi, T. Arimura, Y. Koga, M. Takahashi, H. Shibata, K. Teraoka, T. Chikamori, A. Yamashina, and A. Kimura. 2006. Alpha B-crystallin mutation in dilated cardiomyopathy. *Biochem Biophys Res Commun*. 342:379-386.

Ingber, D.E., and M. Levin. 2007. What lies at the interface of regenerative medicine and developmental biology? *Development*. 134:2541-2547.

Jackson, S.E. 2013. Hsp90: structure and function. *Top Curr Chem*. 328:155-240.

Jacoby, A.S., E. Busch-Nentwich, R.J. Bryson-Richardson, T.E. Hall, J. Berger, S. Berger, C. Sonntag, C. Sachs, R. Geisler, D.L. Stemple, and P.D. Currie. 2009. The zebrafish dystrophic mutant softy maintains muscle fibre viability despite basement membrane rupture and muscle detachment. *Development*. 136:3367-3376.

Jani, K., and F. Schock. 2007. Zasp is required for the assembly of functional integrin adhesion sites. *J Cell Biol*. 179:1583-1597.

Janiesch, P.C., J. Kim, J. Mouysset, R. Barikbin, H. Lochmuller, G. Cassata, S. Krause, and T. Hoppe. 2007. The ubiquitin-selective chaperone CDC-48/p97 links myosin assembly to human myopathy. *Nat Cell Biol*. 9:379-390.

Johnson, S.L., and L.I. Zon. 1999. Genetic backgrounds and some standard stocks and strains used in zebrafish developmental biology and genetics. *Methods Cell Biol*. 60:357-359.

Jungebluth, P., and P. Macchiarini. 2011. Stem cell-based therapy and regenerative approaches to diseases of the respiratory system. *Br Med Bull*.

Just, S., B. Meder, I.M. Berger, C. Etard, N. Trano, E. Patzel, D. Hassel, S. Marquart, T. Dahme, B. Vogel, M.C. Fishman, H.A. Katus, U. Strahle, and W. Rottbauer. 2011. The myosin-interacting protein SMYD1 is essential for sarcomere organization. *J Cell Sci*. 124:3127-3136.

Kachur, T., W. Ao, J. Berger, and D. Pilgrim. 2004. Maternal UNC-45 is involved in cytokinesis and colocalizes with non-muscle myosin in the early Caenorhabditis elegans embryo. *J Cell Sci*. 117:5313-5321.

Kachur, T.M., A. Audhya, and D.B. Pilgrim. 2008. UNC-45 is required for NMY-2 contractile function in early embryonic polarity establishment and germline cellularization in C. elegans. *Dev Biol*. 314:287-299.

Kagawa, M., N. Sato, and T. Obinata. 2006. Effects of BTS (N-benzyl-p-toluene sulphonamide), an inhibitor for myosin-actin interaction, on myofibrillogenesis in skeletal muscle cells in culture. *Zoolog Sci*. 23:969-975.

Kahn, J., Y. Shwartz, E. Blitz, S. Krief, A. Sharir, D.A. Breitel, R. Rattenbach, F. Relaix, P. Maire, R.B. Rountree, D.M. Kingsley, and E. Zelzer. 2009. Muscle contraction is necessary to maintain joint progenitor cell fate. *Dev Cell*. 16:734-743.

Katsura, I. 1987. Determination of bacteriophage lambda tail length by a protein ruler. *Nature*. 327:73-75.

Keller, G., M. Kennedy, T. Papayannopoulou, and M.V. Wiles. 1993. Hematopoietic commitment during embryonic stem cell differentiation in culture. *Mol Cell Biol*. 13:473-486.

Kettleborough, R.N., E.M. Busch-Nentwich, S.A. Harvey, C.M. Dooley, E. de Bruijn, F. van Eeden, I. Sealy, R.J. White, C. Herd, I.J. Nijman, F. Fenyes, S. Mehroke, C. Scahill, R. Gibbons, N. Wali, S. Carruthers, A. Hall, J. Yen, E. Cuppen, and D.L. Stemple. 2013. A systematic genome-wide analysis of zebrafish protein-coding gene function. *Nature*. 496:494-497.

Khaner, O., and F. Wilt. 1990. The influence of cell interactions and tissue mass on differentiation of sea urchin mesomeres. *Development*. 109:625-634.

Kharitonova, M.A., and J.M. Vasiliev. 2004. Length control is determined by the pattern of cytoskeleton. *J Cell Sci*. 117:1955-1960.

Kim, J., T. Lowe, and T. Hoppe. 2008. Protein quality control gets muscle into shape. *Trends Cell Biol*. 18:264-272.

Kim, S.S., S. Rhee, K.H. Lee, J.H. Kim, H.S. Kim, M.S. Kang, and C.H. Chung. 1998. Inhibitors of the proteasome block the myogenic differentiation of rat L6 myoblasts. *FEBS Lett*. 433:47-50.

Kimmel, C.B., W.W. Ballard, S.R. Kimmel, B. Ullmann, and T.F. Schilling. 1995. Stages of embryonic development of the zebrafish. *Dev Dyn*. 203:253-310.

Klaavuniemi, T., A. Kelloniemi, and J. Ylanne. 2004. The ZASP-like motif in actinin-associated LIM protein is required for interaction with the alpha-actinin rod and for targeting to the muscle Z-line. *J Biol Chem*. 279:26402-26410.

Klimanskaya, I., Y. Chung, S. Becker, S.-J. Lu, and R. Lanza. 2006. Human embryonic stem cell lines derived from single blastomeres. *Nature*. 444:481-485.

Knoll, R., M. Hoshijima, H.M. Hoffman, V. Person, I. Lorenzen-Schmidt, M.L. Bang, T. Hayashi, N. Shiga, H. Yasukawa, W. Schaper, W. McKenna, M. Yokoyama, N.J. Schork, J.H. Omens, A.D. McCulloch, A. Kimura, C.C. Gregorio, W. Poller, J. Schaper, H.P. Schultheiss, and K.R. Chien. 2002. The cardiac mechanical stretch sensor machinery involves a Z disc complex that is defective in a subset of human dilated cardiomyopathy. *Cell*. 111:943-955.

Kontrogianni-Konstantopoulos, A., M.A. Ackermann, A.L. Bowman, S.V. Yap, and R.J. Bloch. 2009. Muscle giants: molecular scaffolds in sarcomerogenesis. *Physiol Rev*. 89:1217-1267.

Krone, P.H., T.G. Evans, and S.R. Blechinger. 2003. Heat shock gene expression and function during zebrafish embryogenesis. *Semin Cell Dev Biol*. 14:267-274.

Krone, P.H., Z. Lele, and J.B. Sass. 1997. Heat shock genes and the heat shock response in zebrafish embryos. *Biochem Cell Biol*. 75:487-497.

Krukenberg, K.A., T.O. Street, L.A. Lavery, and D.A. Agard. 2011. Conformational dynamics of the molecular chaperone Hsp90. *Q Rev Biophys*. 44:229-255.

Labeit, S., T. Gibson, A. Lakey, K. Leonard, M. Zeviani, P. Knight, J. Wardale, and J. Trinick. 1991. Evidence that nebulin is a protein-ruler in muscle thin filaments. *FEBS Lett*. 282:313-316.

Laing, N.G., and K.J. Nowak. 2005. When contractile proteins go bad: the sarcomere and skeletal muscle disease. *Bioessays*. 27:809-822.

Lam, M.T., S. Sim, X. Zhu, and S. Takayama. 2006. The effect of continuous wavy micropatterns on silicone substrates on the alignment of skeletal muscle myoblasts and myotubes. *Biomaterials*. 27:4340-4347.

Landsverk, M.L., S. Li, A.H. Hutagalung, A. Najafov, T. Hoppe, J.M. Barral, and H.F. Epstein. 2007. The UNC-45 chaperone mediates sarcomere assembly through myosin degradation in Caenorhabditis elegans. *J Cell Biol*. 177:205-210.

Lange, S., F. Xiang, A. Yakovenko, A. Vihola, P. Hackman, E. Rostkova, J. Kristensen, B. Brandmeier, G. Franzen, B. Hedberg, L.G. Gunnarsson, S.M. Hughes, S. Marchand, T. Sejersen, I. Richard, L. Edstrom, E. Ehler, B. Udd, and M. Gautel. 2005. The kinase domain of titin controls muscle gene expression and protein turnover. *Science*. 308:1599-1603.

Ledee, D.R., B.K. Tripathi, and P.S. Zelenka. 2007. The CDK5 activator, p39, binds specifically to myosin essential light chain. *Biochem Biophys Res Commun*. 354:1034-1039.

Lee, C.F., A.V. Hauenstein, J.K. Fleming, W.C. Gasper, V. Engelke, B. Sankaran, S.I. Bernstein, and T. Huxford. 2011a. X-ray crystal structure of the UCS domain-containing UNC-45 myosin chaperone from Drosophila melanogaster. *Structure*. 19:397-408.

Lee, C.F., G.C. Melkani, Q. Yu, J.A. Suggs, W.A. Kronert, Y. Suzuki, L. Hipolito, M.G. Price, H.F. Epstein, and S.I. Bernstein. 2011b. Drosophila UNC-45 accumulates in embryonic blastoderm and in muscles, and is essential for muscle myosin stability. *J Cell Sci*. 124:699-705.

Levitsky, D.I., N.V. Khvorov, V.L. Shnyrov, N.S. Vedenkina, E.A. Permyakov, and B.F. Poglazov. 1990. Domain structure of myosin subfragment-1. Selective denaturation of the 50 kDa segment. *FEBS Lett*. 264:176-178.

Liew, C.C., and V.J. Dzau. 2004. Molecular genetics and genomics of heart failure. *Nature reviews. Genetics*. 5:811-825.

Lin-Jones, J., L. Sohlberg, A. Dose, J. Breckler, D.W. Hillman, and B. Burnside. 2009. Identification and localization of myosin superfamily members in fish retina and retinal pigmented epithelium. *J Comp Neurol*. 513:209-223.

Lin, D.I., O. Barbash, K.G. Kumar, J.D. Weber, J.W. Harper, A.J. Klein-Szanto, A. Rustgi, S.Y. Fuchs, and J.A. Diehl. 2006. Phosphorylation-dependent ubiquitination of cyclin D1 by the SCF(FBX4-alphaB crystallin) complex. *Mol Cell*. 24:355-366.

Lin, Z.X., S. Holtzer, T. Schultheiss, J. Murray, T. Masaki, D.A. Fischman, and H. Holtzer. 1989. Polygons and adhesion plaques and the disassembly and assembly of myofibrils in cardiac myocytes. *J Cell Biol*. 108:2355-2367.

Lindon, C., O. Albagli, C. Pinset, and D. Montarras. 2001. Cell density-dependent induction of endogenous myogenin (myf4) gene expression by Myf5. *Dev Biol*. 240:574-584.

Linke, W.A., M. Ivemeyer, P. Mundel, M.R. Stockmeier, and B. Kolmerer. 1998. Nature of PEVK-titin elasticity in skeletal muscle. *Proc Natl Acad Sci U S A*. 95:8052-8057.

Lisse, T.S., F. Thiele, H. Fuchs, W. Hans, G.K. Przemeck, K. Abe, B. Rathkolb, L. Quintanilla-Martinez, G. Hoelzlwimmer, M. Helfrich, E. Wolf, S.H. Ralston, and M. Hrabe de Angelis. 2008. ER stress-mediated apoptosis in a new mouse model of osteogenesis imperfecta. *PLoS Genet*. 4:e7.

Liu, B., and Z. Li. 2008. Endoplasmic reticulum HSP90b1 (gp96, grp94) optimizes B-cell function via chaperoning integrin and TLR but not immunoglobulin. *Blood*. 112:1223-1230.
Liu, C., R.P. Gersch, T.J. Hawke, and M. Hadjiargyrou. 2010. Silencing of Mustn1 inhibits myogenic fusion and differentiation. *Am J Physiol Cell Physiol*. 298:1100-1108.
Liu, F., J.M. Barral, C.C. Bauer, I. Ortiz, R.G. Cook, M.F. Schmid, and H.F. Epstein. 1997. Assemblases and coupling proteins in thick filament assembly. *Cell Struct Funct*. 22:155-162.
Liu, L., R. Srikakulam, and D.A. Winkelmann. 2008. Unc45 activates Hsp90-dependent folding of the myosin motor domain. *J Biol Chem*. 283:13185-13193.
Machado, C., and D.J. Andrew. 2000. D-Titin: a giant protein with dual roles in chromosomes and muscles. *J Cell Biol*. 151:639-652.
Manisastry, S.M., K.J. Zaal, and R. Horowits. 2009. Myofibril assembly visualized by imaging N-RAP, alpha-actinin, and actin in living cardiomyocytes. *Exp Cell Res*. 315:2126-2139.
Marino, T.A., L. Kuseryk, and I.K. Lauva. 1987. Role of contraction in the structure and growth of neonatal rat cardiocytes. *Am J Physiol*. 253:H1391-1399.
Maruyama, I.N., D.M. Miller, and S. Brenner. 1989. Myosin heavy chain gene amplification as a suppressor mutation in Caenorhabditis elegans. *Mol Gen Genet*. 219:113-118.
Maruyama, K. 1976. Connectin, an elastic protein from myofibrils. *J Biochem*. 80:405-407.
Mase, V.J., Jr., J.R. Hsu, S.E. Wolf, J.C. Wenke, D.G. Baer, J. Owens, S.F. Badylak, and T.J. Walters. 2010. Clinical application of an acellular biologic scaffold for surgical repair of a large, traumatic quadriceps femoris muscle defect. *Orthopedics*. 33:511.
Mathew, A., and R.I. Morimoto. 1998. Role of the heat-shock response in the life and death of proteins. *Ann N Y Acad Sci*. 851:99-111.
Mayans, O., P.F. van der Ven, M. Wilm, A. Mues, P. Young, D.O. Furst, M. Wilmanns, and M. Gautel. 1998. Structural basis for activation of the titin kinase domain during myofibrillogenesis. *Nature*. 395:863-869.
Mayer, M.P. 2010. Gymnastics of molecular chaperones. *Mol Cell*. 39:321-331.
Melkani, G.C., C.F. Lee, A. Cammarato, and S.I. Bernstein. 2010. Drosophila UNC-45 prevents heat-induced aggregation of skeletal muscle myosin and facilitates refolding of citrate synthase. *Biochem Biophys Res Commun*. 396:317-322.
Miller, D.M., 3rd, I. Ortiz, G.C. Berliner, and H.F. Epstein. 1983. Differential localization of two myosins within nematode thick filaments. *Cell*. 34:477-490.
Miller, G., H. Musa, M. Gautel, and M. Peckham. 2003. A targeted deletion of the C-terminal end of titin, including the titin kinase domain, impairs myofibrillogenesis. *J Cell Sci*. 116:4811-4819.
Moerman, D.G., and B.D. Williams. 2006. Sarcomere assembly in C. elegans muscle. *WormBook*:1-16.
Morimoto, R.I., A. Tissières, and C. Georgopoulos. 1994. The Biology of heat shock proteins and molecular chaperones. Cold Spring Harbor Laboratory Press, Plainview , N.Y. vii, 610 p. pp.
Morita, H., J. Seidman, and C.E. Seidman. 2005. Genetic causes of human heart failure. *J Clin Invest*. 115:518-526.
Mugita, N., Y. Honda, H. Nakamura, T. Fujiwara, K. Tanaka, S. Omura, N. Shimbara, M. Ogawa, H. Saya, and M. Nakao. 1999. The involvement of proteasome in myogenic

differentiation of murine myocytes and human rhabdomyosarcoma cells. *Int J Mol Med*. 3:127-137.
Muller, S., S. Lange, M. Gautel, and M. Wilmanns. 2007. Rigid conformation of an immunoglobulin domain tandem repeat in the A-band of the elastic muscle protein titin. *J Mol Biol*. 371:469-480.
Mullins, M.C., M. Hammerschmidt, P. Haffter, and C. Nusslein-Volhard. 1994. Large-scale mutagenesis in the zebrafish: in search of genes controlling development in a vertebrate. *Curr Biol*. 4:189-202.
Musa, H., S. Meek, M. Gautel, D. Peddie, A.J. Smith, and M. Peckham. 2006. Targeted homozygous deletion of M-band titin in cardiomyocytes prevents sarcomere formation. *J Cell Sci*. 119:4322-4331.
Myhre, J.L., and D.B. Pilgrim. 2010. Cellular differentiation in primary cell cultures from single zebrafish embryos as a model for the study of myogenesis. *Zebrafish*. 7:255-266.
Myhre, J.L., and D.B. Pilgrim. 2012. At the Start of the Sarcomere: A Previously Unrecognized Role for Myosin Chaperones and Associated Proteins during Early Myofibrillogenesis. *Biochem Res Int*. 2012:712315.
Neff, M.M., E. Turk, and M. Kalishman. 2002. Web-based primer design for single nucleotide polymorphism analysis. *Trends Genet*. 18:613-615.
Ni, M., and A.S. Lee. 2007. ER chaperones in mammalian development and human diseases. *FEBS Lett*. 581:3641-3651.
Ni, W., A.H. Hutagalung, S. Li, and H.F. Epstein. 2011. The myosin-binding UCS domain but not the Hsp90-binding TPR domain of the UNC-45 chaperone is essential for function in Caenorhabditis elegans. *J Cell Sci*. 124:3164-3173.
Norris, W., C. Neyt, P.W. Ingham, and P.D. Currie. 2000. Slow muscle induction by Hedgehog signalling in vitro. *J Cell Sci*. 113 (Pt 15):2695-2703.
Nowlan, N.C., J. Sharpe, K.A. Roddy, P.J. Prendergast, and P. Murphy. 2010. Mechanobiology of embryonic skeletal development: Insights from animal models. *Birth defects research. Part C, Embryo today : reviews*. 90:203-213.
Ober, E.A., and S. Schulte-Merker. 1999. Signals from the yolk cell induce mesoderm, neuroectoderm, the trunk organizer, and the notochord in zebrafish. *Dev Biol*. 215:167-181.
Obermann, W.M., M. Gautel, K. Weber, and D.O. Furst. 1997. Molecular structure of the sarcomeric M band: mapping of titin and myosin binding domains in myomesin and the identification of a potential regulatory phosphorylation site in myomesin. *Embo J*. 16:211-220.
Obinata, M. 1997. Conditionally immortalized cell lines with differentiated functions established from temperature-sensitive T-antigen transgenic mice. *Genes Cells*. 2:235-244.
Opitz, C.A., M. Kulke, M.C. Leake, C. Neagoe, H. Hinssen, R.J. Hajjar, and W.A. Linke. 2003. Damped elastic recoil of the titin spring in myofibrils of human myocardium. *Proc Natl Acad Sci U S A*. 100:12688-12693.
Page, S.G., and H.E. Huxley. 1963. Filament Lengths in Striated Muscle. *J Cell Biol*. 19:369-390.

Pan, C., C. Kumar, S. Bohl, U. Klingmueller, and M. Mann. 2009. Comparative proteomic phenotyping of cell lines and primary cells to assess preservation of cell type-specific functions. *Mol Cell Proteomics*. 8:443-450.

Pardo, J.V., J.D. Siliciano, and S.W. Craig. 1983. A vinculin-containing cortical lattice in skeletal muscle: transverse lattice elements ("costameres") mark sites of attachment between myofibrils and sarcolemma. *Proc Natl Acad Sci U S A*. 80:1008-1012.

Patton, E.E., and L.I. Zon. 2001. The art and design of genetic screens: zebrafish. *Nat Rev Genet*. 2:956-966.

Paulus, J.D., G.B. Willer, J.R. Willer, R.G. Gregg, and M.C. Halloran. 2009. Muscle contractions guide rohon-beard peripheral sensory axons. *J Neurosci*. 29:13190-13201.

Peckham, M., P. Young, and M. Gautel. 1997. Constitutive and variable regions of Z-disk titin/connectin in myofibril formation: a dominant-negative screen. *Cell Struct Funct*. 22:95-101.

Peng, J., K. Raddatz, S. Labeit, H. Granzier, and M. Gotthardt. 2005. Muscle atrophy in titin M-line deficient mice. *J Muscle Res Cell Motil*. 26:381-388.

Peng, J., K. Raddatz, J.D. Molkentin, Y. Wu, S. Labeit, H. Granzier, and M. Gotthardt. 2007. Cardiac hypertrophy and reduced contractility in hearts deficient in the titin kinase region. *Circulation*. 115:743-751.

Person, V., S. Kostin, K. Suzuki, S. Labeit, and J. Schaper. 2000. Antisense oligonucleotide experiments elucidate the essential role of titin in sarcomerogenesis in adult rat cardiomyocytes in long-term culture. *J Cell Sci*. 113 Pt 21:3851-3859.

Pfeffer, G., R. Barresi, I.J. Wilson, S.A. Hardy, H. Griffin, J. Hudson, H.R. Elliott, A.V. Ramesh, A. Radunovic, J.B. Winer, S. Vaidya, A. Raman, M. Busby, M.E. Farrugia, A. Ming, C. Everett, H.C. Emsley, R. Horvath, V. Straub, K. Bushby, H. Lochmuller, P.F. Chinnery, and A. Sarkozy. 2013. Titin founder mutation is a common cause of myofibrillar myopathy with early respiratory failure. *J Neurol Neurosurg Psychiatry*.

Pichler, F.B., S. Laurenson, L.C. Williams, A. Dodd, B.R. Copp, and D.R. Love. 2003. Chemical discovery and global gene expression analysis in zebrafish. *Nat Biotechnol*. 21:879-883.

Pirskanen, A., J.C. Kiefer, and S.D. Hauschka. 2000. IGFs, insulin, Shh, bFGF, and TGF-beta1 interact synergistically to promote somite myogenesis in vitro. *Dev Biol*. 224:189-203.

Price, M.G., M.L. Landsverk, J.M. Barral, and H.F. Epstein. 2002. Two mammalian UNC-45 isoforms are related to distinct cytoskeletal and muscle-specific functions. *J Cell Sci*. 115:4013-4023.

Puchner, E.M., A. Alexandrovich, A.L. Kho, U. Hensen, L.V. Schafer, B. Brandmeier, F. Grater, H. Grubmuller, H.E. Gaub, and M. Gautel. 2008. Mechanoenzymatics of titin kinase. *Proc Natl Acad Sci U S A*. 105:13385-13390.

Qadota, H., and G.M. Benian. 2010. Molecular structure of sarcomere-to-membrane attachment at M-Lines in C. elegans muscle. *J Biomed Biotechnol*. 2010:864749.

Raeker, M.O., A.N. Bieniek, A.S. Ryan, H.J. Tsai, K.M. Zahn, and M.W. Russell. 2010. Targeted deletion of the zebrafish obscurin A RhoGEF domain affects heart, skeletal muscle and brain development. *Dev Biol*. 337:432-443.

Rauch, G.-J., M. Granato, and P. Haffter. 1997. A polymorphic zebrafish line for genetic mapping using SSLPs on high-percentage agarose gels. *Technical Tips Online*. 2:148-150.

Rauch, G.J., Lyons, D.A., Middendorf, I., Friedlander, B., Arana, N., Reyes, T., and Talbot, W.S. 2003. Submission and Curation of Gene Expression Data. . *In* ZFIN Direct Data Submission (http://zfin.org).

Rhee, D., J.M. Sanger, and J.W. Sanger. 1994. The premyofibril: evidence for its role in myofibrillogenesis. *Cell Motil Cytoskeleton*. 28:1-24.

Riveline, D., E. Zamir, N.Q. Balaban, U.S. Schwarz, T. Ishizaki, S. Narumiya, Z. Kam, B. Geiger, and A.D. Bershadsky. 2001. Focal contacts as mechanosensors: externally applied local mechanical force induces growth of focal contacts by an mDia1-dependent and ROCK-independent mechanism. *J Cell Biol*. 153:1175-1186.

Robu, M.E., J.D. Larson, A. Nasevicius, S. Beiraghi, C. Brenner, S.A. Farber, and S.C. Ekker. 2007. p53 activation by knockdown technologies. *PLoS Genet*. 3.

Rooney, J.E., J.V. Welser, M.A. Dechert, N.L. Flintoff-Dye, S.J. Kaufman, and D.J. Burkin. 2006. Severe muscular dystrophy in mice that lack dystrophin and alpha7 integrin. *J Cell Sci*. 119:2185-2195.

Rosser, B.W., M. Wick, D.M. Waldbillig, D.J. Wright, C.M. Farrar, and E. Bandman. 1998. Expression of myosin heavy chain isoforms during development of domestic pigeon pectoralis muscle. *Int J Dev Biol*. 42:653-661.

Roy, S., C. Wolff, and P.W. Ingham. 2001. The u-boot mutation identifies a Hedgehog-regulated myogenic switch for fiber-type diversification in the zebrafish embryo. *Genes Dev*. 15:1563-1576.

Rui, Y., J. Bai, and N. Perrimon. 2010. Sarcomere formation occurs by the assembly of multiple latent protein complexes. *PLoS Genet*. 6:e1001208.

Sandquist, J.C., K.I. Swenson, K.A. Demali, K. Burridge, and A.R. Means. 2006. Rho kinase differentially regulates phosphorylation of nonmuscle myosin II isoforms A and B during cell rounding and migration. *J Biol Chem*. 281:35873-35883.

Sanger, J.M., B. Mittal, M.B. Pochapin, and J.W. Sanger. 1986. Myofibrillogenesis in living cells microinjected with fluorescently labeled alpha-actinin. *J Cell Biol*. 102:2053-2066.

Sanger, J.M., and J.W. Sanger. 2008. The dynamic Z bands of striated muscle cells. *Sci Signal*. 1:pe37.

Sanger, J.W., S. Kang, C.C. Siebrands, N. Freeman, A. Du, J. Wang, A.L. Stout, and J.M. Sanger. 2005. How to build a myofibril. *J Muscle Res Cell Motil*. 26:343-354.

Sanger, J.W., B. Mittal, and J.M. Sanger. 1984. Analysis of myofibrillar structure and assembly using fluorescently labeled contractile proteins. *J Cell Biol*. 98:825-833.

Sanger, J.W., J. Wang, Y. Fan, J. White, and J.M. Sanger. 2010. Assembly and dynamics of myofibrils. *J Biomed Biotechnol*. 2010:858606.

Sanger, J.W., J.S. Wang, B. Holloway, A.P. Du, and J.M. Sanger. 2009. Myofibrillogenesis in Skeletal Muscle Cells in Zebrafish. *Cell Motil Cytoskeleton*. 66:556-566.

Sato, Y., H.C. Probst, R. Tatsumi, Y. Ikeuchi, M.S. Neuberger, and C. Rada. 2010. Deficiency in APOBEC2 leads to a shift in muscle fiber type, diminished body mass, and myopathy. *J Biol Chem*. 285:7111-7118.

Schwander, M., M. Leu, M. Stumm, O.M. Dorchies, U.T. Ruegg, J. Schittny, and U. Muller. 2003. Beta1 integrins regulate myoblast fusion and sarcomere assembly. *Dev Cell*. 4:673-685.

Seeley, M., W. Huang, Z. Chen, W.O. Wolff, X. Lin, and X. Xu. 2007. Depletion of zebrafish titin reduces cardiac contractility by disrupting the assembly of Z-discs and A-bands. *Circ Res*. 100:238-245.

Sela, I., I. Milman Krentsis, Z. Shlomai, M. Sadeh, R. Dabby, Z. Argov, H. Ben-Bassat, and S. Mitrani-Rosenbaum. 2011. The proteomic profile of hereditary inclusion body myopathy. *PLoS One*. 6:e16334.

Selcen, D., and A.G. Engel. 2011. Myofibrillar myopathies. *Handb Clin Neurol*. 101:143-154.

Sharp, W.W., D.G. Simpson, T.K. Borg, A.M. Samarel, and L. Terracio. 1997. Mechanical forces regulate focal adhesion and costamere assembly in cardiac myocytes. *Am J Physiol*. 273:H546-556.

Shi, H., and G. Blobel. 2010. UNC-45/CRO1/She4p (UCS) protein forms elongated dimer and joins two myosin heads near their actin binding region. *Proc Natl Acad Sci U S A*. 107:21382-21387.

Shimizu, K., H. Fujita, and E. Nagamori. 2009. Alignment of skeletal muscle myoblasts and myotubes using linear micropatterned surfaces ground with abrasives. *Biotechnol Bioeng*. 103:631-638.

Siegers, K., T. Waldmann, M.R. Leroux, K. Grein, A. Shevchenko, E. Schiebel, and F.U. Hartl. 1999. Compartmentation of protein folding in vivo: sequestration of non-native polypeptide by the chaperonin-GimC system. *Embo J*. 18:75-84.

Silberstein, L., S.G. Webster, M. Travis, and H.M. Blau. 1986. Developmental progression of myosin gene expression in cultured muscle cells. *Cell*. 46:1075-1081.

Simpson, D.G., M.L. Decker, W.A. Clark, and R.S. Decker. 1993. Contractile activity and cell-cell contact regulate myofibrillar organization in cultured cardiac myocytes. *J Cell Biol*. 123:323-336.

Skwarek-Maruszewska, A., P. Hotulainen, P.K. Mattila, and P. Lappalainen. 2009. Contractility-dependent actin dynamics in cardiomyocyte sarcomeres. *J Cell Sci*. 122:2119-2126.

Soeno, Y., Y. Shimada, and T. Obinata. 1999. BDM (2,3-butanedione monoxime), an inhibitor of myosin-actin interaction, suppresses myofibrillogenesis in skeletal muscle cells in culture. *Cell and tissue research*. 295:307-316.

Sparrow, J.C., and F. Schock. 2009. The initial steps of myofibril assembly: integrins pave the way. *Nat Rev Mol Cell Biol*. 10:293-298.

Srikakulam, R., L. Liu, and D.A. Winkelmann. 2008. Unc45b forms a cytosolic complex with Hsp90 and targets the unfolded myosin motor domain. *PLoS One*. 3:e2137.

Srikakulam, R., and D.A. Winkelmann. 1999. Myosin II folding is mediated by a molecular chaperonin. *J Biol Chem*. 274:27265-27273.

Srikakulam, R., and D.A. Winkelmann. 2004. Chaperone-mediated folding and assembly of myosin in striated muscle. *J Cell Sci*. 117:641-652.

Steffen, L.S., J.R. Guyon, E.D. Vogel, M.H. Howell, Y. Zhou, G.J. Weber, L.I. Zon, and L.M. Kunkel. 2007. The zebrafish runzel muscular dystrophy is linked to the titin gene. *Dev Biol*. 309:180-192.

Streisinger, G., C. Walker, N. Dower, D. Knauber, and F. Singer. 1981. Production of clones of homozygous diploid zebra fish (Brachydanio rerio). *Nature*. 291:293-296.
Sun, L., C.S. Bradford, C. Ghosh, P. Collodi, and D.W. Barnes. 1995. ES-like cell cultures derived from early zebrafish embryos. *Mol Mar Biol Biotechnol*. 4:193-199.
Swailes, N.T., M. Colegrave, P.J. Knight, and M. Peckham. 2006. Non-muscle myosins 2A and 2B drive changes in cell morphology that occur as myoblasts align and fuse. *J Cell Sci*. 119:3561-3570.
Takeda, K., Z.X. Yu, S. Qian, T.K. Chin, R.S. Adelstein, and V.J. Ferrans. 2000. Nonmuscle myosin II localizes to the Z-lines and intercalated discs of cardiac muscle and to the Z-lines of skeletal muscle. *Cell Motil Cytoskeleton*. 46:59-68.
Tamaki, T., Y. Okada, Y. Uchiyama, K. Tono, M. Masuda, M. Wada, A. Hoshi, T. Ishikawa, and A. Akatsuka. 2007. Clonal multipotency of skeletal muscle-derived stem cells between mesodermal and ectodermal lineage. *Stem Cells*. 25:2283-2290.
Tan, X., J. Rotllant, H. Li, P. De Deyne, and S.J. Du. 2006. SmyD1, a histone methyltransferase, is required for myofibril organization and muscle contraction in zebrafish embryos. *Proc Natl Acad Sci U S A*. 103:2713-2718.
te Velthuis, A.J., and C.P. Bagowski. 2007. PDZ and LIM domain-encoding genes: molecular interactions and their role in development. *ScientificWorldJournal*. 7:1470-1492.
Thisse, B., V. Heyer, A. Lux, V. Alunni, A. Degrave, I. Seiliez, J. Kirchner, J.P. Parkhill, and C. Thisse. 2004. Spatial and temporal expression of the zebrafish genome by large-scale in situ hybridization screening. *Methods Cell Biol*. 77:505-519.
Thompson, O., M. Edgley, P. Strasbourger, S. Flibotte, B. Ewing, R. Adair, V. Au, I. Chaudry, L. Fernando, H. Hutter, A. Kieffer, J. Lau, N. Lee, A. Miller, G. Raymant, B. Shen, J. Shendure, J. Taylor, E. Turner, L. Hillier, D.G. Moerman, and R.H. Waterston. 2013. The Million Mutation Project: A new approach to genetics in Caenorhabditis elegans. *Genome Res*.
Toh, B.H., A. Yildiz, J. Sotelo, O. Osung, E.J. Holborow, and A. Fairfax. 1979. Distribution of actin and myosin in muscle and non-muscle cells. *Cell Tissue Res*. 199:117-126.
Tokuyasu, K.T. 1989. Immunocytochemical studies of cardiac myofibrillogenesis in early chick embryos. III. Generation of fasciae adherentes and costameres. *J Cell Biol*. 108:43-53.
Tokuyasu, K.T., and P.A. Maher. 1987. Immunocytochemical studies of cardiac myofibrillogenesis in early chick embryos. II. Generation of alpha-actinin dots within titin spots at the time of the first myofibril formation. *J Cell Biol*. 105:2795-2801.
Trinick, J. 1996. Titin as a scaffold and spring. Cytoskeleton. *Curr Biol*. 6:258-260.
Tskhovrebova, L., and J. Trinick. 2002. Role of titin in vertebrate striated muscle. *Philos Trans R Soc Lond B Biol Sci*. 357:199-206.
Tskhovrebova, L., and J. Trinick. 2003. Titin: properties and family relationships. *Nat Rev Mol Cell Biol*. 4:679-689.
Tullio, A.N., D. Accili, V.J. Ferrans, Z.X. Yu, K. Takeda, A. Grinberg, H. Westphal, Y.A. Preston, and R.S. Adelstein. 1997. Nonmuscle myosin II-B is required for normal development of the mouse heart. *Proc Natl Acad Sci U S A*. 94:12407-12412.
Turnacioglu, K.K., B. Mittal, G.A. Dabiri, J.M. Sanger, and J.W. Sanger. 1997. Zeugmatin is part of the Z-band targeting region of titin. *Cell Struct Funct*. 22:73-82.

Turner, N.J., and S.F. Badylak. 2011. Regeneration of skeletal muscle. *Cell and tissue research*.

Turner, W.S., X. Wang, S. Johnson, C. Medberry, J. Mendez, S.F. Badylak, M.G. McCord, and K.E. McCloskey. 2012. Cardiac tissue development for delivery of embryonic stem cell-derived endothelial and cardiac cells in natural matrices. *J Biomed Mater Res B Appl Biomater*. 100:2060-2072.

Udd, B. 2012. Distal myopathies--new genetic entities expand diagnostic challenge. *Neuromuscul Disord*. 22:5-12.

Valentin, J.E., N.J. Turner, T.W. Gilbert, and S.F. Badylak. 2010. Functional skeletal muscle formation with a biologic scaffold. *Biomaterials*. 31:7475-7484.

van der Loop, F.T., P.F. van der Ven, D.O. Furst, M. Gautel, G.J. van Eys, and F.C. Ramaekers. 1996. Integration of titin into the sarcomeres of cultured differentiating human skeletal muscle cells. *Eur J Cell Biol*. 69:301-307.

van der Ven, P.F., J.W. Bartsch, M. Gautel, H. Jockusch, and D.O. Furst. 2000. A functional knock-out of titin results in defective myofibril assembly. *J Cell Sci*. 113 (Pt 8):1405-1414.

van der Ven, P.F., and D.O. Furst. 1997. Assembly of titin, myomesin and M-protein into the sarcomeric M band in differentiating human skeletal muscle cells in vitro. *Cell Struct Funct*. 22:163-171.

van Eeden, F.J., M. Granato, U. Schach, M. Brand, M. Furutani-Seiki, P. Haffter, M. Hammerschmidt, C.P. Heisenberg, Y.J. Jiang, D.A. Kane, R.N. Kelsh, M.C. Mullins, J. Odenthal, R.M. Warga, M.L. Allende, E.S. Weinberg, and C. Nusslein-Volhard. 1996. Mutations affecting somite formation and patterning in the zebrafish, Danio rerio. *Development*. 123:153-164.

Venolia, L., W. Ao, S. Kim, C. Kim, and D. Pilgrim. 1999. unc-45 gene of Caenorhabditis elegans encodes a muscle-specific tetratricopeptide repeat-containing protein. *Cell Motil Cytoskeleton*. 42:163-177.

Vleminckx, V., P. Van Damme, K. Goffin, H. Delye, L. Van Den Bosch, and W. Robberecht. 2002. Upregulation of HSP27 in a transgenic model of ALS. *Journal of neuropathology and experimental neurology*. 61:968-974.

Vogel, B., B. Meder, S. Just, C. Laufer, I. Berger, S. Weber, H.A. Katus, and W. Rottbauer. 2009. In-vivo characterization of human dilated cardiomyopathy genes in zebrafish. *Biochem Biophys Res Commun*. 390:516-522.

Volk, T., L.I. Fessler, and J.H. Fessler. 1990. A role for integrin in the formation of sarcomeric cytoarchitecture. *Cell*. 63:525-536.

von der Mark, K., and M. Ocalan. 1989. Antagonistic effects of laminin and fibronectin on the expression of the myogenic phenotype. *Differentiation*. 40:150-157.

Wainwright, J.M., C.A. Czajka, U.B. Patel, D.O. Freytes, K. Tobita, T.W. Gilbert, and S.F. Badylak. 2010. Preparation of cardiac extracellular matrix from an intact porcine heart. *Tissue Eng Part C Methods*. 16:525-532.

Walker, M.G. 2001. Pharmaceutical target identification by gene expression analysis. *Mini Rev Med Chem*. 1:197-205.

Walsh, D., J. Grantham, X.O. Zhu, J. Wei Lin, M. van Oosterum, R. Taylor, and M. Edwards. 1999. The role of heat shock proteins in mammalian differentiation and development. *Environ Med*. 43:79-87.

Wang, A., X. Ma, M.A. Conti, and R.S. Adelstein. 2011. Distinct and redundant roles of the non-muscle myosin II isoforms and functional domains. *Biochem Soc Trans*. 39:1131-1135.

Wang, K., R. McCarter, J. Wright, J. Beverly, and R. Ramirez-Mitchell. 1993. Viscoelasticity of the sarcomere matrix of skeletal muscles. The titin-myosin composite filament is a dual-stage molecular spring. *Biophys J*. 64:1161-1177.

Wang, L., C. Cerdan, P. Menendez, and M. Bhatia. 2006. Derivation and characterization of hematopoietic cells from human embryonic stem cells. *Methods Mol Biol*. 331:179-200.

Wang, X., R. Klevitsky, W. Huang, J. Glasford, F. Li, and J. Robbins. 2003. AlphaB-crystallin modulates protein aggregation of abnormal desmin. *Circ Res*. 93:998-1005.

Wang, Y.H., Y.H. Chen, J.H. Lu, and H.J. Tsai. 2005. A 23-amino acid motif spanning the basic domain targets zebrafish myogenic regulatory factor myf5 into nucleolus. *DNA Cell Biol*. 24:651-660.

Weinert, S., N. Bergmann, X. Luo, B. Erdmann, and M. Gotthardt. 2006. M line-deficient titin causes cardiac lethality through impaired maturation of the sarcomere. *J Cell Biol*. 173:559-570.

Wells, C., D. Coles, A. Entwistle, and M. Peckham. 1997. Myogenic cells express multiple myosin isoforms. *J Muscle Res Cell Motil*. 18:501-515.

Westerfield, M. 2000. The Zebrafish Book: A guide for the laboratory use of zebrafish (Danio rerio). University of Oregon Press, Eugene, OR.

Whiting, A., J. Wardale, and J. Trinick. 1989. Does titin regulate the length of muscle thick filaments? *J Mol Biol*. 205:263-268.

Williams, B.D., and R.H. Waterston. 1994. Genes critical for muscle development and function in Caenorhabditis elegans identified through lethal mutations. *J Cell Biol*. 124:475-490.

Willis, M.S., J.C. Schisler, A.L. Portbury, and C. Patterson. 2009. Build it up-Tear it down: protein quality control in the cardiac sarcomere. *Cardiovasc Res*. 81:439-448.

Wohlgemuth, S.L. 2007. Characterization of *unc45b* in zebrafish muscle development. *In* Biological Sciences. Vol. Doctor of Philosophy. University of Alberta, Edmonton. 185.

Wohlgemuth, S.L., B.D. Crawford, and D.B. Pilgrim. 2007. The myosin co-chaperone UNC-45 is required for skeletal and cardiac muscle function in zebrafish. *Dev Biol*. 303:483-492.

Xu, X., S.E. Meiler, T.P. Zhong, M. Mohideen, D.A. Crossley, W.W. Burggren, and M.C. Fishman. 2002. Cardiomyopathy in zebrafish due to mutation in an alternatively spliced exon of titin. *Nat Genet*. 30:205-209.

Yaffe, D., and O. Saxel. 1977. Serial passaging and differentiation of myogenic cells isolated from dystrophic mouse muscle. *Nature*. 270:725-727.

Zhu, J.J., Y.Q. Xu, J.H. He, H.P. Yu, C.J. Huang, J.M. Gao, Q.X. Dong, Y.X. Xuan, and C.Q. Li. 2013. Human cardiotoxic drugs delivered by soaking and microinjection induce cardiovascular toxicity in zebrafish. *Journal of applied toxicology : JAT*.

Zoeller, J.J., A. McQuillan, J. Whitelock, S.Y. Ho, and R.V. Iozzo. 2008. A central function for perlecan in skeletal muscle and cardiovascular development. *J Cell Biol*. 181:381-394.

Zou, P., M. Gautel, A. Geerlof, M. Wilmanns, M.H. Koch, and D.I. Svergun. 2003. Solution scattering suggests cross-linking function of telethonin in the complex with titin. *J Biol Chem*. 278:2636-2644.

Zou, P., N. Pinotsis, S. Lange, Y.H. Song, A. Popov, I. Mavridis, O.M. Mayans, M. Gautel, and M. Wilmanns. 2006. Palindromic assembly of the giant muscle protein titin in the sarcomeric Z-disk. *Nature*. 439:229-233.